WCAP-8945

WESTINGHOUSE CLASS 3
CUSTOMER-DESIGNATED DISTRIBUTION

FRACTURE MECHANICS EVALUATION OF THE FLORIDA POWER AND LIGHT COMPANY TURKEY POINT UNIT NO. 4 REACTOR PRESSURE VESSEL SUBJECTED TO POSTULATED ACCIDENT TRANSIENTS

O. Meeuwis
R. W. Fleming
P. J. Morris

May 1977

Prepared by Westinghouse for Florida Power and Light Company

APPROVED: _____
J. N. Chirigos, Manager
Structural Materials Engineering

Work Performed Under EKDP-200

WESTINGHOUSE ELECTRIC CORPORATION
Nuclear Energy Systems
P. O. Box 355
Pittsburgh, Pennsylvania 15230

ABSTRACT

This report presents an integrity evaluation of the Turkey Point Unit No. 4 reactor pressure vessel for a postulated Loss-of-Coolant Accident (LOCA) and a Large Steam Line Break (LSB).

Principles of the linear elastic fracture mechanics technology were used to assess the potential for brittle failure of the reactor vessel for both faulted condition transients. The results of the fracture mechanics analysis were evaluated relative to conservative initiation and arrest criteria pertaining to the integrity of nuclear reactor pressure vessels.

This study was performed as part of the contractual commitments called for in the Florida Power & Light Company purchase order No. 95599-83717 of September 13, 1976 as amended by Supplement No. 2 dated December 7, 1976.

PREFACE

This report has been technically reviewed and the calculations checked.

J. J. McGowan

TABLE OF CONTENTS

Section	Title	Page
1	SUMMARY OF RESULTS	1-1
	1-1. Westinghouse Copper Trend Curves	1-1
	1-2. Regulatory Guide 1.99 Trend Curve	1-1
2	INTRODUCTION	2-1
	2-1. Background	2-1
	2-2. Analysis Performed	2-1
3	DESCRIPTION OF THE FAULTED CONDITION TRANSIENT FOR THE LOSS-OF-COOLANT ACCIDENT AND LARGE STEAM LINE BREAK	3-1
	3-1. Loss-of-Coolant Accident (LOCA)	3-1
	3-2. Large Steam Line Break (LSB)	3-2
4	THERMAL ANALYSIS	4-1
	4-1. Thermal Analysis Method	4-1
	4-2. Large LOCA	4-3
	4-3. Large Steam Line Break	4-4
5	FRACTURE MECHANICS ANALYSIS	5-1
	5-1. Basis for Analytical Method	5-1
	5-2. Stress Intensity Factor Expression	5-2
	5-3. Fluence Calculations	5 3
	5-4. Irradiation Effects	5-4
	5-5. Fracture Analysis	5-6

TABLE OF CONTENTS (cont)

Section	Title	Page
6	MATERIAL INPUT	6-1
	6-1. Basis for Selection of Base Material Properties	6-2
	6-2. Basis for Selection of the Circumferential Weldment Properties	6-2
7	RESULTS AND CONCLUSIONS	7-1
	7-1. Loss-of-Coolant Accident	7-1
	7-2. Longitudinal Flaw (Evaluation at 40 Calendar Years)	7-1
	7-3. Circumferential Flaw (Evaluation at 40 Calendar Years)	7-3
	7-4. Evaluation at 26.25 Calendar Years (R.G. 1.99 Trend Curves)	7-4
	7-5. Conclusion for LOCA Analysis	7-4
	7-6. Large Steam Line Break	7-5
	7-7. Longitudinal Flaw (Evaluation at 40 Calendar Years)	7-5
	7-8. Circumferential Flaw (Evaluation at 40 Calendar Years)	7-7
	7-9. Evaluation at 31.25 Calendar Years LSB (With Off-Site Power)	7-8
	7-10. Evaluation at 25 Calendar Years LSB (With Off-Site Power)	7-8
	7-11. Conclusion for LSB Analysis	7-8
	7-12. Remarks on LOCA-LSB Analysis	7-9
	APPENDIX A	A-1

LIST OF ILLUSTRATIONS

Figure	Title	Page
3-1	Safety Injection System for the Turkey Point Unit No. 4 Power Plant	3-5
3-2	Flow Rate Versus Pressure for the Turkey Point Unit No. 4 Safety Injection System	3-6
3-3	Pressurizer Pressure and Cold Leg Temperature During a Large Steam Line Break With Off-Site Power	3-7
3-4	Pressurizer Pressure and Cold Leg Temperature During a Large Steam Line Break Without Off-Site Power	3-8
3-5	Reactor Coolant Flow During a Large Steam Line Break Without Off-Site Power	3-9
4-1	Heat Transfer Coefficients Applied in the LOCA Transient	4-5
4-2	LOCA Temperature Distribution Through the Vessel Wall	4-6
4-3	LOCA Thermal Hoop Stress Distribution Through the Vessel Wall	4-7
4-4	LOCA Thermal Axial Stress Distribution Through the Vessel Wall	4-8
4-5	Heat Transfer Coefficients Applied in the LSB Transient (With Off-Site Power)	4-9
4-6	Heat Transfer Coefficients Applied in the LSB Transient (Without Off-Site Power)	4-10
4-7	LSB (With Off-Site Power) Temperature Distribution Through the Vessel Wall	4-11
4-8	LSB (With Off-Site Power) Pressure and Thermal Hoop Stress Distribution Through the Vessel Wall	4-12
4-9	LSB (With Off-Site Power) Pressure and Thermal Axial Stress Distribution Through the Vessel Wall	4-13
4-10	LSB (Without Off-Site Power) Temperature Distribution Through the Vessel Wall	4-14
4-11	LSB (Without Off-Site Power) Pressure and Thermal Hoop Stress Distribution Through the Vessel Wall	4-15
4-12	LSB (Without Off-Site Power) Pressure and Thermal Axial Stress Distribution Through the Vessel Wall	4-16

LIST OF ILLUSTRATIONS (cont)

Figure	Title	Page
5-1	Magnification Factors for Longitudinal Crack in Cylinder (t/R = 0.1)	5-7
5-2	Magnification Factors for Circumferential Crack in Cylinder (t/R = 0.1)	5-8
5-3	Fast Neutron Fluence Distribution Through the Vessel Wall (End of Life, 2300 MWt)	5-9
5-4	Azimuthal Variation of the Fast Neutron Fluence at the Reactor Vessel Inner Surface (End of Life, 2300 MWt)	5-10
5-5	Westinghouse Copper Trend Curves: "Effect of Fluence and Copper Content on RT_{NDT} for Reactor Vessel Steels Exposed to Irradiation at 550°F"	5-11
5-6	Regulatory Guide 1.99 Trend Curves: "Predicted Adjustment of Reference Temperature, ΔRT_{NDT} as a Function of Fluence and Copper Content"	
5-7	ΔRT_{NDT} of the Core Region Girth Weld as a Function of Fractional Distance Through the Vessel Wall (End of Life, 2300 MWt)	5-13
6-1	Pre- and Postirradiation Impact Properties of Turkey Point Weldment Samples	6-4
7-1	K_{IC}, K_{IR} and K_I After 500 Seconds in the LOCA (Longitudinal Flaw, 40 Calendar Years, Westinghouse Copper Trend Curves)	7-10
7-2	K_{IC}, K_{IR} and K_I After 700 Seconds in the LOCA (Longitudinal Flaw, 40 Calendar Years, Westinghouse Copper Trend Curves)	7-11
7-3	K_{IC}, K_{IR} and K_I After 800 Seconds in the LOCA (Longitudinal Flaw, 40 Calendar Years, R.G. 1.99 Trend Curves)	7-12
7-4	K_{IC}, K_{IR} and K_I After 2300 Seconds in the LOCA (Longitudinal Flaw, 40 Calendar Years, R.G. 1.99 Trend Curves)	7-13
7-5	K_{IC}, K_{IR} and K_I After 300 Seconds in the LOCA (Circumferential Flaw, 40 Calendar Years, Westinghouse and R.G. 1.99 Trend Curves)	7-14
7-6	K_{IC}, K_{IR} and K_I After 2400 Seconds in the LOCA (Circumferential Flaw, 40 Calendar Years, Westinghouse and R.G. 1.99 Trend Curves)	7-15

LIST OF ILLUSTRATIONS (cont)

Figure	Title	Page
7-7	Longitudinal Flaw Initiation Depth and Arrest Depth for the LOCA (40 Calendar Years, Westinghouse Copper Trend Curves)	7-16
7-8	Longitudinal Flaw Initiation Depth and Arrest Depth for the LOCA (40 Calendar Years, R.G. 1.99 Trend Curves)	7-17
7-9	Circumferential Flaw Initiation Depth and Arrest Depth for the LOCA (40 Calendar Years, Westinghouse Copper Trend Curves)	7-18
7-10	Circumferential Flaw Initiation Depth and Arrest Depth for the LOCA (40 Calendar Years, R.G. 1.99 Trend Curves)	7-19
7-11	K_{IC}, K_{IR} and K_I After 300 Seconds in the LOCA (Circumferential Flaw, 26.25 Calendar Years, R.G. 1.99 Trend Curves)	7-20
7-12	K_{IC}, K_{IR} and K_I after 2400 Seconds in LOCA (Circumferential Flaw, 26.25 Calendar Years, R.G. 1.99 Trend Curves)	7-21
7-13	Circumferential Flaw Initiation Depth and Arrest Depth for the LOCA (26.25 Calendar Years, R.G. 1.99 Trend Curves)	7-22
7-14	K_{IC}, K_{IR} and K_I after 600 Seconds in the LSB, With Off-Site Power (Longitudinal Flaw, 40 Calendar Years, R.G. 1.99 and Westinghouse Trend Curves)	7-23
7-15	K_{IC}, K_{IR} and K_I after 6000 Seconds in the LSB, With Off-Site Power (Longitudinal Flaw, 40 Calendar Years, Westinghouse and R.G. 1.99 Trend Curves)	7-24
7-16	K_{IC}, K_{IR} and K_I after 600 Seconds in the LSB - Without Off-Site Power (Longitudinal Crack, 40 Calendar Years, Westinghouse and R.G. 1.99 Trend Curves)	7-25
7-17	K_{IC}, K_{IR} and K_I after 6000 Seconds in the LSB - Without Off-Site Power (Longitudinal Flaw, 40 Calendar Years, Westinghouse and R.G. 1.99 Trend Curves)	7-26
7-18	Longitudinal Flaw Initiation Depth and Arrest Depth for the LSB - With Off-Site Power (40 Calendar Years, Westinghouse and R.G. 1.99 Trend Curves)	7-27
7-19	Longitudinal Flaw Initiation Depth and Arrest Depth for the LSB - Without Off-Site Power (40 Calendar Years, Westinghouse and R.G. 1.99 Trend Curves)	7-28
7-20	K_{IC}, K_{IR} and K_I after 600 Seconds in the LSB - With Off-Site Power (Circumferential Flaw, 40 Calendar Years, Westinghouse and R.G. 1.99 Trend Curves)	7-29

LIST OF ILLUSTRATIONS (cont)

Figure	Title	Page
7-21	K_{IC}, K_{IR} and K_I after 600 Seconds in the LSB - Without Off-Site Power (Circumferential Flaw, 40 Calendar Years, Westinghouse Copper Trend Curves)	7-30
7-22	K_{IC}, K_{IR} and K_I after 1600 Seconds in the LSB - With Off-Site Power (Circumferential Flaw, 40 Calendar Years, Westinghouse Copper Trend Curves)	7-31
7-23	K_{IC}, K_{IR} and K_I after 1500 Seconds in the LSB - Without Off-Site Power (Circumferential Flaw, 40 Calendar Years, Westinghouse Copper Trend Curves)	7-32
7-24	K_{IC}, K_{IR} and K_I after 3100 Seconds in the LSB - With Off-Site Power (Circumferential Flaw, 40 Calendar Years, R.G. 1.99 Trend Curves)	7-33
7-25	K_{IC}, K_{IR} and K_I after 400 Seconds in the LSB - Without Off-Site Power (Circumferential Flaw, 40 Calendar Years, R.G. 1.99 Trend Curves)	7-34
7-26	K_{IC}, K_{IR} and K_I after 6000 Seconds in the LSB - Without Off-Site Power (Circumferential Flaw, 40 Calendar Years, R.G. 1.99 Trend Curves)	7-35
7-27	Circumferential Flaw Initiation Depth and Arrest Depth for the LSB - With Off-Site Power (40 Calendar Years, Westinghouse and R.G. 1.99 Trend Curves)	7-36
7-28	Circumferential Flaw Initiation Depth and Arrest Depth for the LSB - Without Off-Site Power (40 Calendar Years, Westinghouse and R.G. 1.99 Trend Curves)	7-37
7-29	K_{IC}, K_{IR} and K_I after 500 Seconds in the LSB - With Off-Site Power (Circumferential Crack, 31.25 Calendar Years, Westinghouse and R.G. 1.99 Trend Curves)	7-38
7-30	K_{IC}, K_{IR} and K_I after 2800 Seconds in the LSB - With Off-Site Power (Circumferential Flaw, 31.25 Calendar Years, Westinghouse and R.G. 1.99 Trend Curves)	7-39
7-31	Circumferential Flaw Initiation Depth and Arrest Depth for the LSB - Off-Site Power Available (31.25 Calendar Years, Westinghouse and R.G. Trend Curves)	7-40
7-32	K_{IC}, K_{IR} and K_I after 400 Seconds in the LSB - Without Off-Site Power (Circumferential Flaw, 25 Calendar Years, R.G. 1.99 Trend Curves)	7-41
7-33	K_{IC}, K_{IR} and K_I after 3300 Seconds in the LSB - Without Off-Site Power (Circumferential Flaw, 25 Calendar Years, R.G. 1.99 Trend Curves)	7-42
7-34	Circumferential Crack Initiation Depth and Arrest Depth for the LSB - Without Off-Site Power (25 Calendar Years, R.G. 1.99 Trend Curves)	7-43

LIST OF TABLES

Table	Title	Page
7-1	Turkey Point Unit No. 4 — LOCA Analysis Crack Initiation and Arrest Depth for Continuous Surface Crack in Reactor Vessel Belt Line Region	7-2
7-2	Turkey Point Unit No. 4 — LSB Analysis Crack Initiation and Arrest Depth for Continuous Surface Crack in Reactor Vessel Belt Line Region	7-6

SECTION 1
SUMMARY OF RESULTS

In this study of the integrity of the reactor pressure vessel for the postulated faulted condition transients, the Westinghouse copper trend curves and the Regulatory Guide 1.99 radiation damage curves were used in the determination of the critical depths of postulated continuous surface cracks in the cylindrical belt line region of the vessel.

The following results were obtained in the fracture mechanics analysis of the Turkey Point Unit No. 4 reactor vessel for a postulated Loss-of-Coolant Accident and Large Steam Line Break occurring during the 40-calendar-year life of the plant.

1-1. WESTINGHOUSE COPPER TREND CURVES

The integrity of the Turkey Point Unit No. 4 reactor vessel subjected to a postulated LOCA or LSB at the end of life will be maintained using the Westinghouse copper trend curves for predicting the end-of-life shift of the core region girth weld RT_{NDT}.

A longitudinal crack in the base material is not initiated during the LOCA or LSB provided the depth does not exceed 3.66 inches or 3.05 inches, respectively. A small circumferential crack in the weldment may be initiated, but arrest will occur within 67.9 percent and 43.2 percent of the wall thickness for the LOCA and the LSB, respectively.

1-2. REGULATORY GUIDE 1.99 TREND CURVE

For a LOCA postulated to occur at the end of life, a longitudinal crack in the base material will arrest within 71.1 percent of the vessel wall thickness.

For an LSB postulated to occur at the end of life, longitudinal flaws in the base material less than 3.05 inch deep will not be initiated.

For a postulated circumferential crack in the weldment, the Turkey Point Unit No. 4 reactor vessel will conform to the vessel integrity criteria during a maximum period of 26.25 calendar years and 25 calendar years for a LOCA and LSB, respectively.

As explained in appendix A, this report also updates results of a previously performed fracture mechanics evaluation of the Turkey Point Unit No. 3 reactor vessel since:

- The results of the present analysis for continuous cracks assumed in the circumferential weldment in the belt line region of Turkey Point Unit No. 4 are equally applicable to Turkey Point Unit No. 3.
- The results for the continuous longitudinal flaws assumed in the belt line region base material, with the exception of the results obtained for the LOCA using Regulatory Guide 1.99, are also applicable to the Turkey Point Unit No. 3 reactor vessel.

SECTION 2
INTRODUCTION

2-1. BACKGROUND

The ability of nuclear power plant reactor vessels to withstand extremely low probability faulted condition transients is an important issue. Safe system shutdown following such an event, whose consequences are such that the integrity and operability may be impaired, is the only consideration.

If an accident transient takes place, the reactor vessel could be subjected to a thermal shock due to activation of safety injection systems, as a result of which fast fracture could occur. To assess the potential for brittle failure, Westinghouse performed a fracture mechanics study of the Turkey Point Unit No. 4 reactor vessel subjected to two postulated faulted condition transients that are considered as most severe, i.e., a Loss-of-Coolant Accident and a Large Steam Line Break.

Florida Power and Light Company has been commercially operating the Turkey Point Unit No. 4 Nuclear Power Plant since 1972. The reactor pressure vessel for this plant was constructed by Babcock & Wilcox following the requirements of the 1965 edition of the ASME Boiler and Pressure Vessel Code, Sections II, III, and IX,[1] and in accordance with the applicable Westinghouse design specifications.

2-2. ANALYSIS PERFORMED

The core belt line region of the reactor pressure vessel is exposed to neutron irradiation, causing changes in material properties such as a shift to higher temperatures in the reference temperature (RT_{NDT})[2]. With time, these embrittlement effects increase the potential for crack instability. Therefore, the integrity evaluation for the Loss-of-Coolant Accident (LOCA) and Large Steam Line Break (LSB) has been applied to the core belt line region of the reactor pressure vessel. The Westinghouse copper trend curves and the methods of

---

1. ASME Boiler and Pressure Vessel Code, Section II, III and IX, Nuclear Power Plant Components, ASME, New York, 1971.
2. L. E. Steele, G. W. Knighton, and U. Potapovs, "Radiation Embrittlement of Pressure Vessels and Procedures for Limiting This Effect in Power Reactors," Nucl. Appl., 4, 230-244, (1968).

Regulatory Guide 1.99[1] have been used to determine the shift of RT_{NDT} as a function of neutron fluence and material chemistry. The impact of each method on the calculated critical crack sizes has also been evaluated. Principles of linear elastic fracture mechanics technology have been applied in this analysis, which considers, for conservatism, postulated continuous longitudinal flaws using the most limiting properties of the core region base material and postulated continuous circumferential flaws using the material properties of the circumferential girth weld in the core region.

The results of this analysis have been evaluated relative to conservative initiation and arrest criteria pertaining to the integrity of nuclear reactor pressure vessels. These criteria are:

- The minimum critical flaw depth required for initiation is equal to, or greater than, one inch, consistent with conservatively established minimum capabilities of ultrasonic inspection techniques, or
- The maximum depth at which a propagating crack will arrest, is equal to 75 percent of the vessel wall thickness. This criterion is consistent with the ASME Code, Section XI.[2]

1. U. S. Nuclear Regulatory Commission, Regulatory Guide 1.99, Revision 1, Office of Standards Development, January 1976.
2. ASME Boiler and Pressure Vessel Code, Section XI, Appendix A Evaluation of Flaw Indications, ASME, New York, 1974.

SECTION 3

DESCRIPTION OF THE FAULTED CONDITION TRANSIENT FOR THE LOSS-OF-COOLANT ACCIDENT AND LARGE STEAM LINE BREAK

The following is a description of the safety injection system's performance, upon which the evaluation of the resistance-to-failure of the reactor vessel has been based.

Figure 3-1 describes the pumping systems under consideration in this study. The four shared safety injection pumps are arranged to deliver the flow of refueling water down one header with branch lines to each of the three cold legs of the unit undergoing the accident. Upon initiation, the system delivers water from the two refueling water storage tanks by means of four safety injection pumps. This figure also shows the two residual heat removal pumps that deliver a flow of refueling water through a header and branch lines to each of the three cold legs. Figure 3-2 describes the flow rates versus reactor backpressure from the safety injection pumps to the cold legs of the reactor coolant loops.

All injection pumps take suction from the refueling water storage tanks that are located outside the Auxiliary Building. Because of the outside location of the tanks, the minimum temperature of the injection water has been conservatively taken as 39°F, the minimum recent historic outside air temperature for the area of the plant.

3-1. LOSS-OF-COOLANT ACCIDENT (LOCA)

During a double-ended hot leg break in the main coolant loop pipe, the reactor vessel blows down rapidly and the downcomer region is refilled at least above the core centerline with 90°F water from the accumulators. Within 20 to 30 seconds from the start of the accident, the safety injection pumps are started and begin to deliver 155°F flow from the boron injection tank. The minimum volume of boric acid (900 gallons) is delivered in 48 seconds (68 to 78 seconds from start of accident). The flow is then from the refueling water storage tank, and the temperature of the delivered water drops to 39°F. The maximum flow rate is 780 gpm into two intact loops, assuming that the reactor pressure and containment pressure are near ambient. The injection flow enters the reactor coolant piping through the accumulator connections.

The two residual heat removal pumps also start on demand and begin to deliver refueling water to the loops within about 30 seconds of the start of the accident. The total flow is 2810 gpm from the low-head injection system if the reactor backpressure is near zero.

The injection phase is considered to last for about 40 minutes from the start of the accident until the refueling water storage tank has emptied. At this time, long-term recirculation flow paths are set up; the flow rates will be decreased by operator action. The temperature of the water is estimated to be between 100 and 250°F, depending on the decay heat at the time, because it is recirculated from the containment sump. However, a more conservative approach is followed in establishing the recirculation water temperature.

In this analysis the conservative assumption is made that the only source of heat is provided by the spilled coolant, i.e., no residual heat from the core or sensible heat from the system metal or steam generators has been taken into account. As a result, the temperature of the coolant and refueling water after mixing will be 63°F for a conservatively low refueling water temperature of 39°F. The flow rate depends on the actions of the operator, but it is reasonable to assume that the minimum recirculation flow occurs if the system is aligned for high-head injection only, as per emergency instructions. This total flow rate would be about 680 gpm. A minimum flow rate of 680 gpm is conservative because higher flow rates will heat the vessel and reduce the stresses at a higher rate.

Note that the flow rate from the residual heat removal pumps during the injection phase is conservatively high because the refueling water storage tank has been assumed to be completely full throughout the transient. The added suction boost has a significant effect on these low-head pumps.

3-2. LARGE STEAM LINE BREAK (LSB)

During a Large Steam Line Break, the reactor coolant temperature and pressure rapidly decrease as energy is released from the faulted steam generator through the break. As it cools, the reactor coolant becomes more dense, shrinking in volume and causing pressurizer level to fall. Following a no-load break, the pressurizer empties in approximately 30 seconds. The safety injection pumps begin to deliver flow to the reactor when the reactor coolant pressure decreases below 1450 psig. The flow rate to the three cold legs is dependent on the reactor coolant pressure as described by figure 3-2. Initially, the pumps deliver boric acid from the boron injection tank (as described for the LOCA, above) at a temperature of 155°F. After the stored volume of 900 gallons has been delivered, flow begins from the refueling water storage tank, whereupon the temperature of the pumped fluid is assumed to decrease to 39°F.

Several minutes after the break occurs, water again enters the surge line and pressurizer as the volumetric delivery rate of water to the system begins to exceed the rate of shrink from the cooldown. The steam remaining in the pressurizer begins to compress causing system pressure to increase as it would normally if charging flow were to cause pressurizer level to rise. Pressurizer pressure does not rise to the nominal value of 2250 psia unless charging pumps are allowed to run for a very long time, but it begins to rise again slowly as soon as the surge line starts filling.

Also, the residual heat removal pumps are not expected to deliver refueling water because their developed head is not sufficient to overcome the reactor pressure expected during an LSB.

For the Large Steam Line Break, the following conditions are assumed:

- Initial Conditions

  a. No-load conditions (no-load temperature 547°F)

  b. Reactor coolant system pressure 2250 psia

  c. Reactor coolant flow 268,500 gpm (corresponds to 199 ft^3/sec loop flow).

- The largest inside containment break is assumed (4.37 ft^2). The check valve in the broken loop is assumed to fail, resulting in steam flow from the unbroken steam generators. This steam flow is limited by the 1.4 ft^2 flow restrictor in the steam lines. Isolation of the unbroken loops occurs 10 seconds after the break.

- The main feed system delivers the nominal plant flow to the broken loop for 60 seconds following the break. The total capacity of the auxiliary feed system is supplied to the broken loop for 10 minutes.

- Thick-metal heat capacity and reverse heat transfer from the intact steam generators are included.

- No return to criticality in the core is permitted and no decay heat is assumed.

- All four safety injection pumps operate, delivering a flow as indicated above. In addition, two charging pumps are assumed to operate, delivering a total of 150 gpm. Safety injection and charging are assumed to be terminated by operator action ten minutes after initiation of the transient.

Two cases are considered in the study of the Large Steam Line Break. In the first case, off-site power is assumed available throughout the transient and reactor coolant flow is maintained. In the second case, a loss of off-site power with a reactor coolant system flow coastdown is assumed at the time of the LSB.

Figure 3-3 shows the reactor coolant system pressure and cold leg temperature variations as a function of time if off-site power is available. Figure 3-4 shows the reactor coolant system pressure and cold leg temperature variations; figure 3-5 shows the reactor coolant flow as a function of time coincident with a loss of off-site power.

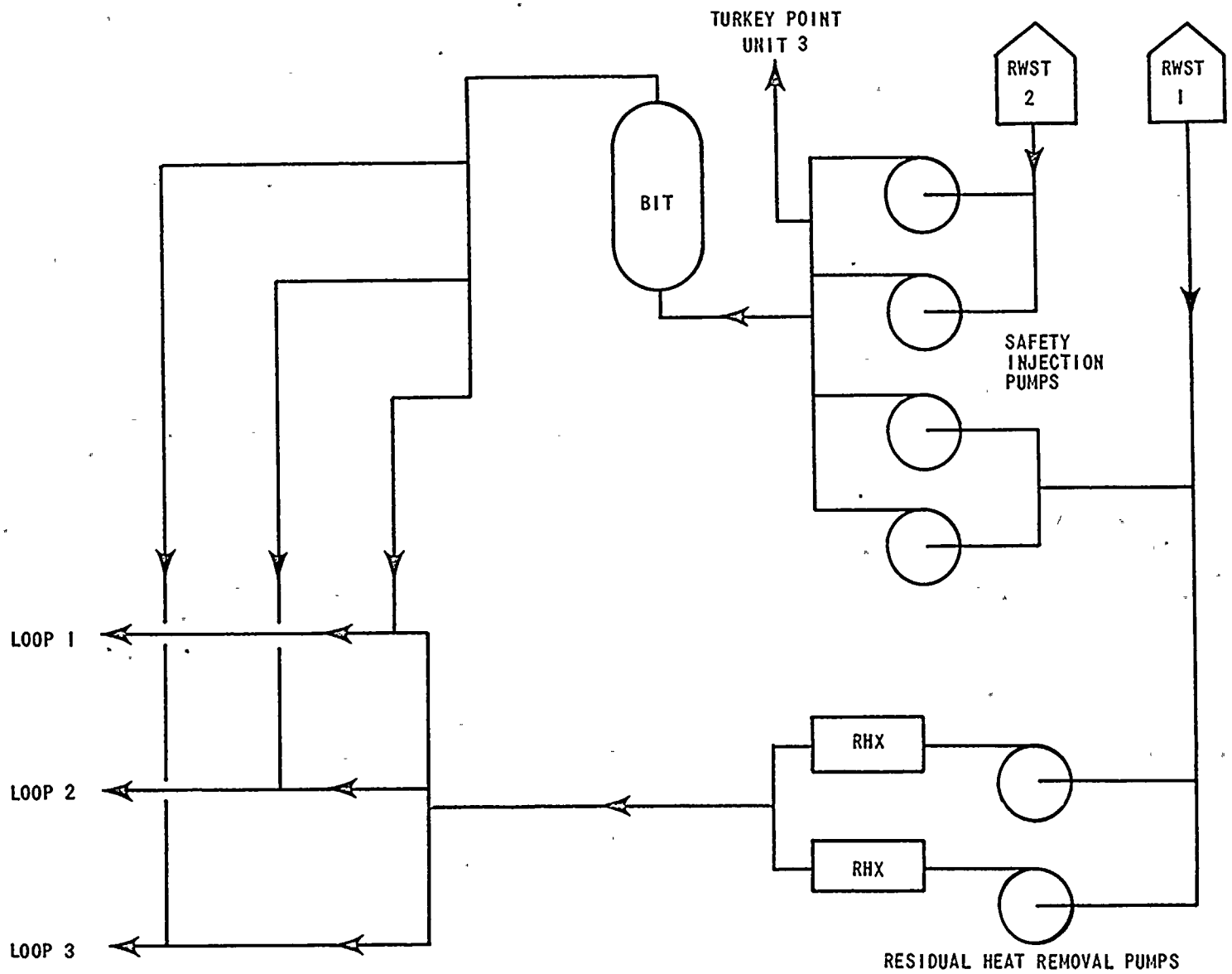

Figure 3-1. Safety Injection System for the Turkey Point Unit No. 4 Power Plant

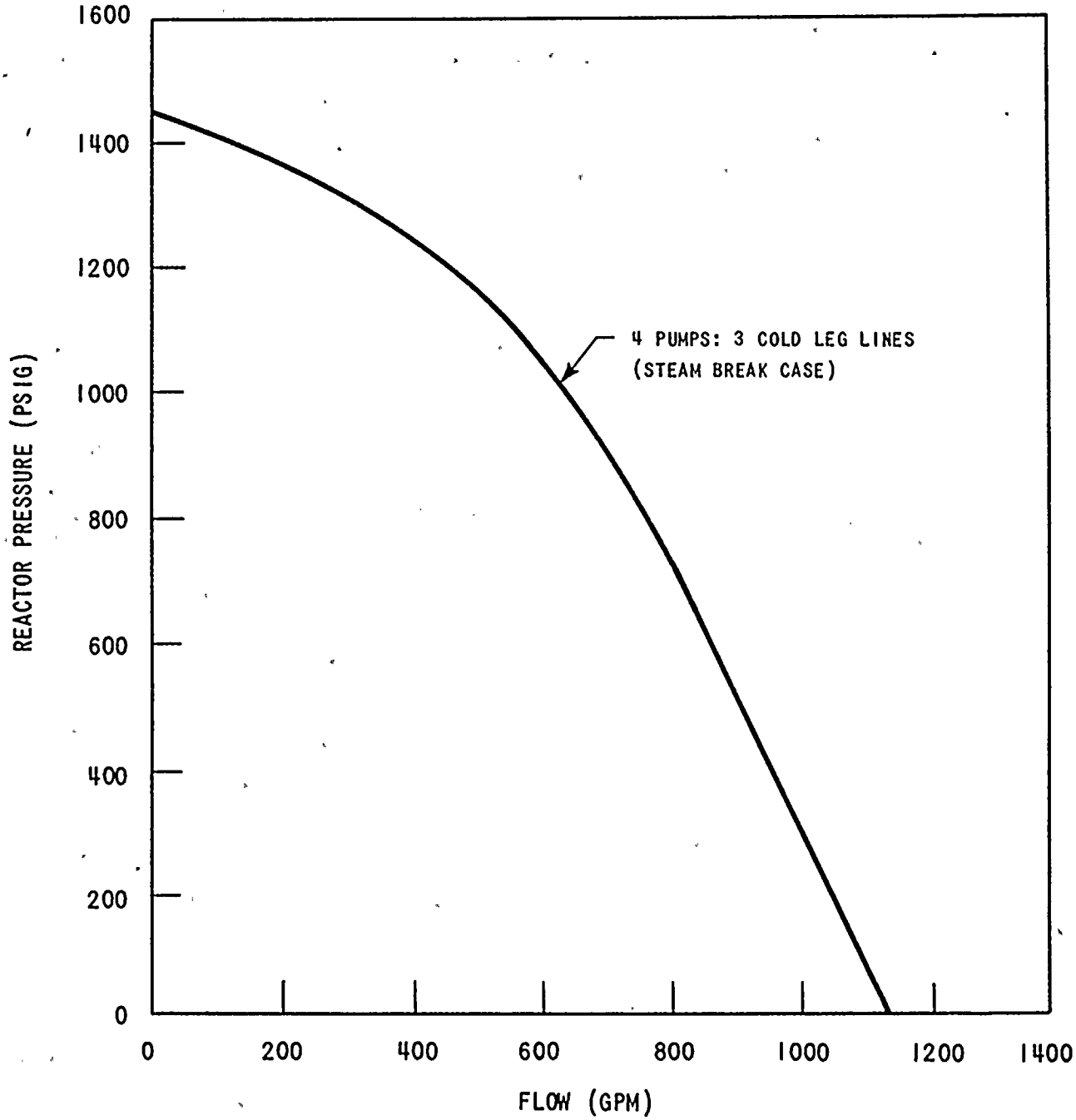

Figure 3-2. Flow Rate Versus Pressure for the Turkey Point Unit No. 4 Safety Injection System

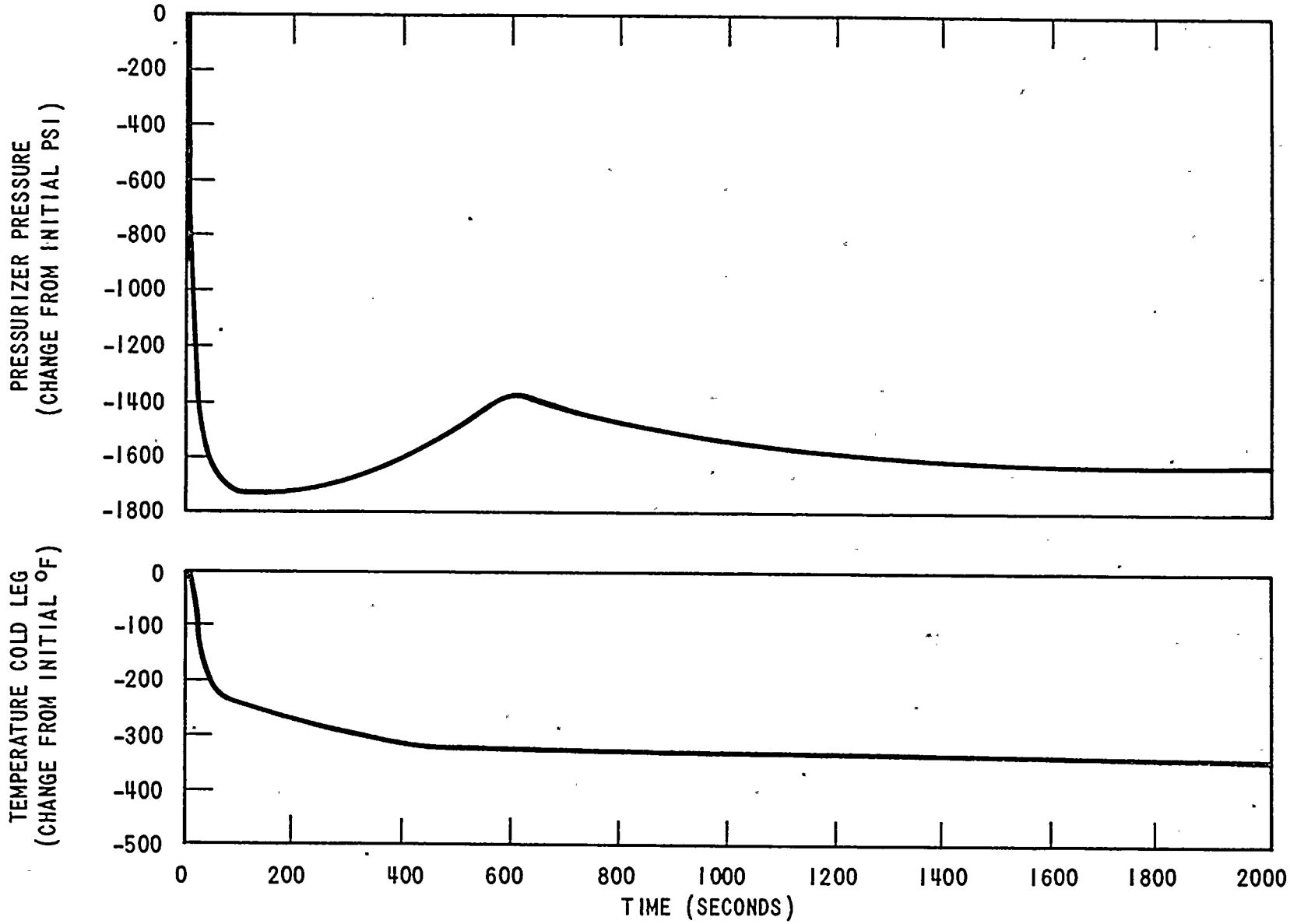

Figure 3-3. Pressurizer Pressure and Cold Leg Temperature During a Large Steam Line Break With Off-Site Power

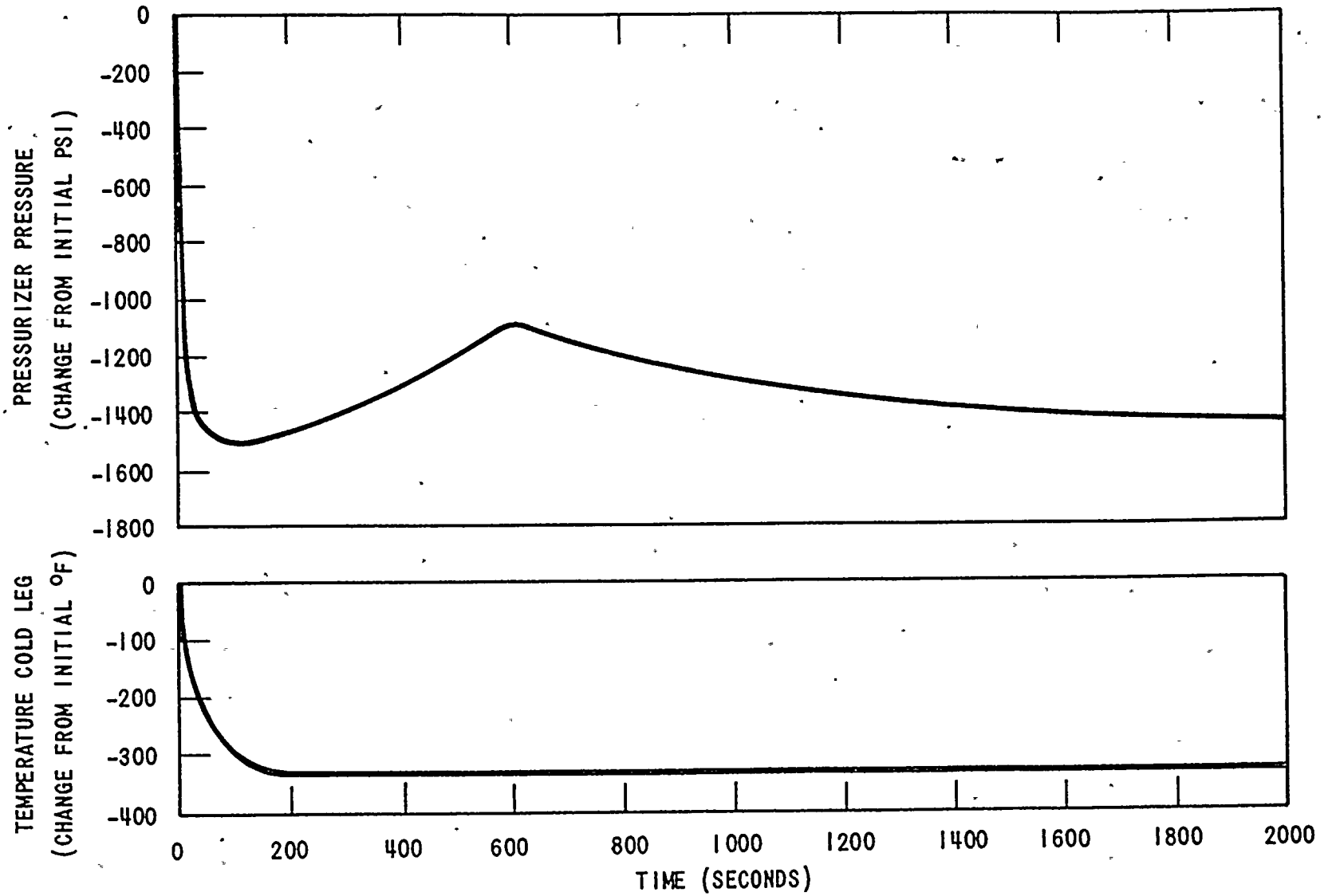

Figure 3-4. Pressurizer Pressure and Cold Leg Temperature During a Large Steam Line Break Without Off-Site Power

11,114-34

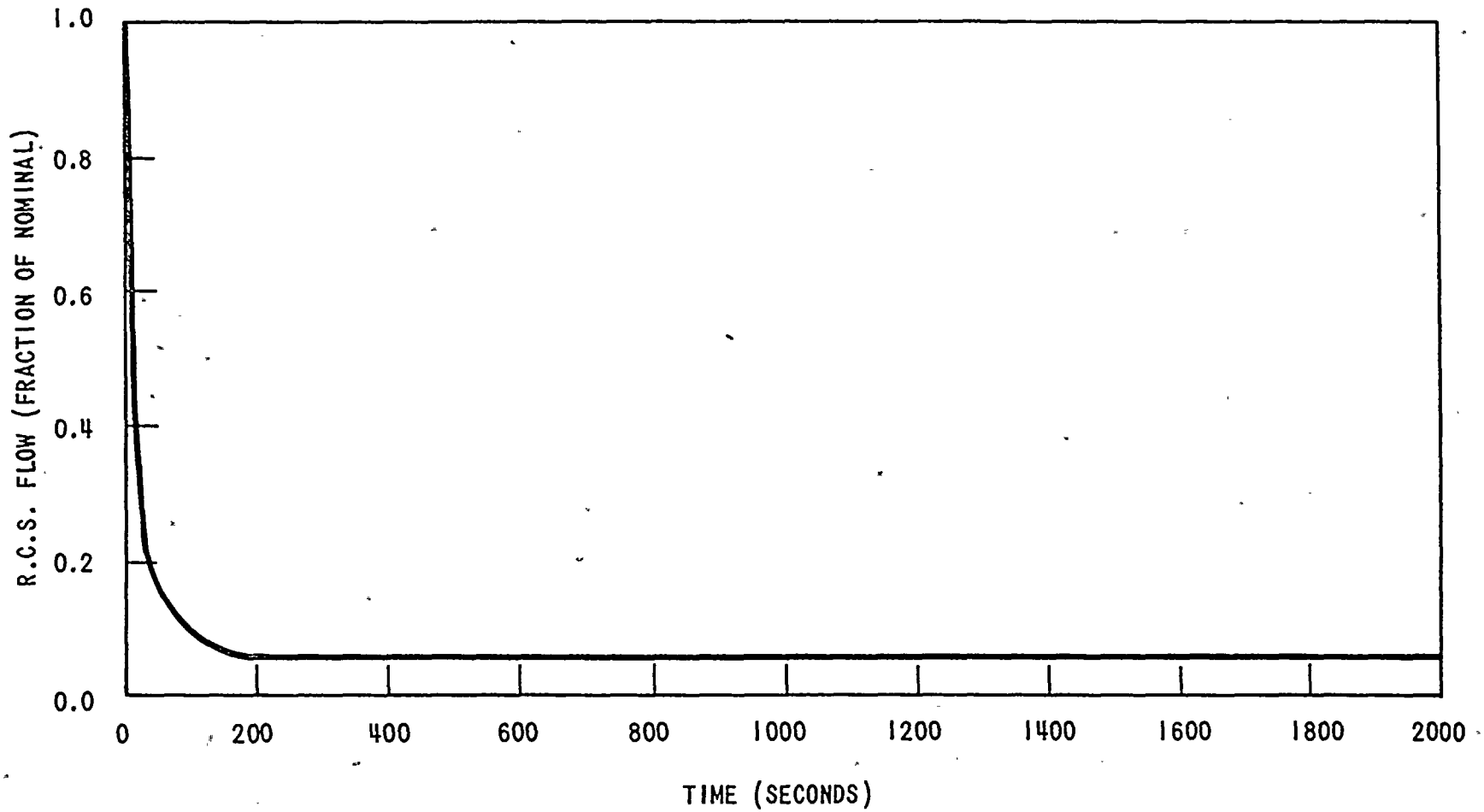

Figure 3-5. Reactor Coolant Flow During a Large Steam Line Break Without Off-Site Power

SECTION 4
THERMAL ANALYSIS

4-1. THERMAL ANALYSIS METHOD

The thermal analysis for faulted condition transients, such as the Loss-of-Coolant Accident and the Large Steam Line Break, requires that the temperature and thermal stress profiles in the vessel be calculated as a function of time.

The input to the thermal analysis consists of the following:

- Vessel-barrel annulus volumetric flow rate history
- Flow temperature history
- Vessel-barrel annulus pressure history
- Vessel and stainless steel cladding geometry and material properties

The temperature profiles are determined by a finite difference calculation technique; the thermal stress profiles are determined by the use of thermal stress equations for thick-walled cylinders[1] modified to include the effect of the stainless steel cladding.

The thermal properties of the reactor vessel cladding and base material used in the analysis are as follows:

	Carbon Steel Material	Stainless Steel Cladding
C_p specific heat (Btu/lb-°F)	0.128	0.125
ρ density (lb/ft^3)	490	497
k thermal conductivity (Btu/hr-ft-°F)	25.2	9.8

1. S. P. Timoshenko, and J. N. Goodier, Theory of Elasticity, 2nd Edition, McGraw-Hill Book Company, New York, 1951.

These constants yield thermal diffusivity values of 0.402 and 0.158 ft^2/hr for carbon steel and stainless steel, respectively. These values are appropriate for the temperature range of interest.

The change from two-phase boiling heat transfer to convection heat transfer in the initial portion of the large LOCA transient is determined by simultaneously calculating the heat flux from the vessel surface by both methods of heat transfer. The analysis assumes nucleate boiling to occur until the calculated heat flux for the vessel inner surface due to convection exceeds that due to nucleate boiling. The thermal analysis considers a hot leg large LOCA so that the safety injection flow rate is maximized in the vessel-barrel annulus. This produces the maximum forced convection heat transfer coefficients on the vessel inner surface. The heat transfer film coefficients for forced convection are calculated using the Dittus-Boelter[1] forced-convection correlation:

$$H = 0.023\ f \frac{k}{D} Re^{0.8}\ Pr^{0.4} \tag{4-1}$$

where

f = safety coefficient (= 1.5)

k = thermal conductivity of the fluid (Btu/hr-ft-°F)

D = hydraulic diameter (ft)

$Re = \rho VD/\mu$ = Reynolds number

ρ = density of the fluid (lb/ft^3)

V = fluid velocity (ft/hr)

μ = fluid viscosity (lb/hr-ft)

$Pr = C_p\ \mu/k$ = Prandtl number

C_p = specific heat (Btu/lb-°F)

This correlation generally has an accuracy of ±25 percent with regard to the data scatter of the correlation. An additional 25 percent margin is considered in this analysis as an added safety margin to account for any geometric effects of the vessel-barrel annulus. Therefore, an ample margin is added to the forced convection film coefficients calculated from equation (4-1) before it is used in the temperature and stress analysis.

---

1. F. W. Dittus, and L. M. K. Boelter, Heat Transfer in Automobile Radiators of the Tubular Type, Calif. Univ. Publication in Eng. 2, No. 13, 443-461 (1930).

Free convection heat transfer coefficients are determined using the following free convection correlation for vertical flat plates[1].

$$H = 0.021\ (Gr\ Pr)^{0.4}\ k/L \qquad (4\text{-}2)$$

where

Gr = Grashof number = $[g\beta\rho^2L^3/\mu^2] \times [T_{surface} - T_{bulk}]$

g = gravitational constant (ft/sec^2)

β = volume coefficient of expansion (°F^{-1})

L = characteristic length

4-2. LARGE LOCA

During the initial portion, (0-50 seconds), of the large LOCA, the reactor coolant system (RCS) is depressurized from 2250 to ~30 psia and various emergency core cooling systems (ECCS) are initiated. During this initial portion of the transient the vessel inner surface temperature is significantly higher than the saturation temperature corresponding to the vessel-barrel annulus pressure. Therefore, boiling occurs on the vessel inner surface. During this portion of the large LOCA transient a constant nucleate boiling heat transfer coefficient of 10,000 Btu/hr-ft^2-°F is applied with a sink temperature equal to the saturation temperature. This heat transfer coefficient is sufficiently high to limit the vessel heat transfer conduction. This means that the largest portion of the thermal resistance is due to conduction in the vessel wall, whereas the boiling heat transfer coefficient at the vessel surface offers negligible thermal resistance.

If the calculated boiling heat transfer heat flux decreases below the calculated convection heat flux, the heat transfer method in the thermal analyses becomes convection heat transfer with correspondingly lower heat transfer coefficients and a sink temperature equal to the bulk fluid temperature. The long-term (> 50 seconds) heat transfer from the vessel surface during the large LOCA is by opposed mixed convection. Opposed mixed convection is the combined forced and free convection resulting from the forced convection due to the downward pumped safety injection flow and the opposed free convection due to the upward flow of the buoyant effects of free convection. The heat transfer mechanism (free or forced convection) providing the highest calculated heat transfer coefficient is conservatively applied in the Turkey Point Unit No. 4 thermal analysis. Including the safety factor of 1.5, these heat transfer coefficients as a function of time in the transient are graphically shown in figure 4-1.

1. E. R. G. Eckert, T. W. Jackson, Analysis of Turbulent Free Convection Boundary Layer on a Flat Plate, NASA Report, 1015, 1951.

Figures 4-2, 4-3, and 4-4 show the temperature profiles and the resulting hoop and axial thermal stress distributions through the vessel wall at various time steps in the LOCA transient (pressure stresses are negligible because P = 30 psia).

4-3. LARGE STEAM LINE BREAK

Two transient cases are considered in the thermal analysis of the Large Steam Line Break. The first case is the one occurring with off-site power available (100 percent of main RCS pump flow assumed). The second case assumes that there is a coincident loss of off-site power (main RCS pump flow decays toward zero flow). Forced convection is the dominant mechanism of convection heat transfer for both cases. This results from the high RCS pump flow during Case 1 (with off-site power) and the relatively high RCS flow during the time period of concern (< 4000 seconds) for Case 2 (without off-site power). The flow through the vessel barrel annulus at long time periods (> 4000 seconds) for Case 2 will still be relatively high due to the natural circulation occurring in the primary system.

For Case 1 (with off-site power) the higher of the free or forced convection heat transfer coefficient calculated from equations (4-1) and (4-2), varies from 9862 Btu/hr-ft^2-°F after 6000 seconds in the transient. For Case 2 (without off-site power) these values are 9862 and 734 Btu/hr-ft^2-°F, respectively. Figures 4-5 and 4-6 show as a function of time the applied heat transfer coefficients for Case 1 and Case 2, respectively.

The resulting temperature profiles and the combined thermal and pressure hoop and axial stress profiles at several time steps are presented in figures 4-7, 4-8 and 4-9 for Case 1 and in figures 4-10, 4-11 and 4-12 for Case 2.

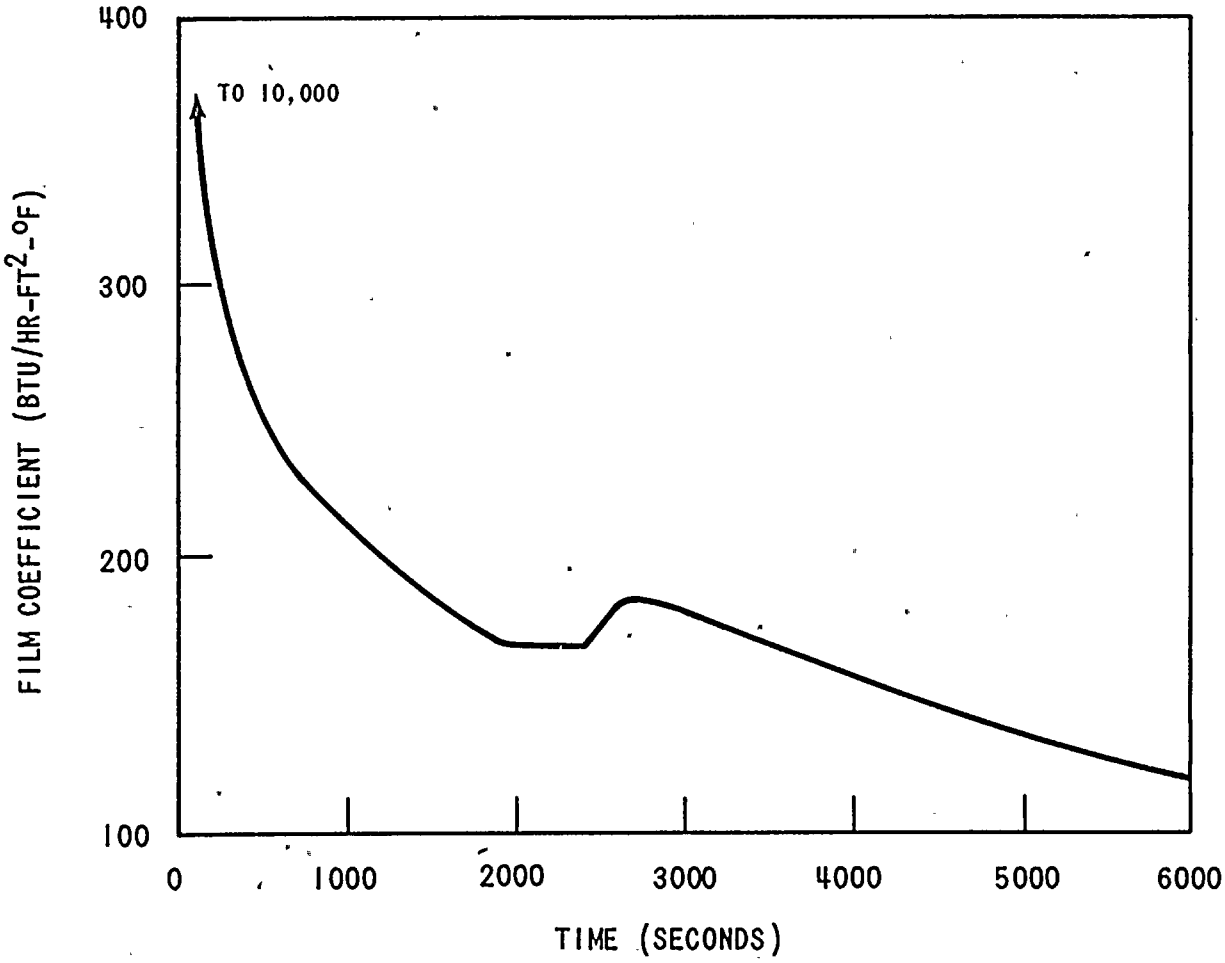

Figure 4-1. Heat Transfer Coefficients Applied in the LOCA Transient

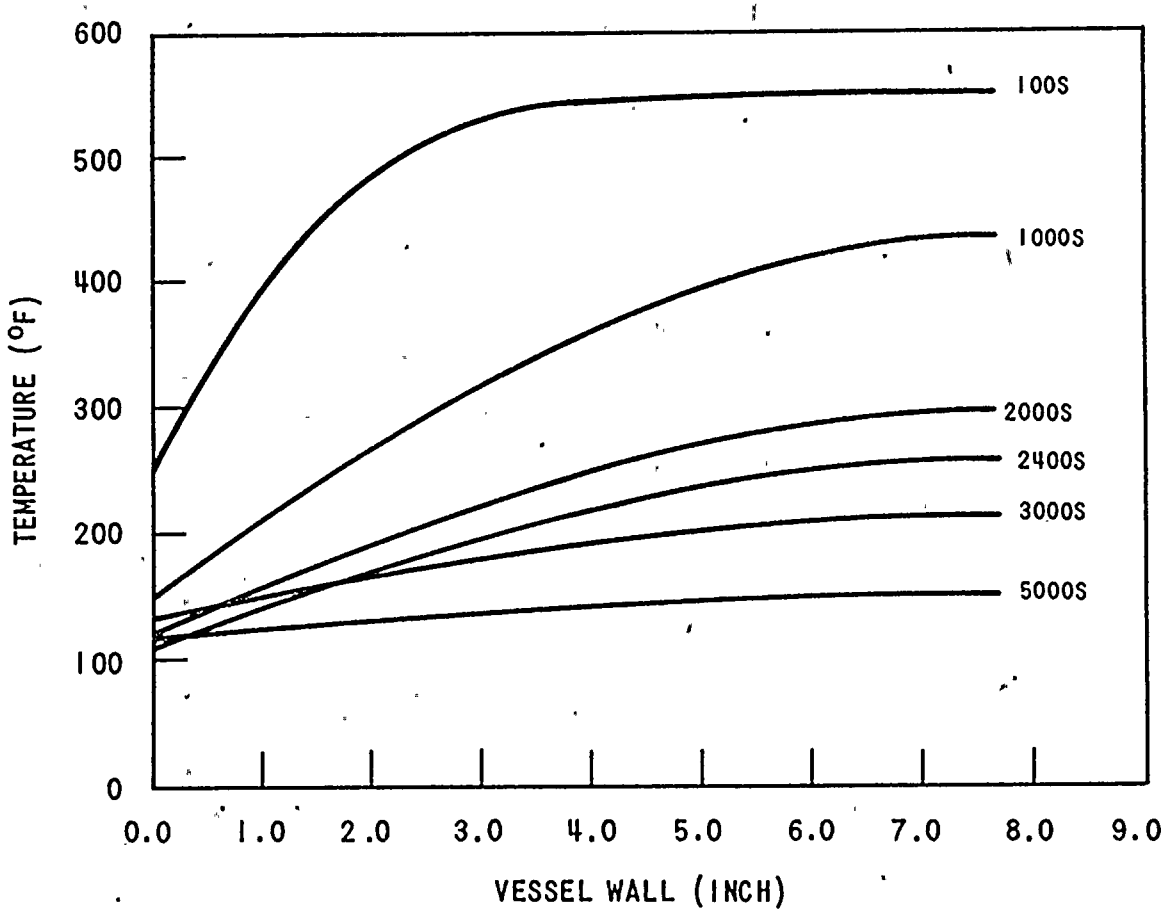

Figure 4-2. LOCA Temperature Distribution Through the Vessel Wall

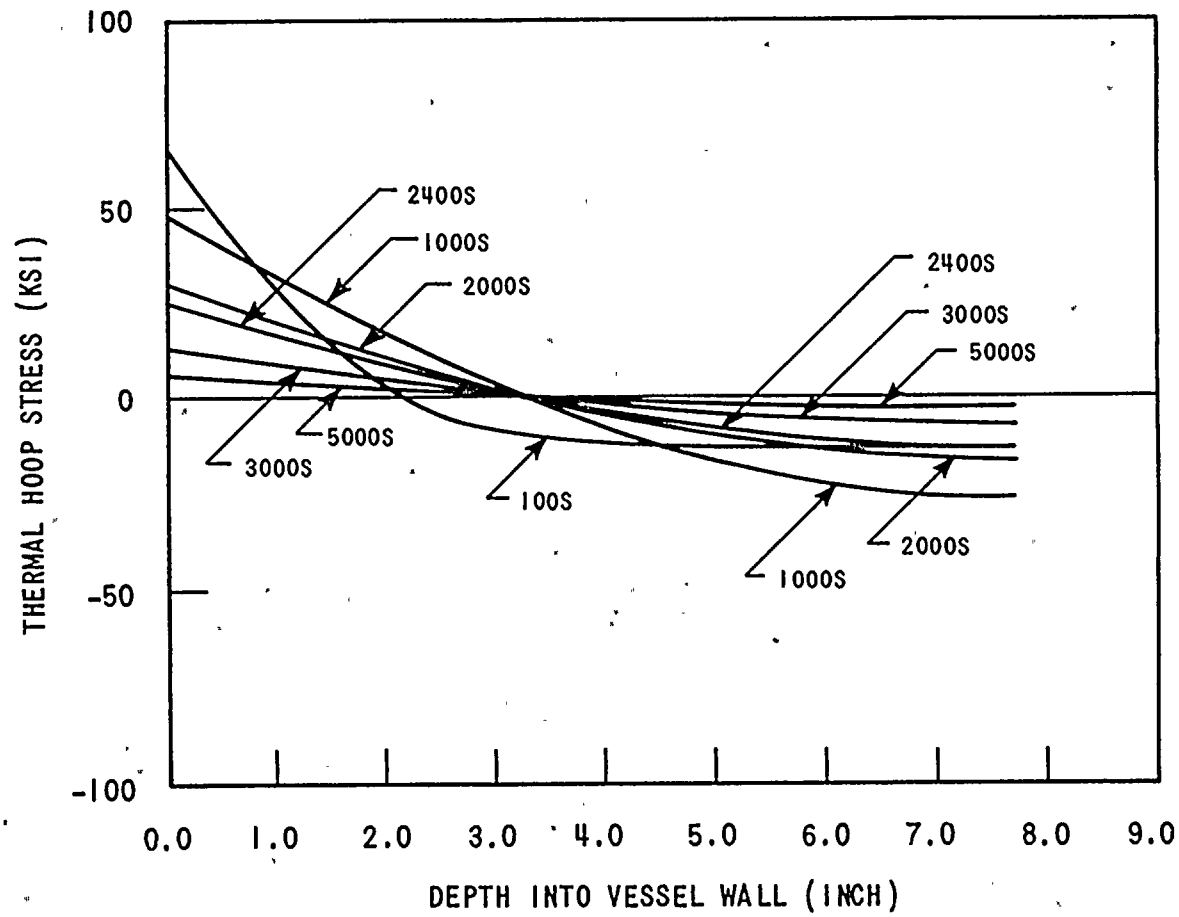

Figure 4-3. LOCA Thermal Hoop Stress Distribution Through the Vessel Wall

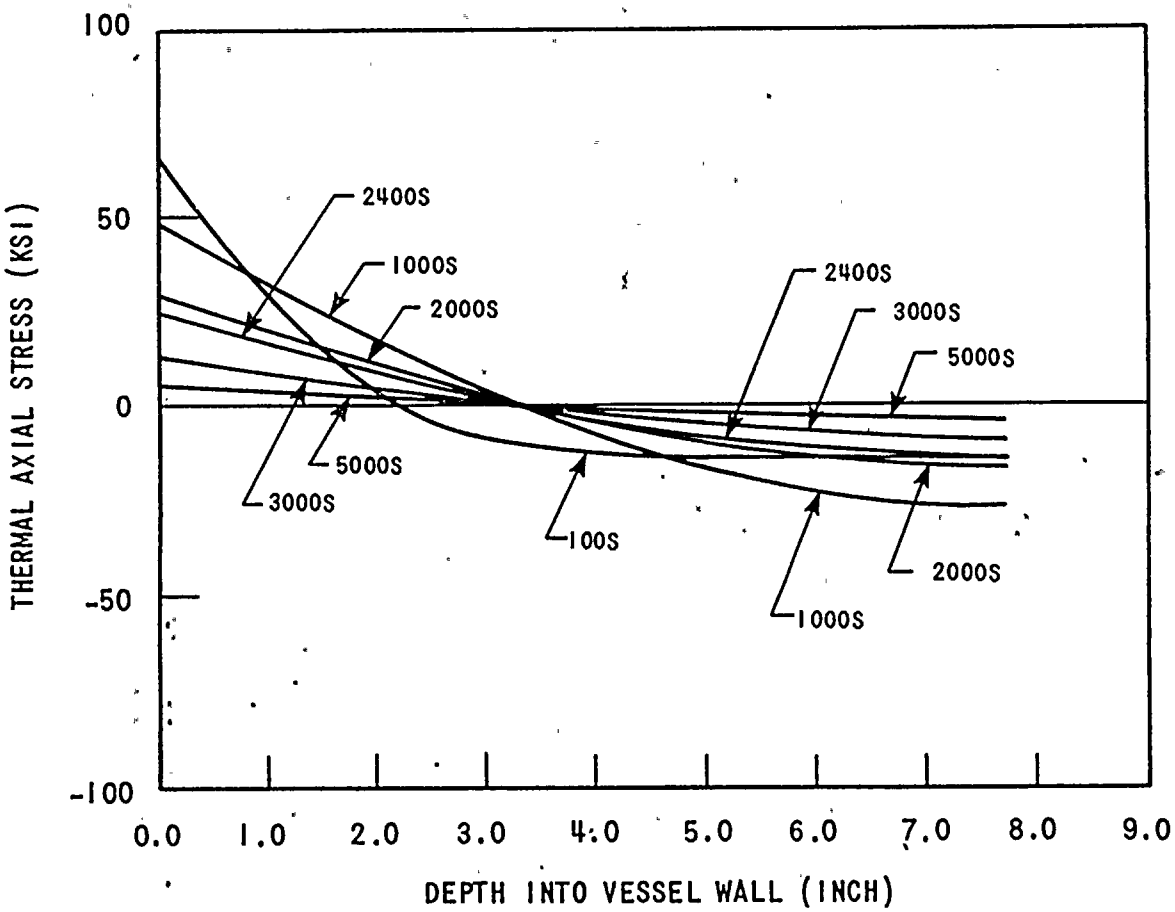

Figure 4-4. LOCA Thermal Axial Stress Distribution Through the Vessel Wall

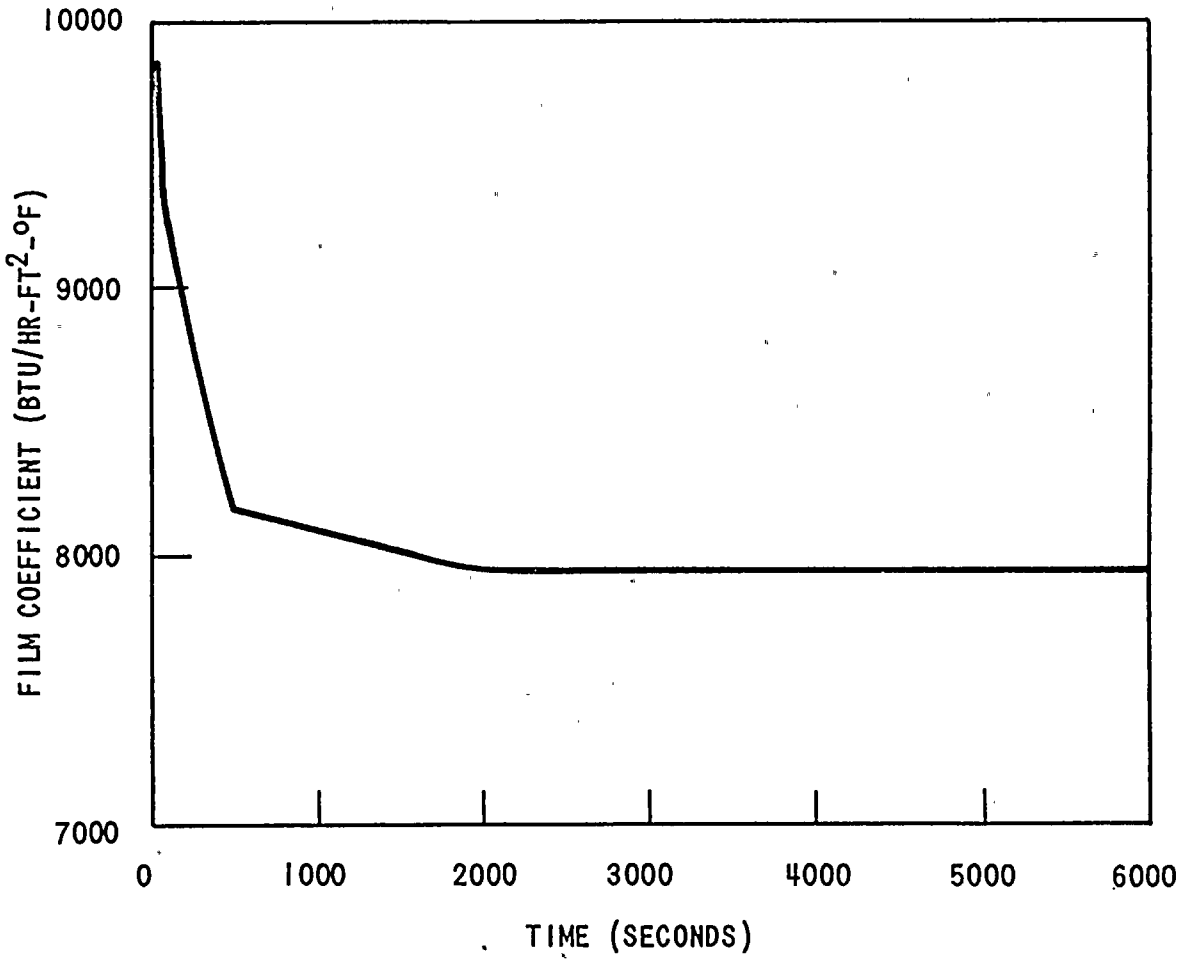

Figure 4-5. Heat Transfer Coefficients Applied in the LSB Transient (With Off-Site Power)

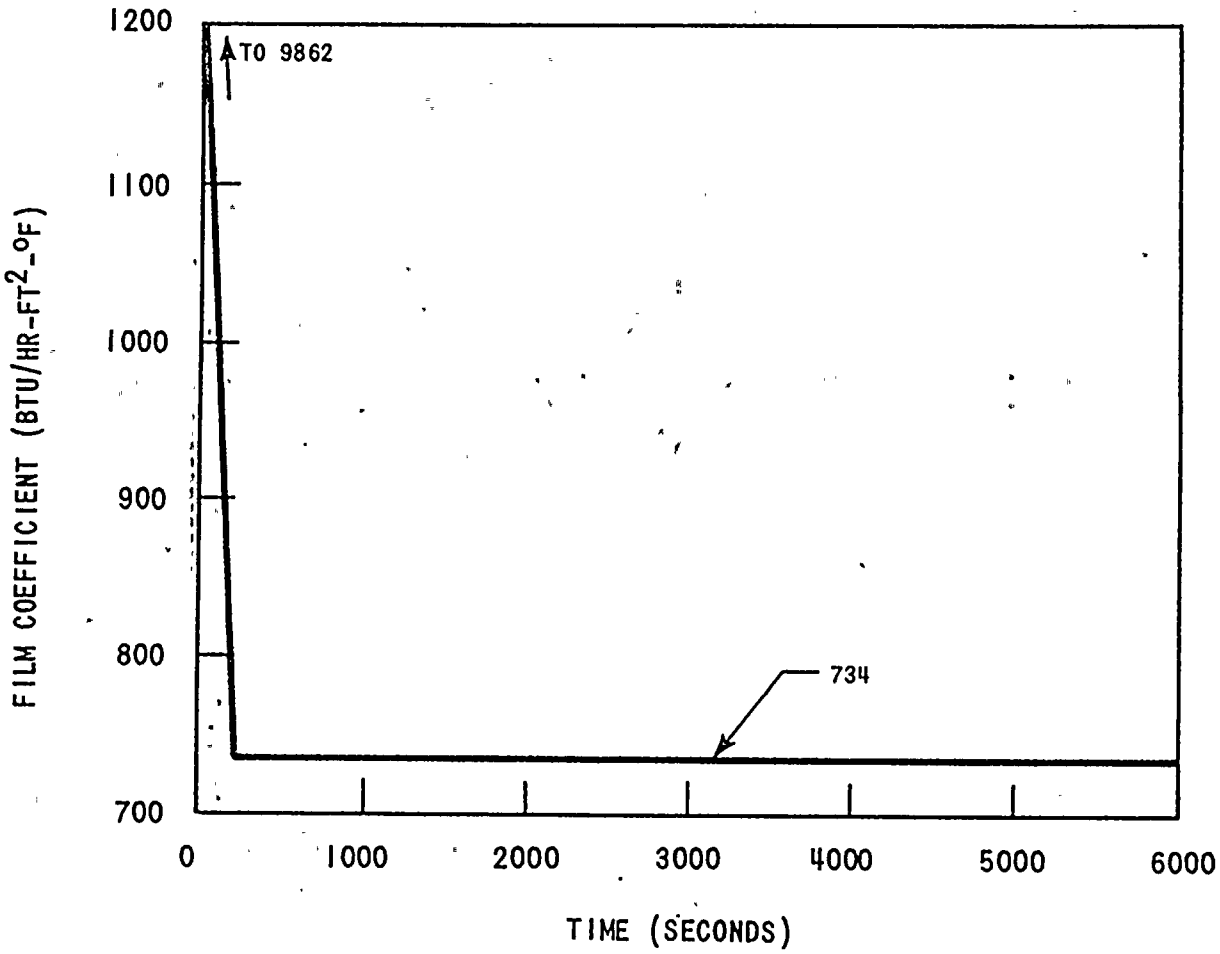

Figure 4-6. Heat Transfer Coefficients Applied in the LSB Transient (Without Off-Site Power)

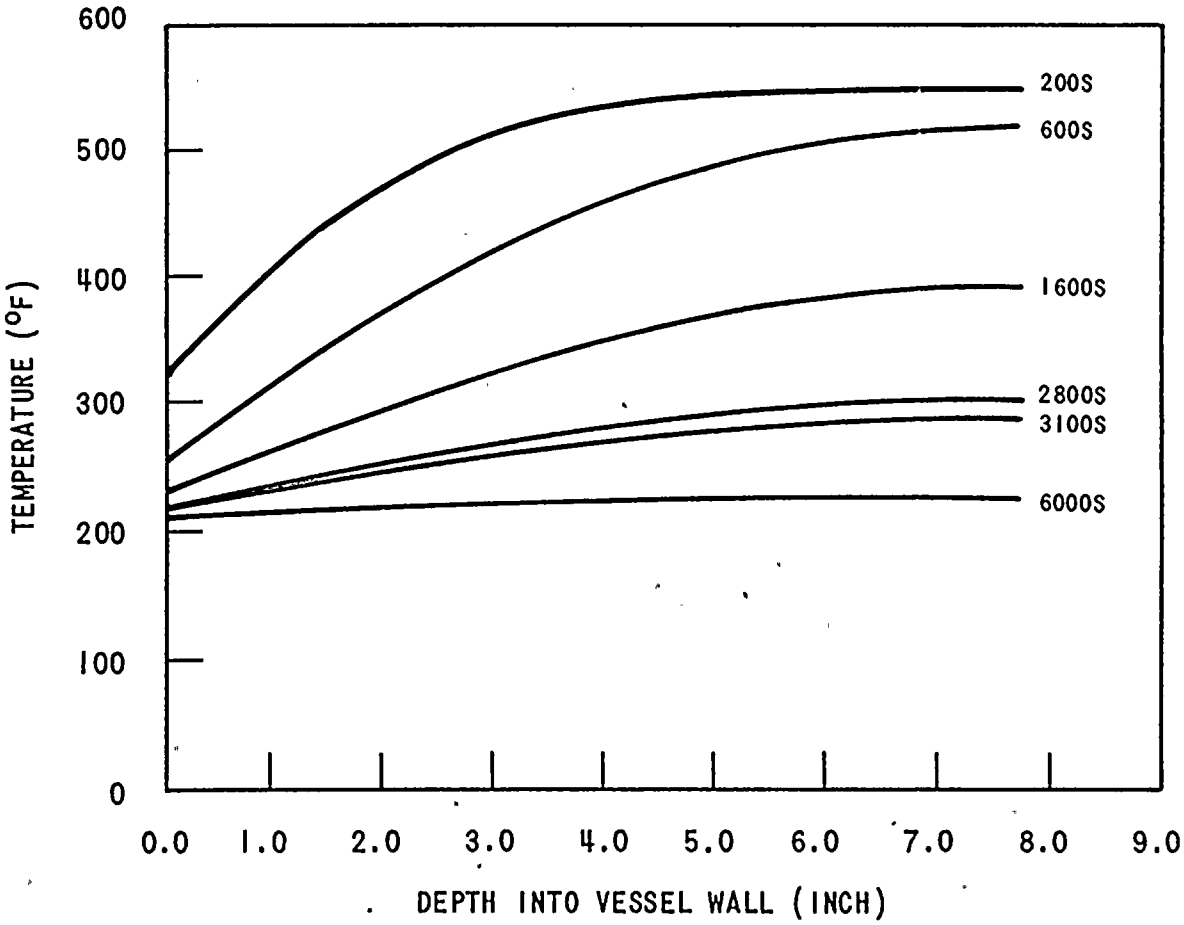

Figure 4-7. LSB (With Off-Site Power) Temperature Distribution Through the Vessel Wall

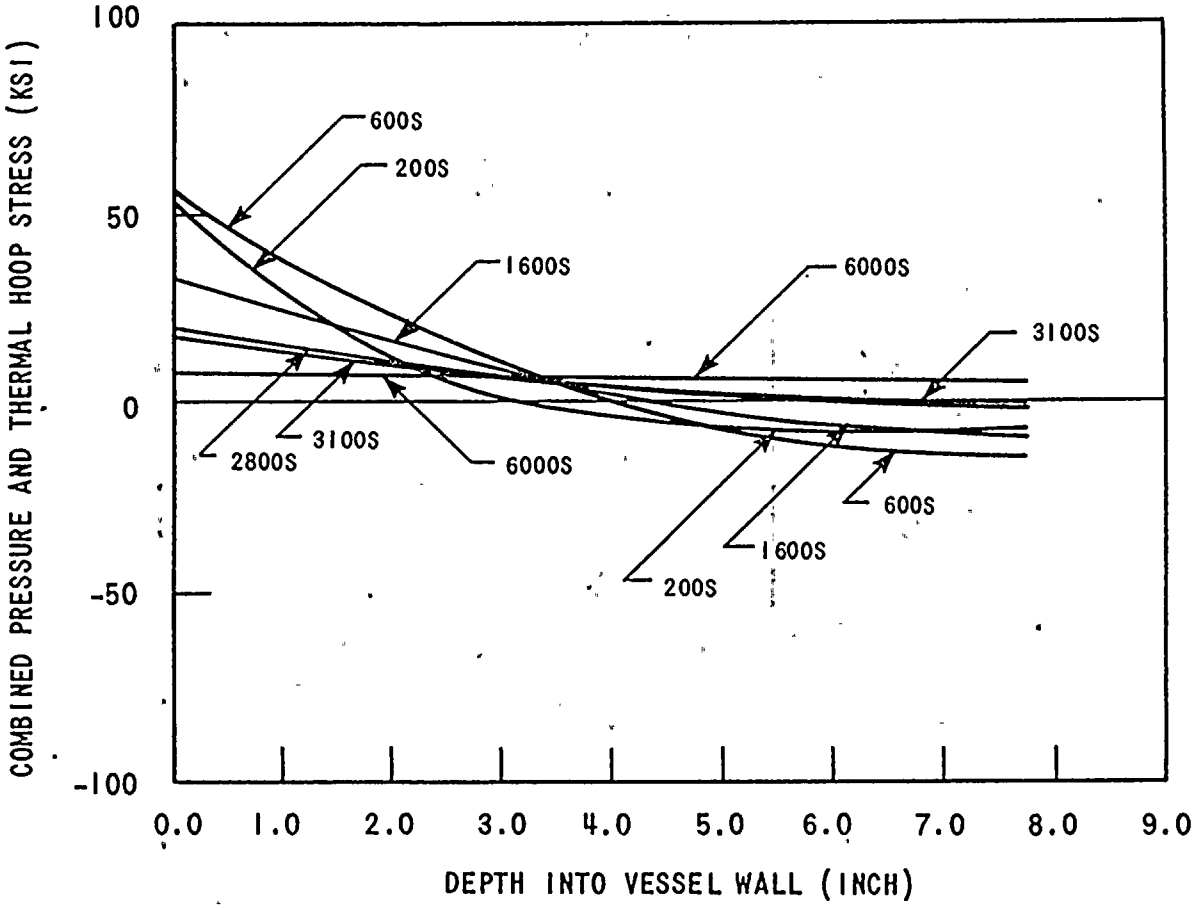

Figure 4-8. LSB (With Off-Site Power) Pressure and Thermal Hoop Stress Distribution Through the Vessel Wall

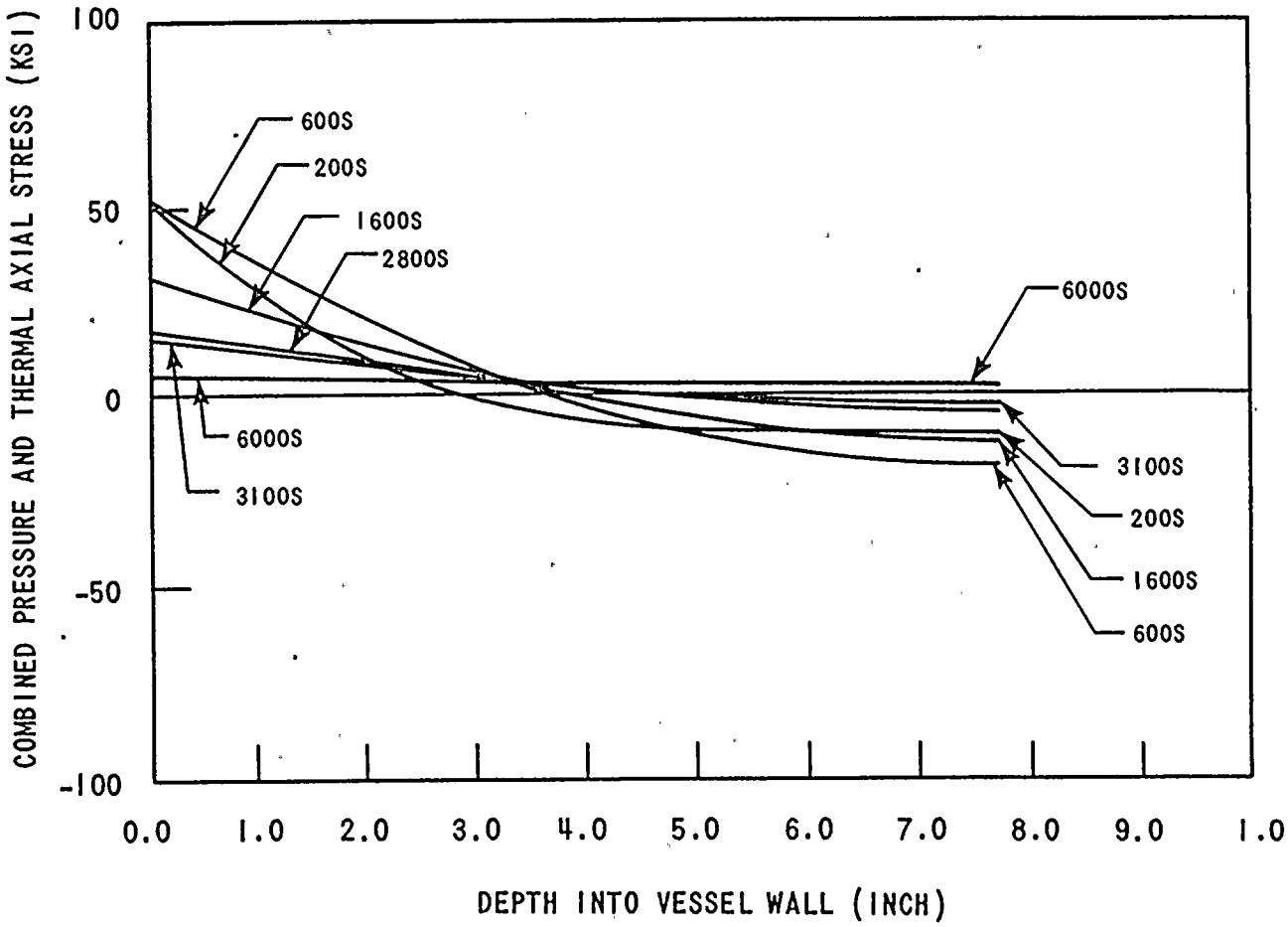

Figure 4-9. LSB (With Off-Site Power) Pressure and Thermal Axial Stress Distribution Through the Vessel Wall

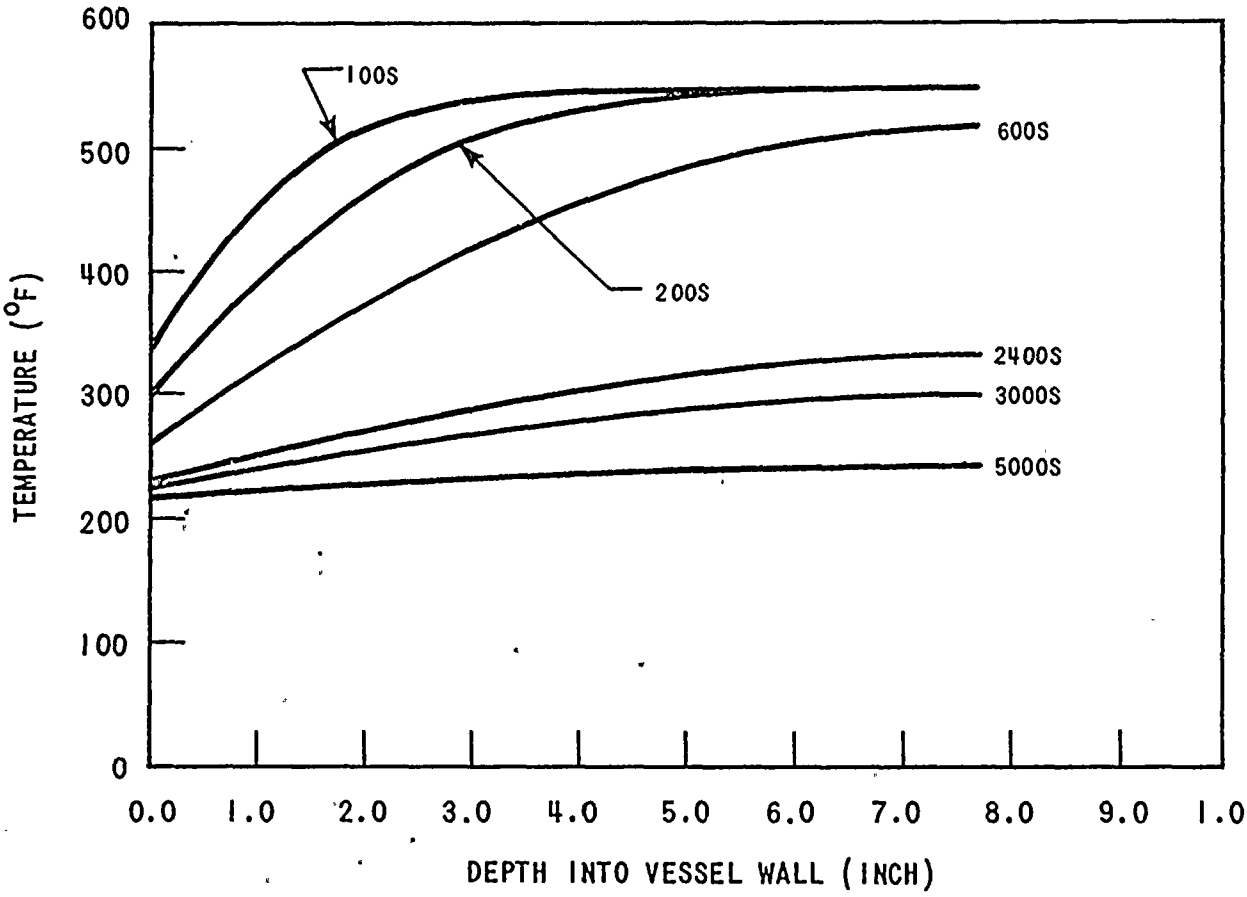

Figure 4-10. LSB (Without Off-Site Power) Temperature Distribution Through the Vessel Wall

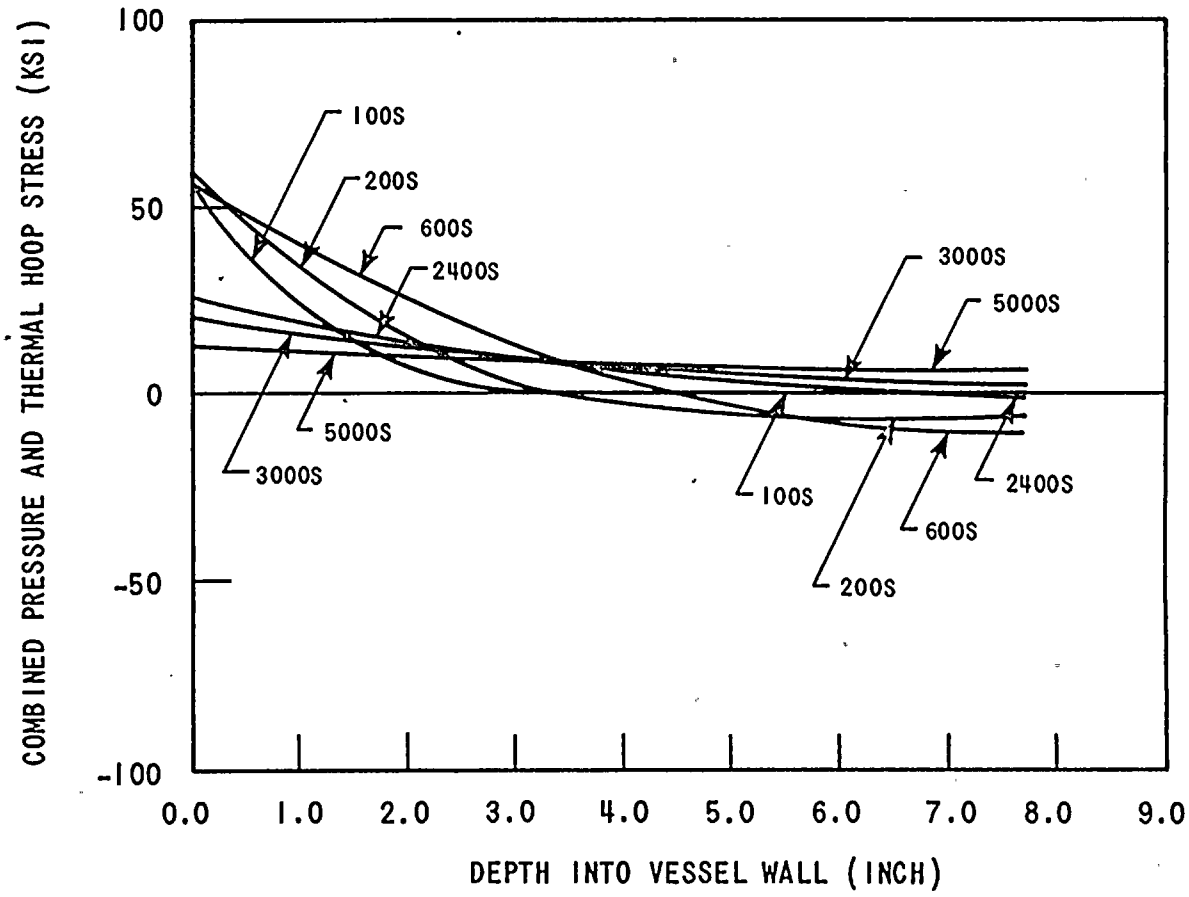

Figure 4-11. LSB (Without Off-Site Power) Pressure and Thermal Hoop Stress Distribution Through the Vessel Wall

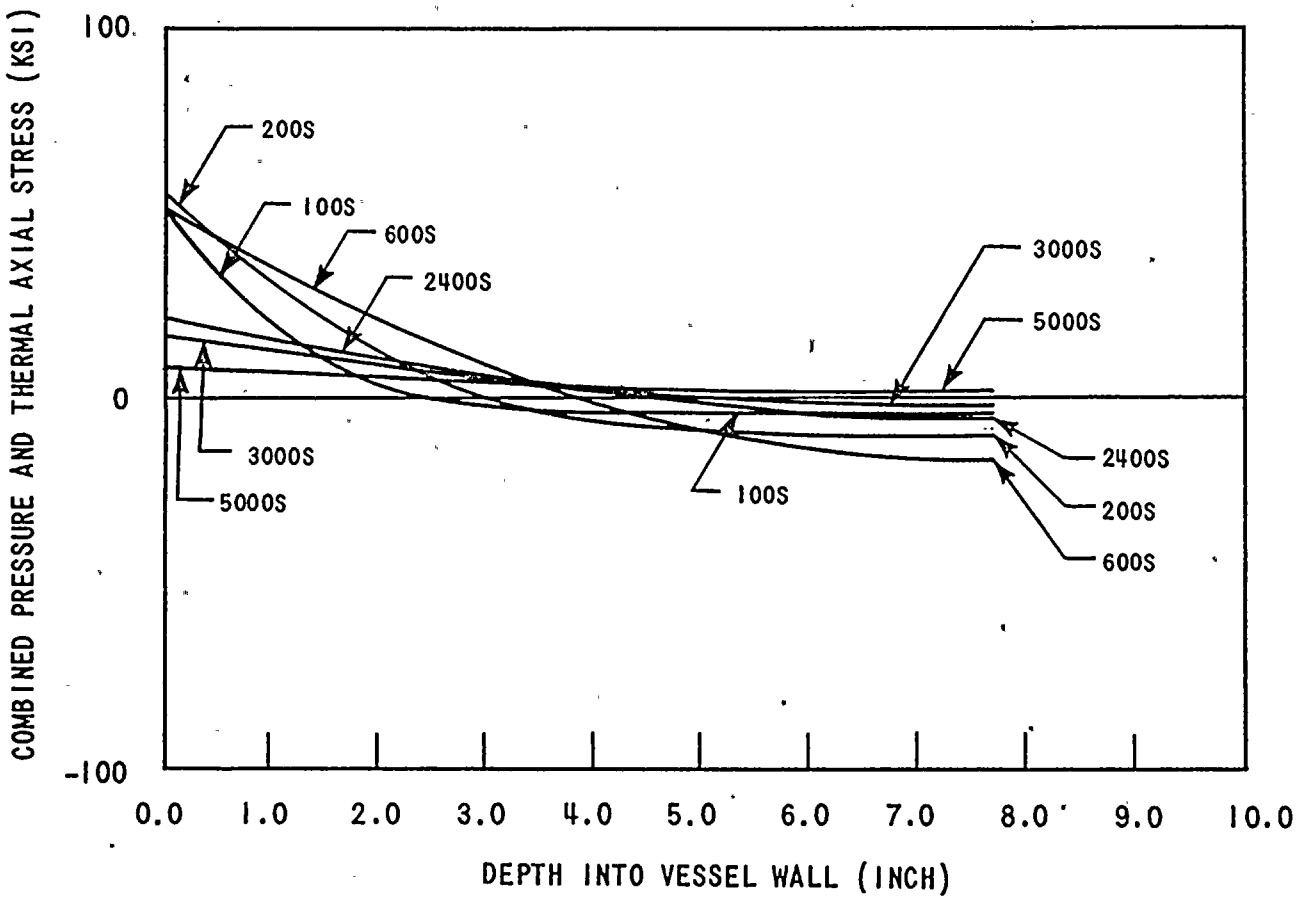

Figure 4-12. LSB (Without Off-Site Power) Pressure and Thermal Axial Stress Distribution Through the Vessel Wall

SECTION 5
FRACTURE MECHANICS ANALYSIS

5-1. BASIS FOR ANALYTICAL METHOD

After calculation of the stresses and temperatures in the reactor vessel belt line region resulting from the LOCA and LSB transients, fracture mechanics techniques have been used to determine the limiting conditions throughout the entire course of the accidents. More specifically, critical crack depths which must be exceeded before fracture initiation can occur have been determined using principles of the linear-elastic fracture mechanics (LEFM) technology.

The LEFM approach to the design against failure is basically a stress intensity factor consideration in which criteria are established for fracture instability in the presence of a crack[1]. Consequently, a basic assumption employed in LEFM is that a crack or crack-like defect exists in the structure. The essence of the approach is to relate the stress field developed in the vicinity of the crack tip to the applied nominal stress on the structure, the material properties, and the size of defect necessary to cause failure.

The elastic stress field at the crack tip in any cracked body is described by a single parameter designated as the stress intensity factor K. The magnitude of K is a function of the geometry of the body containing the crack, the size and location of the crack, and the magnitude and distribution of the stress. The criterion for failure in the presence of a crack is that failure will occur whenever K exceeds some critical value.

For the opening mode of loading (stresses perpendicular to the major plane of the crack) the stress intensity factor is designated as K_I and the critical stress intensity factor is designated K_{IC}. Commonly called the plane strain fracture toughness, K_{IC} is an inherent material property that is a function of temperature and strain rate. Any combination of applied load, structural configuration, crack geometry and size which yields a stress intensity factor greater than K_{IC} for the material, will result in crack instability or fast fracture.

1. T. R. Mager, C. Buchalet, and J. F. Enrietto, "Discussion of Fracture Mechanics Concepts," WCAP-7841, March 1972.

While K_{IC} is associated with crack initiation and is determined by static fracture toughness testing, another LEFM parameter, the reference fracture toughness, K_{IR} (K_{IA}), is associated with arrest of an unstable propagating crack.

Whenever the stress intensity factor K_I of a propagating crack becomes equal to K_{IR} at the same material temperature, crack arrest will occur as long as K_I for increasing crack depths becomes less than K_{IR}.

The (static) fracture toughness versus temperature curve, K_{IC}, represents the lower bound K_{IC} values of A-533 Grade B Class 1 and A-508 Class 2 reactor steels and weld metal. The reference fracture toughness versus temperature curve, K_{IR}, represents the lower bound dynamic and arrest fracture toughness values for both types of reactor steels. WCAP-8912 gives the justification and information on the K_{IC} and K_{IR} upper shelf toughness[1].

The temperature scale of the K_{IC} and K_{IR} curves is defined relative to the reference temperature, RT_{NDT}. The RT_{NDT} is a nonphysical constant related to the brittle-to-ductile fracture transition temperature; it is determined by both dropweight tests and Charpy V impact tests. RT_{NDT} is defined in Article NB 2331 of the Summer 1972 Addenda to the ASME Section III Boiler and Pressure Vessel Code[2].

The K_{IC} curve[3] is analytically described by:

$$K_{IC} = 33.194 + 2.806 \exp\left[0.02\left(T - RT_{NDT} + 100\right)\right] \tag{5-1}$$

The K_{IR} (K_{IA}) curve[3] is given by:

$$K_{IR} = 26.78 + 1.223 \exp\left[0.0145\left(T - RT_{NDT} + 160\right)\right] \tag{5-2}$$

5-2. STRESS INTENSITY FACTOR EXPRESSION

The fracture mechanics analysis requires the determination of the stress intensity factor solution for the continuous longitudinal and circumferential inside surface cracks that are postulated to exist in the cylindrical belt line region. Furthermore, the steep stress gradients developed in the vessel wall during the postulated accidents require that the actual stress profile be used in the stress intensity factor expressions.

---

1. P. J. Fields, "ASME III, Appendix G Analysis of the Florida Power and Light Co. Turkey Point Units No. 3 and No. 4 Reactor Vessels," WCAP-8912, June 1977.
2. ASME Boiler and Pressure Vessel Code, Section II, III and IX, Nuclear Power Plant Components, ASME, New York, 1971.
3. ASME Boiler and Pressure Vessel Code, Section XI, Appendix A Evaluation of Flaw Indications, ASME, New York, 1974.

The stress intensity factor for a continuous crack in an infinite structure subjected to an arbitrary nominal stress field σ (x, o) can be written as follows:[1]

$$K_I = \sqrt{\pi a}\ [A_o\ F_1 + \frac{2a}{\pi}\ A_1\ F_2 + \frac{a^2}{2}\ A_2\ F_3 + \frac{4a^3}{3\pi}\ A_3\ F_4] \qquad (5\text{-}3)$$

where

a = the crack length

F_1, F_2, F_3, F_4 = the magnification factors for the particular geometry considered relative to $\sigma = A_o$, $\sigma = A_1x$, $\sigma = A_2x^2$, $\sigma = A_3x^3$, respectively.

The applied stress profile σ (x, o) is expressed as a third-degree polynomial:

$$\sigma\ (x,\ o) = A_o + A_1x + A_2x^2 + A_3x^3 \qquad (5\text{-}4)$$

Buchalet and Bamford determined the magnification factors that are to be applied in the terms in equation (5-3) for continuous circumferential and longitudinal surface flaws in cylindrical vessels with a radius-to-wall-thickness ratio of 10. They developed a two-dimensional finite element model of a cylindrical geometry containing continuous longitudinal or circumferential surface cracks to calculate the stress intensity factor relative to this geometry. Their results, presented in terms of magnification factors versus fractional distance through the wall, are shown in figures 5-1 and 5-2 for the longitudinal and circumferential orientation, respectively.

5-3. FLUENCE CALCULATIONS

The determination of the shift of RT_{NDT} at any distance through the vessel wall and at the position of interest, requires that the neutron flux energy and the spatial distribution within the reactor vessel geometry be computed. A two-dimensional multigroup discrete ordinate transport computer code is used for these computations. The radial and azimuthal distributions are obtained from an R, θ calculation wherein the reactor core and the water and steel

1. Buchalet, C. B. and Bamford, W. H., "Stress Intensity Factor Solutions for Continuous Surface Flaws in Reactor Vessels," in *Mechanics of Crack Growth*, ASTM-STP-590, pp. 385-402. American Society for Testing and Materials, Philadelphia, 1976.

annuli surrounding it are modeled explicitly. The axial variations are then obtained from an R, Z calculation using the equivalent cylindrical core concept. The neutron flux at any point in the geometry is then given by

$$\phi(E, R, \theta, Z) = \phi(E, R, \theta)\ F(Z) \qquad (5\text{-}5)$$

where $\phi(E, R, \theta)$ is obtained directly from the R, θ calculation and F(Z) is a normalized function obtained from the R, Z analysis. The core power distributions used in both the R, θ and R, Z computations represent the expected average over the life of the plant.

Applicable neutron fluence values (neutrons per square cm, E > 1 MeV) are obtained by multiplying the neutron flux with the plant operating calendar time and the plant load factor.

A plant load factor of 0.8 and a nominal power of 2300 MWt (net) has been used in this analysis. The (radial) distribution of the neutron fluence through the reactor vessel wall of the Turkey Point Unit No. 4 after 40 calendar years of operation, is shown in figure 5-3. Figure 5-4 is a plot of the azimuthal variation of the maximum fluence.

5-4. IRRADIATION EFFECTS

Neutron irradiation has been shown to produce embrittlement which reduces the toughness properties of reactor vessel steels[1]. The decrease in the toughness properties can be assessed by determining the shift to higher temperatures of the reference temperature RT_{NDT}. Because the copper content of reactor vessel steel has been identified as a major contributor to radiation embrittlement, Westinghouse has developed copper trend curves to relate the magnitude of the shift of RT_{NDT} to the amount of neutron fluence.

The Westinghouse copper trend curves are shown in figure 5-5. These curves have been developed using the 30 ft-lb energy criterion, i.e., the shift of RT_{NDT} (ΔRT_{NDT}) is equal to the difference in temperature at which 30 ft-lb impact energy is obtained on unirradiated and irradiated Charpy V-notch specimens. The greater sensitivity of weld material to irradiation is generally accounted for by adding 0.05 weight percent copper to the actual copper content of the weld material to produce the trend curve applicable to weld material. However, available data on the Unit No. 4 girth weld indicate that this would result in an unduly conservative trend curve. Therefore, for Turkey Point Unit No. 4

1. U. Potapovs, J. R. Hawthorne, "The Effect of Residual Elements on 550°F Irradiation Response on Selected Pressure Vessel Steels and Weldments," NRL 6803, September 1968.

the appropriate trend curve is obtained by substituting 0.31 for the copper content in the equation for the Westinghouse copper trend curves given below.

For $Cu \leq 0.1$	ΔRT_{NDT}	$= [420\ (Cu - 0.05) + 21]\ (F)^{.2615}$
$0.1 < Cu \leq 0.15$	ΔRT_{NDT}	$= [420\ (Cu - 0.10) + 37]\ (F)^{.2699}$
$0.15 < Cu \leq 0.20$	ΔRT_{NDT}	$= [420\ (Cu - 0.15) + 53]\ (F)^{.2710}$
$0.20 < Cu \leq 0.25$	ΔRT_{NDT}	$= [420\ (Cu - 0.20) + 67]\ (F)^{.2830}$
$0.25 < Cu \leq 0.30$	ΔRT_{NDT}	$= [420\ (Cu - 0.25) + 79]\ (F)^{.2841}$
$Cu > 0.30$	ΔRT_{NDT}	$= [420\ (Cu - 0.30) + 91]\ (F)^{.2841}$ (5-6)

where

Cu = weight percent of Cu in base metal (for weld use actual Cu + 0.05)

F = fluence x 10^{-18} (n/cm^2, $E > 1$ MeV)

Regulatory Guide 1.99, Revision 1, "Effects of Residual Elements on Predicted Radiation Damage to Reactor Vessel Materials"[1] presents an alternative procedure for predicting the shift of RT_{NDT} as a function of fluence, copper content and phosphorus content. Figure 5-6 shows the R.G. 1.99 trend curves.

The R.G. 1.99 trend curves are given by the following expression:

$$\Delta RT_{NDT} = [40 + 1000\ (\%\ Cu - 0.08) + 5000\ (\%\ P - 0.008)]\ \sqrt{0.1\ F} \qquad (5\text{-}7)$$

For $Cu < 0.08$ weight percent, use 0.08, and for $P < 0.008$ weight percent, use 0.008.

Both prediction methods have been applied in this analysis. Based on the initial RT_{NDT} values of the core region girth weld and the limiting intermediate shell forging and their respective copper and phosphorus contents, the RT_{NDT} values are determined from the respective trend curves for given levels of irradiation. Figure 5-7 shows the shift of RT_{NDT} of the core region girth weld after 40 calendar years of reactor operation, using the Westinghouse and R.G. 1.99 prediction methods. The reference fracture toughness (K_{IR}) curve and the static fracture toughness (K_{IC}) curve, both indexed to RT_{NDT}, are shifted along the temperature scale with a value equal to the respective RT_{NDT} to allow calculation of the K_{IR} and K_{IC} as a function of the fractional depth through the reactor vessel wall.

1. U.S. Nuclear Regulatory Commission, Regulatory Guide 1.99, Revision 1, Office of Standards Development, January 1976.

The fluence distribution through the reactor vessel wall has been used to determine the RT_{NDT} at any point in the reactor vessel wall. Since the fluence varies azimuthally around the vessel, the fluence in the area of the assumed flaw should be used. For the continuous longitudinal flaws postulated in the base material, the maximum fluence has been used because a flaw may exist in the area of maximum fluence. For the continuous circumferential flaws postulated in the core region circumferential weld, the maximum fluence has also been used. Note that this is conservative because the fluence varies azimuthally while a continuous circumferential flaw cannot exist entirely in the maximum fluence region.

5-5. FRACTURE ANALYSIS

A fracture analysis method has been applied to calculate the initiation and arrest flaw depths from stress intensity factor calculations for cracked bodies subjected to mechanical and/or thermal stresses. Equations (5-1) and (5-2) for K_{IC} and K_{IR} (K_{IA}), respectively, are used to determine the crack depth required for crack initiation and to determine the maximum depth at which a running crack arrests.

The K_{IC} and K_{IR} curves are transformed to obtain the respective values as a function of the fractional distance through the wall rather than functions of temperature to facilitate the calculations of the initiation and arrest flaw depths. The minimum crack initiation depth is obtained at the first intersection of the stress intensity factor (K_I) curve with the static fracture toughness (K_{IC}) curve. Intersection of the K_I curve and the arrest toughness (K_{IR}) curve determines the crack arrest size, provided that for increasing crack depths the K_I curve drops below the K_{IR} curve.

The results are presented per time step and the K_I, K_{IC} and K_{IR} versus the fractional distance through the wall at these time steps are graphically presented.

The basic flow of logic employed in the fracture analysis is simple. From the input, supplied as the temperature and the combined stresses as a function of the time and the fractional distance through the vessel wall, calculations from the analytical expressions for K_I, K_{IC} and K_{IR} are performed. Once these values have been calculated at each discrete time step, the intersections are determined and hence the critical crack sizes.

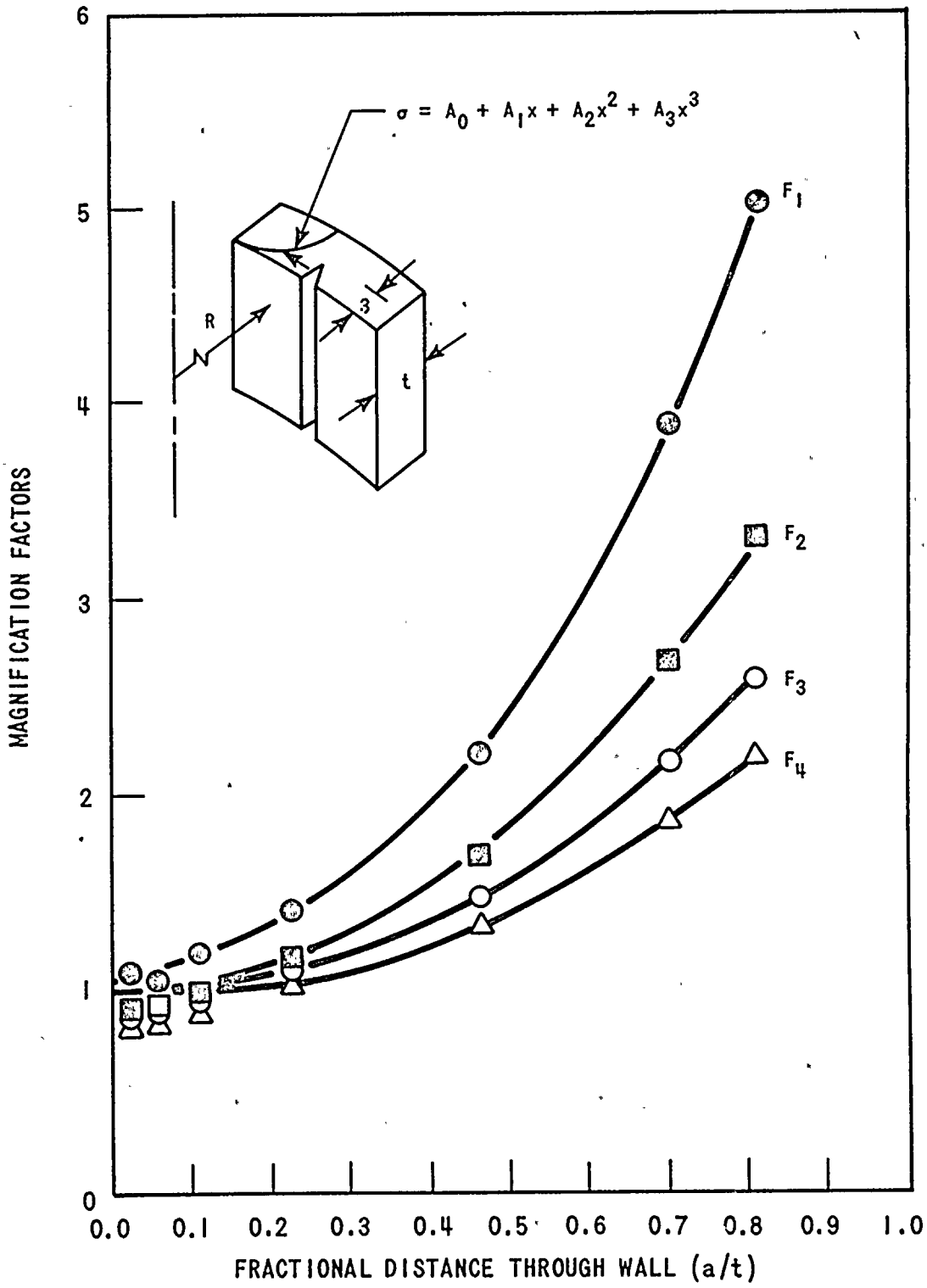

$$K_I = \sqrt{\pi a}\left[A_0F_1 + \frac{2a}{\pi}A_1F_2 + \frac{a^2}{2}A_2F_3 + \frac{4}{3}\frac{a^3}{\pi}A_3F_4\right]$$

Figure 5-1. Magnification Factors for Longitudinal Crack in Cylinder (t/R = 0.1)

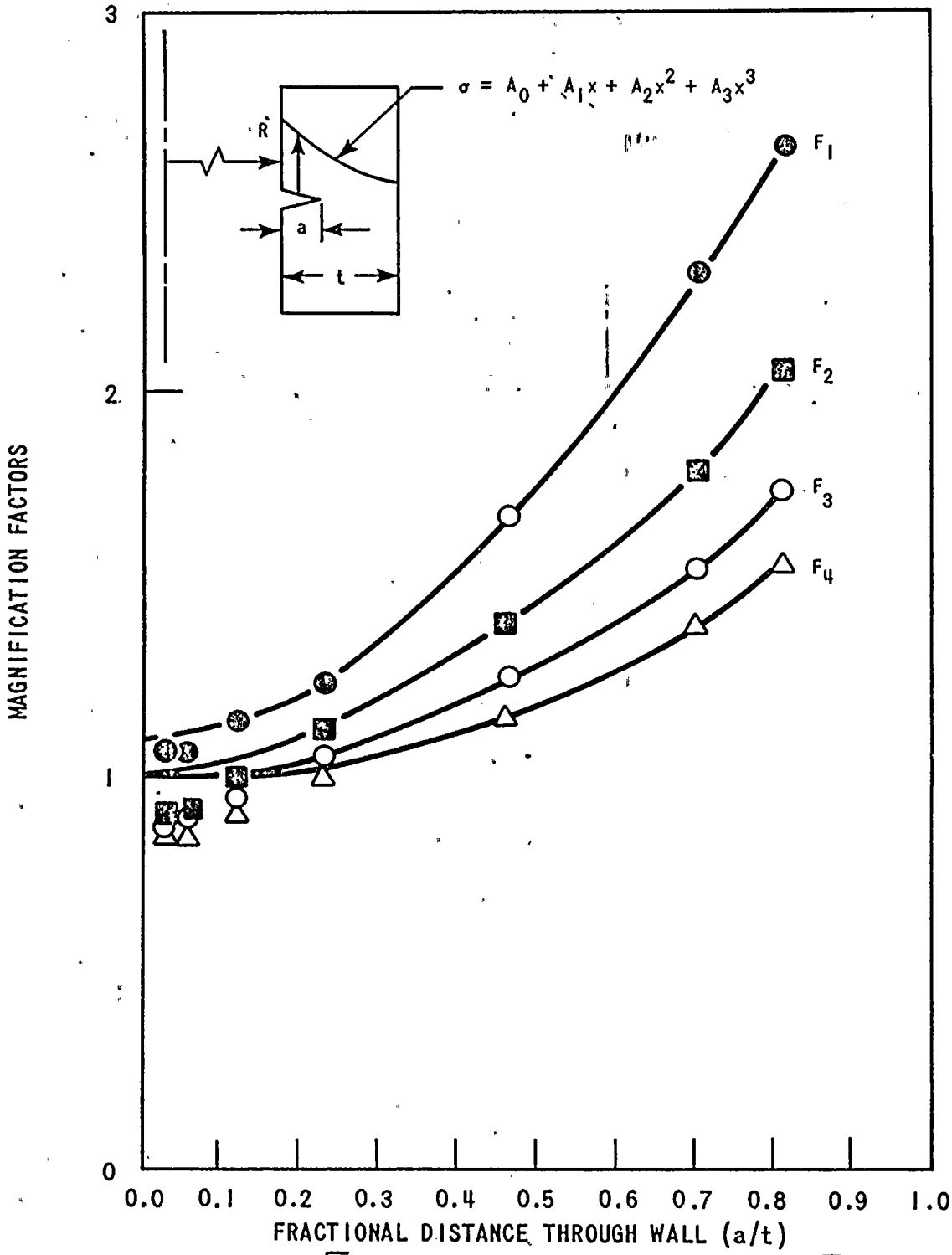

$$K_I = \sqrt{\pi a}\left[A_0F_1 + \frac{2a}{\pi}A_1F_2 + \frac{a^2}{2}A_2F_3 + \frac{4}{3}\frac{a^3}{\pi}A_3F_4\right]$$

Figure 5-2. Magnification Factors for Circumferential Crack in Cylinder (t/R = 0.1)

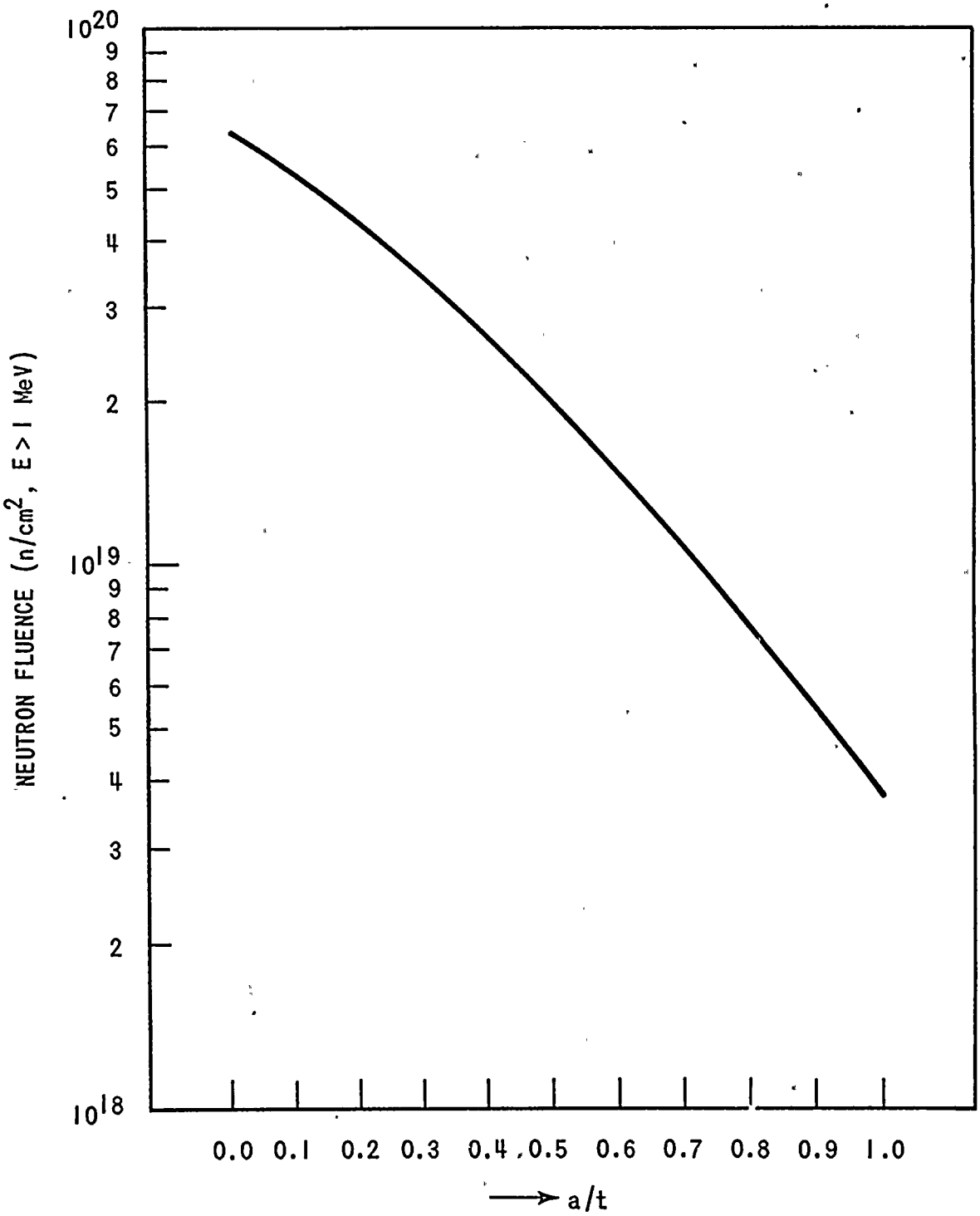

Figure 5-3. Fast Neutron Fluence Distribution Through the Vessel Wall (End of Life, 2300 MWt)

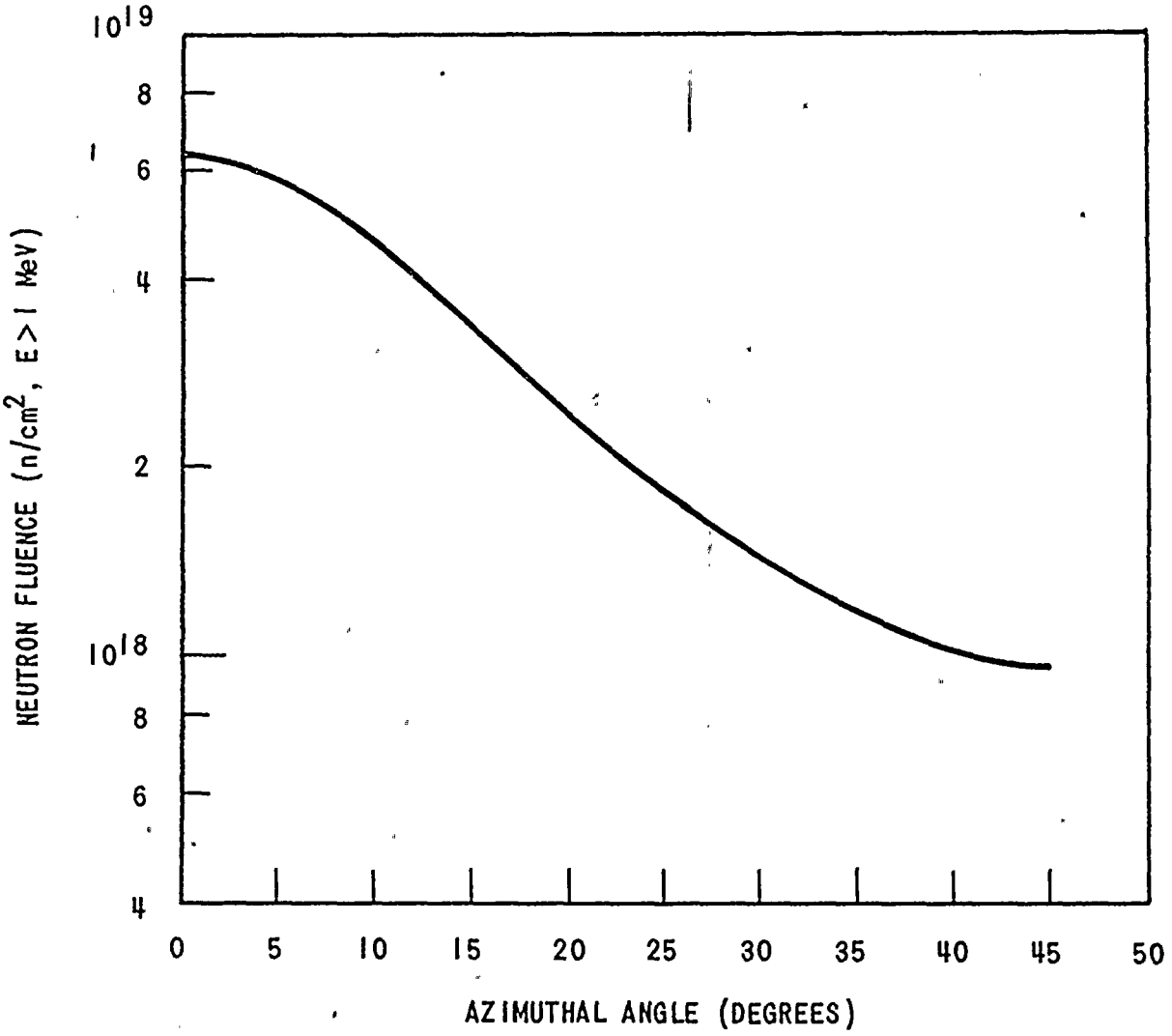

Figure 5-4. Azimuthal Variation of the Fast Neutron Fluence at the Reactor Vessel Inner Surface (End of Life, 2300 MWt)

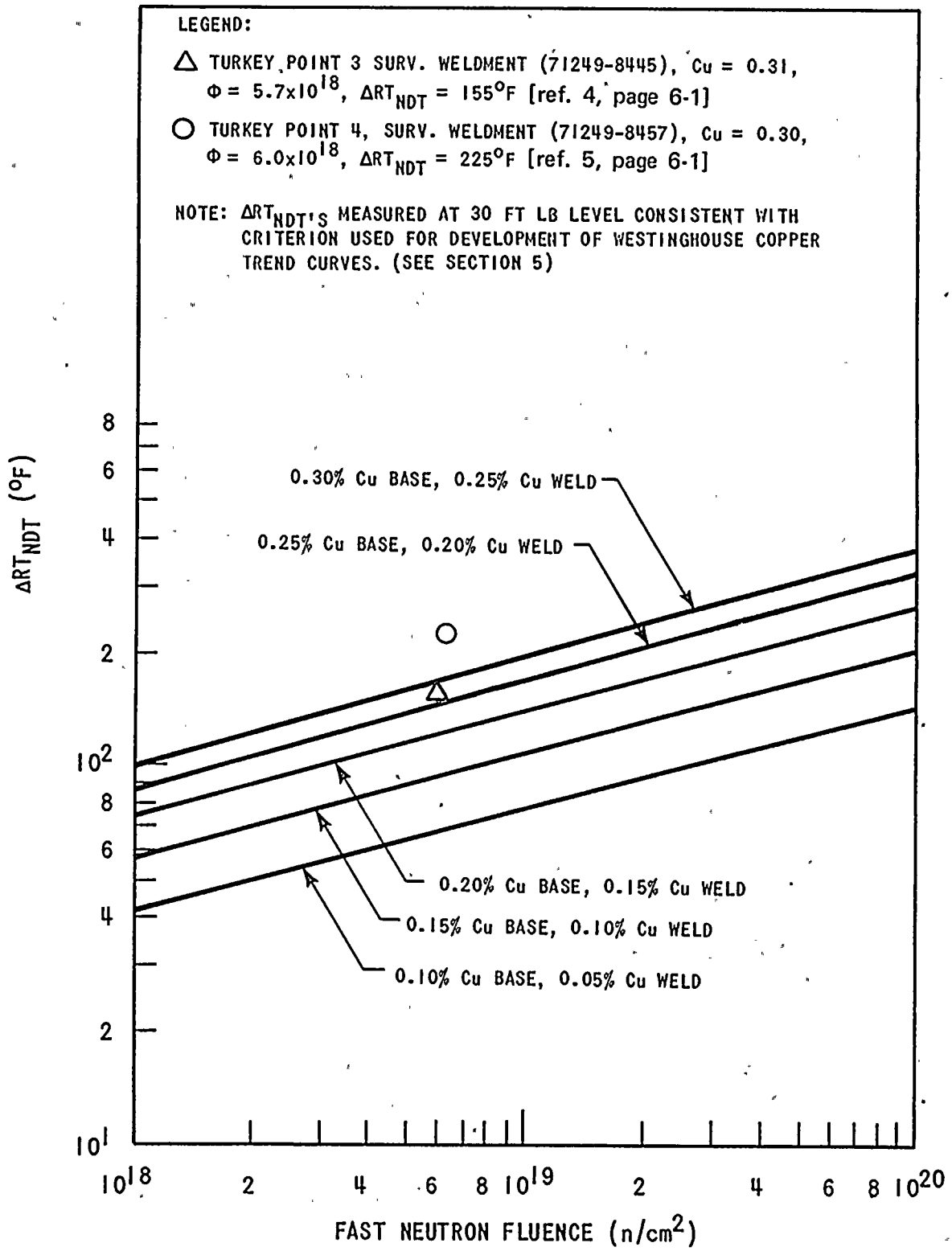

Figure 5-5. Westinghouse Copper Trend Curves: "Effect of Fluence and Copper Content on RT_{NDT} for Reactor Vessel Steels Exposed to Irradiation at 550°F"

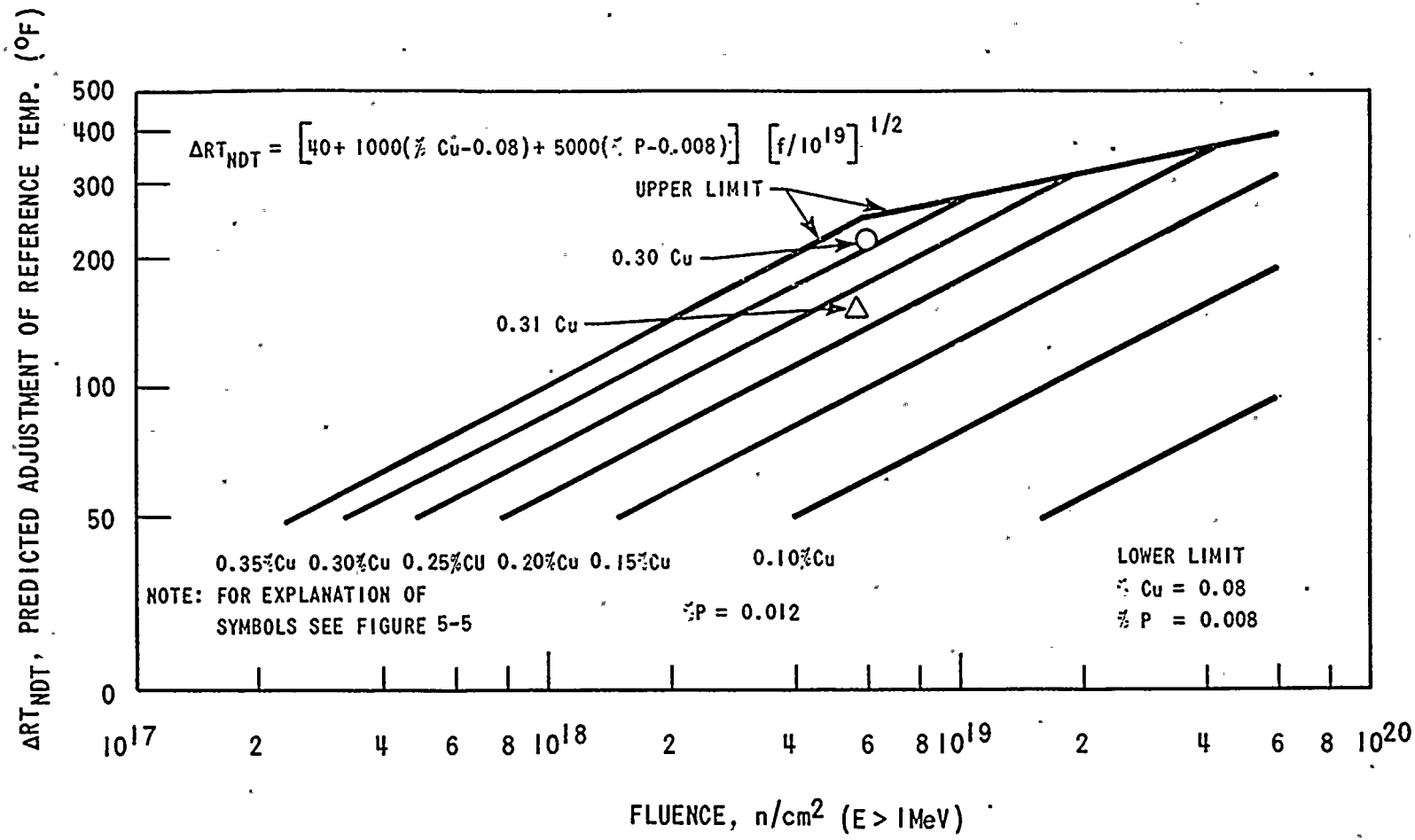

Figure 5-6. Regulatory Guide 1.99 Trend Curves: "Predicted Adjustment of Reference Temperature, ΔRT_{NDT} as a Function of Fluence and Copper Content"

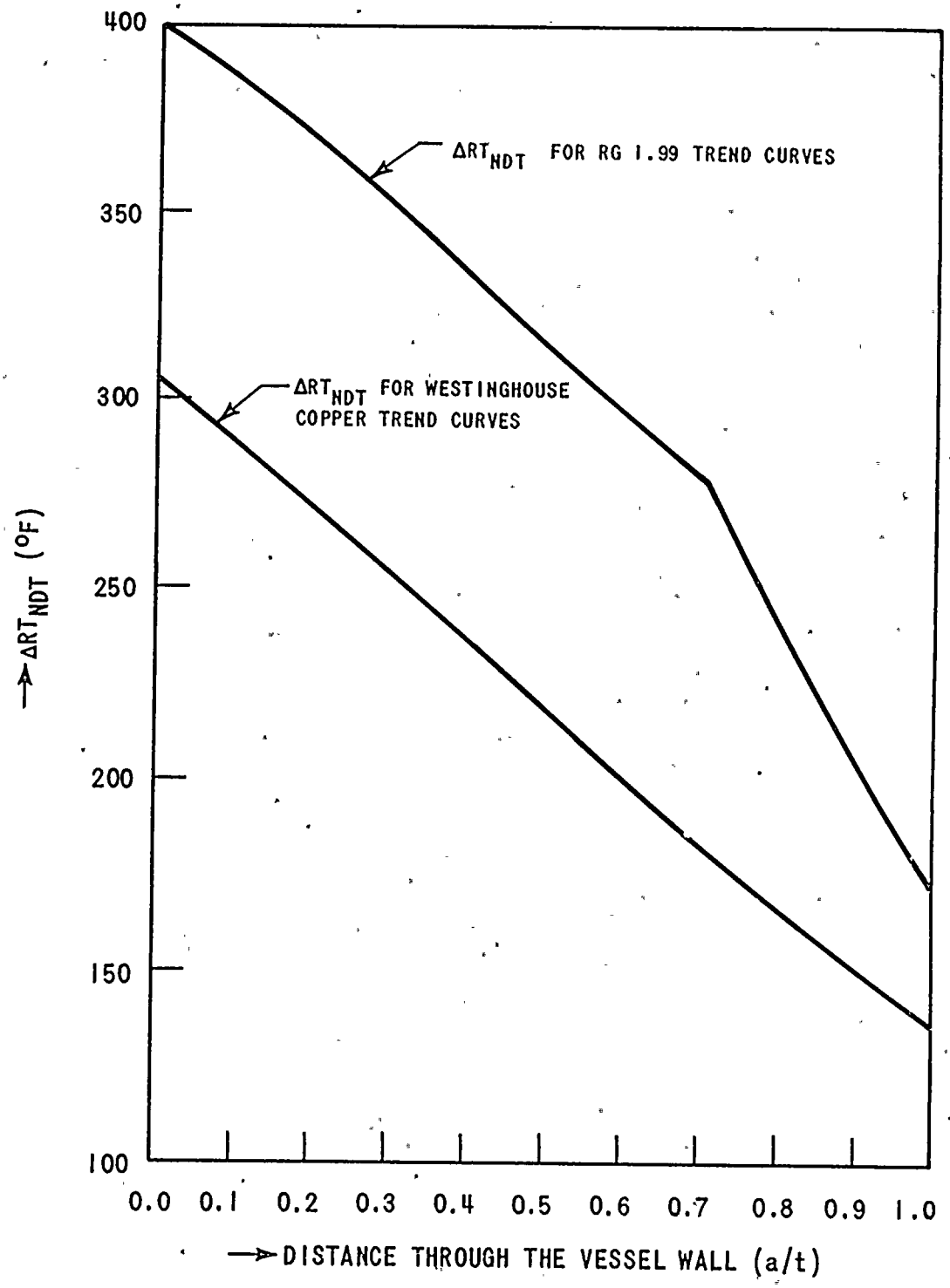

Figure 5-7. ΔRT_{NDT} of the Core Region Girth Weld as a Function of Fractional Distance Through the Vessel Wall (End of Life, 2300 MWt)

SECTION 6
MATERIAL INPUT

The Turkey Point Unit No. 4 reactor vessel core belt line region was fabricated from two ring forgings (intermediate and lower shell course) joined by one circumferential girth weld.

In the analysis of postulated continuous longitudinal flaws, the following most limiting material properties of the intermediate shell course forging have been used.

- Base Material Properties[1, 2, 3]

Copper Content:	0.054 weight percent
Phosphorus Content:	0.010 weight percent
Initial RT_{NDT}:	50°F

Unirradiated and irradiated upper shelf fracture toughness: 200 ksi $\sqrt{in.}$

In the analysis of continuous circumferential flaws postulated in the core region girth weld, the following properties have been used.

- Circumferential Weldment Properties[4, 5]

Copper Content:	0.31 weight percent
Phosphorus Content:	0.011 weight percent
Initial RT_{NDT}:	+3°F

Unirradiated and irradiated upper shelf fracture toughness: 200 ksi $\sqrt{in.}$

---

1. S. E. Yanichko, "Florida Power and Light Co., Turkey Point Unit No. 4 Reactor Vessel Radiation Surveillance Program," WCAP-7660, May 1971.
2. U.S. Nuclear Regulatory Commission, "Regulatory Standard Review Plan," Section 5.3.2.
3. P. J. Fields, "ASME III, Appendix G Analysis of the Florida Power and Light Co. Turkey Point Units No. 3 and No. 4 Reactor Vessels," WCAP-8912, June 1977.
4. S. E. Yanichko, et. al., "Analysis of Capsule T from the Florida Power and Light Company, Turkey Point Unit No. 3 Reactor Vessel Radiation Surveillance Program," WCAP-8631, December 1975.
5. E. B. Norris, "Reactor Vessel Material Surveillance Program for Turkey Point Unit No. 4; Analysis of Capsule T," SWRI Project No. 02-4221, June 14, 1976.

6-1. BASIS FOR SELECTION OF BASE MATERIAL PROPERTIES

Yanichko[1] provides the chemistry data on the intermediate shell course as well as the full Charpy V-notch impact curve obtained from longitudinally oriented Charpy specimens machined from this shell.

The nil-ductility transition temperature, NDTT, is 50°F as determined from the dropweight tests. At NDTT + 60°F, the estimated transverse impact properties are greater than 50 ft-lb and 35 mils lateral expansion. Per definition it then follows that the RT_{NDT} is equal to NDTT.

The estimation of the transverse impact properties from the longitudinal Charpy data was performed consistent with the NRC Regulatory Standard Review Plan, previously referenced.

Justification for the upper shelf fracture toughness value of 200 ksi $\sqrt{in.}$ for base and weld material in the unirradiated and irradiated condition is presented in Appendix A contained in WCAP-8912, previously referenced.

6-2. BASIS FOR SELECTION OF THE CIRCUMFERENTIAL WELDMENT PROPERTIES

Turkey Point Unit No. 3 pre- and postirradiation surveillance weldment data of WCAP-8631 have been used to represent the unirradiated and irradiated properties of the circumferential girth weld in the belt line region of the Turkey Point Unit No. 4 reactor vessel for the following reason.

The belt line region girth weld in the Turkey Point Units No. 3 and 4 reactor vessels and the weldment samples contained in the Unit No. 3 surveillance capsules were made with weld wire heat No. 71249 and flux lot No. 8445. The weldment samples in the Turkey Point Unit No. 4 were made with the same weld wire heat number but with a different lot of flux (flux lot No. 8457). Figure 6-1 shows for information purposes the pre- and post-irradiation Charpy V-notch impact data obtained from the Units No. 3 and No. 4 weldment samples as described by Yanichko in WCAPs 7660 and 8631 and by Morris in SWRI Project 02-4221, previously referenced.

The behavior of the reactor vessel steels under neutron irradiation can only be accurately assessed from samples that are identical to the materials to be monitored.

---

1. S. E. Yanichko, "Florida Power and Light Co., Turkey Point Unit No. 4 Reactor Vessel Radiation Surveillance Program," WCAP-7660, May 1971.

This is the case with the Turkey Point Unit No. 3 surveillance weldment samples. Because the belt line region dimensions, the core structure and geometry, and other components governing the reactor operating conditions are identical for both units, the thermal and irradiation conditions are the same for Units No. 3 and No. 4.[1, 2]

Therefore, it follows that the Turkey Point Unit No. 3 surveillance weldment properties should be used for assessing the neutron-radiation-induced changes in the properties of the Turkey Point Unit No. 4 core region girth weld.

Using the Westinghouse copper trend curves shown in figure 5-5 for the prediction of the (30 ft-lb) shift of RT_{NDT} for the three different weld material samples, it follows that the predicted shift of RT_{NDT} for Unit No. 3 weld material samples corresponds reasonably, but yet conservatively, to the actual shift (measured at the 30 ft-lb level).

Using the R.G. 1.99 trend curves (figure 5-6) and the actual 30 ft-lb shift of RT_{NDT}, it follows that R.G. 1.99 amply overestimates the ΔRT_{NDT} of Unit No. 3 weld material.

1. J. J. McGowan et.al., "Fatigue Crack Growth Evaluation of the Florida Power & Light Co. Turkey Point Units No. 3 and No. 4 Reactor Vessel," WCAP-8884, June, 1977.
2. Communication with S. L. Anderson, Westinghouse PWRSD, Radiation & Environmental Systems, January 1977.

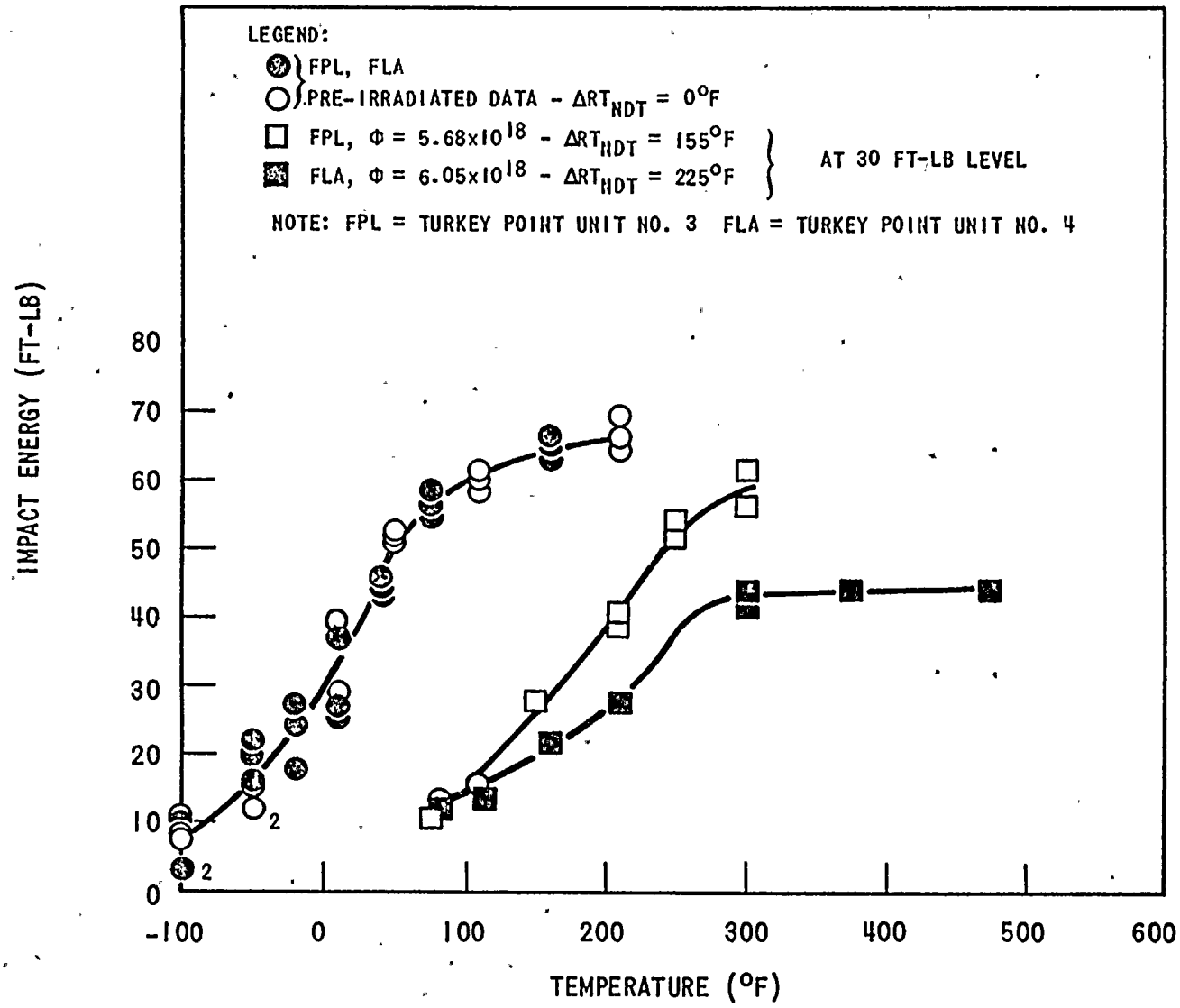

Figure 6-1. Pre- and Postirradiation Impact Properties of Turkey Point Weldment Samples

SECTION 7
RESULTS AND CONCLUSIONS

This analysis has been performed using LEFM methods to determine the critical depths required for initiation of postulated continuous surface cracks, and to determine the maximum depths at which crack arrest takes place. Westinghouse Copper Trend Curves and the method of Regulatory Guide 1.99 have been applied for the calculation of the shift of RT_{NDT}. For the cases that do not meet the criteria pertaining to the integrity of nuclear reactor pressure vessels, the maximum number of calendar years of plant operation that satisfy these criteria have been determined.

7-1. LOSS-OF-COOLANT ACCIDENT

The LOCA conditions are summarized in section 3. The stress intensity factor K_I for a continuous longitudinal and continuous circumferential flaw, as a function of progressive crack depth, has been calculated from equation (5-3) at time intervals of 100 seconds throughout the LOCA transient. The critical crack depth required for unstable growth is determined from the intersection of the K_I curve with the K_{IC} curve, and the crack arrest depth is determined from the intersection of the K_I curve with the K_{IR} curve. Table 7-1 summarizes the results of the LOCA analysis. Figures 7-1 through 7-6 present plots of K_{IC}, K_{IR}, and K_I at the time steps in the LOCA transient at which the minimum initiation depth and maximum arrest depth have been obtained for end-of-life conditions (40 calendar years). Figures 7-7 through 7-10 show the plots of flaw initiation depth and arrest depth as a function of time during the LOCA, for end-of-life conditions, the flaw orientations and RT_{NDT} adjustment methods considered.

7-2. Longitudinal Flaw (Evaluation at 40 Calendar Years)

- Westinghouse Copper Trend Curves

  Throughout the LOCA, the critical depths for initiation and arrest depths are determined from intersections of the K_I curve and the upper shelf of the K_{IC} K_{IR} curve. Consequently, the initiation and arrest depths are very large. After 500 seconds in the transient the initiation depth reaches a minimum value of

TABLE 7-1

TURKEY POINT UNIT NO. 4 – LOCA ANALYSIS
CRACK INITIATION AND ARREST DEPTH FOR CONTINUOUS SURFACE
CRACK IN REACTOR VESSEL VELT LINE REGION

Operation Period	Flaw Orientation	Minimum Crack Initiation Depth		Maximum Crack Initiation Depth		Maximum Crack Arrest Depth	ΔRT_{NDT} Shift Method
		a_c (min)	Time	a_c (max)	Time	a_a (max)	
40 Calendar Years	Longitudinal	3.66 inch 0.472 a/t	500	<7.63 inch <0.985	700	7.63 inch 98.5%	W Method
	Circumferential	0.16 inch 0.021 a/t	300	4.21 inch 0.543 a/t	2400	5.26 inch 67.9%	W Method
	Longitudinal	0.30 inch 0.039 a/t	800	1.71 inch 0.221 a/t	2300	5.51 inch 71.1%	R.G. 1.99
	Circumferential	0.149 inch 0.019 a/t	300	5.76 inch 0.743 a/t	2400	6.18 inch 79.8%	R.G. 1.99
26.25[a] Calendar Years	Circumferential	0.152 inch 0.020 a/t	300	5.24 inch 0.677 a/t	2400	5.80 inch 74.9%	R.G. 1.99

a. Maximum number of calendar years of operation for which integrity criterion $a_{arrest} \leq$ 75 percent of wall thickness is satisfied.

3.66 inch (0.472 a/t) as is shown in figure 7-1. After 700 seconds the arrest depth is maximum and equals 7.63 inches (0.985 a/t), as is illustrated in figure 7-2. Also, it follows from this figure that the maximum crack initiation depth is smaller than 7.63 inch. Figure 7-7 shows the critical crack depth as a function of time during the LOCA for this case.

- R.G. 1.99 Trend Curves

Due to the much greater shift of RT_{NDT} (about 100°F up to 70 percent of the wall thickness, see figure 5-7) obtained by using the R.G. 1.99 method, intersection of the K_I curve occurs in the lower portion of the K_{IC}, K_{IR} curves, and the minimum crack depth required for initiation is 0.30 inch (0.039 a/t) after 800 seconds as is shown in figure 7-3. The maximum initiation depth is 1.71 inches (0.221 a/t) at 2300 seconds, and the corresponding maximum arrest depth is 5.51 inches or 71.1 percent of the wall thickness, as is shown in figure 7-4. Up to 1400 seconds, the K_I curves also intersect the K_{IC}, K_{IR} curves in the upper shelf region, a situation that is identical to the one described for the Westinghouse Copper Trend Curves. Thus, up to 1400 seconds into the transient, a longitudinal continuous surface crack with a depth between 3.66 and 7.63 inches could be initiated and would arrest at a depth between 81 and 98.5 percent of the wall thickness. This is depicted in figure 7-8, which shows also that a crack with a depth between 1.71 and 3.66 inches will not be initiated throughout this transient.

7-3. Circumferential Flaw (Evaluation at 40 Calendar Years)

- Westinghouse Copper Trend Curves

At 300 seconds after beginning of the LOCA, a minimum critical flaw depth of 0.16 inch (0.021 a/t) is obtained from the first intersection of the K_I curve and the K_{IC} curve in figure 7-5. This flaw, however, arrests within 28 percent of the wall thickness. The maximum initiation depth is 4.21 inches (0.543 a/t) at 2400 seconds, but this crack arrests within 67.9 percent of the wall thickness, as is illustrated in figure 7-6. Figure 7-9 shows the initiation and corresponding arrest depth as a function of time in the transient for this case.

- R.G. 1.99 Trend Curves

Similar results for the minimum crack initiation depth as described for the previous case are obtained, because initiation throughout the LOCA is governed by the intersection of the K_I curve and the nearly flat lower portion of the

K_{IC} curve. The minimum initiation depth is 0.149 inch (0.019 a/t) at 300 seconds into the transient (see figure 7-5). This crack arrests within 44.1 percent of the wall. Due to the greater shift in the K_{IC}, K_{IR} curves, the maximum initiation depth is 5.76 inches (0.743 a/t) at 2400 seconds, and the maximum arrest depth is 6.18 inches (0.798 a/t), as shown in figure 7-6. The initiation and arrest depths as a function of the time in the LOCA are presented in figure 7-10.

Thus, using the R.G. 1.99 method for predicting ΔRT_{NDT} the integrity criterion of section 2.2 is not satisfied since the maximum arrest depth of circumferential flaws is greater than 0.75 a/t. Therefore, the maximum period of operation has been determined for which the arrest depth is within 75 percent of the wall thickness. This period is equal to 26.25 calendar years (21 effective full-power years).

7-4. Evaluation at 26.25 Calendar Years (R.G. 1.99 Trend Curves)

For this period the minimum circumferential flaw initiation depth during the LOCA is 0.152 inch (0.020 a/t) after 300 seconds, as is shown in figure 7-11, and the maximum arrest depth is 5.80 inch (0.749 a/t) at 2400 seconds, as is illustrated in figure 7-12. Figure 7-13 shows the critical crack depths as a function of time in the LOCA after 26.25 calendar years.

7-5. CONCLUSION FOR LOCA ANALYSIS

The circumferential flaws in the weldment joining the intermediate and lower shell course forgings represent the most severe fracture condition for the Turkey Point Unit No. 4 if a large LOCA were to occur at the end of the plant design life.

The greater potential for brittle fracture of the girth weld by initiation of a circumferential flaw results from the much greater shift of the reference temperature (RT_{NDT}) and, consequently, a greater shift in the K_{IC} and K_{IR} curves for the weldment. This is due to the high copper content of the weld material compared with the low copper content of the shell forgings.

The fracture analysis results obtained using the Westinghouse method for predicting the shift of RT_{NDT} with neutron irradiation, demonstrate that the Turkey Point Unit No. 4 reactor vessel subjected to a large LOCA at end of life will not be impaired because: (1) small circumferential flaws in the weldment will arrest within 67.9 percent of the wall thickness; and (2) the minimum initiation depth for a longitudinal flaw (3.66 inches) is so large that a crack this deep would be readily detected during a regular in-service inspection.

Using the Regulatory Guide 1.99 method for determining the end-of-life ΔRT_{NDT}, the results for longitudinal cracks satisfy the integrity criterion of section 2.2 because the maximum arrest depth of relatively small cracks is less than 0.75 a/t, whereas a crack between 1.71 and 3.66 inches deep is not initiated. For circumferential flaws the maximum arrest depth is greater than 75 percent of the wall thickness. However, it has been demonstrated that 26.25 calendar years of plant operation are required before the reactor vessel integrity criterion may be violated should a LOCA take place.

7-6. LARGE STEAM LINE BREAK

The Large Steam Line Break conditions are summarized in section 3.

Two cases have been considered. In Case 1, off-site power is assumed to be available throughout the transient. In Case 2, a loss of off-site power with a reactor coolant system flow coastdown takes place during the LSB.

The methods of LEFM technology have been used and K_I has been determined for continuous longitudinal and continuous circumferential flaws.

Figures 7-14 through 7-28 present plots of K_I, K_{IC}, and K_{IR} at the critical flaw times (minimum and maximum initiation depths) and plots of the crack initiation and arrest depths as a function of time during the LSB for the various cases analyzed. Table 7-2 summarizes the results for the various cases.

7-7. Longitudinal Flaw (Evaluation at 40 Calendar Years)

- Westinghouse Copper Trend Curves

  At 600 seconds after the start of the Large Steam Line Break, a minimum critical flaw initiation depth of 3.28 inches (0.423 a/t) and 3.05 inches (0.393 a/t) for Case 1 (with off-site power) and Case 2 (without off-site power) respectively, have been determined by this analysis. The maximum initiation depth occurs at the end of this transient, and is equal to approximately 7.25 inches (0.935 a/t) and 6.44 inches (0.83 a/t) for Case 1 and Case 2, respectively. Figures 7-14 and 7-15 show K_I, K_{IC} and K_{IR} curves at 600 and 6000 seconds for Case 1, and figures 7-16 and 7-17 show these curves for Case 2. The critical crack depths as a function of time is plotted in figure 7-18 (Case 1) and in figure 7-19 (Case 2). For both cases the crack initiation depths are throughout the transient determined by intersection of the K_I curves and the upper shelf of the K_{IC} curve.

TABLE 7-2

TURKEY POINT UNIT NO. 4 – LSB ANALYSIS
CRACK INITIATION AND ARREST DEPTH FOR CONTINUOUS SURFACE
CRACK IN REACTOR VESSEL BELT LINE REGION

Case/ Operation Period	Flaw Orientation	Minimum Crack Initiation		Maximum Crack Initiation		Maximum Crack Arrest Depth	ΔRT_{NDT} Shift Method
		a_c (min)	Time	a_c (max)	Time	a_a (max)	
Large Steam Line Break (With Off-Site Power) 40 Calendar Years	Longitudinal	3.28 inch .423 a/t	600	~7.25 inch ~0.935 a/t	≥6000	No Arrest	W Method & R.G. 1.99
	Circumferential	0.26 inch .033 a/t	600	1.85 inch 0.238 a/t	1600	3.35 inch 43.2%	W Method
	Circumferential	0.19 inch .025 a/t	600	5.26 inch 0.679 a/t	3100	6.41 inch 82.7%	R.G. 1.99
Large Steam Line Break (With Off-Site Power) 31.25 Calendar Years[a]	Circumferential	0.20 inch 0.026 a/t	500	4.63 inch 0.598 a/t	2800	5.81 inch 75.0%	R.G. 1.99
		0.29 inch 0.038 a/t	600	1.32 inch 0.171 a/t	1300	2.78 inch 35.8%	W Method
Large Steam Line Break (Without Off-Site Power) 40 Calendar Years	Longitudinal	3.05 inch .393 a/t	600	~6.44 inch ~0.83 a/t	≥6000	No Arrest	W Method & R.G. 1.99
	Circumferential	0.27 inch .035 a/t	600	1.71 inch 0.220 a/t	1500	3.28 inch 42.3%	W Method
	Circumferential	0.19 inch .025 a/t	400	~6.36 inch ~0.82 a/t	≥6000	No Arrest	R.G. 1.99
Large Steam Line Break (Without Off-Site Power) 25 Calendar Years[a]	Circumferential	0.21 inch .027 a/t	400	4.53 inch 0.584 a/t	3300	5.79 inch 74.7%	R.G. 1.99

a. Maximum number of calendar years of operation for which integrity criterion $a_{arrest} \leq$ 75 percent of wall thickness is satisfied.

- R.G. 1.99 Trend Curves

  The results are identical to the results obtained for the Westinghouse ΔRT_{NDT} adjustment method because the critical crack depths are throughout the transient governed by intersection of the K_I curve with the upper shelf of the K_{IC}, K_{IR} curves shown in figures 7-14 through 7-17.

7-8. Circumferential Flaw (Evaluation at 40 Calendar Years)

- For Case 1 and Case 2 the minimum crack initiation depths are 0.26 inch (0.033 a/t) and 0.27 inch (0.035 a/t), respectively, after 600 seconds into the LSB. These cracks arrest, however, within 30.8 percent of the wall thickness. Figures 7-20 and 7-21 show the K_I, K_{IC} and K_{IR} curves at 600 seconds. For Case 1 the maximum initiation depth is 1.85 inches (0.238 a/t) at 1600 seconds and the corresponding arrest depth is 3.35 inches or 43.2 percent of the wall thickness, as is shown in figure 7-22. For Case 2 these values are 1.71 inches (0.220 a/t) and 3.28 inches (42.3 percent), respectively, as illustrated in figure 7-23. The transient time-dependent initiation and arrest depths are shown in figures 7-27 (Case 1) and 7-28 (Case 2).

- R.G. 1.99 Trend Curves

  The minimum initiation depth for Case 1 is 0.19 inch (0.025 a/t) at 600 seconds, the corresponding arrest depth is 4.03 inches (0.520 a/t) as shown in figure 7-20. The maximum depth required for brittle fracture is 5.26 inches (0.679 a/t) at 3100 seconds and the maximum arrest depth is 6.41 inches (0.827 a/t) as depicted in figure 7-24. For Case 2 the same initiation depth of 0.19 inch (0.025 a/t) has been obtained after 400 seconds in the transient, and, as is indicated in figure 7-25, this crack has an arrest depth of 3.41 inches (0.440 a/t). The maximum initiation depth of 6.36 inches (0.82 a/t) for the LSB without off-site power occurs at the end of the transient, but this crack will not arrest, as seen from figure 7-26. The critical crack depths as a function of time in the transient have been plotted in figure 7-27 for the LSB with off-site power, and in figure 7-28 for the LSB coincident with a loss of off-site power.

  Thus, the results obtained for the circumferential flaws using R.G. 1.99 methods do not meet the integrity criteria should an LSB occur at the end of design life.

Therefore, repetitive calculations for successively decreasing numbers of calendar years have been performed, using R.G. 1.99 Trend Curves, to determine the operational periods at the end of which the arrest criterion can just be met. This period is 31.25 calendar years for the LSB with off-site power, and 25 calendar years for the LSB with coincident loss of off-site power.

7-9. Evaluation at 31.25 Calendar Years — LSB (With Off-Site Power)

The minimum initiation depth of 0.20 inch (0.026 a/t) is obtained after 500 seconds into the transient from the K_I and K_{IC} curves in figure 7-29. This crack arrests within 43.5 percent of the wall thickness. The maximum arrest depth is 75 percent of the wall thickness at 2800 seconds for a crack with a maximum initiation depth of 4.63 inches (0.598 a/t) as is shown in figure 7-30. The critical crack depths during this transient are plotted in figure 7-31. Note that figures 7-29 through 7-31 also illustrate the K_{IC}, K_{IR} curves and the three-dependent critical cracks that would result if the Westinghouse copper trend curves are used for the determination of ΔRT_{NDT}.

7-10. Evaluation at 25 Calendar Years — LSB (Without Off-Site Power)

Figures 7-32 through 7-34 show for this case the K_I, K_{IC}, and K_{IR} curves and the critical crack depths during this transient. The minimum initiation depth is 0.21 inch (0.027 a/t) at 400 seconds, the maximum arrest depth is 74.7 percent of the wall thickness of a circumferential crack with a (maximum) initiation depth for 4.53 inches.

7-11. CONCLUSION FOR LSB ANALYSIS

As is the case with the LOCA transient, the continuous circumferential crack in the weldment exhibits the greatest potential for fast fracture of the reactor vessel because the shift of the K_{IC} and K_{IR} curves for the weld metal relative to the base metal is much greater due to the high copper content in the former.

Based upon the Westinghouse copper trend curves, the results demonstrate that the integrity of the reactor vessel of the Turkey Point Unit No. 4 will not be impaired in the hypothetical case of an LSB occurring at the end of the design life. The depth of a longitudinal flaw in the base material must exceed 42 percent of the component thickness before crack initiation will occur. This depth amply exceeds the minimum capabilities of current in-serivce inspection techniques. A circumferential flaw in the girth weld in the core belt line region with a depth up to 1.85 inches will, after initiation, arrest within a distance of 43.2 percent of the wall.

Based on the Regulatory Guide 1.99 method for adjusting RT_{NDT}, the results obtained for a longitudinal crack in the base material demonstrate that the integrity of the reactor vessel will be maintained should an LSB take place at the end of plant life. The crack depth required for initiation is 3.28 inches. This is well within the detection limits of current inspection techniques.

For circumferential cracks postulated in the weldment, the results obtained using R.G. 1.99 methods indicate that the vessel integrity will not be impaired should an LSB (with off-site power) occur after 32.25 calendar years or an LSB (without off-site power) after 25 calendar years.

7-12. REMARKS ON LOCA-LSB ANALYSIS

Up to February 28, 1977, Turkey Point Unit No. 4 has effectively operated for 2.37 calendar years. Therefore, an additional period of about 22 calendar years would be required, using conservative assumptions and methods, before a potential integrity problem could manifest itself. During this period, a number of radiation surveillance capsules will be removed from Turkey Point Unit No. 3, thus allowing ahead of time a reliable assessment of end-of-life girth weld properties that also apply to Unit No. 4.

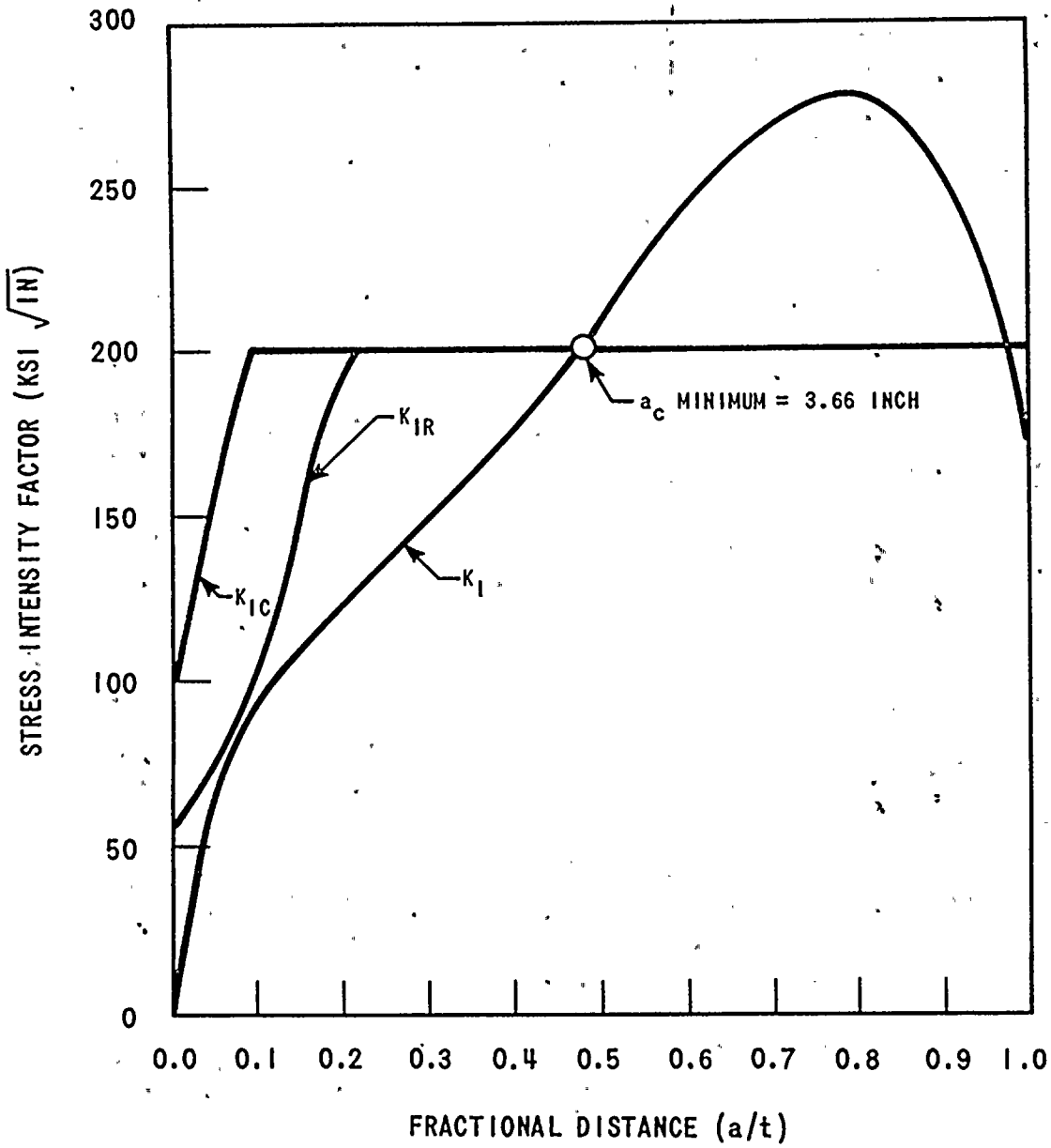

Figure 7-1. K_{IC}, K_{IR} and K_I After 500 Seconds in the LOCA (Longitudinal Flaw, 40 Calendar Years, Westinghouse Copper Trend Curves)

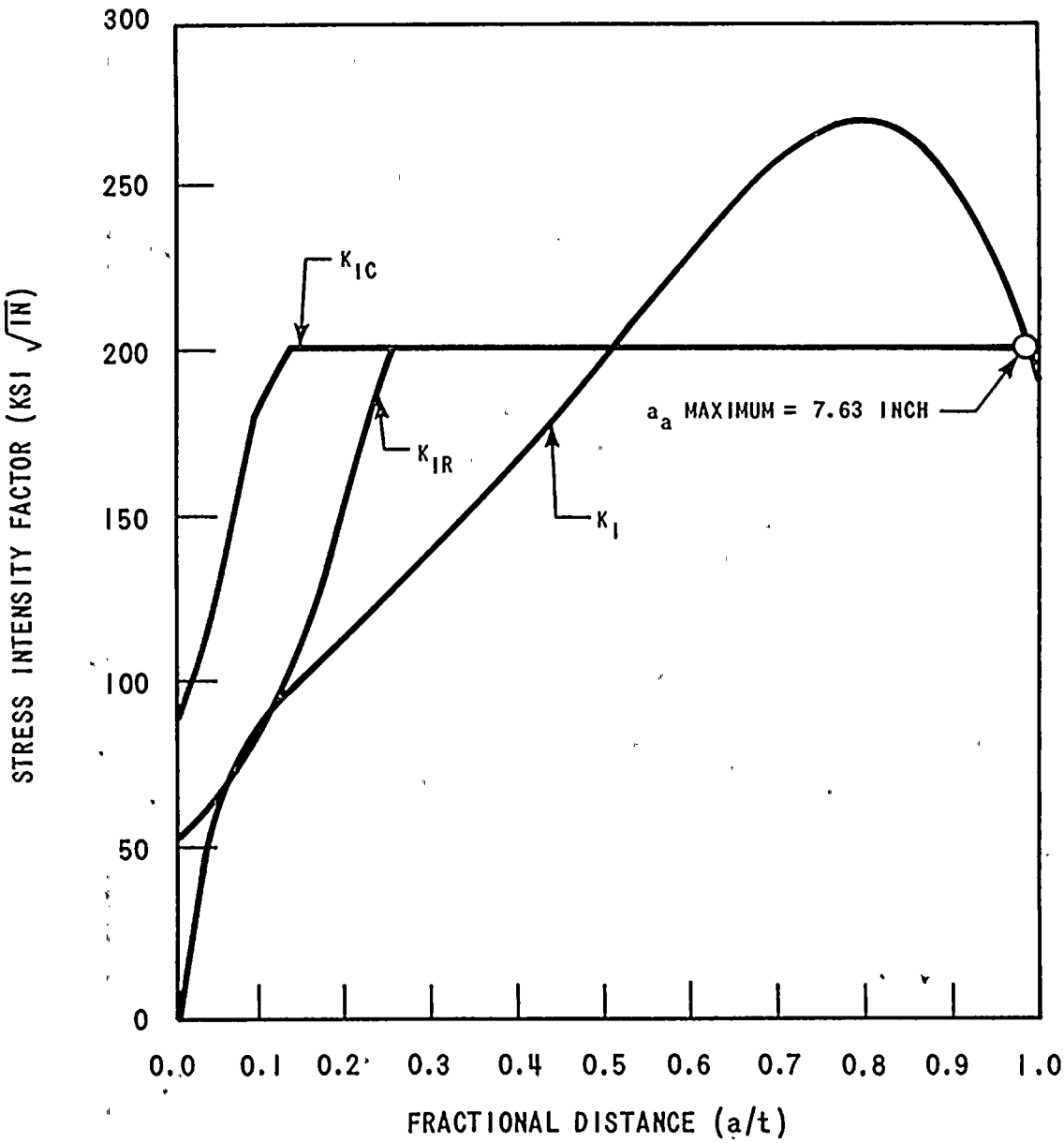

Figure 7-2. K_{IC}, K_{IR} and K_I After 700 Seconds in the LOCA (Longitudinal Flaw, 40 Calendar Years, Westinghouse Copper Trend Curves)

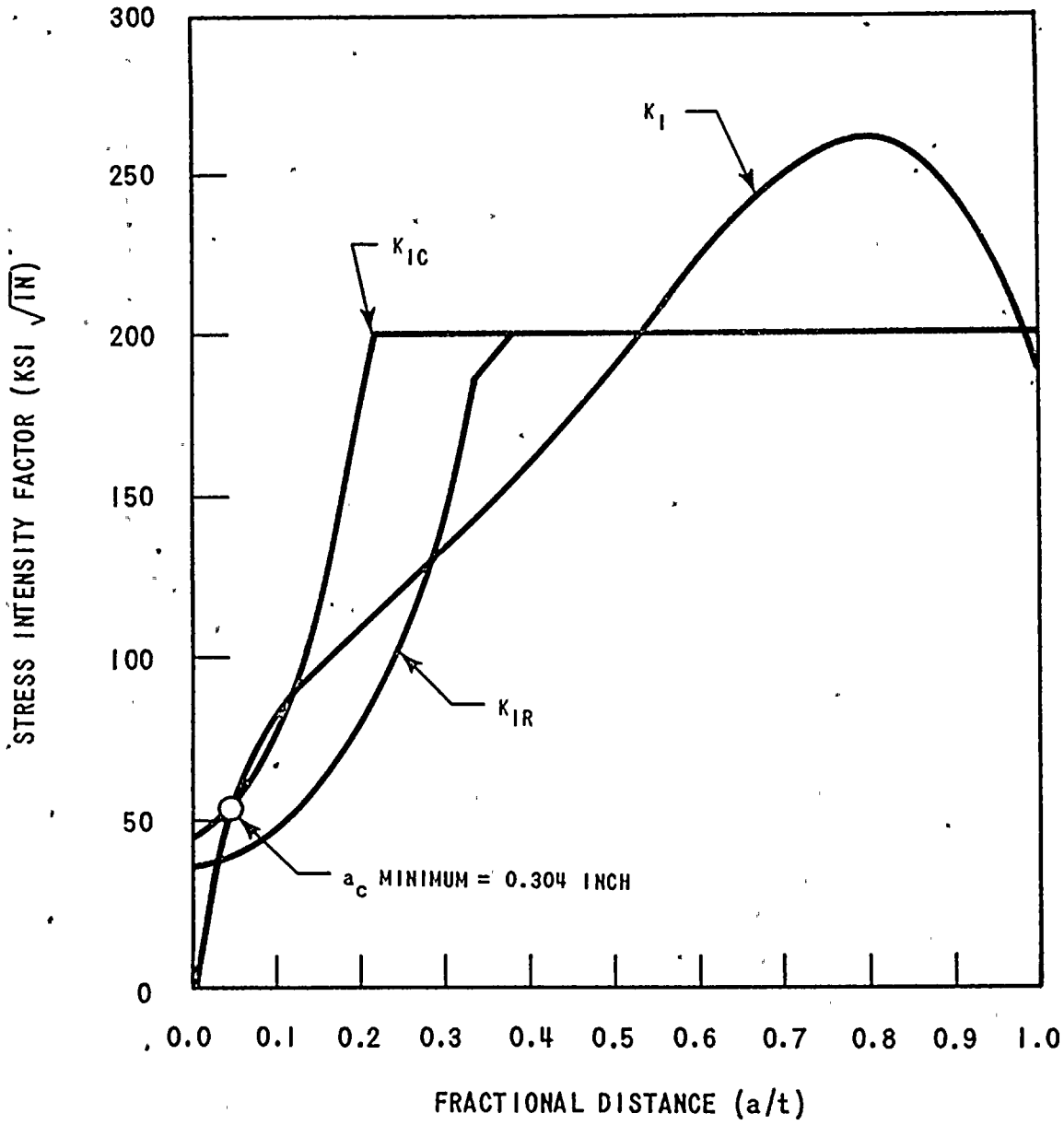

Figure 7-3. K_{IC}, K_{IR} and K_I After 800 Seconds in the LOCA (Longitudinal Flaw, 40 Calendar Years, R.G. 1.99 Trend Curves)

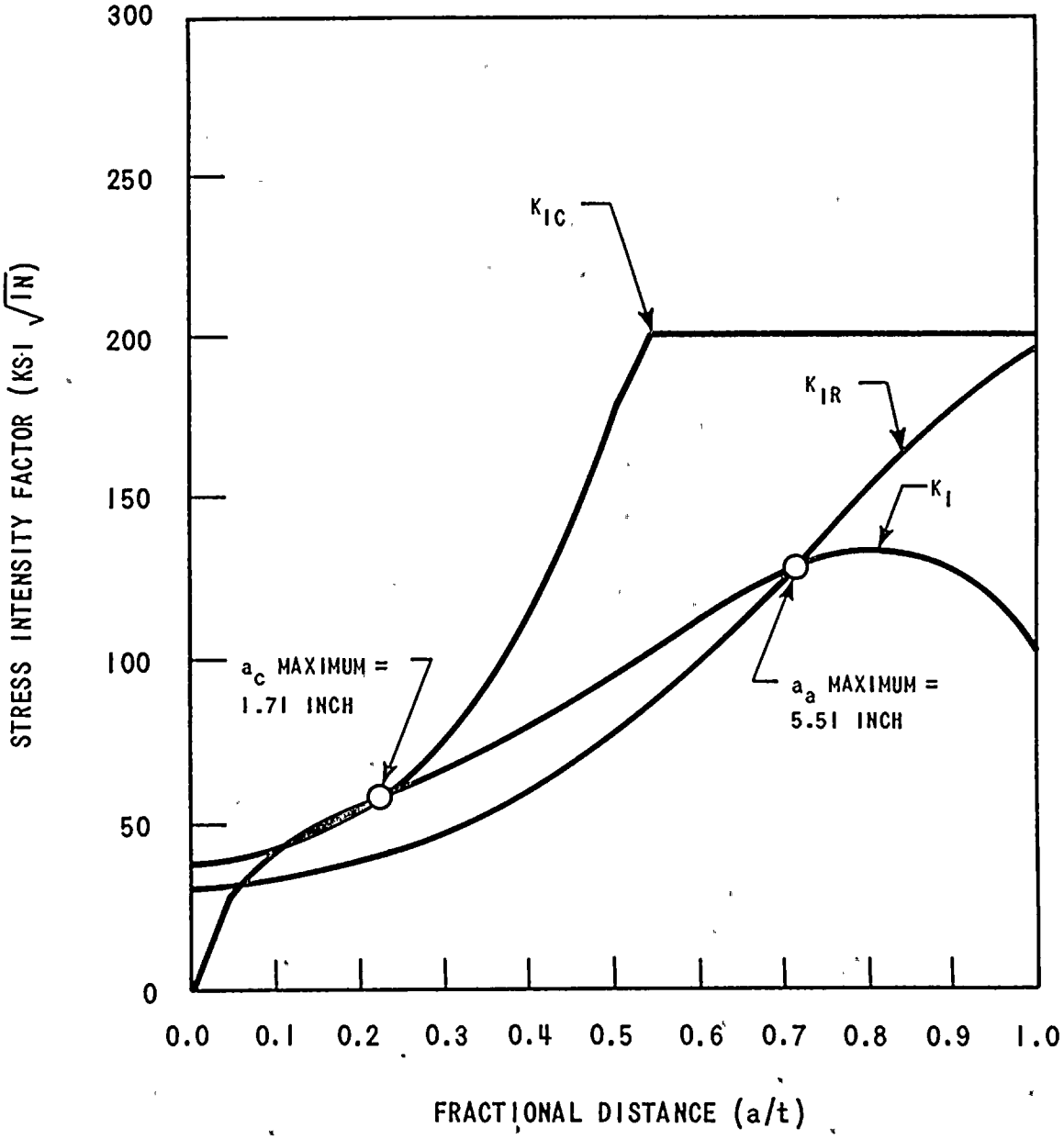

Figure 7-4. K_{IC}, K_{IR} and K_I After 2300 Seconds in the LOCA (Longitudinal Flaw, 40 Calendar Years, R.G. 1.99 Trend Curves)

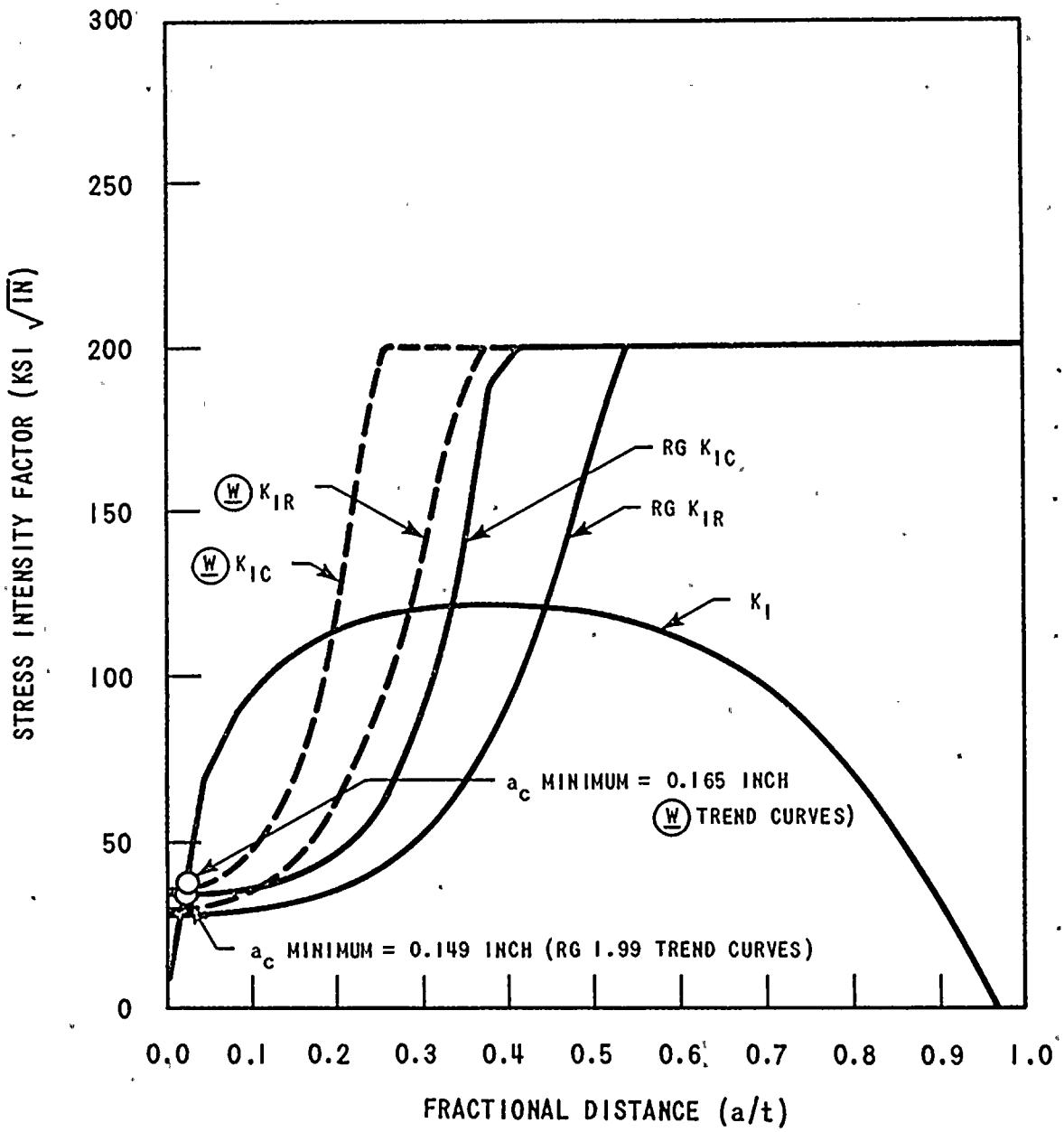

Figure 7-5. K_{IC}, K_{IR} and K_I After 300 Seconds in the LOCA (Circumferential Flaw, 40 Calendar Years, Westinghouse and R.G. 1.99 Trend Curves)

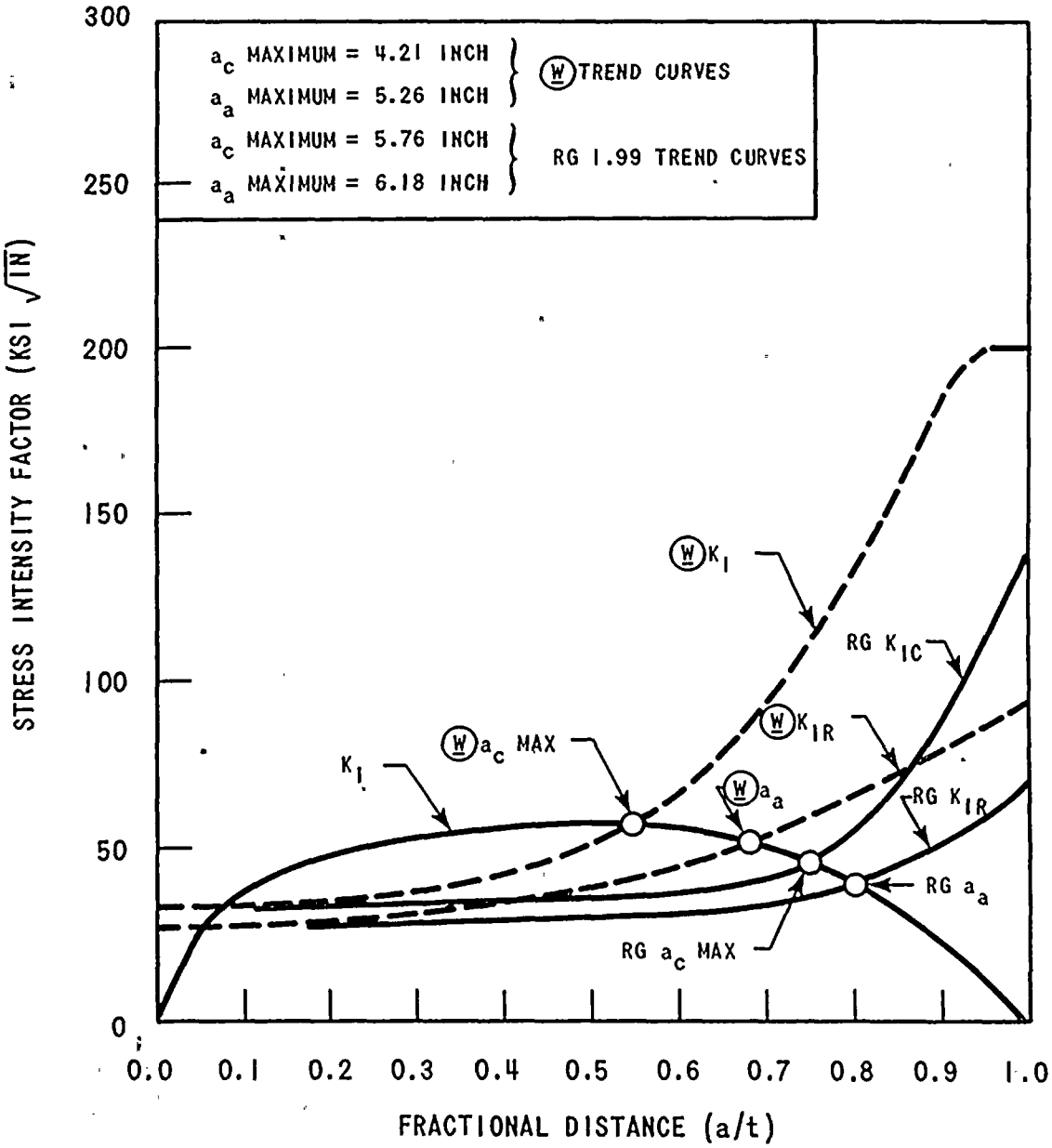

Figure 7-6. K_{IC}, K_{IR} and K_I After 2400 Seconds in the LOCA (Circumferential Flaw, 40 Calendar Years, Westinghouse and R.G. 1.99 Trend Curves)

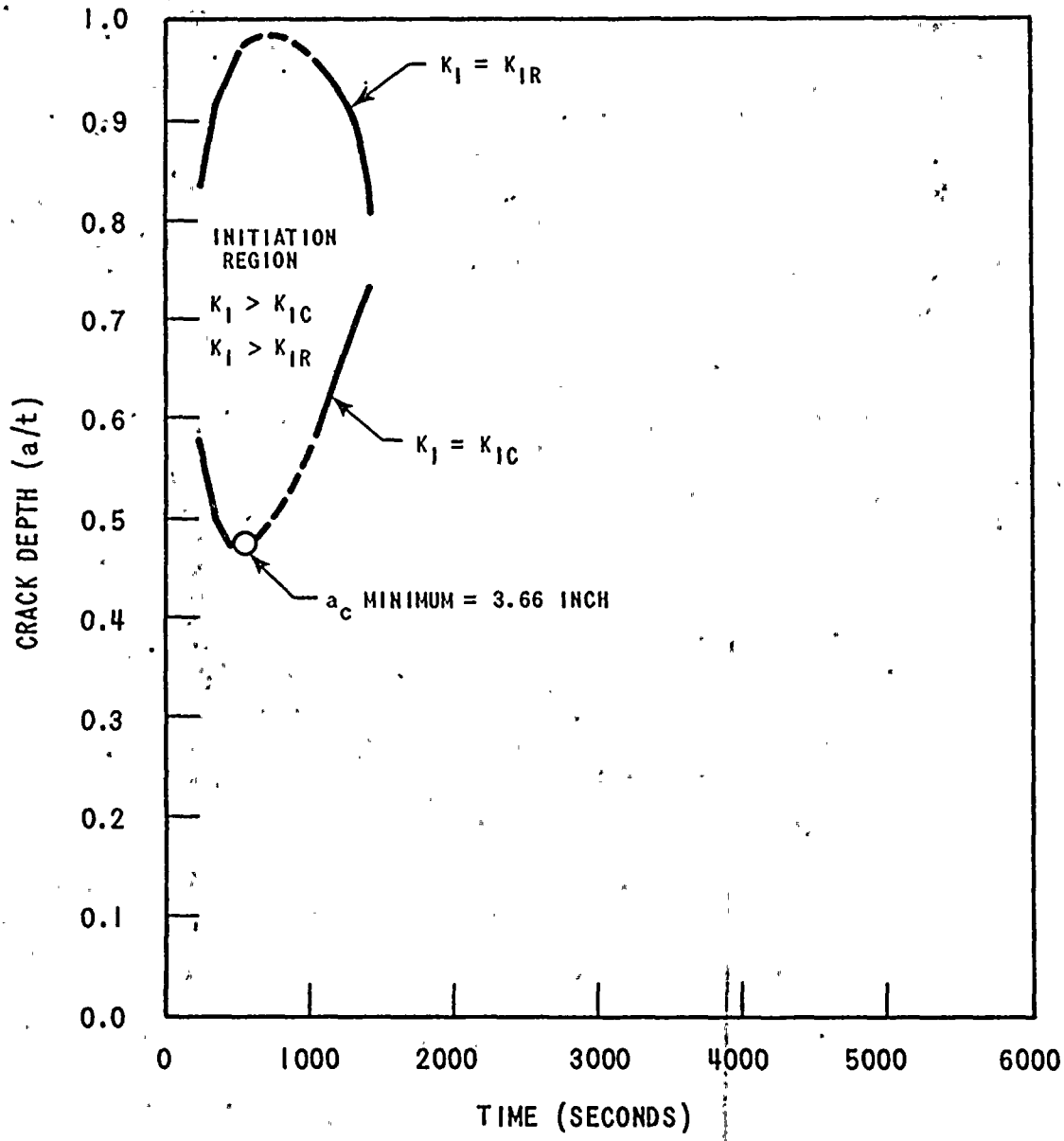

Figure 7-7. Longitudinal Flaw Initiation Depth and Arrest Depth for the LOCA (40 Calendar Years, Westinghouse Copper Trend Curves)

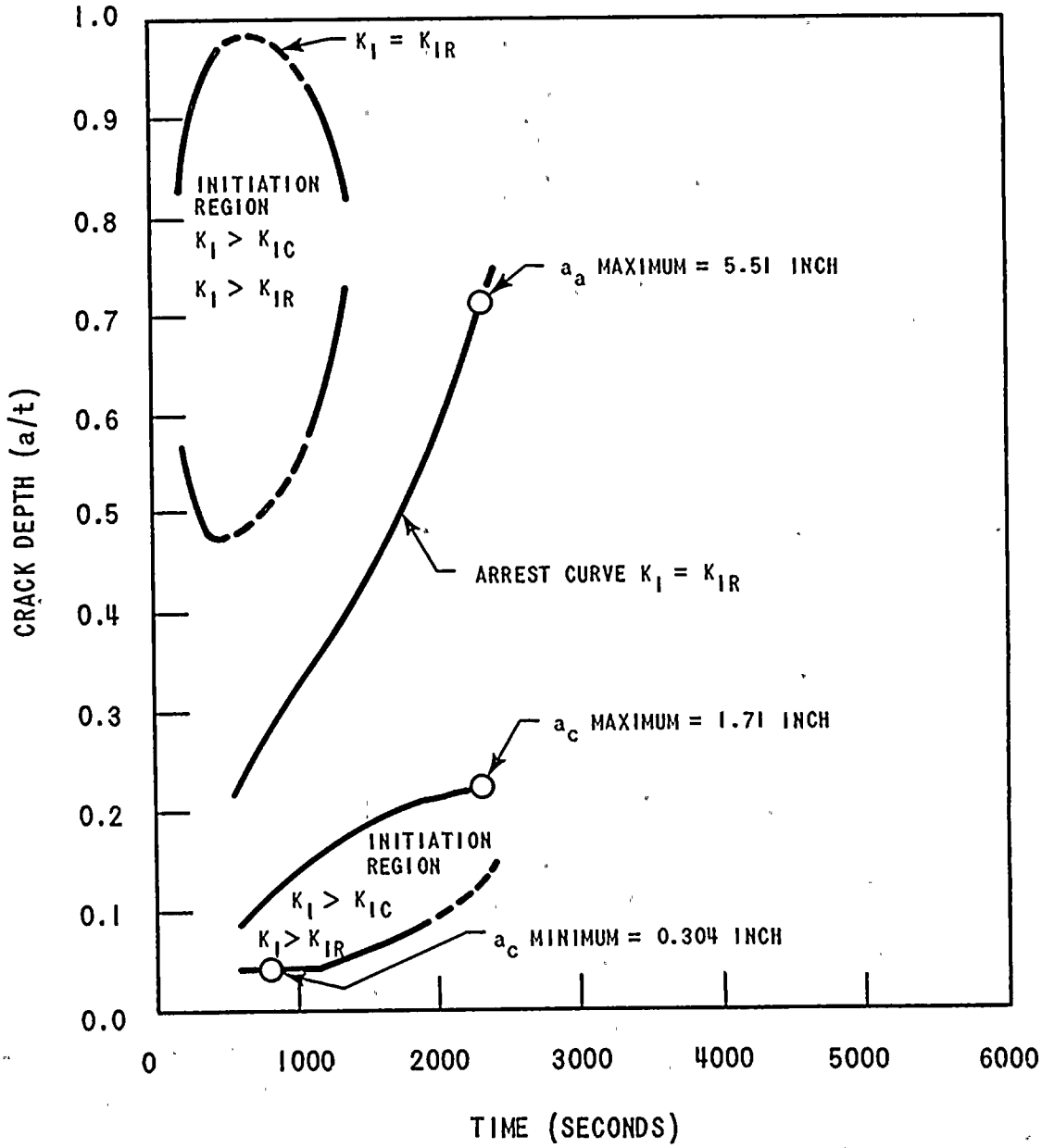

Figure 7-8. Longitudinal Flaw Initiation Depth and Arrest Depth for the LOCA (40 Calendar Years, R.G. 1.99 Trend Curves)

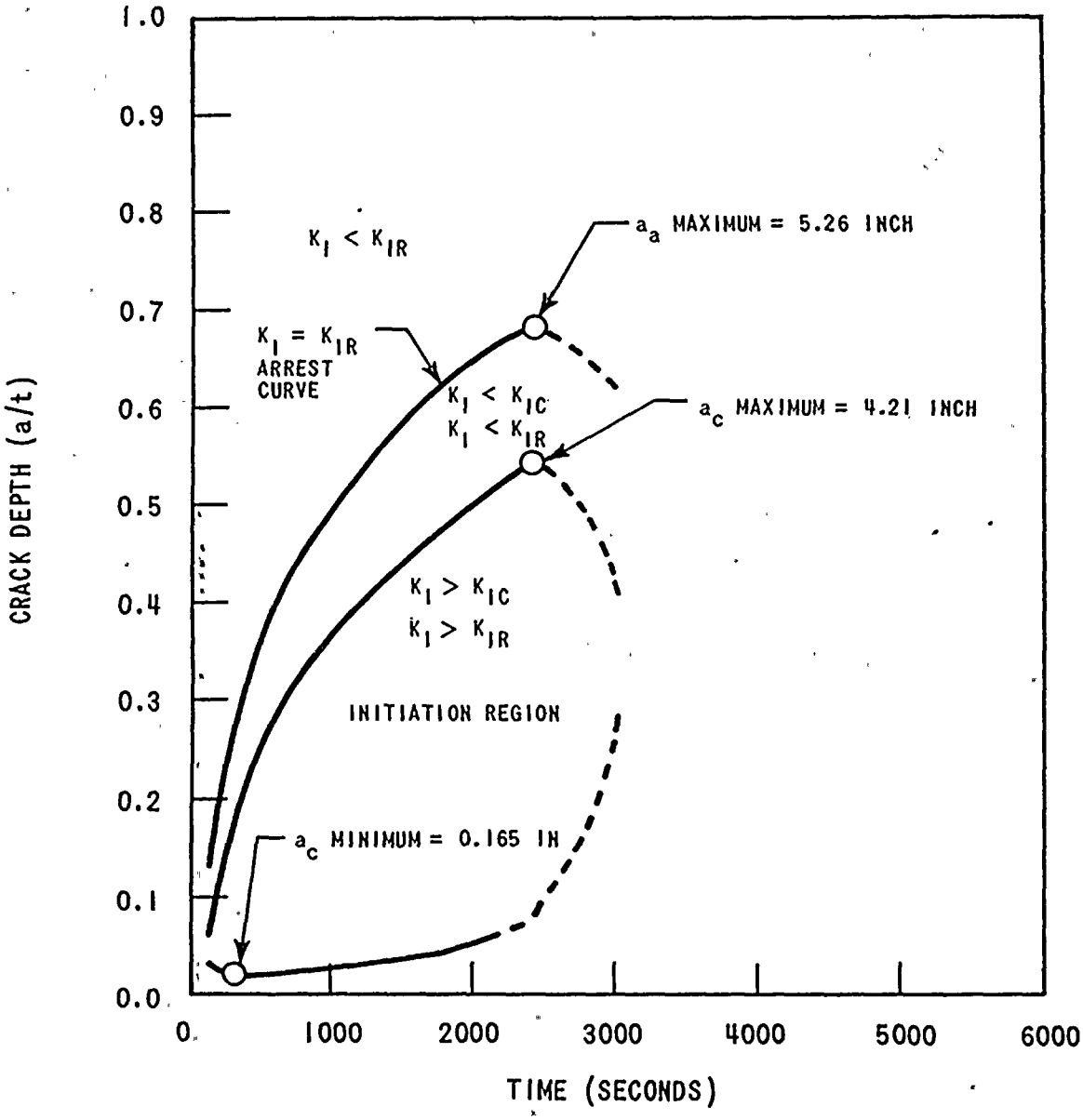

Figure 7-9. Circumferential Flaw Initiation Depth and Arrest Depth for the LOCA (40 Calendar Years, Westinghouse Copper Trend Curves)

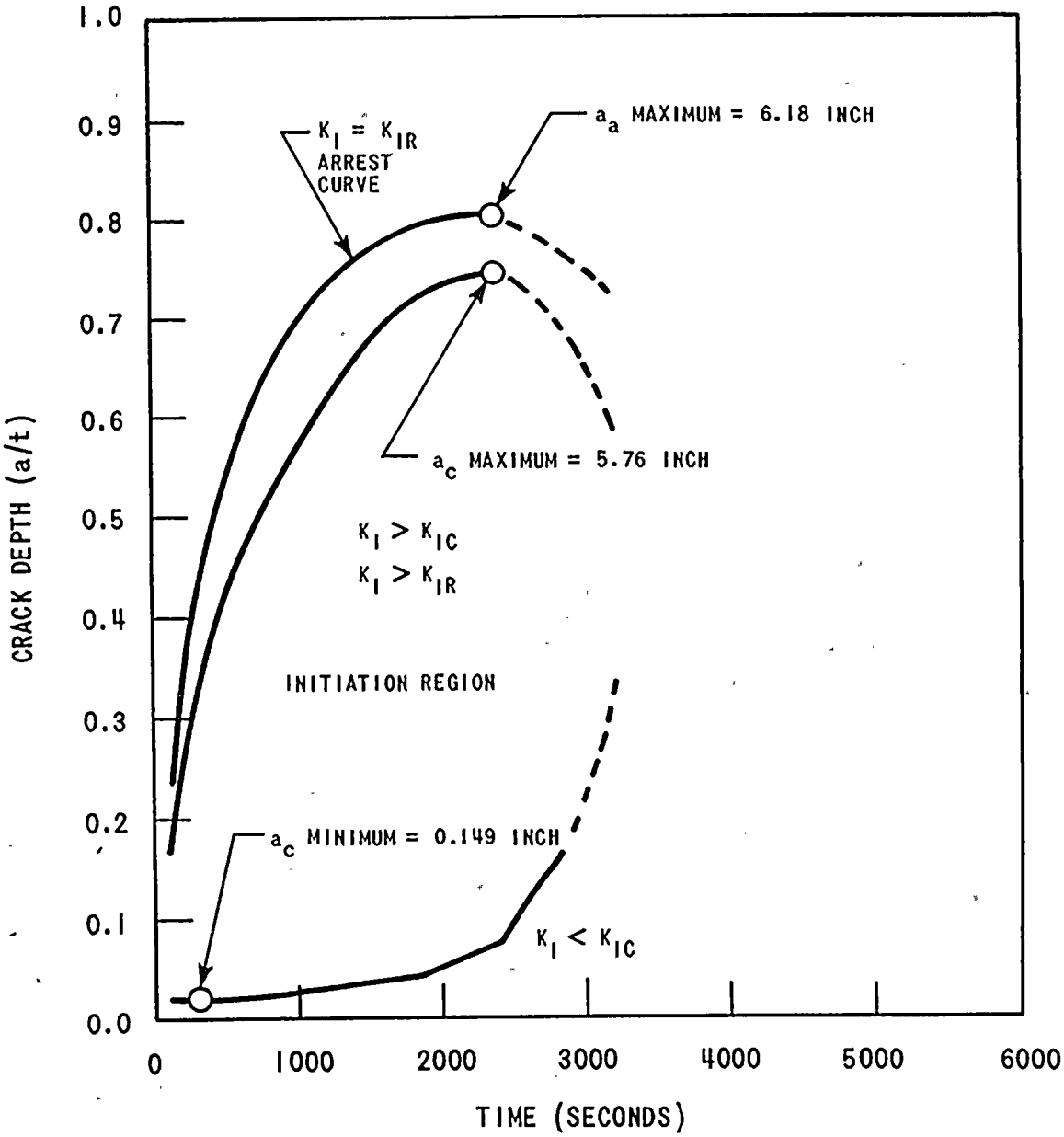

Figure 7-10. Circumferential Flaw Initiation Depth and Arrest Depth for the LOCA (40 Calendar Years, R.G. 1.99 Trend Curves)

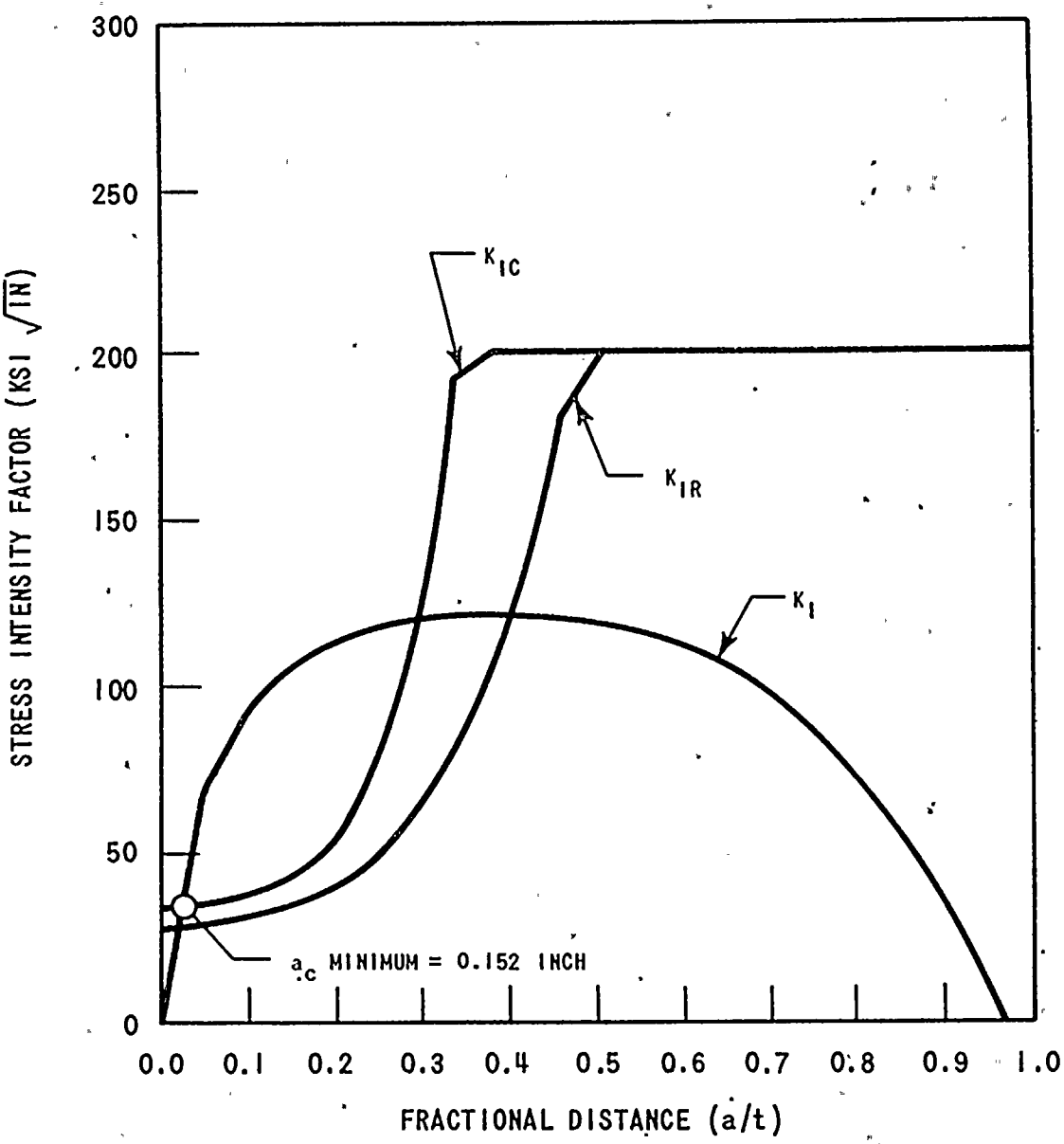

Figure 7-11. K_{IC}, K_{IR} and K_I after 300 Seconds in the LOCA (Circumferential Flaw, 26.25 Calendar Years, R.G. 1.99 Trend Curves)

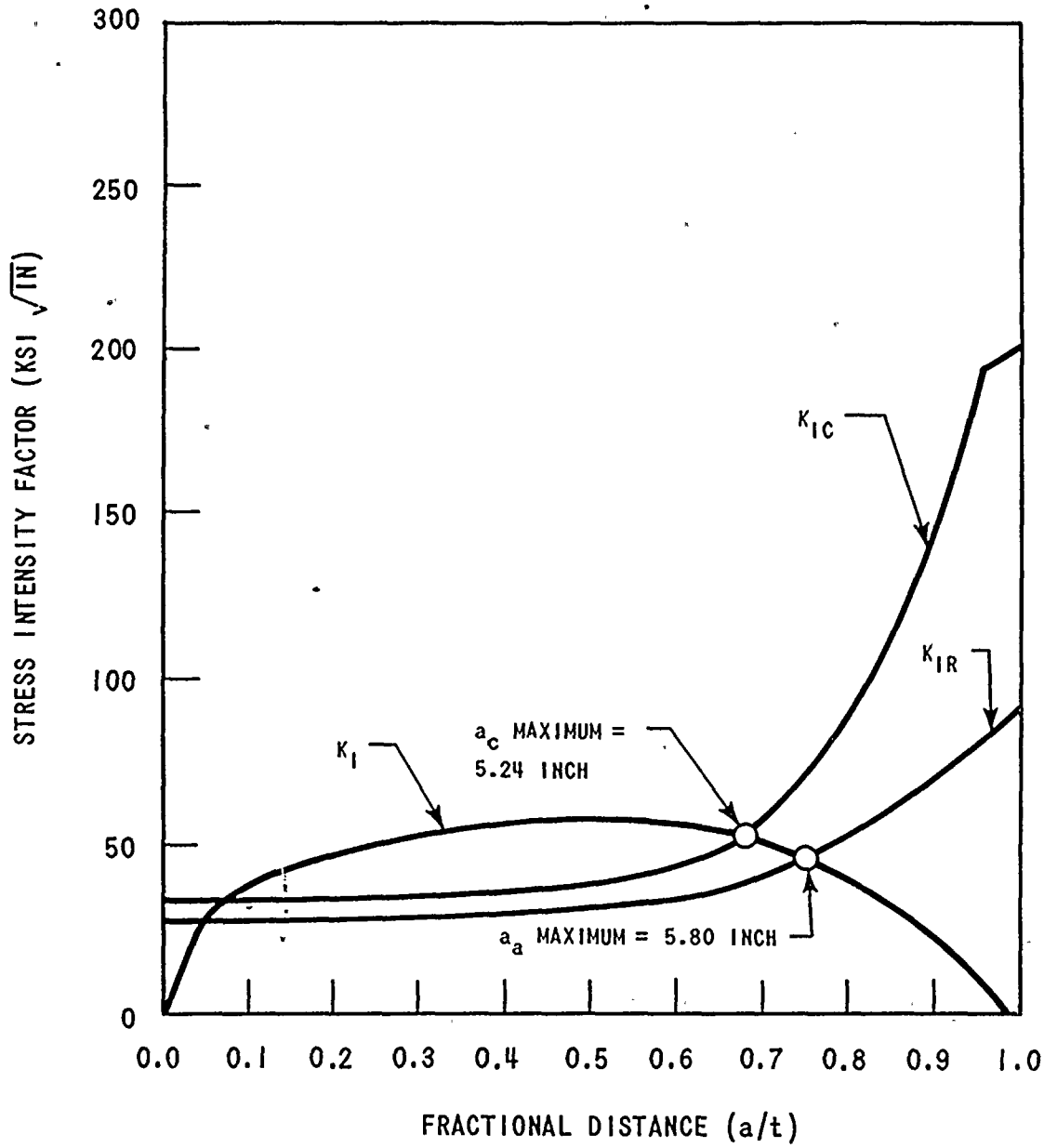

Figure 7-12. K_{IC}, K_{IR} and K_I After 2400 Seconds in LOCA (Circumferential Flaw, 26.25 Calendar Years, R.G. 1.99 Trend Curves)

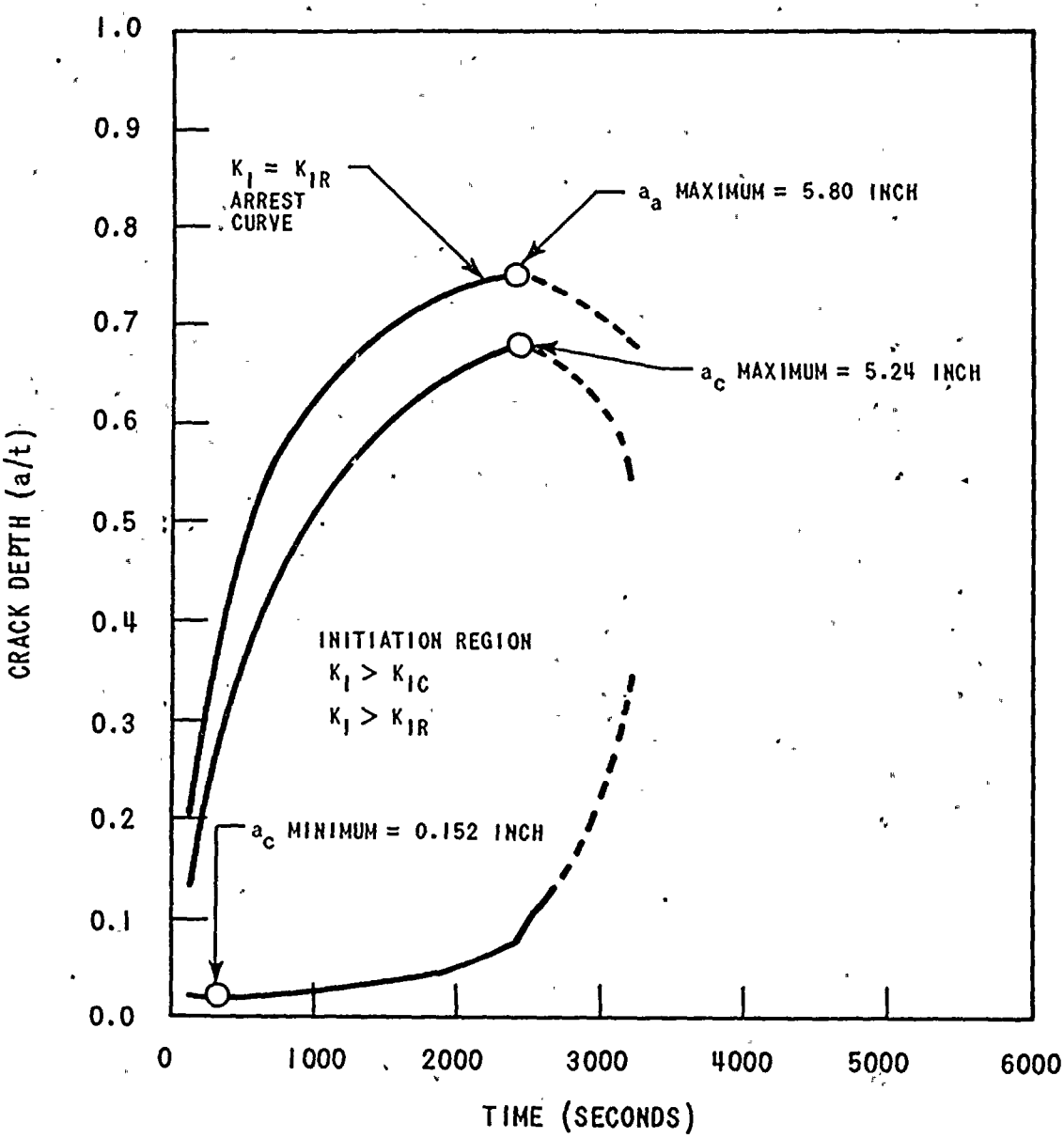

Figure 7-13. Circumferential Flaw Initiation Depth and Arrest Depth for the LOCA (26.25 Calendar Years, R.G. 1.99 Curves)

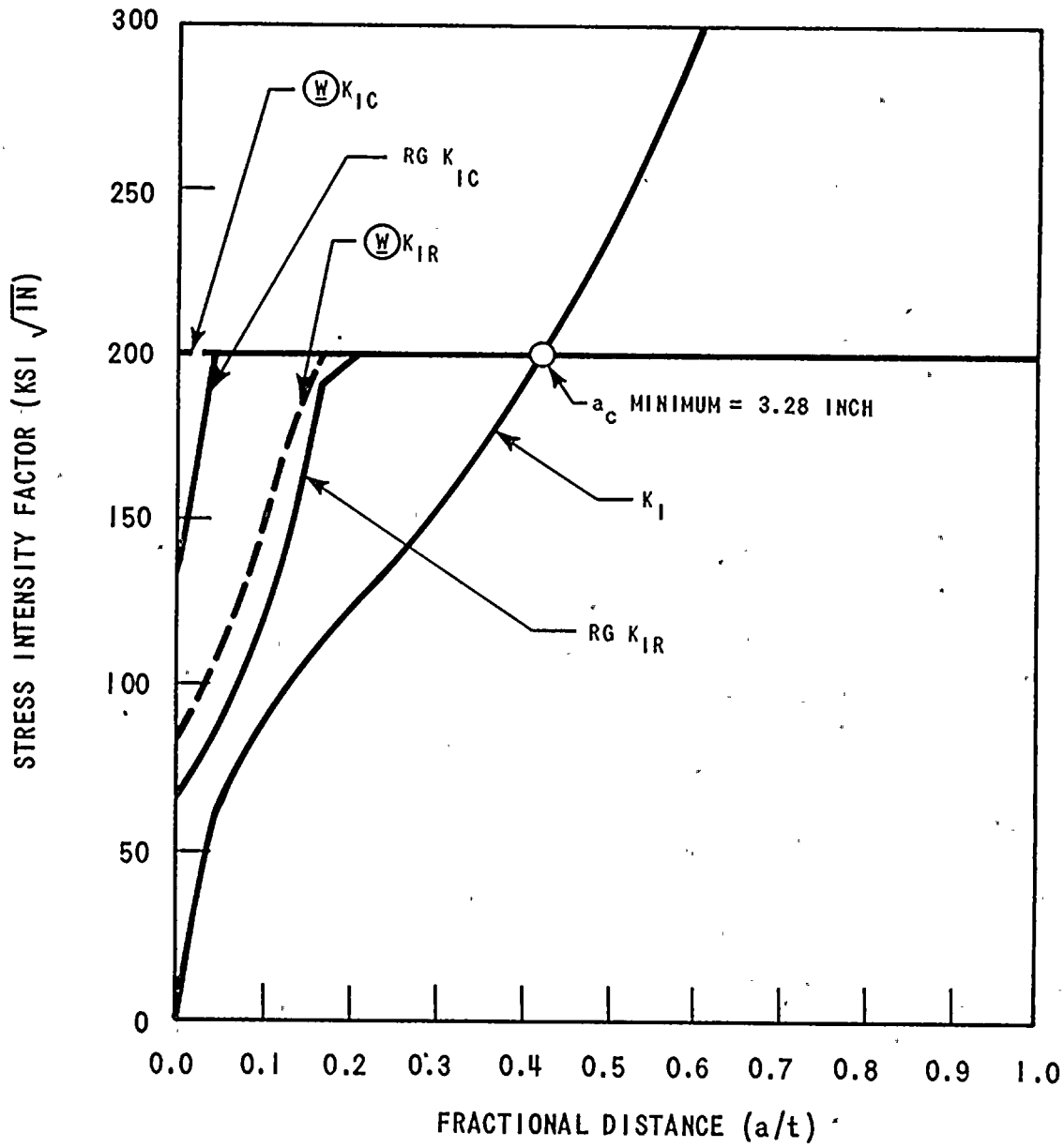

Figure 7-14. K_{IC}, K_{IR} and K_I after 600 Seconds in the LSB With Off-Site Power (Longitudinal Flaw, 40 Calendar Years, R.G. 1.99 and Westinghouse Trend Curves)

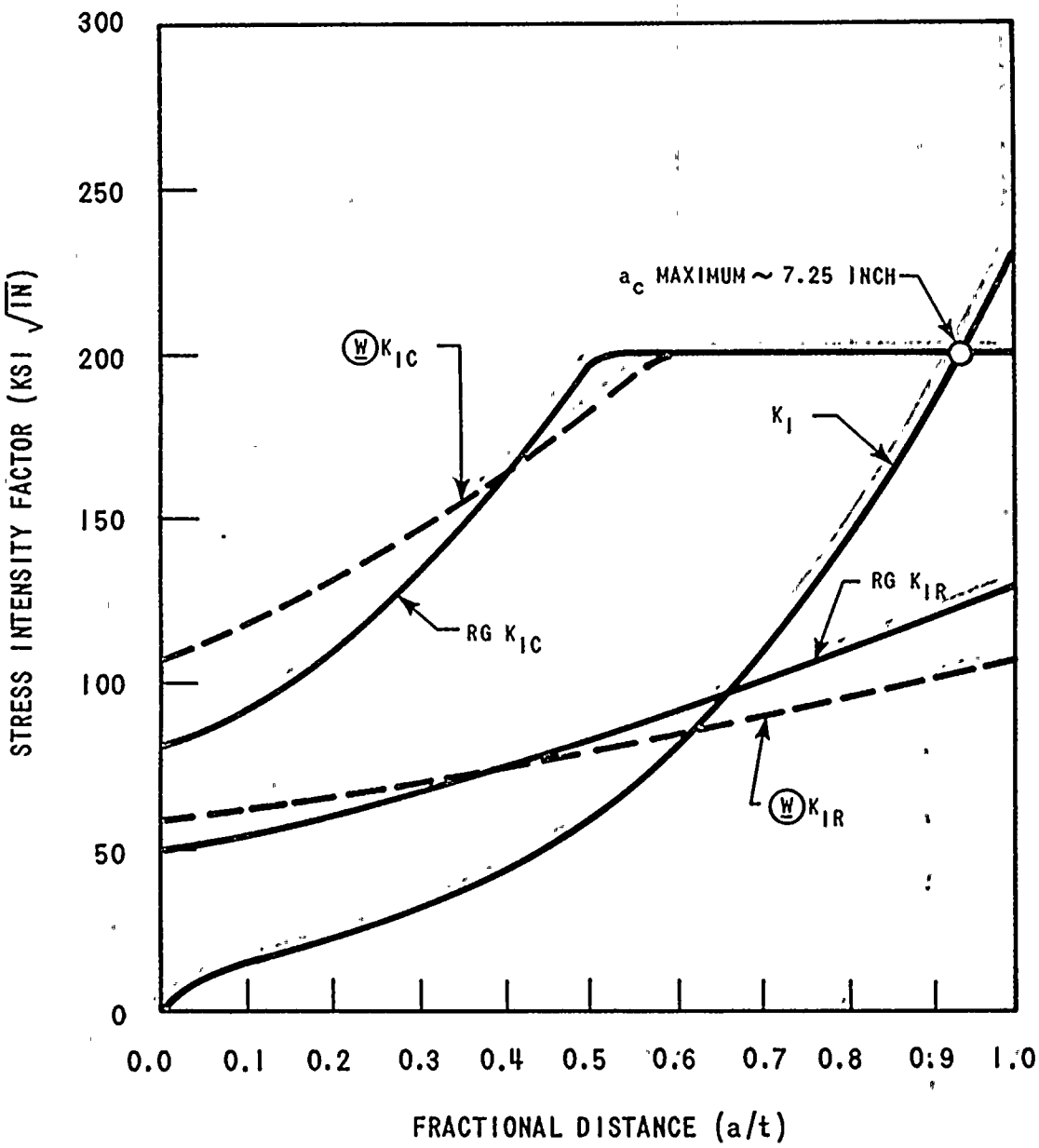

Figure 7-15. K_{IC}, K_{IR} and K_I after 6000 Seconds in the LSB With Off-Site Power (Longitudinal Flaw, 40 Calendar Years, Westinghouse and R.G. 1.99 Trend Curves)

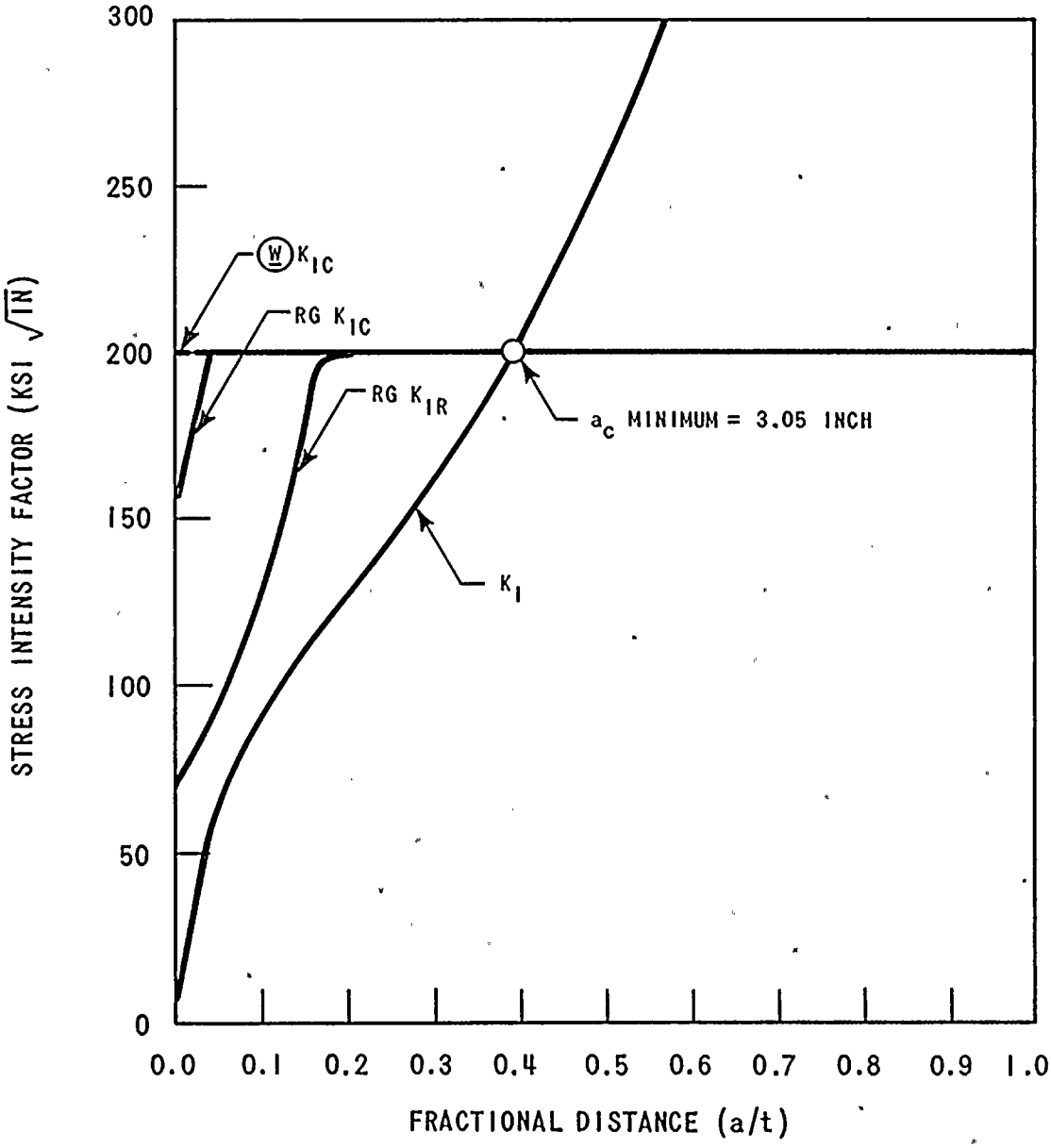

Figure 7-16. K_{IC}, K_{IR} and K_I After 600 Seconds in the LSB - Without Off-Site Power (Longitudinal Crack, 40 Calendar Years, Westinghouse and R.G. 1.99 Trend Curves)

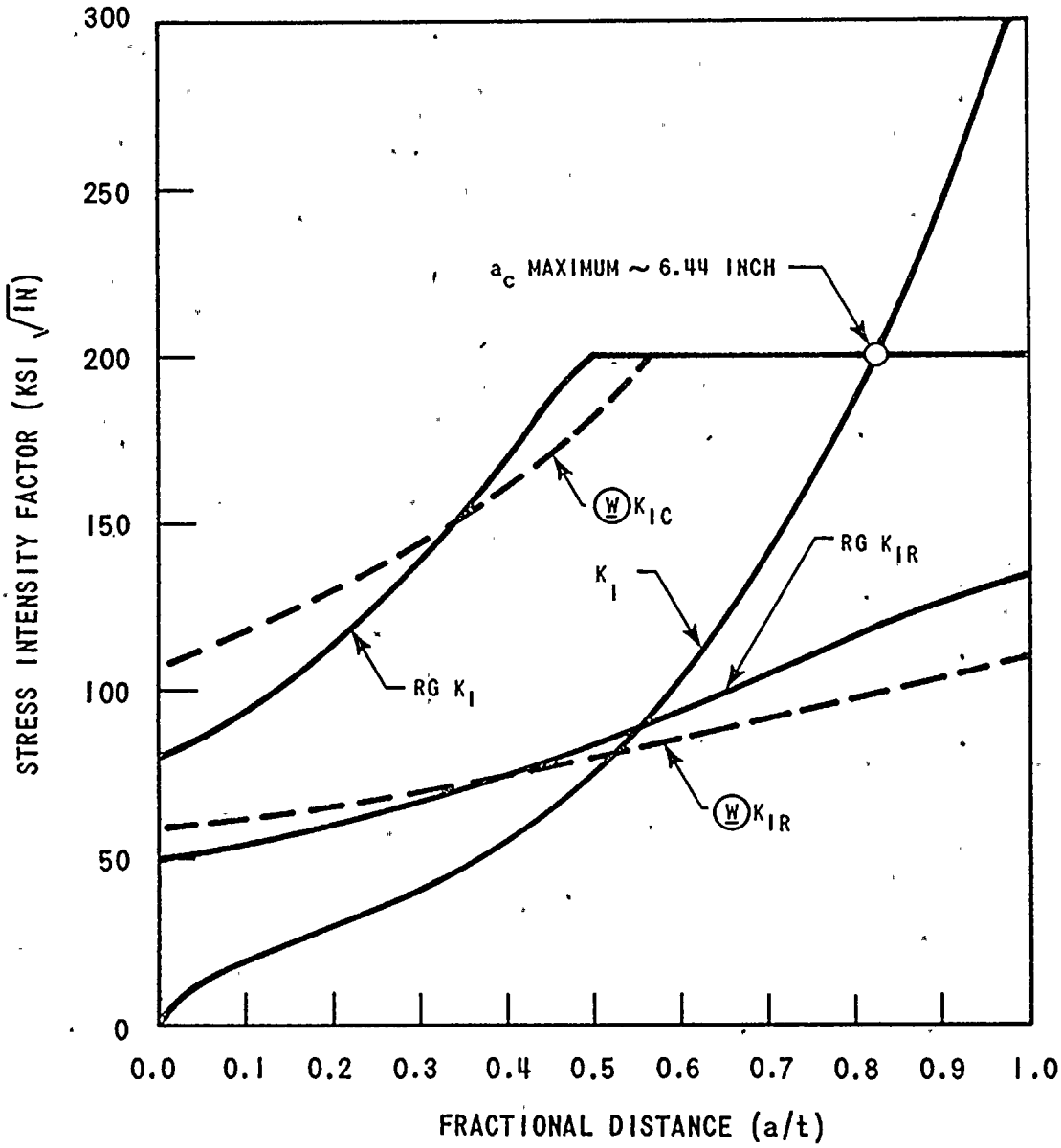

Figure 7-17. K_{IC}, K_{IR} and K_I After 6000 Seconds in the LSB - Without Off-Site Power (Longitudinal Flaw, 40 Calendar Years, Westinghouse and R.G. 1.99 Trend Curves)

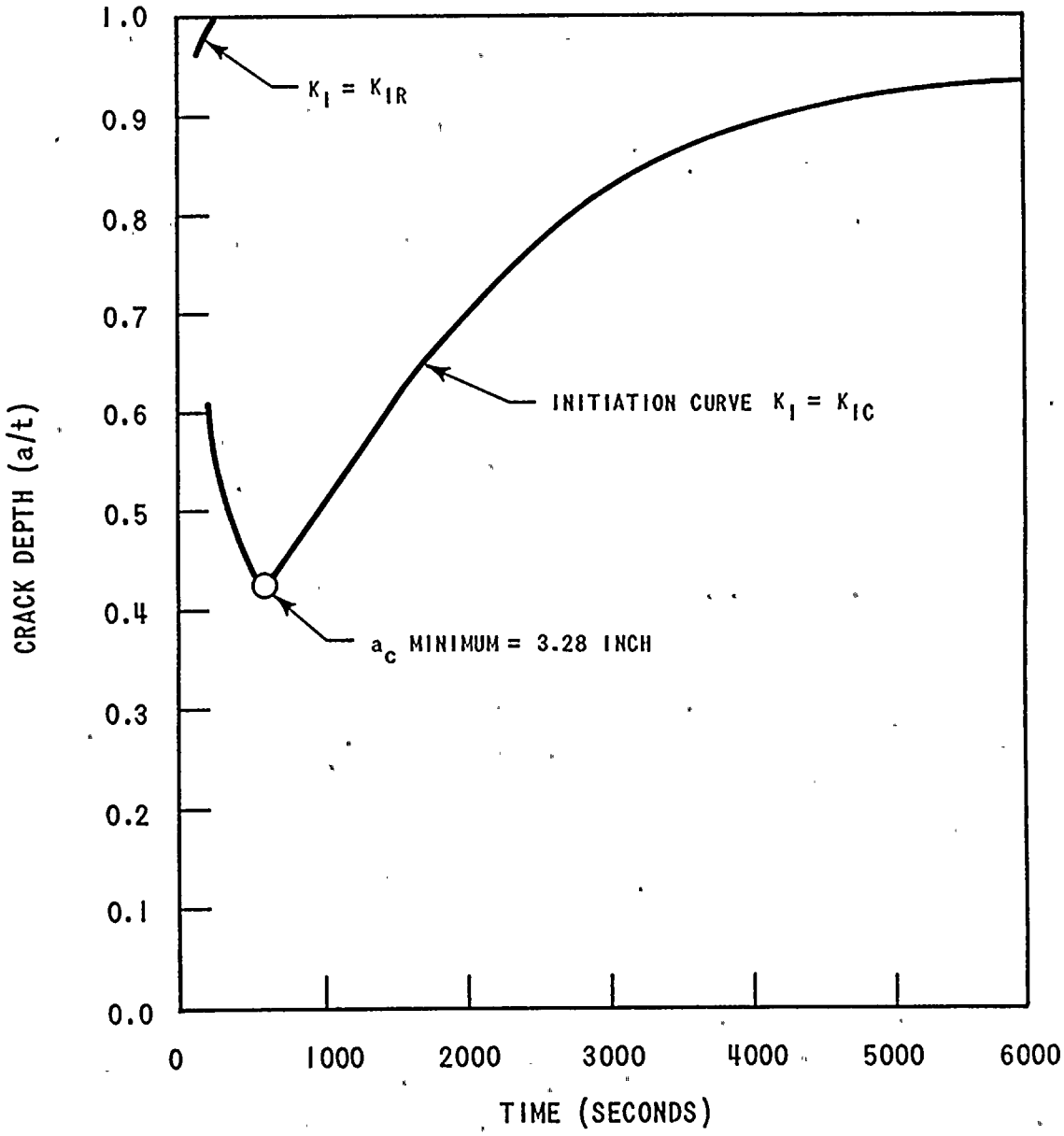

Figure 7-18. Longitudinal Flaw Initiation Depth and Arrest Depth for the LSB - With Off-Site Power (40 Calendar Years, Westinghouse and R.G. 1.99 Trend Curves).

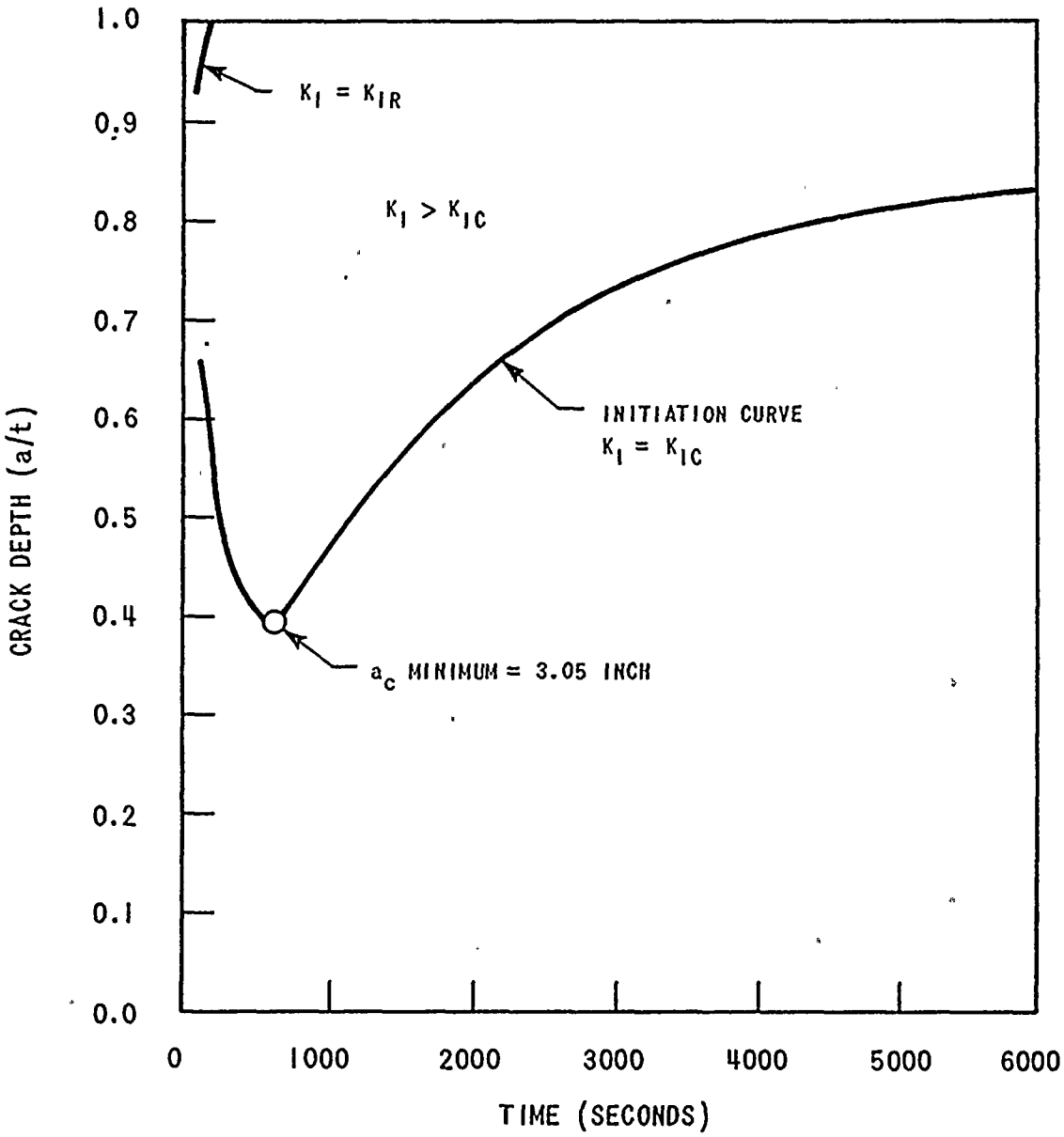

Figure 7-19. Longitudinal Flaw Initiation Depth and Arrest Depth for the LSB - Without Off-Site Power (40 Calendar Years, Westinghouse and R.G. 1.99 Trend Curves)

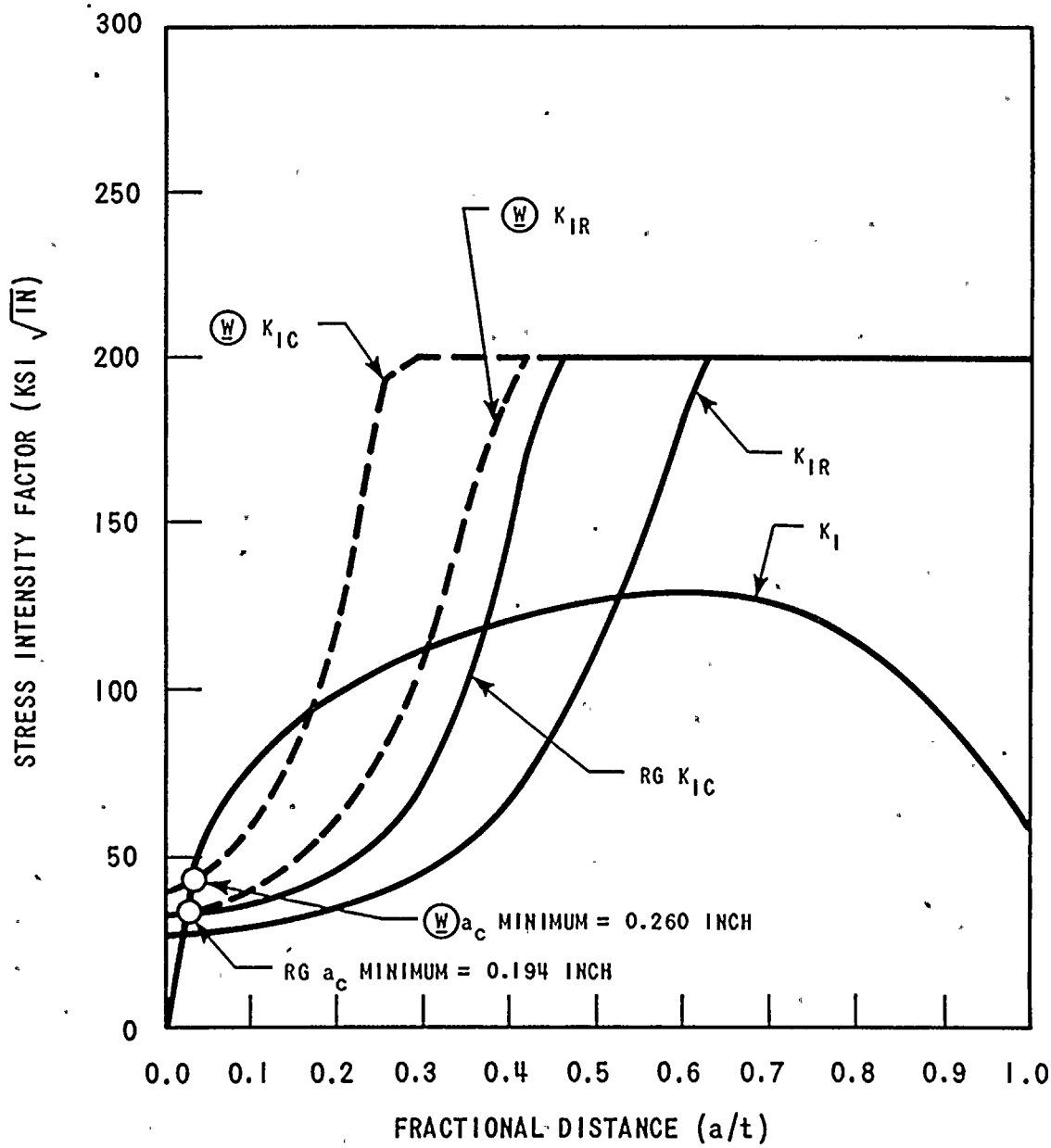

Figure 7-20. K_{IC}, K_{IR} and K_I After 600 Seconds in the LSB - With Off-Site Power (Circumferential Flaw, 40 Calendar Years, Westinghouse and R.G. 1.99 Trend Curves)

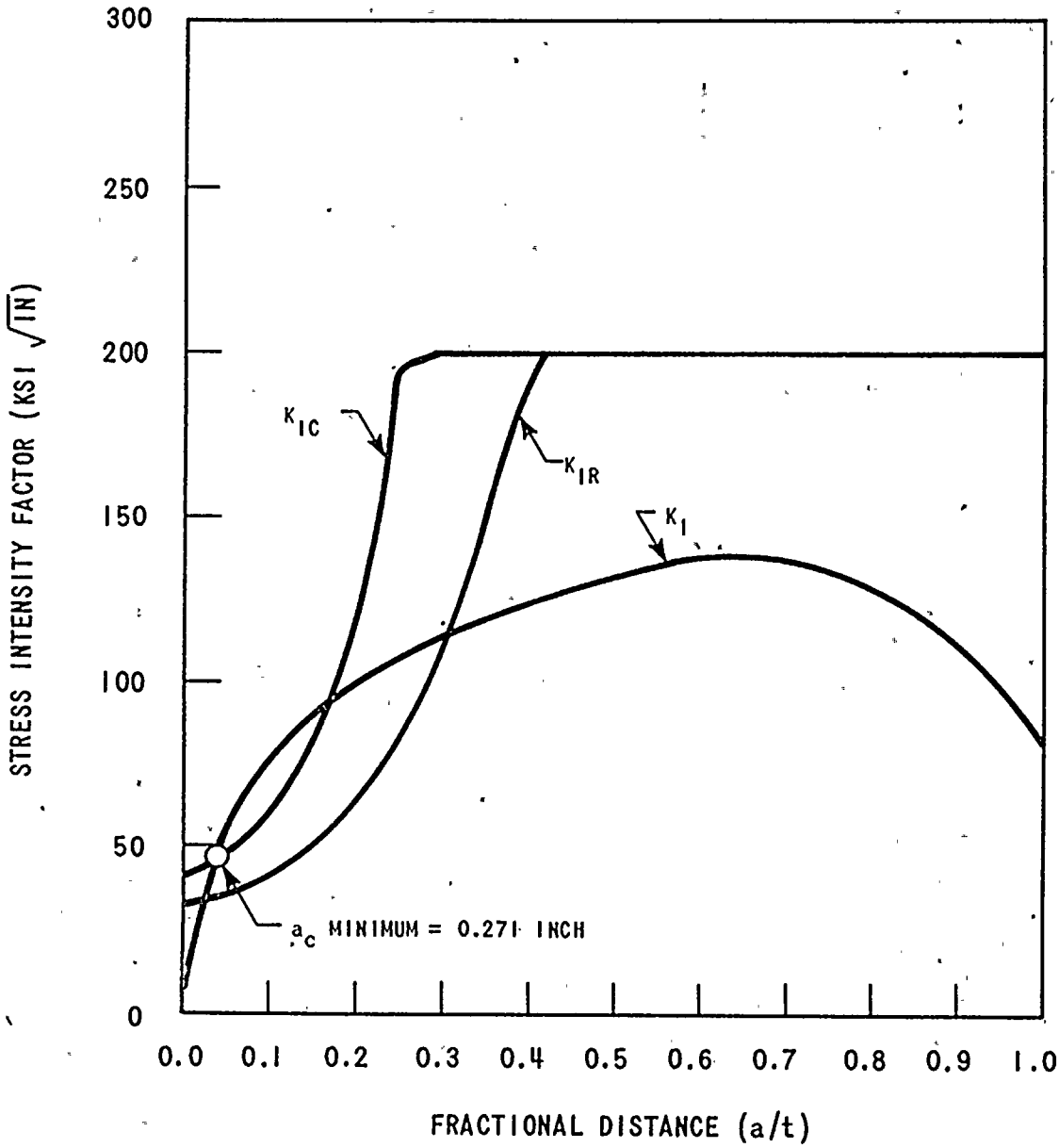

Figure 7-21. K_{IC}, K_{IR} and K_I After 600 Seconds in the LSB - Without Off-Site Power (Circumferential Flaw, 40 Calendar Years, Westinghouse Copper Trend Curves)

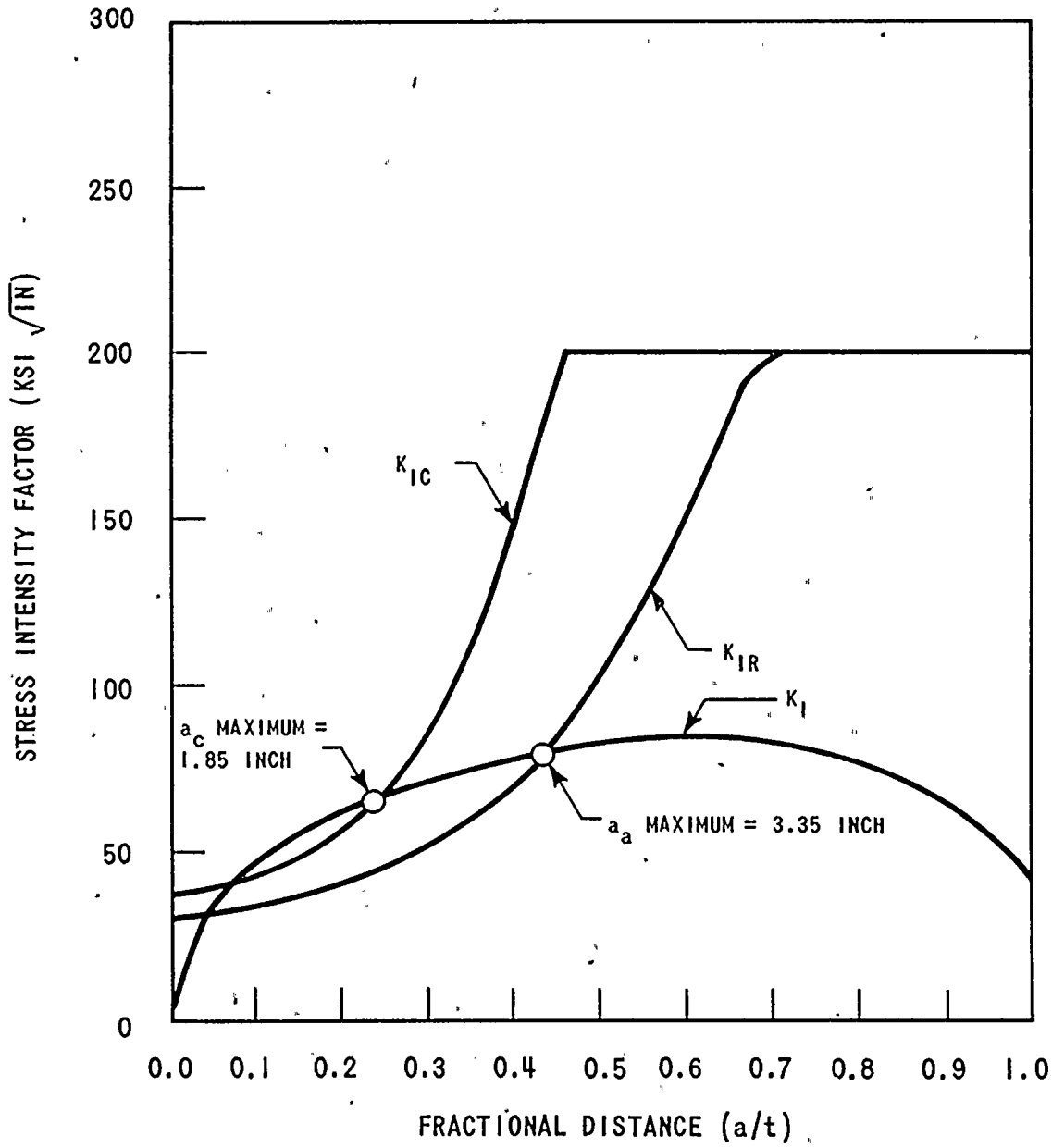

Figure 7-22. K_{IC}, K_{IR} and K_I After 1600 Seconds in the LSB - With Off-Site Power (Circumferential Flaw, 40 Calendar Years, Westinghouse Copper Trend Curves)

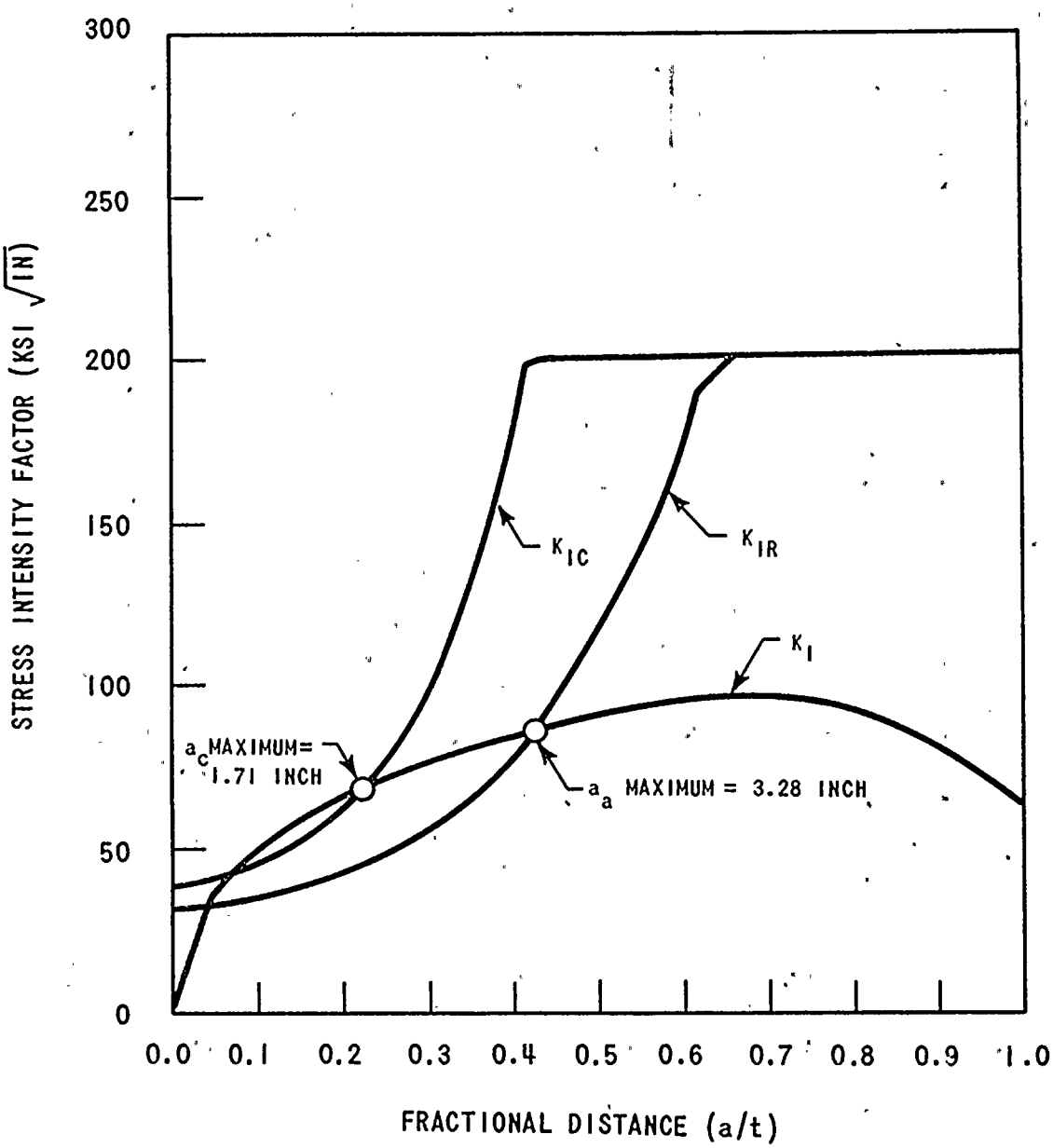

Figure 7-23. K_{IC}, K_{IR} and K_I After 1500 Seconds in the LSB - Without Off-Site Power (Circumferential Flaw, 40 Calendar Years, Westinghouse Copper Trend Curves)

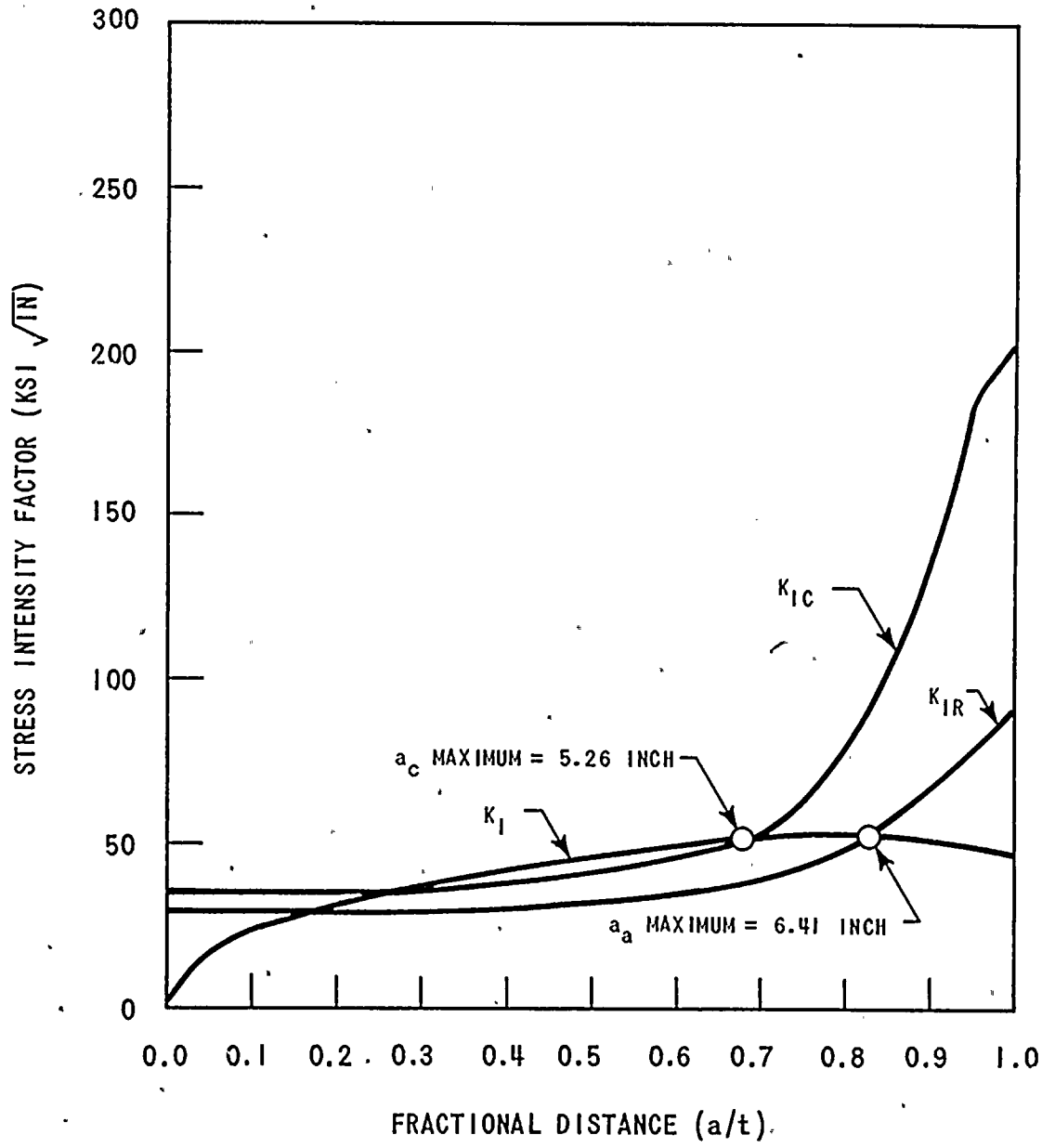

Figure 7-24. K_{IC}, K_{IR} and K_I After 3100 Seconds in the LSB - With Off-Site Power (Circumferential Flaw, 40 Calendar Years, R.G. 1.99 Trend Curves)

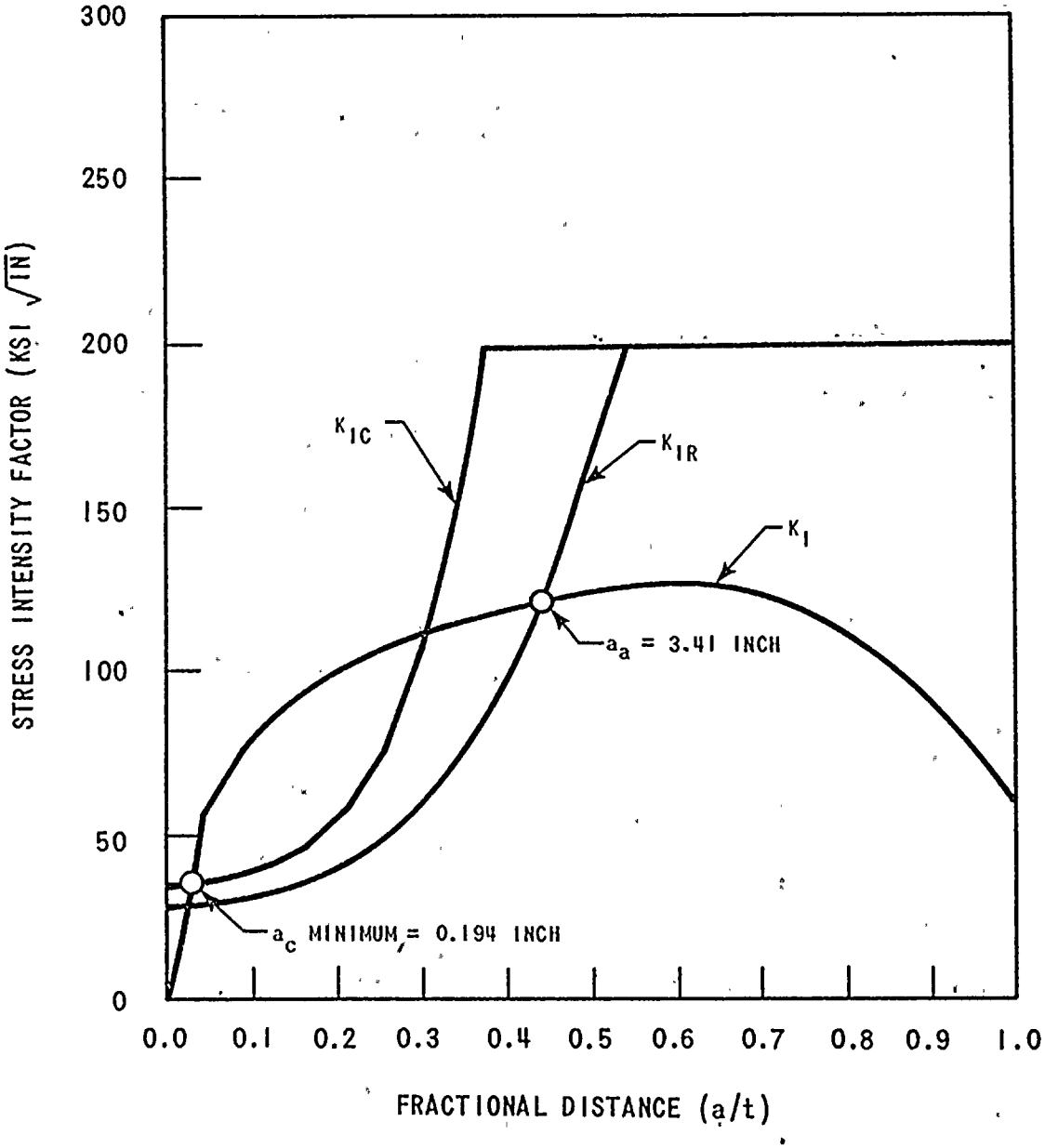

Figure 7-25. K_{IC}, K_{IR} and K_I After 400 Seconds in the LSB - Without Off-Site Power (Circumferential Flaw, 40 Calendar Years, R.G. 1.99 Trend Curves)

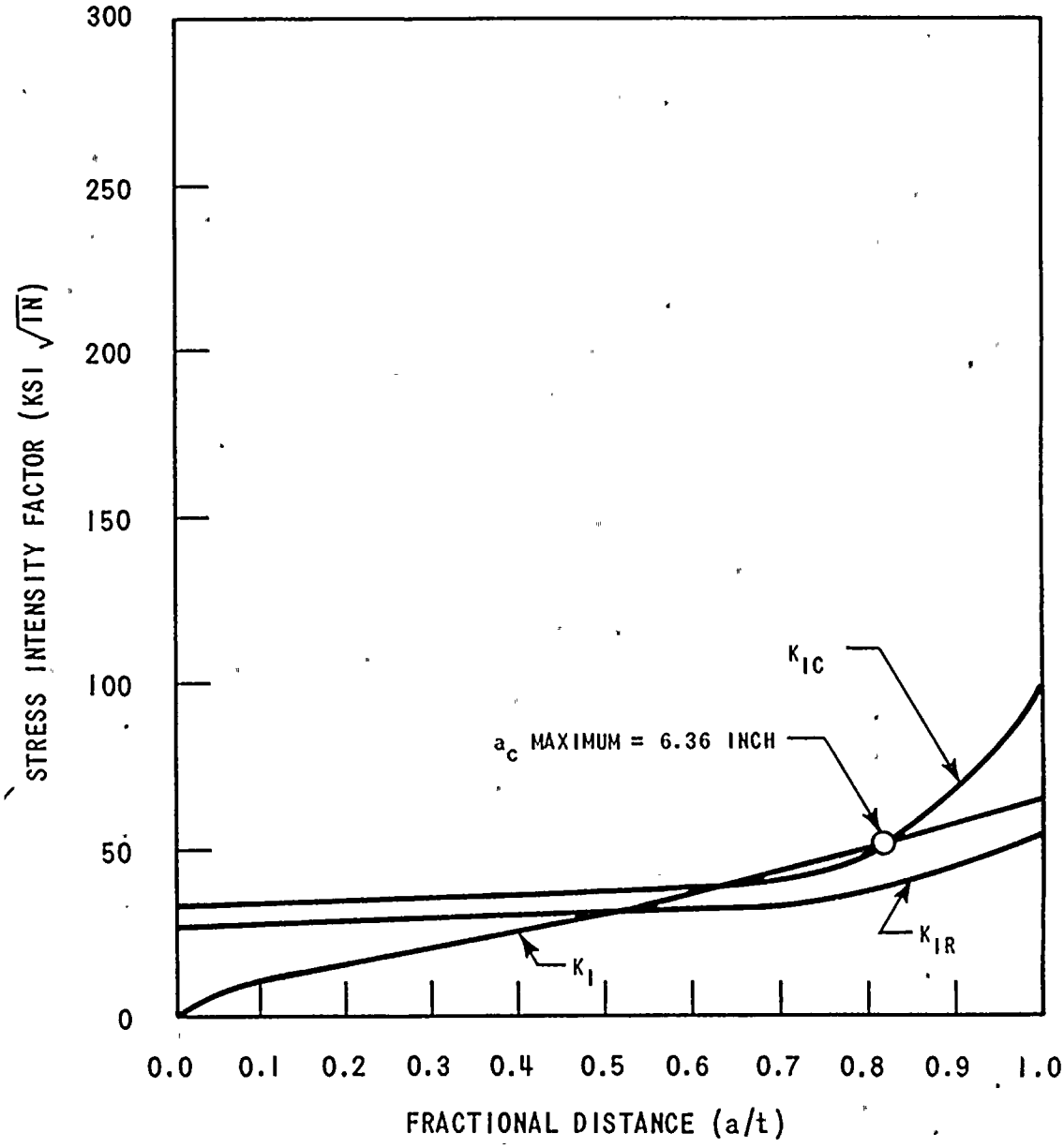

Figure 7-26. K_{IC}, K_{IR} and K_I After 6000 Seconds in the LSB - Without Off-Site Power (Circumferential Flaw, 40 Calendar Years, R.G. 1.99 Trend Curves)

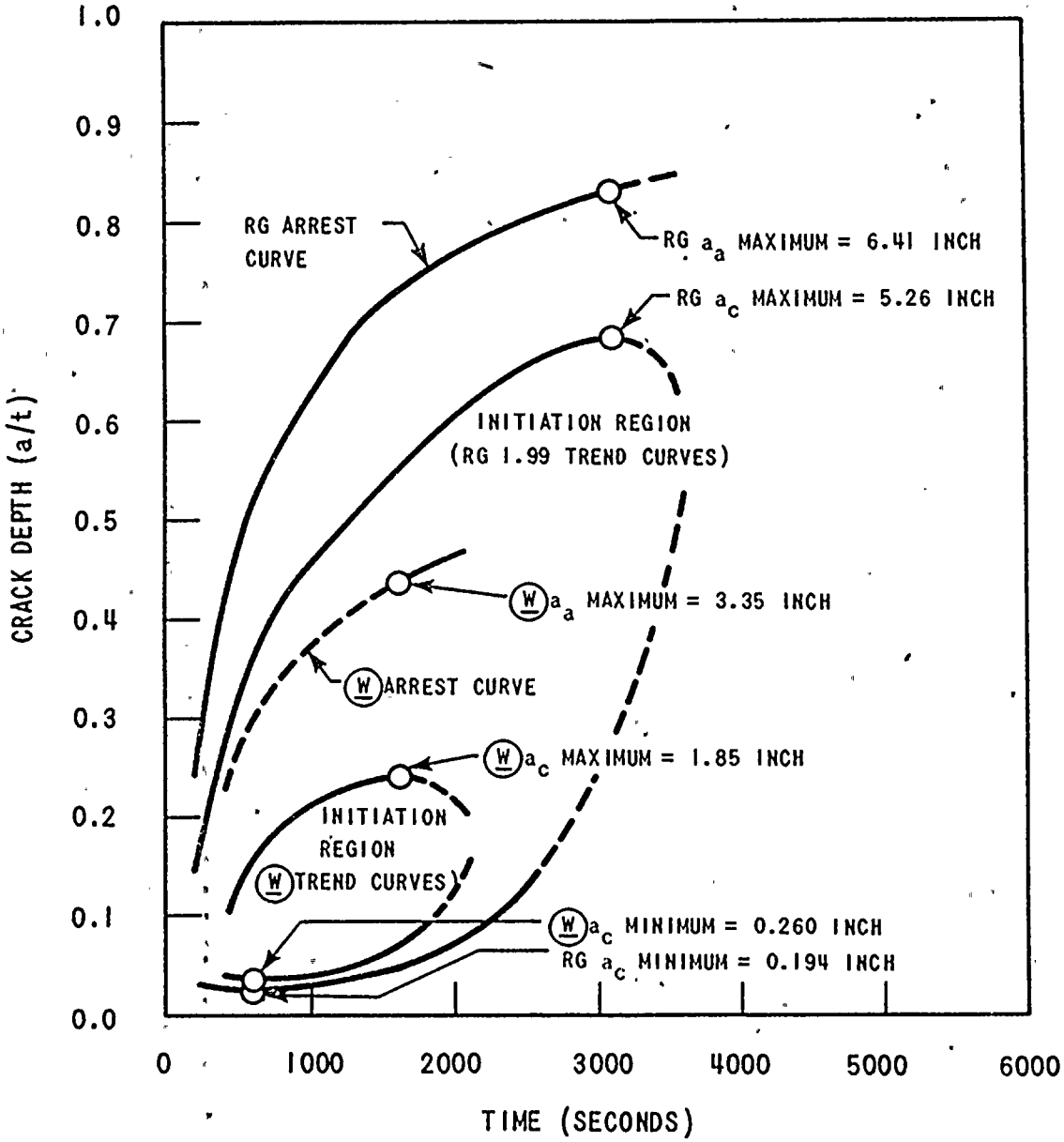

Figure 7-27. Circumferential Flaw Initiation Depth and Arrest Depth for the LSB - With Off-Site Power (40 Calendar Years, Westinghouse and R.G. 1.99 Trend Curves)

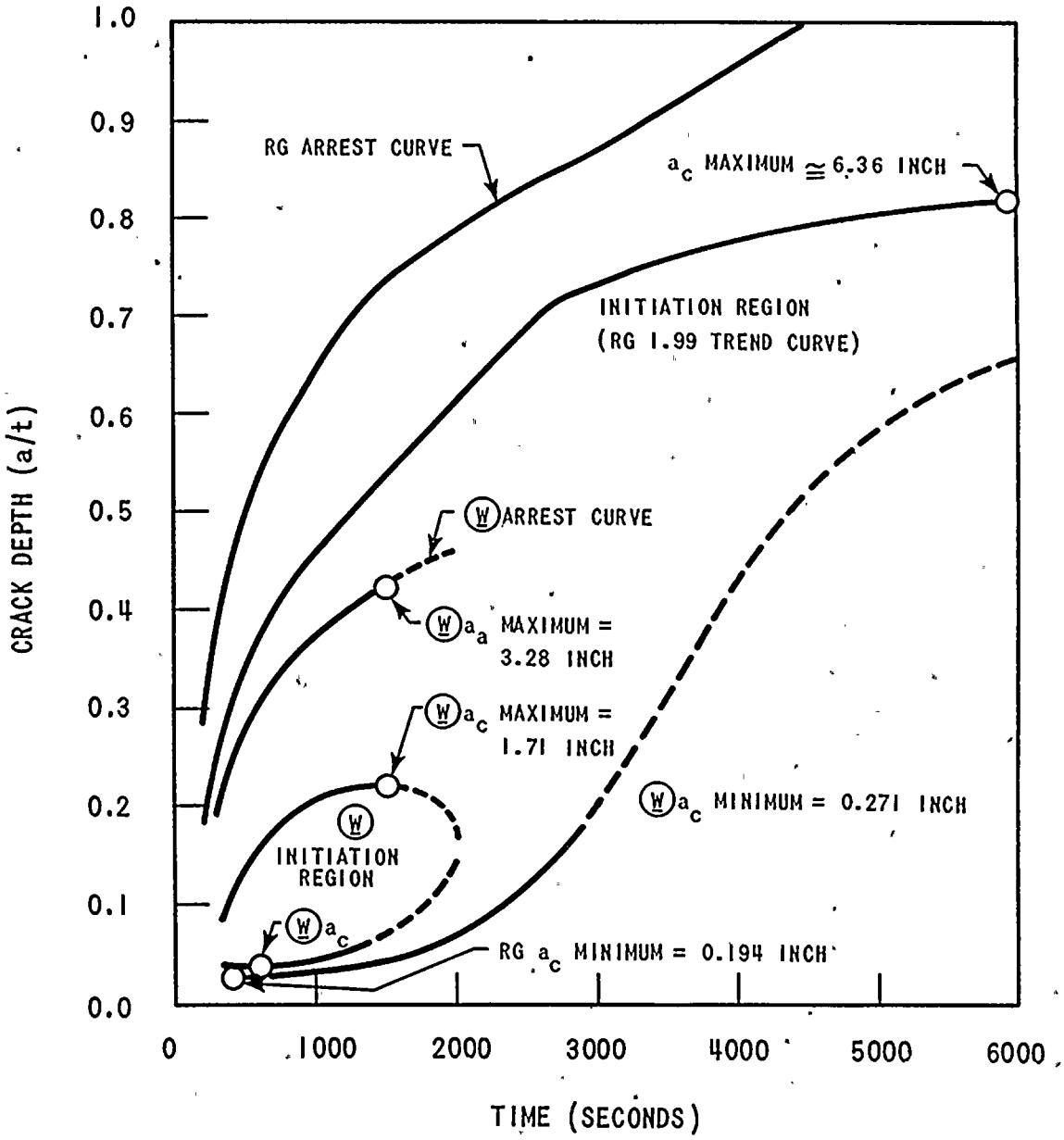

Figure 7-28. Circumferential Flaw Initiation Depth and Arrest Depth for the LSB - Without Off-Site Power (40 Calendar Years, Westinghouse and R.G. 1.99 Trend Curves)

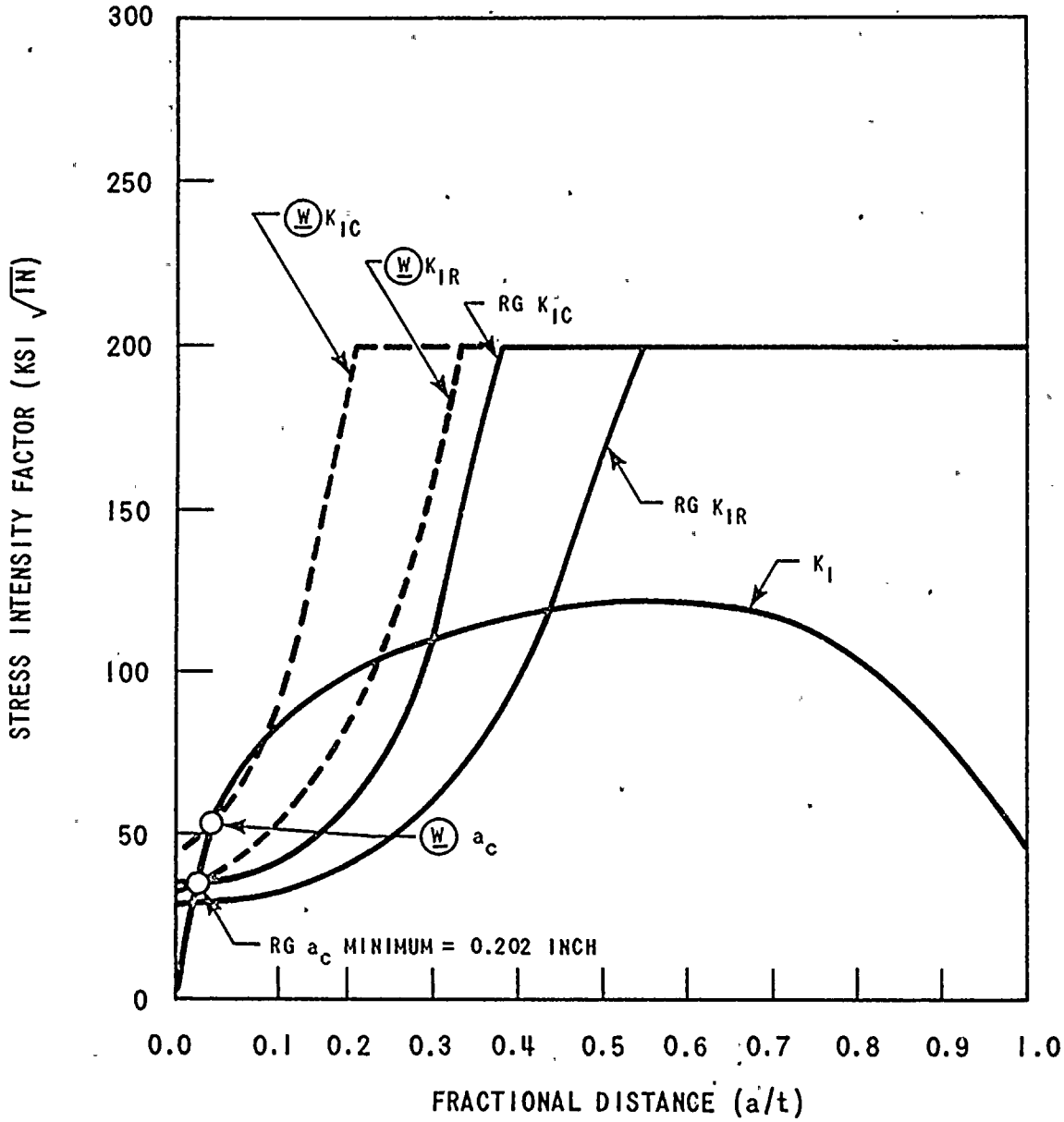

Figure 7-29. K_{IC}, K_{IR} and K_I After 500 Seconds in the LSB - With Off-Site Power (Circumferential Crack, 31.25 Calendar Years, Westinghouse and R. G. 1.99 Trend Curves)

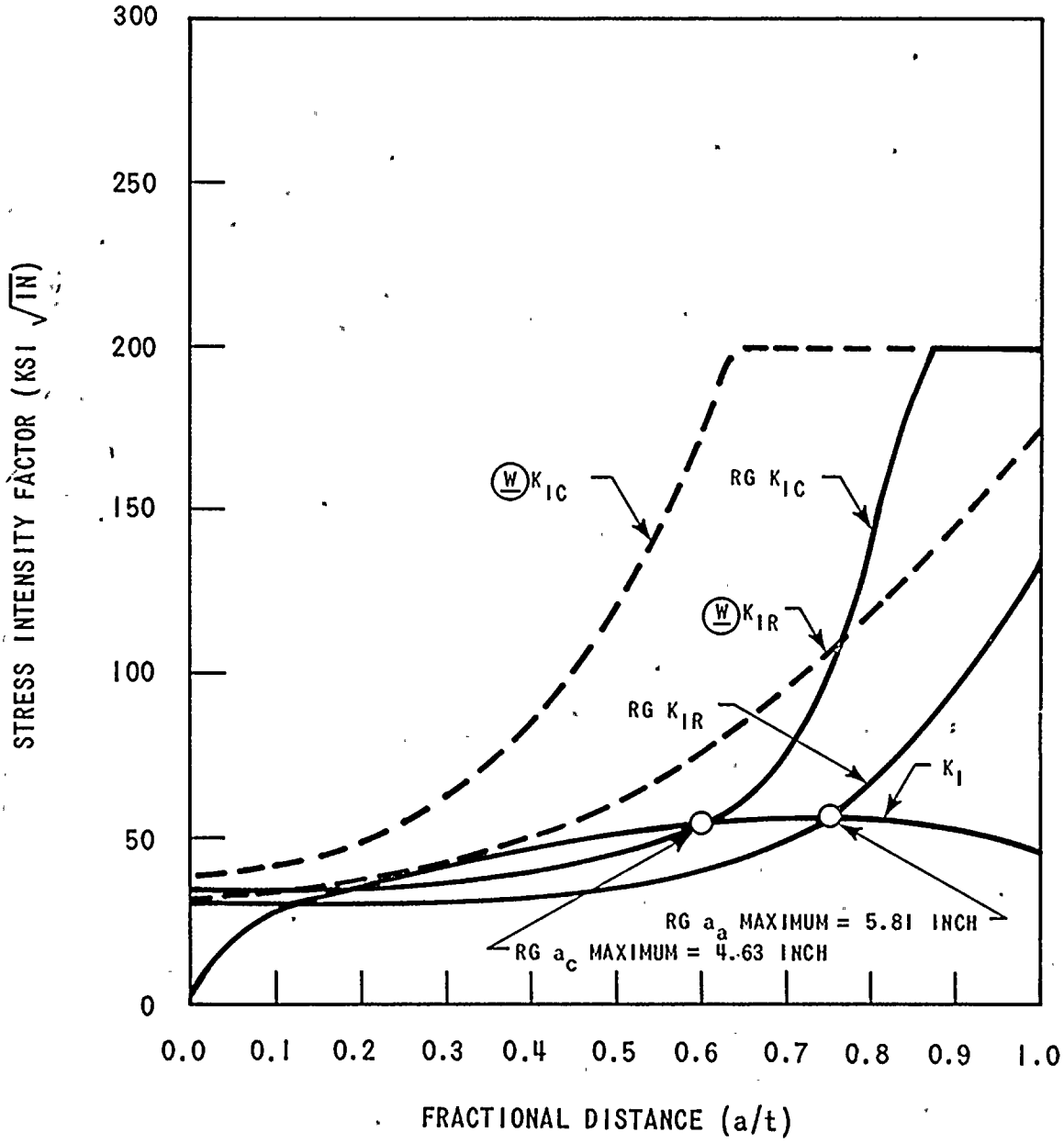

Figure 7-30. K_{IC}, K_{IR} and K_I After 2800 Seconds in the LSB - With Off-Site Power (Circumferential Flaw, 31.25 Calendar Years, Westinghouse and R. G. 19

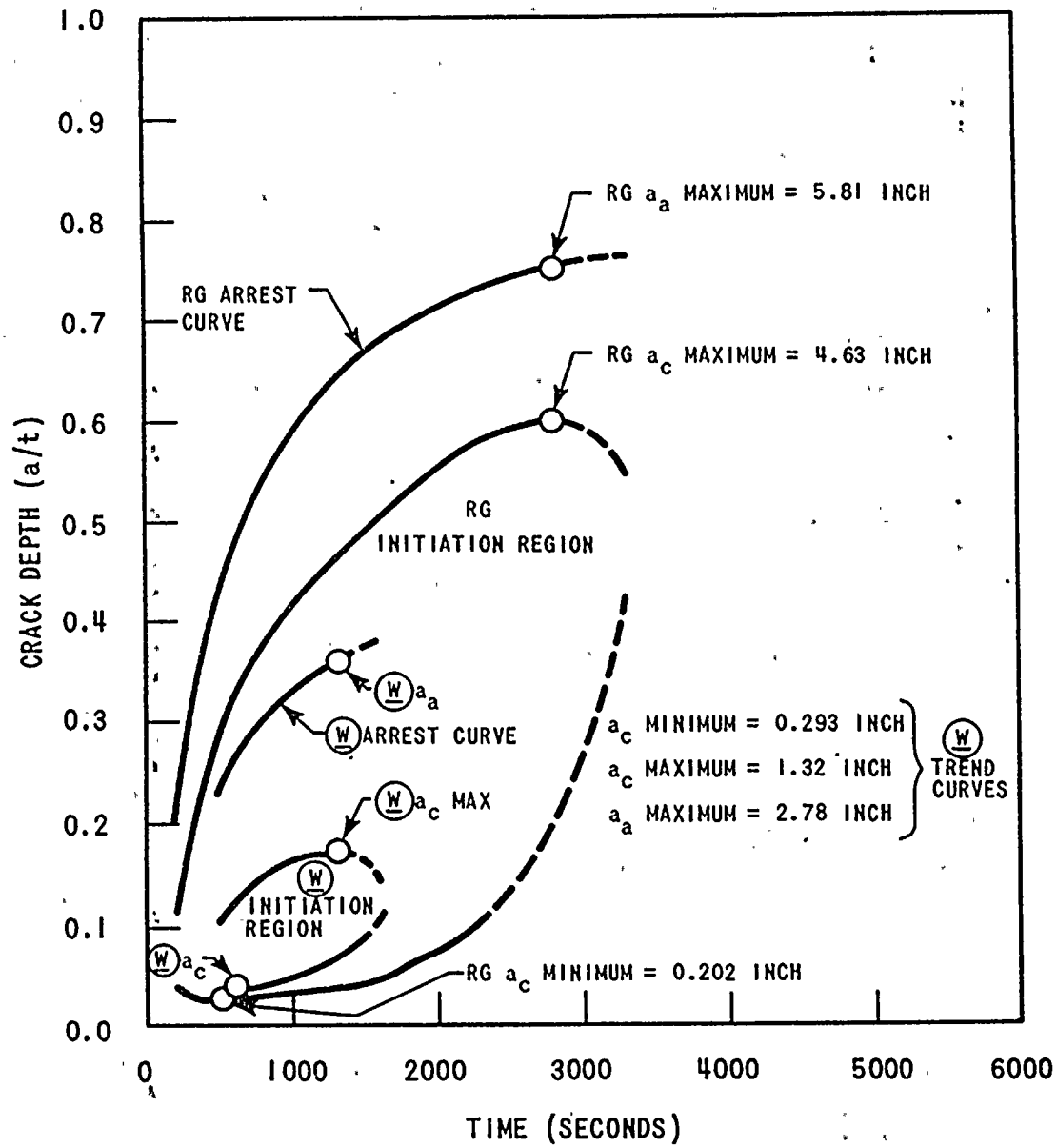

Figure 7-31. Circumferential Flaw Initiation Depth and Arrest Depth for the LSB - With Off-Site Power (31.25 Calendar Years, Westinghouse and R.G. 1.99 Trend Curves)

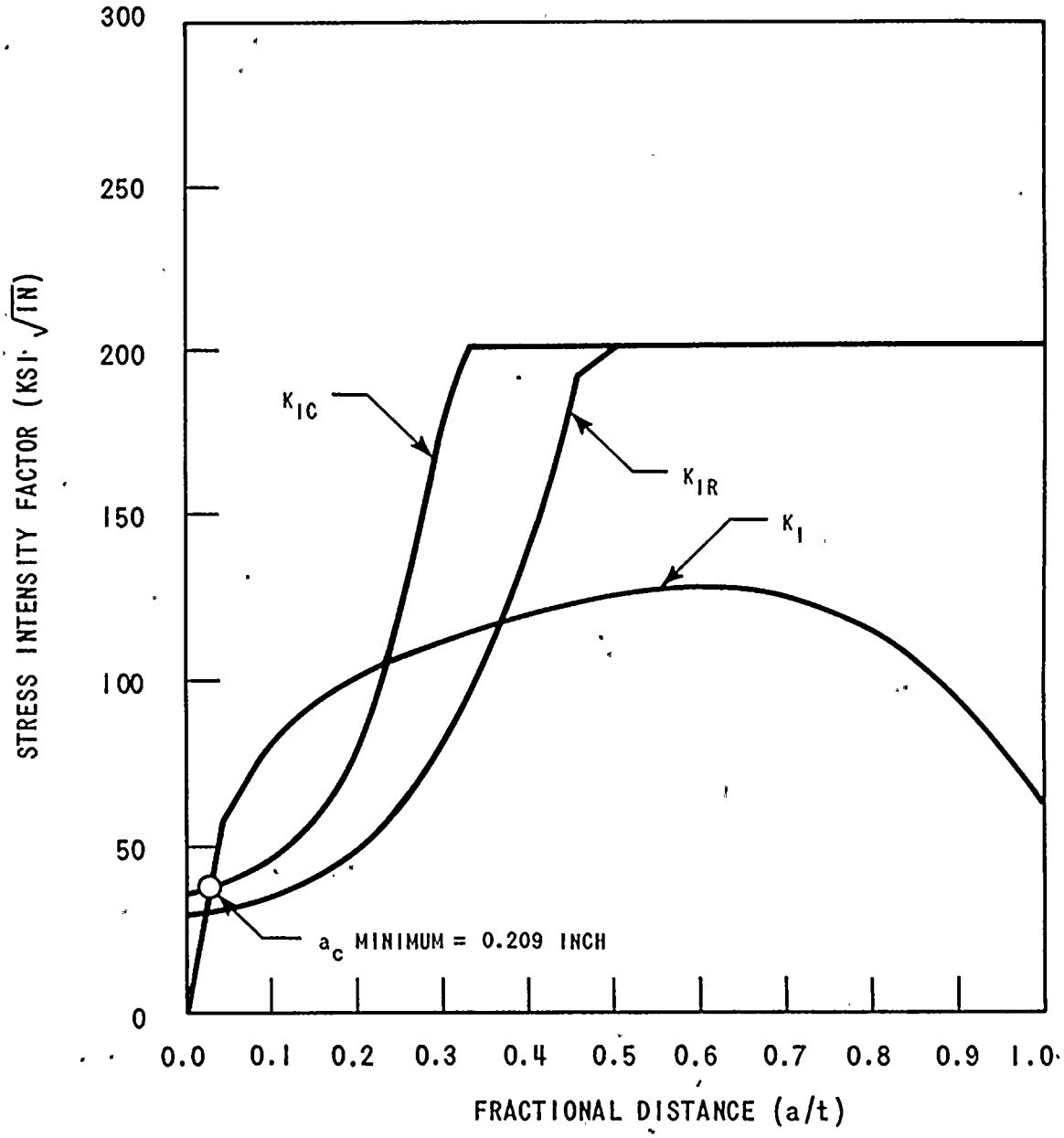

Figure 7-32. K_{IC}, K_{IR} and K_I After 400 Seconds in the LSB - Without Off-Site Power (Circumferential Flaw, 25 Calendar Years, R.G. 1.99 Trend Curves)

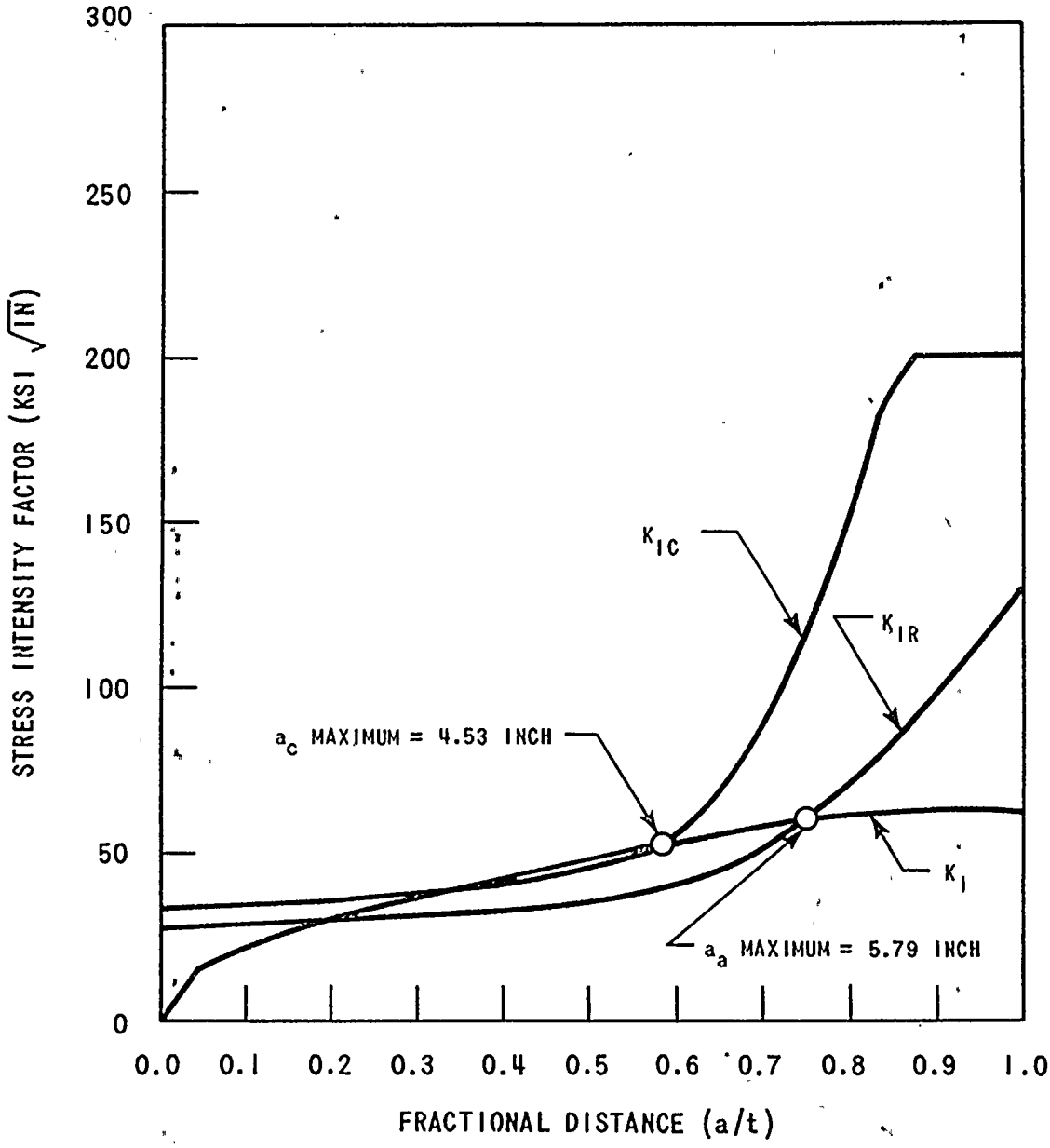

Figure 7-33. K_{IC}, K_{IR} and K_I After 3300 Seconds in the LSB - Without Off-Site Power (Circumferential Flaw, 25 Calendar Years, R.G. 1.99 Trend Curves)

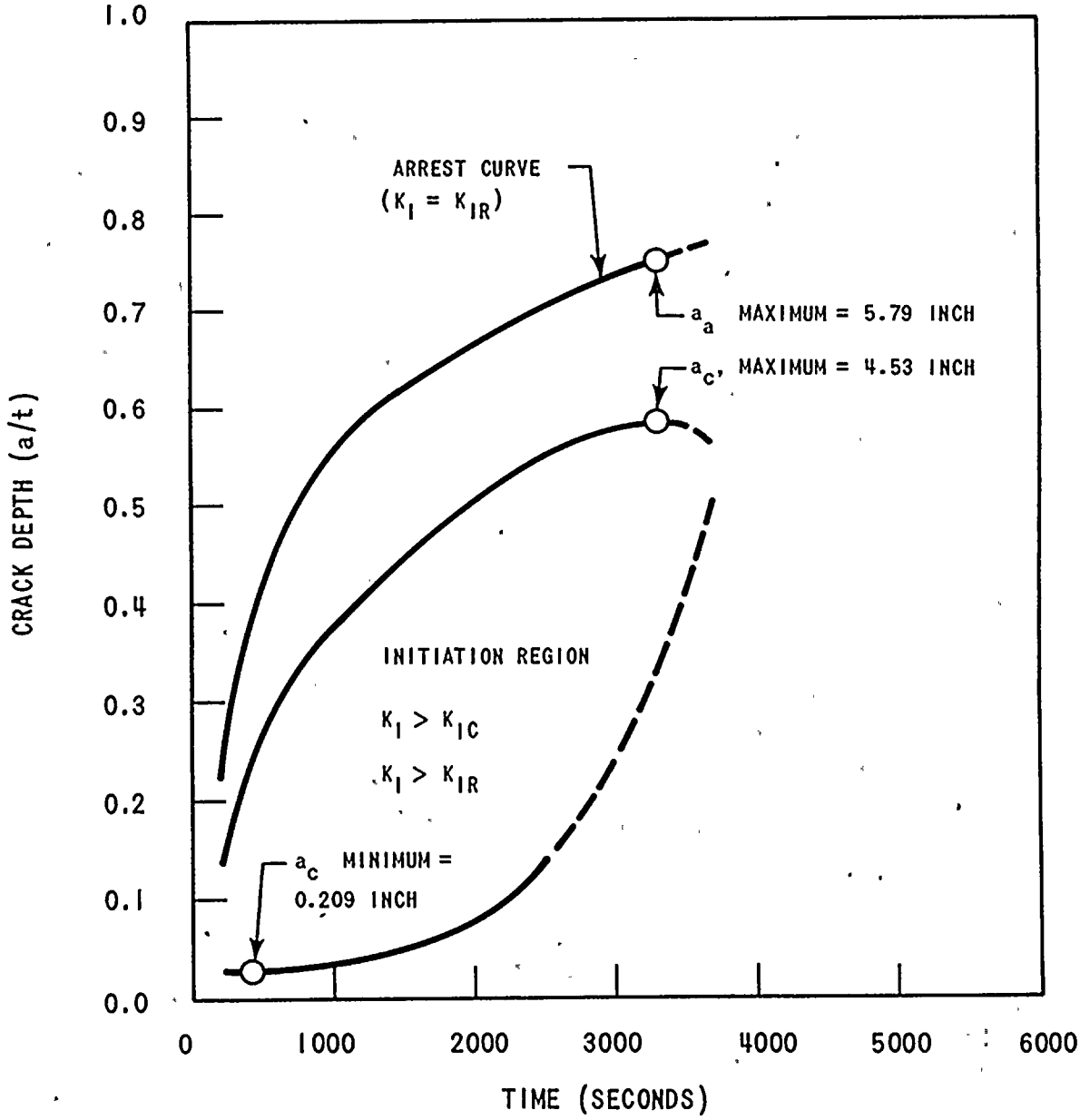

Figure 7-34. Circumferential Crack Initiation Depth and Arrest Depth for the LSB -- Without Off-Site Power (25 Calendar Years, R.G. 1.99 Trend Curves)

APPENDIX A

The results documented in this report for the circumferential weldment are equally applicable to the Turkey Point Unit No. 3 because (1) the properties and the thermal and irradiation conditions are identical as explained previously in section 6 and (2) the LOCA and LSB transients are the same for both units[1].

The limiting initial RT_{NDT} and the copper content of the Turkey Point Unit No. 3 base material differ slightly from the corresponding values for Unit No. 4 (40°F and 0.07 wt-% versus 50°F and 0.054 wt-%.) Therefore, the results for the longitudinal flaw contained herein are applicable to Turkey Point Unit No. 3 only for those cases where the critical crack depths (initiation and/or arrest) have been determined from intersections of the K_I curves with the uppershelf of the K_{IC}, K_{IR} curves.

This report also updates, within the limits outlined before, the results documented in WCAP-8580, "Fracture Mechanics Evaluation of Florida Power and Light Turkey Point Unit No. 3 Reactor Vessel" by J. H. Phillips, et. al., November 1975.

Letter FAII-440, 10-25-76, from P. J. Morris, PWRSD, Functional Analysis II, to O. Meeuwis, PWRSD Structural Materials Engineering.

WCAP-8912

WESTINGHOUSE CLASS 3

CUSTOMER-DESIGNATED DISTRIBUTION

ASME III, APPENDIX G ANALYSIS OF THE FLORIDA POWER AND LIGHT COMPANY TURKEY POINT UNITS NO. 3 AND NO. 4 REACTOR VESSEL

P. J. Fields

June 1977

Prepared by Westinghouse for the Florida Power and Light Company

APPROVED: J. N. Chirigos
J. N. Chirigos, Manager
Structural Materials Engineering

Work Performed Under EKDP-100

Although the information contained in this report is nonproprietary, no distribution shall be made outside Westinghouse or its Licensees without the customer's approval.

WESTINGHOUSE ELECTRIC CORPORATION
Nuclear Energy Systems
P. O. Box 355
Pittsburgh, Pennsylvania 15230

PREFACE

This report has been technically reviewed and the calculations checked.

W. K. Ma

TABLE OF CONTENTS

Section	Title	Page
1	INTRODUCTION	1-1
	1-1. Background	1-1
	1-2. Summary of Analytical Results	1-3
2	ANALYSIS	2-1
	2-1. Determination of the K_{IR} Curve	2-1
	2-2. Typical K_{IR} Curve	2-1
	2-3. Irradiation Effects on the K_{IR} Curve	2-1
	2-4. K_{IR} Curves for the Four Critical Locations	2-3
	2-5. Maximum Postulated Defects	2-9
	2-6. Formulation of the Stress Intensity Factor, K_I	2-9
	2-7. General Formula for K_I	2-9
	2-8. K_I Determined for 1/4-Thickness Flaw	2-11
	2-9. K_I Determined for 1/5-Thickness Flaw	2-12
	2-10. Numerical Calculations of K_I	2-18
	2-11. Comparison of the Combined Stress Intensity Factors with K_{IR} Curves	2-18
	2-12. Transients	2-30
	2-13. Maximum Combined K_I Values	2-30
	2-14. K_I Values	2-30
	2-15. Conservatism of the Analysis	2-30
	2-16. Safety Factors	2-30
	2-17. K_{Ia} Values Included	2-30
	2-18. Flat Plate Assumed	2-38
	2-19. Stresses Assumed Linear	2-38
	2-20. Largest ΔRT_{NDT}	2-38
	2-21. Negative Stresses Not Deduced	2-38

TABLE OF CONTENTS (cont)

Section	Title	Page
3	CONCLUSIONS	3-1
4	REFERENCES	4-1
Appendix A	FRACTURE TOUGHNESS VALUES	A-1
	REFERENCES TO APPENDIX A	A-5

LIST OF ILLUSTRATIONS

Figure	Title	Page
1-1	Critical Locations of the Pressurized Water Reactor Vessel	1-2
2-1	K_{IR} Reference Stress Intensity Factor Curve	2-2
2-2	Effects of Fluence and Copper Content on ΔRT_{NDT} for Reactor Vessel Steels Exposed to Irradiation at 550°F	2-4
2-3	Effect of Fluence, Copper Content, and Phosphorous Content on ΔRT_{NDT} for Reactor Vessel Steels per Regulatory Guide 1.99 (January 1976)	2-5
2-4	Longitudinal Distance versus Multiplying Factor for Peak Fluence	2-6
2-5	Reference Flaw (Appendix G)	2-10
2-6	M_m, M_b versus $\sqrt{\text{Thickness}}$ Curve	2-13
2-7	Q versus $\left(\frac{a}{\sigma_y}\right)$ Curve	2-15
2-8	M_K versus $\left(\frac{a}{T}\right)$ Curve	2-16
2-9	A_b versus $\left(\frac{a}{T}\right)$ Curve	2-17
2-10	Upper Head Region	2-19
2-11	Outlet Nozzle Region	2-20
2-12	Beltline and Lower Head Regions	2-21
2-13	Linearized Representation of Stresses	2-27
2-14	K_{IR} versus Temperature Curve for Upper Head Junction	2-32
2-15	K_{IR} versus Temperature Curve for Outlet Nozzle Junction	2-33
2-16	K_{IR} versus Temperature Curve for Beltline (Longitudinal Flaw)	2-34
2-17	K_{IR} versus Temperature Curve for Beltline (Circumferential Flaw)	2-35
2-18	K_{IR} versus Temperature Curve for Lower Head Junction	2-36
A-1	Instrumented Precracked Charpy Test Results	A-2
A-2	Irradiated Dynamic Fracture Toughness Results	A-4

LIST OF TABLES

Table	Title	Page
2-1	Turkey Point Unit No. 3 Reactor Vessel Material Data	2-7
2-2	Turkey Point Unit No. 4 Reactor Vessel Material Data	2-8
2-3	Stress and K_I Data for the Upper Head Junction	2-22
2-4	Stress and K_I Data for the Outlet Nozzle Junction	2-23
2-5	Hoop Stress and K_I Data for the Beltline	2-24
2-6	Axial Stress and K_I Data for the Beltline	2-25
2-7	Stress and K_I Data for the Lower Head Junction	2-26
2-8	Data for M_m and M_b Calculation by Appendix G Curve	2-28
2-9	Data for M_m and M_b Calculation for the Outlet Nozzle Junction	2-29
2-10	Transients	2-31
2-11	Temperature versus Maximum Combined K_I	2-37

SECTION 1
INTRODUCTION

1-1. BACKGROUND

An analysis has been performed for the Turkey Point Units No. 3 and No. 4 reactor vessels following the procedure of Appendix G of the ASME Code Section III, entitled "Protection Against Nonductile Failure" (hereafter termed Appendix G).[1]

Appendix G is developed on the principle of Linear Elastic Fracture Mechanics. In the analysis, normal, upset, and test conditions are investigated at four critical locations of the reactor vessel (figure 1-1). These locations are:

- Upper Head Junction
- Outlet Nozzle Junction
- Beltline of the Vessel
- Lower Head Junction

Briefly, the Appendix G procedures require the following five basic steps:

- Construct a valid reference fracture toughness curve (K_{IR} versus temperature) for the material of the reactor vessel as the basis for comparison with the calculated stress intensity factors, K_I.
- Assume a certain shape and size of the maximum postulated defect at the critical regions of interest. The typical flaw assumed in Appendix G is a semielliptical crack with an aspect ratio of 1:6. Its depth is assumed to be ~ 1/4 of the wall thickness for all regions except the nozzle where a value of 1/5 of wall thickness is used.
- Calculate the stress intensity factors, K_I, for both primary and secondary stress at the locations of interest under various load conditions (transients) for the postulated flaw size.

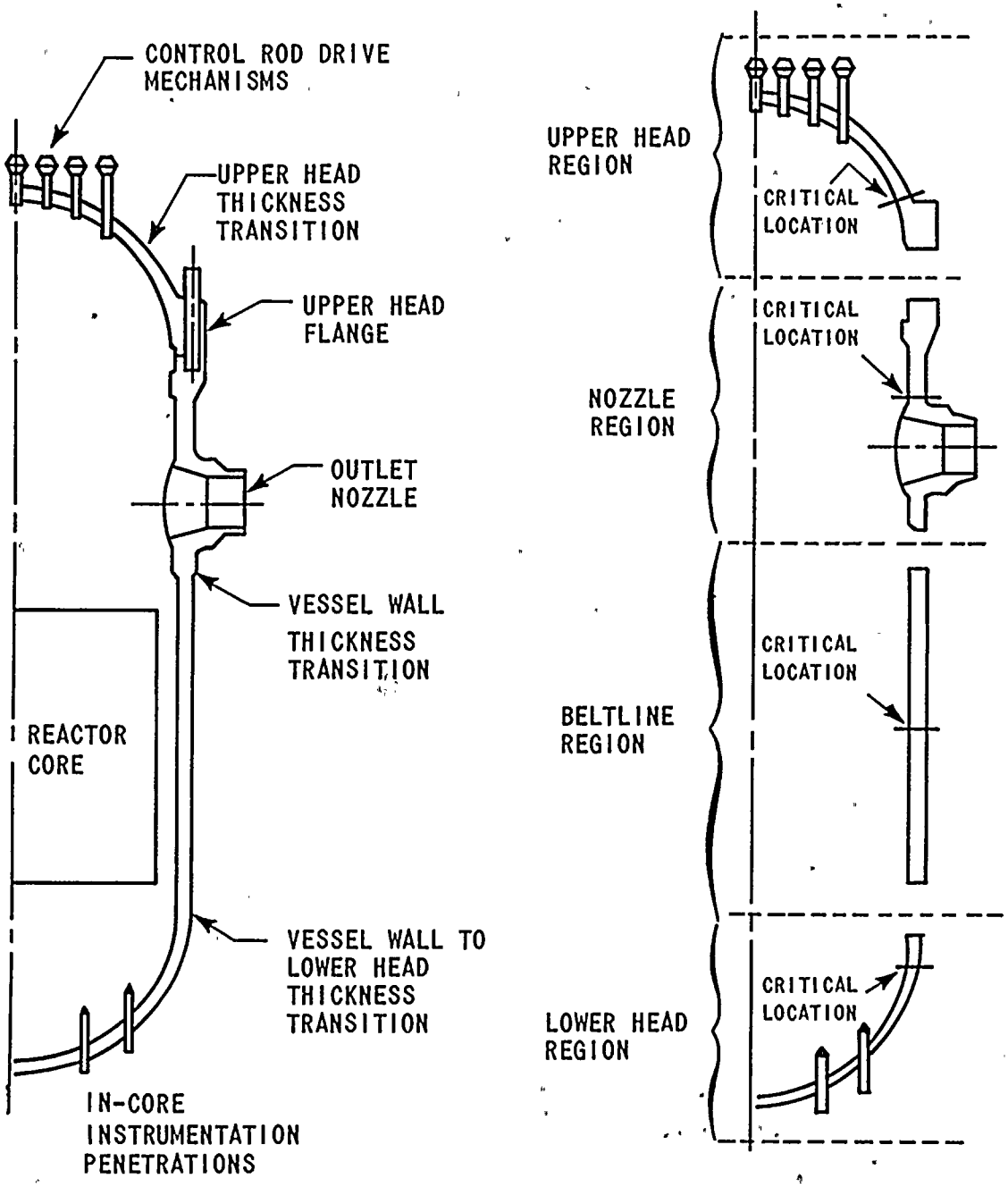

Figure 1-1. Critical Locations of the Pressurized Water Reactor Vessel

- Add up the primary and secondary stress intensity factors (with appropriate safety factors) to find the combined stress intensity factors.
- Compare the combined stress intensity factors with the corresponding fracture toughness curves by plotting the calculated K_I values on the respective curves. Compliance with Appendix G is achieved if the plotted K_I values fall below the corresponding K_{IR} curves.

1-2. SUMMARY OF ANALYTICAL RESULTS

The analysis detailed in section 2 shows that for Turkey Point Units No. 3 and No. 4:

- The maximum combined K_I values of the upper head junction, lower head junction, and the outlet nozzle junction are below the upper shelf limit of 200 ksi $\sqrt{\text{in.}}$ (unirradiated regions).
- The maximum combined K_I values of the beltline of the reactor vessel are less than the upper shelf limit of 200 ksi $\sqrt{\text{in.}}$ (irradiated region).
- The requirements of the rules of Appendix G have been fully satisfied. Protection against nonductile failure of the reactor vessel is shown to be ensured.

Note that this analysis supercedes the previous analysis documented in WCAP-8581.

SECTION 2
ANALYSIS

2-1. DETERMINATION OF THE K_{IR} CURVE

The first step in the Appendix G Analysis is to construct a valid reference fracture toughness curve for reactor vessel material.

2-2. Typical K_{IR} Curve

A typical reference fracture toughness curve (K_{IR} versus temperature) for the reactor vessel material is presented in Appendix G (figure 2-1). This typical curve is based on the lower bound of static, dynamic, and crack-arrest critical K_I values measured as a function of temperature from test specimens of SA-533, Grade B, Class 1, and SA-508, Class 2, Steels and Weldments.

The temperature scale is defined relative to the reference transition temperature or RT_{NDT}. The RT_{NDT}, a nonphysical constant which is related to the brittle-to-ductile fracture transition temperature, is determined by both drop weight tests and Charpy V impact tests.

A K_{IR} upper shelf of 200 ksi $\sqrt{in.}$ has been adopted for unirradiated material and a shelf of 200 ksi $\sqrt{in.}$ has been fixed for irradiated material as well (appendix A).

2-3. Irradiation Effects on the K_{IR} Curve

Neutron irradiation adversely affects the toughness properties of the reactor vessel steel. The neutron embrittlement of the steel has been found to be a function of the copper content of the steel for given fluences.

A consequence of a decrease in the toughness properties is a shift in the fracture toughness curve to a higher temperature. Quantitatively, this shift can be assessed by determining the shift to higher temperatures of the initial reference nil-ductility temperature RT_{NDT}.[2]

Copper trend curves have been developed by Westinghouse to relate the magnitude of shift in RT_{NDT} to the amount of neutron fluence. These curves were based on Charpy impact test results obtained from surveillance capsules as well as testing conducted by the Naval Research Laboratory and tests conducted under the Heavy Section Steel Technology Program.

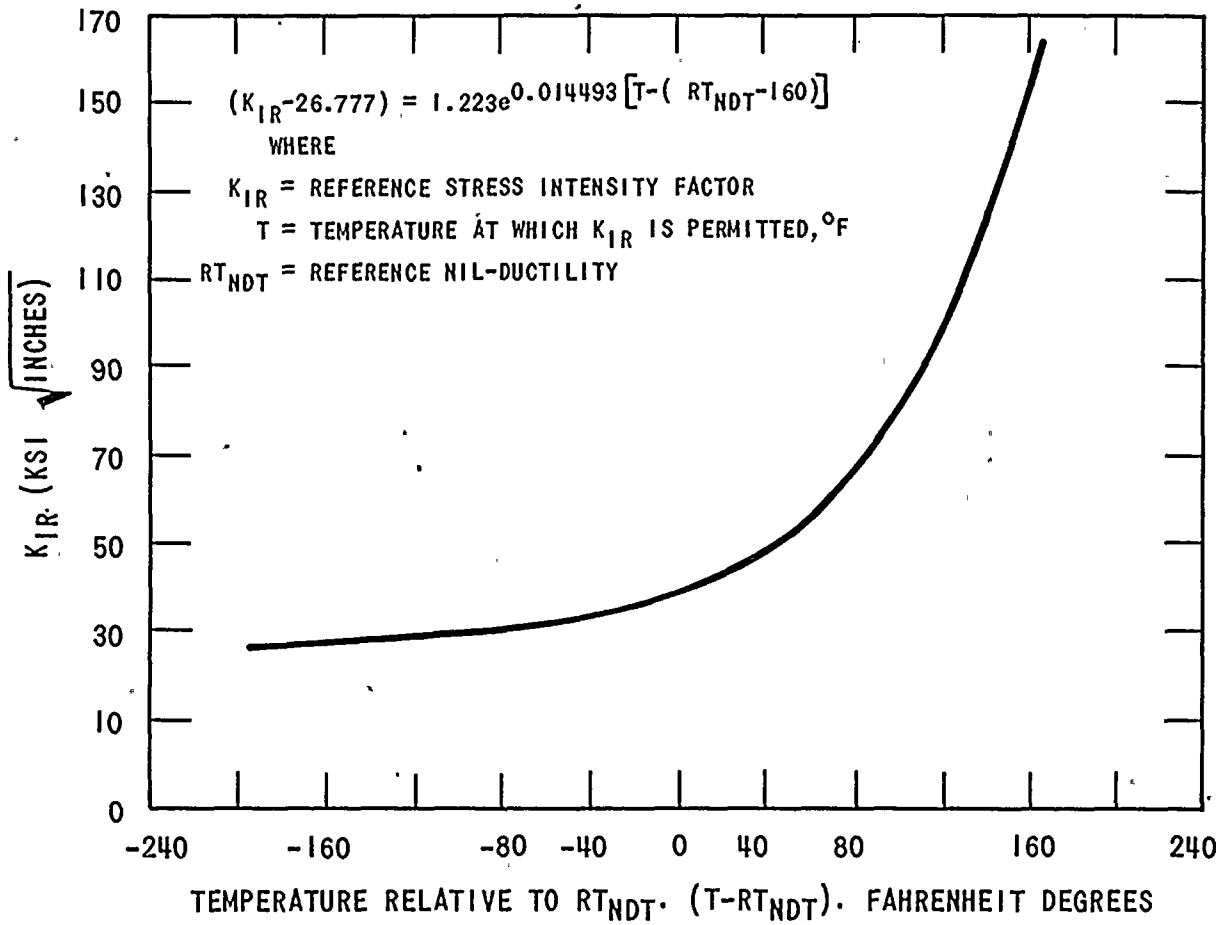

Figure 2-1. K_{IR} Reference Stress Intensity Factor Curve

Tests were conducted on these materials, A302B, A533B, Class 1, and A508, Class 2, as well as associated welds, all of which were irradiated at 550°F. Copper contents of these steels ranged from 0.03 to 0.27 weight percent, and irradiation levels ranged from 2×10^{18} neutrons/cm^2 to 7×10^{19} neutrons/cm^2. The change in RT_{NDT} was determined by comparing the 30 foot pound temperatures of the unirradiated and irradiated Charpy curves. The trend curves are shown in figure 2-2.

The U.S. Nuclear Regulatory Commission has also developed copper trend curves for the prediction of ΔRT_{NDT} versus fluence.[3] These curves are presented in Regulatory Guide 1.99 (figure 2-3). Regulatory Guide 1.99 curves predict RT_{NDT} shift as a function of phosphorous content as well as copper content. Both Westinghouse and NRC curves are used in this analysis.

The fracture toughness curve, indexed to $T\text{-}RT_{NDT}$, therefore, will shift along the abscissa by a value equal to ΔRT_{NDT} for a given level of irradiation and copper content as indicated by the copper trend curves. The RT_{NDT} values at the end of life differ sufficiently for the four critical locations under study that different reference fracture toughness curves are required.

2-4. K_{IR} Curves for the Four Critical Locations

The fluence drops drastically at a short longitudinal distance beyond the vicinity of the core assemblies as illustrated by figure 2-4. For instance, the outlet nozzles of a 3-loop reactor vessel are located more than 30 inches above the top level of the core assembly. The curve in figure 2-4 shows that the fluence is about 0.6 percent of the peak fluence value. Thus, the irradiation effect at the outlet nozzle area becomes insignificant due to its location.

The upper head and lower head junctions are located still farther from the core ensuring that there will be no significant irradiation effect at those locations. Consequently, only the K_{IR} curves of the vessel beltline which is exposed to the maximum irradiation have been adjusted to account for the shift in RT_{NDT} resulting from irradiation.

The material properties of the reactor vessels related to Appendix G analysis are tabulated in table 2-1 and table 2-2 along with the initial RT_{NDT} as determined by drop weight testing and Charpy V impact tests and the predicted end of life RT_{NDT}. The end of life RT_{NDT} is the sum of the initial RT_{NDT} plus the increment ΔRT_{NDT}. The increment is determined from figure 2-2 and figure 2-3.

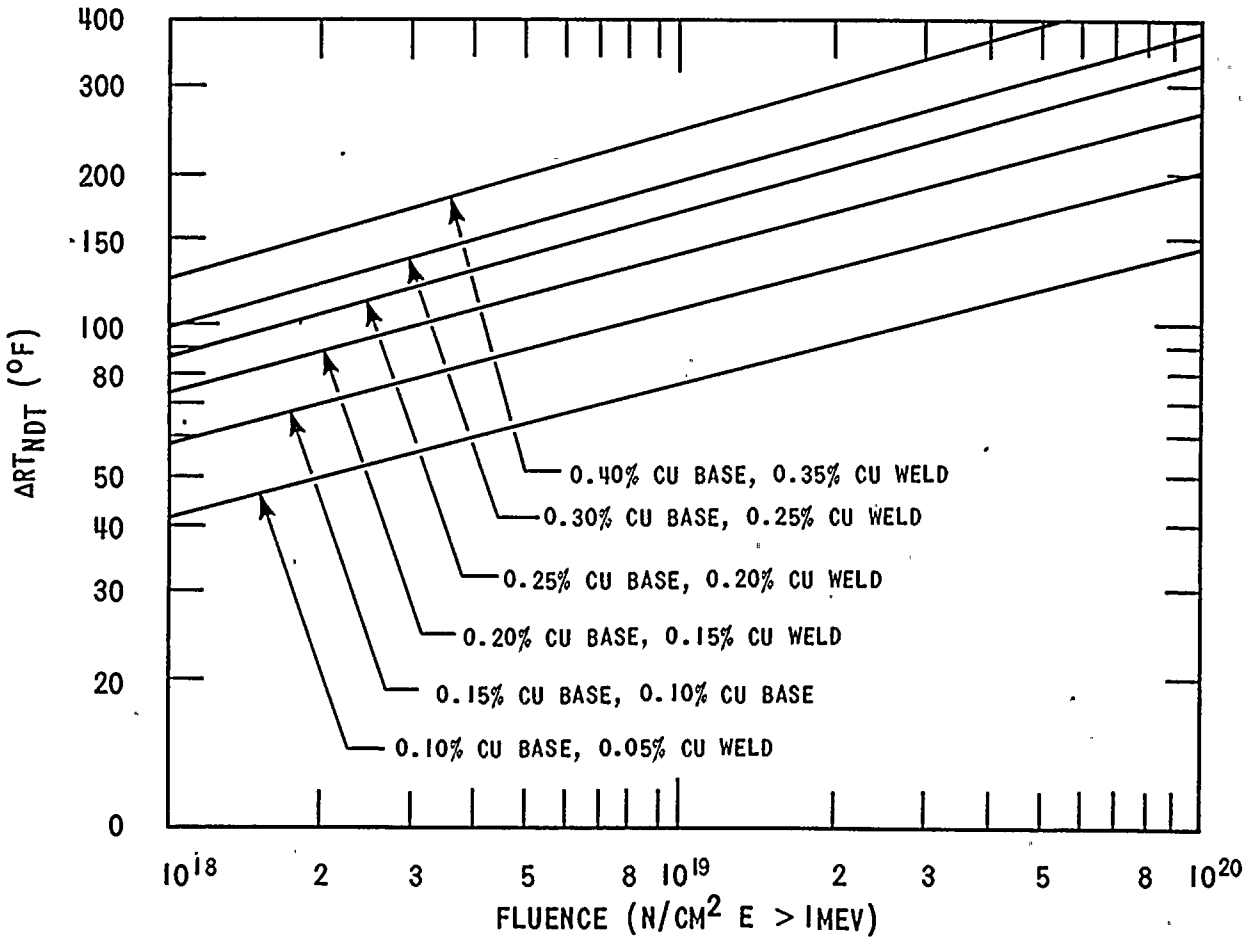

Figure 2-2. Effect of Fluence and Copper Content on ΔRT_{NDT} for Reactor Vessel Steels Exposed to Irradiation at 550°F

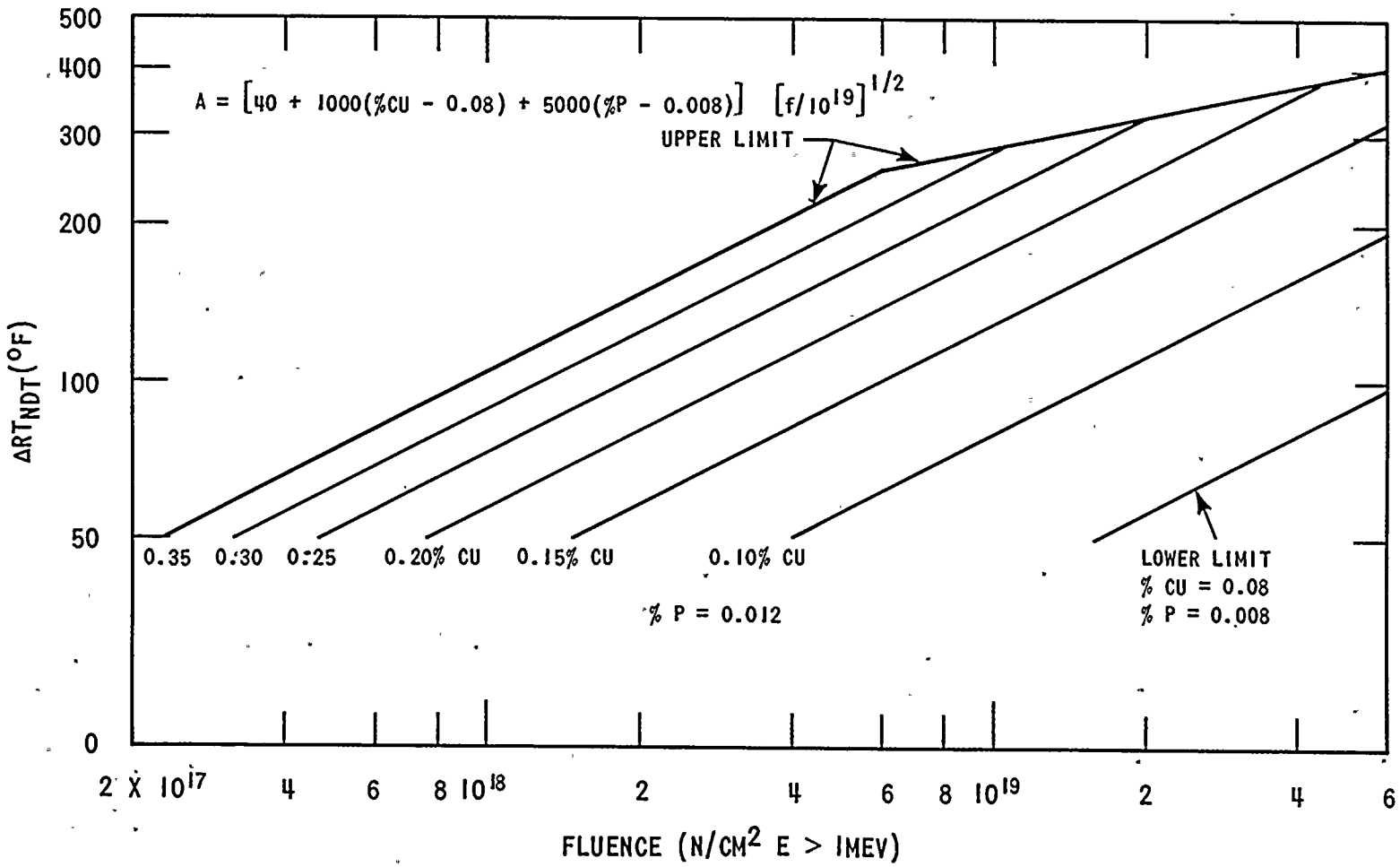

Figure 2-3. Effect of Fluence, Copper Content, and Phosphorus Content on ΔRT_{NDT} for Reactor Vessel Steels per Regulatory Guide 1.99 (January 1976)

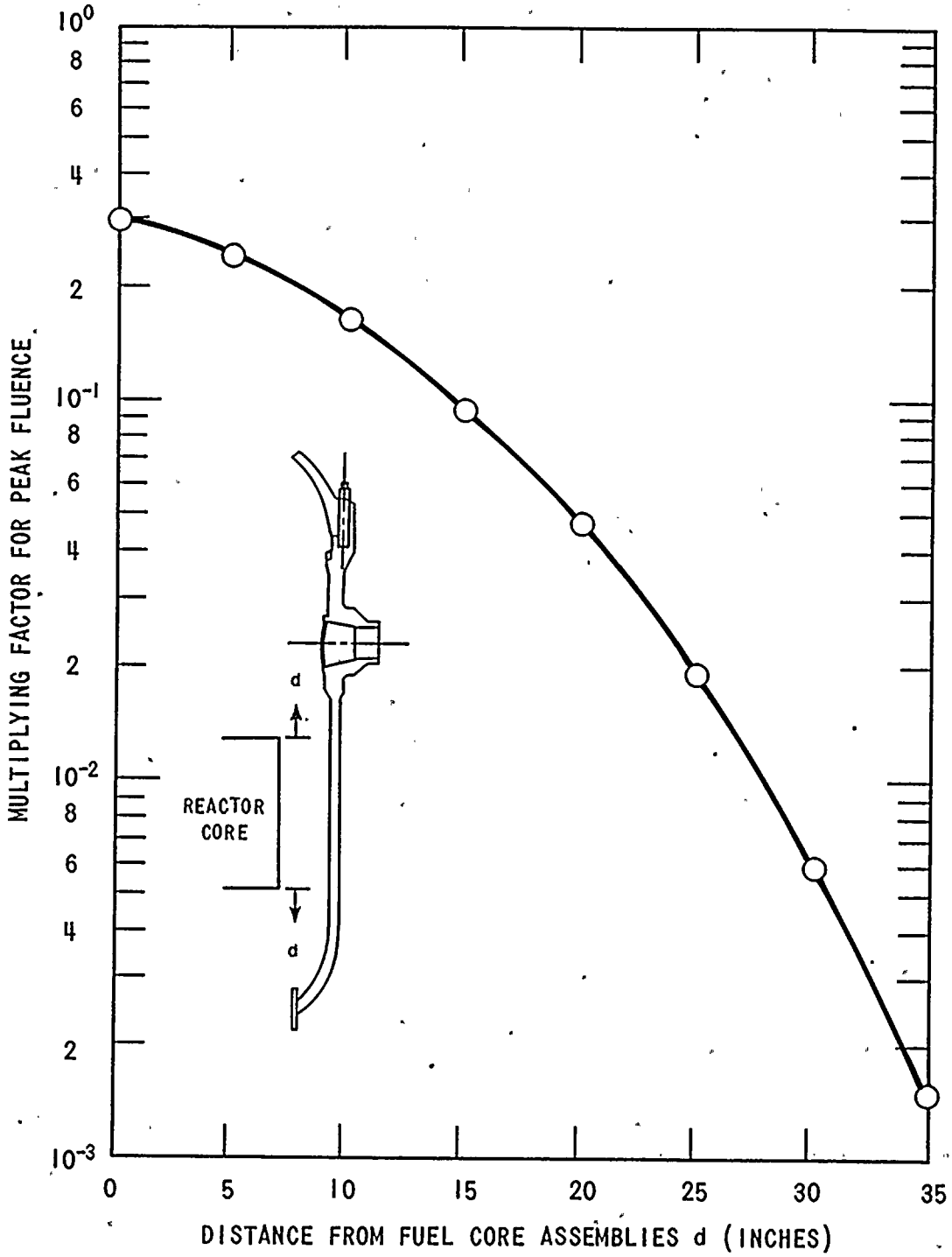

Figure 2-4. Longitudinal Distance Versus Multiplying Factor for Peak Fluence

TABLE 2-1

TURKEY POINT UNIT NO. 3 REACTOR VESSEL MATERIAL DATA[a]

Location	Material	Copper Content (%)	Phos. Content (%)	End of Life Fluence at 1/4 T[b] (n/cm^2)	Initial RT_{NDT} (°F)	Predicted End of Life RT_{NDT}[c] (°F)	
Upper Head	A-302-B	—	—	—	0	0[d]	0[e]
	A-508-Cl 2	—	—	—	44	44	44
Outlet Nozzle	A-508-Cl 2	—	—	—	42	42	42
	A-508-Cl 2	—	—	—	50	50	50
Beltline	A-508-Cl 2	0.079	0.010	3.76×10^{19}	30	116	107
	A-508-Cl 2	0.058	0.010	3.76×10^{19}	40	103	117
	Weld	0.31	0.011	3.76×10^{19}	3	270	367
Lower Head	A-508-Cl 2	—	—	—	60	60	60
	A-302-B	—	—	—	30	30	30

a. See table A-1 in reference 8.

b. See figure A-2 in reference 8.

c. This assumes 32 effective-full-power years.

d. Shift prediction based on the Westinghouse Copper Trend Curves.

e. Shift prediction based on the curves presented in Regulatory Guide 1.99.

TABLE 2-2

TURKEY POINT UNIT NO. 4 REACTOR VESSEL MATERIAL DATA[a]

Location	Material	Copper Content (%)	Phos. Content (%)	End of Life Fluence at 1/4 T[b] (n/cm^2)	Initial RT_{NDT} (°F)	Predicted End of Life RT_{NDT}[c] (°F)	
Upper Head	A-302-B	—	—	—	30	30[d]	30[e]
	A-508-Cl 2	—	—	—	30	30	30
Outlet Nozzle	A-508-Cl 2	—	—	—	60	60	60
	A-508-Cl 2	—	—	—	40	40	40
Beltline	A-508-Cl 2	0.054	0.010	3.76×10^{19}	50	109	127
	A-508-Cl 2	0.056	0.010	3.76×10^{19}	40	101	117
	Weld	0.31	0.011	3.76×10^{19}	3	270	367
Lower Head	A-508-Cl 2	—	—	—	60	60	60
	A-302-B	—	—	—	10	10	10

a. See table 1 in reference 9. For further explanation, see reference 10, section 5.

b. See figure A-2 in reference 8.

c. This assumes 32 effective-full-power years.

d. Shift prediction based on the Westinghouse Copper Trend Curves.

e. Shift prediction based on the curves presented in Regulatory Guide 1.99.

2-5. MAXIMUM POSTULATED DEFECTS

The maximum defect assumed in Appendix G is a sharp surface defect normal to the direction of the maximum stress. The typical flaw is assumed to be semielliptical with an aspect ratio of 1:6. The depth of the reference flaw in the top closure head, the beltline, and the lower head is assumed to be 1/4 of the vessel wall thickness as shown in figure 2-5.

A flaw depth of 1/5 of wall thickness is assumed for the outlet nozzle junction instead of quarter thickness since the wall thickness over this junction is thicker than at any of the other three critical locations.

A nozzle is a region of geometrical discontinuity in which the stresses produced by pressure can be two or three times the membrane stress in the shell region. ASME Appendix G recognizes that the nozzle region cannot be expected to meet its requirements for a one-quarter thickness defect; it states that "smaller defect sizes may be used on an individual case basis if a smaller size of maximum postulated defect can be assured."

WRC bulletin No. 175, "PVRC Recommendations on Toughness Requirements for Ferritic Materials,"[4] provides procedures for considering postulated defect sizes smaller than one-quarter of the wall thickness.

The combination of examinations required by Section III (generally radiography) and the volumetric examination required by Section XI (generally ultrasonic mapping) are capable of detecting flaws much smaller than the magnitude (1/5 wall thickness) assumed for the outlet nozzle junction.

2-6. FORMULATION OF THE STRESS INTENSITY FACTOR, K_I

For the critical regions, the stress intensity factors, K_I, are calculated for both primary and secondary stress during the load transients.

2-7. General Formula for K_I

The value of K_I depends on:

- The geometry of the body in which the crack is postulated
- The shape and size of the crack
- The mode and the magnitude of the stress distribution at the crack surface

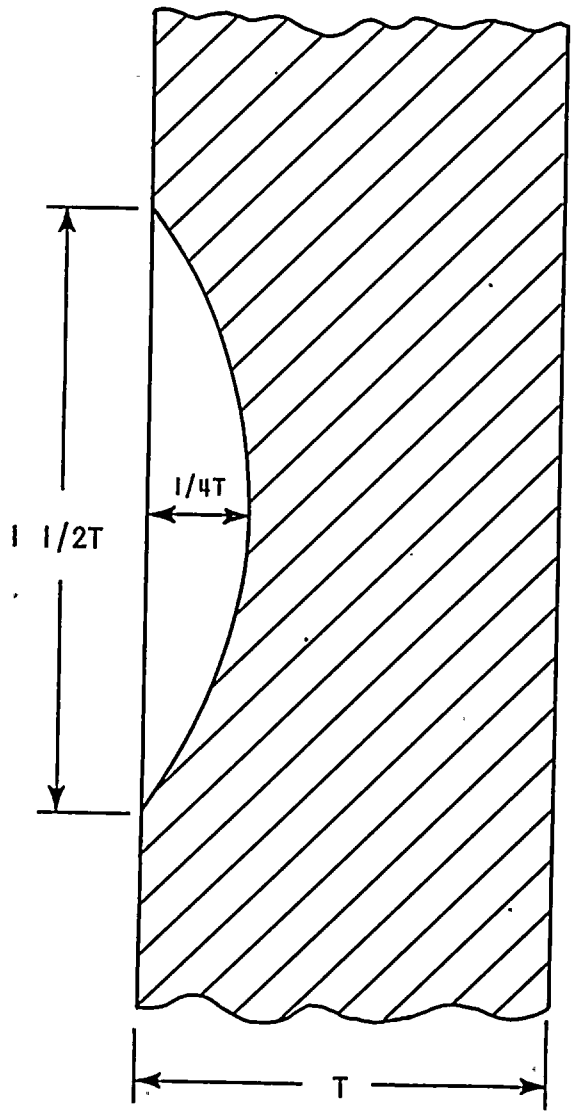

SEMI-ELLIPTICAL SURFACE FLAW

Figure 2-5. Reference Flaw (Appendix G)

The general formula of K_I is

$$K_I = \sqrt{\frac{\pi a}{Q}} (A_m \sigma_m + A_b \sigma_b) \tag{2-1}$$

where

a	=	the flaw depth.
Q	=	the flaw shape factor as a function of stress/yield strength ratio.
A_m, A_b	=	the correction factors for membrane and bending stresses respectively. They depend on the depth and aspect ratio of the crack.
σ_m, σ_b	=	membrane and bending stresses (calculated as if no crack were present).

The general formula is valid for a semielliptical surface flaw in both primary and secondary stress conditions.

K_I for primary and secondary stresses should be added to obtain the combined stress intensity factor. Appendix G requires that a safety factor of 2 be applied to the K_I of primary stresses in normal and upset conditions. A safety factor of 1.5 is to be used for hydrostatic test conditions. Therefore, we have

$$[K_I]_{\text{combined}} = 2\,[K_I]_{\text{primary}} + [K_I]_{\text{secondary}} \tag{2-2}$$

for normal and upset conditions, and

$$[K_I]_{\text{combined}} = 1.5\,[K_I]_{\text{primary}} + [K_I]_{\text{secondary}} \tag{2-3}$$

for hydrostatic test conditions.

2-8. K_I Determined for 1/4-Thickness Flaw

From the general formula, equation (2-1), if the correction factors A_m and A_b are combined with $\sqrt{\frac{\pi a}{Q}}$, equation (2-1) can be expressed as:

$$K_I = M_m \sigma_m + M_b \sigma_b \tag{2-4}$$

where

$$M_m = \sqrt{\frac{\pi a}{Q}}(A_m) \text{ and}$$

$$M_b = \sqrt{\frac{\pi a}{Q}}(A_b)$$

Since A_m and A_b depend on the flaw size, it is logical to simplify equation (2-1) in the form of equation (2-4) when the flaw size is given.

As mentioned in the previous paragraph, a typical flaw of 1:6 ratio and 1/4-thickness deep is assumed in Appendix G. Therefore, M_m and M_b can be plotted against two independent parameters, wall thickness and stress ratio, as shown in figure 2-6.[1]

M_m and M_b for the primary and secondary stress conditions can be determined by figure 2-6. K_I values can be calculated by equation (2-4).

Equations (2-2) and (2-3) for the combined K_I can be expressed as:

$$[K_I]_{\text{combined}} = 2\,[M_m\,\sigma_m + M_b\,\sigma_b]_{\text{primary}} + [M_m\,\sigma_m + M_b\,\sigma_b]_{\text{secondary}} \qquad (2\text{-}5)$$

for normal and upset conditions, and

$$[K_I]_{\text{combined}} = 1.5\,[M_m\,\sigma_m + M_b\,\sigma_b]_{\text{primary}} + [M_m\,\sigma_m + M_b\,\sigma_b]_{\text{secondary}} \qquad (2\text{-}6)$$

for hydrostatic test conditions.

This method is applicable for the top head junction, beltline, and the lower head junction of the reactor vessel where a 1/4-thickness flaw is postulated.

2-9. K_I Determined for 1/5-Thickness Flaw

As previously mentioned, the flaw depth at the outlet nozzle is assumed to be 1/5 of the wall thickness instead of the typical 1/4 of the wall thickness. The curves in figure 2-6, which were developed for a 1/4-thickness flaw, are not applicable for the outlet nozzle.

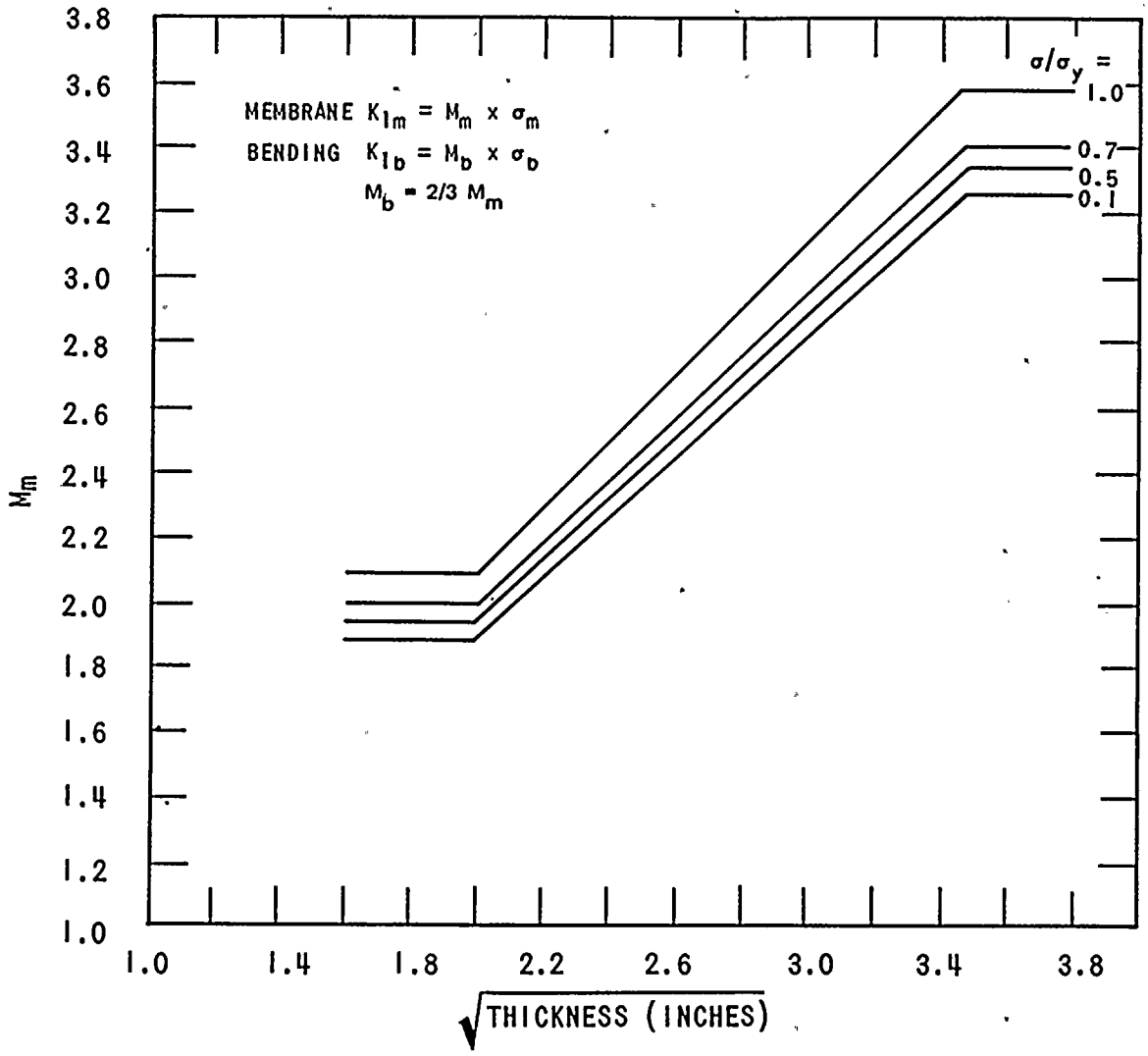

Figure 2-6. M_m, M_b versus $\sqrt{\text{Thickness}}$ Curve

Calculation of the stress intensity factor for a 1/5-thickness semielliptical flaw in the nozzle shell region is by equation (2-1).

$$K_I = \sqrt{\frac{\pi a}{Q}}\,[A_m\,\sigma_m + A_b\,\sigma_b] \qquad (2\text{-}7)$$

where a, σ_m, and σ_b have been defined in the previous paragraphs.

Figure 2-7 gives the value of Q as a function of the $(\frac{\sigma}{\sigma y})$ ratio. A_m, A_b can be determined from figures 2-8 and 2-9 which show the relationships M_k versus $(\frac{a}{T})$ and A_b versus $(\frac{a}{T})$ respectively. Note that $A_m = 1.1\ M_k$.[4]

Equation (2-7) can be transformed to:

$$K_I = M_m\,\sigma_m + M_b\,\sigma_b \qquad (2\text{-}8)$$

This expression is identical with equation (2-4) in which

$$M_m = \left(\sqrt{\frac{\pi a}{Q}}\,A_m\right)$$

and

$$M_b = \left(\sqrt{\frac{\pi a}{Q}}\,A_b\right)$$

Equations (2-5) and (2-6) are applicable for the outlet nozzle also. Namely,

$$[K_I]_{\text{combined}} = 2\,[M_m\,\sigma_m + M_b\,\sigma_b]_{\text{primary}} + [M_m\,\sigma_m + M_b\,\sigma_b]_{\text{secondary}} \qquad (2\text{-}9)$$

for normal and upset conditions, and

$$[K_I]_{\text{combined}} = 1.5\,[M_m\,\sigma_m + M_b\,\sigma_b]_{\text{primary}} + [M_m\,\sigma_m + M_b\,\sigma_b]_{\text{secondary}} \qquad (2\text{-}10)$$

for the hydrostatic test conditions.

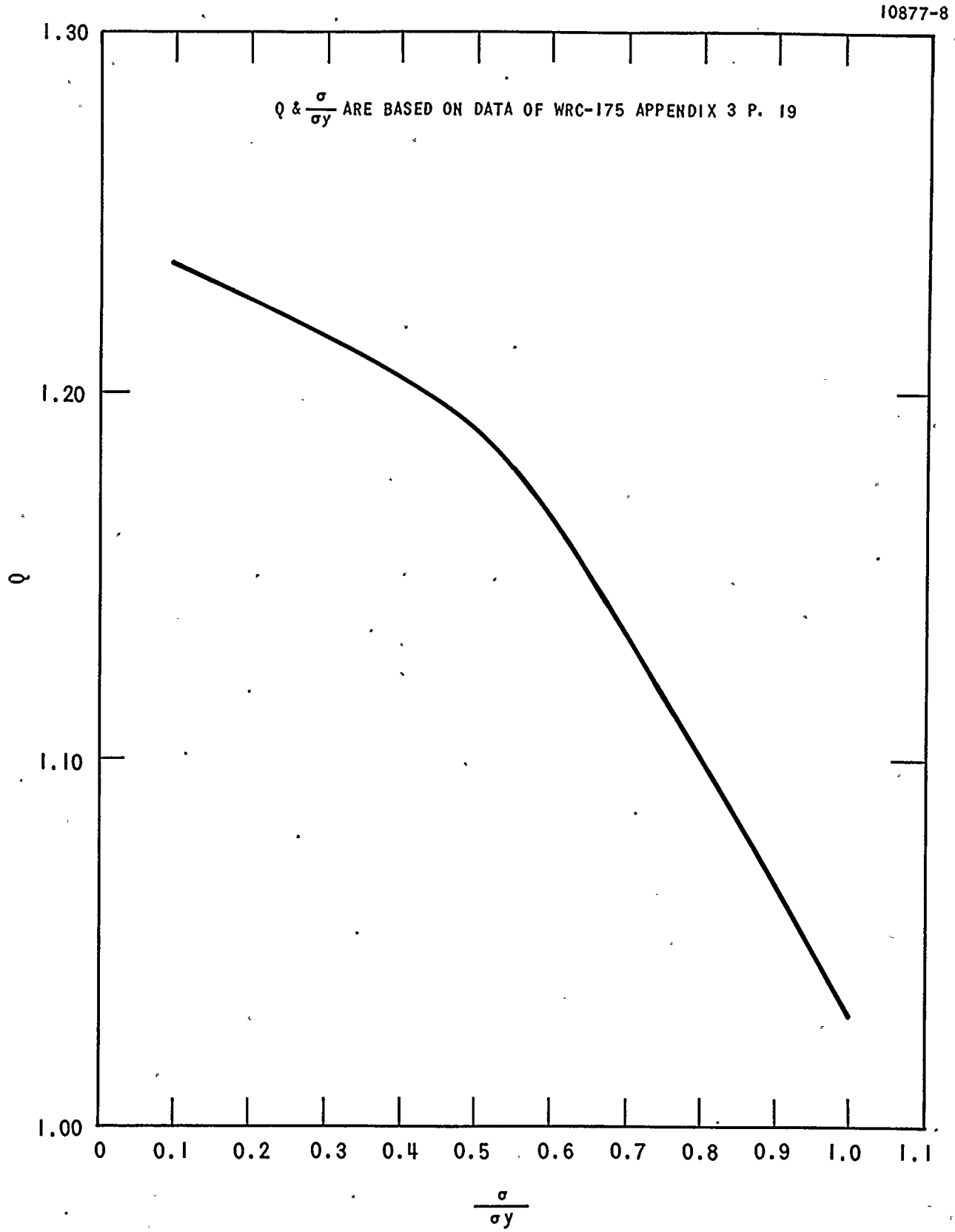

Figure 2-7. Q versus $(\frac{\sigma}{\sigma_y})$ Curve

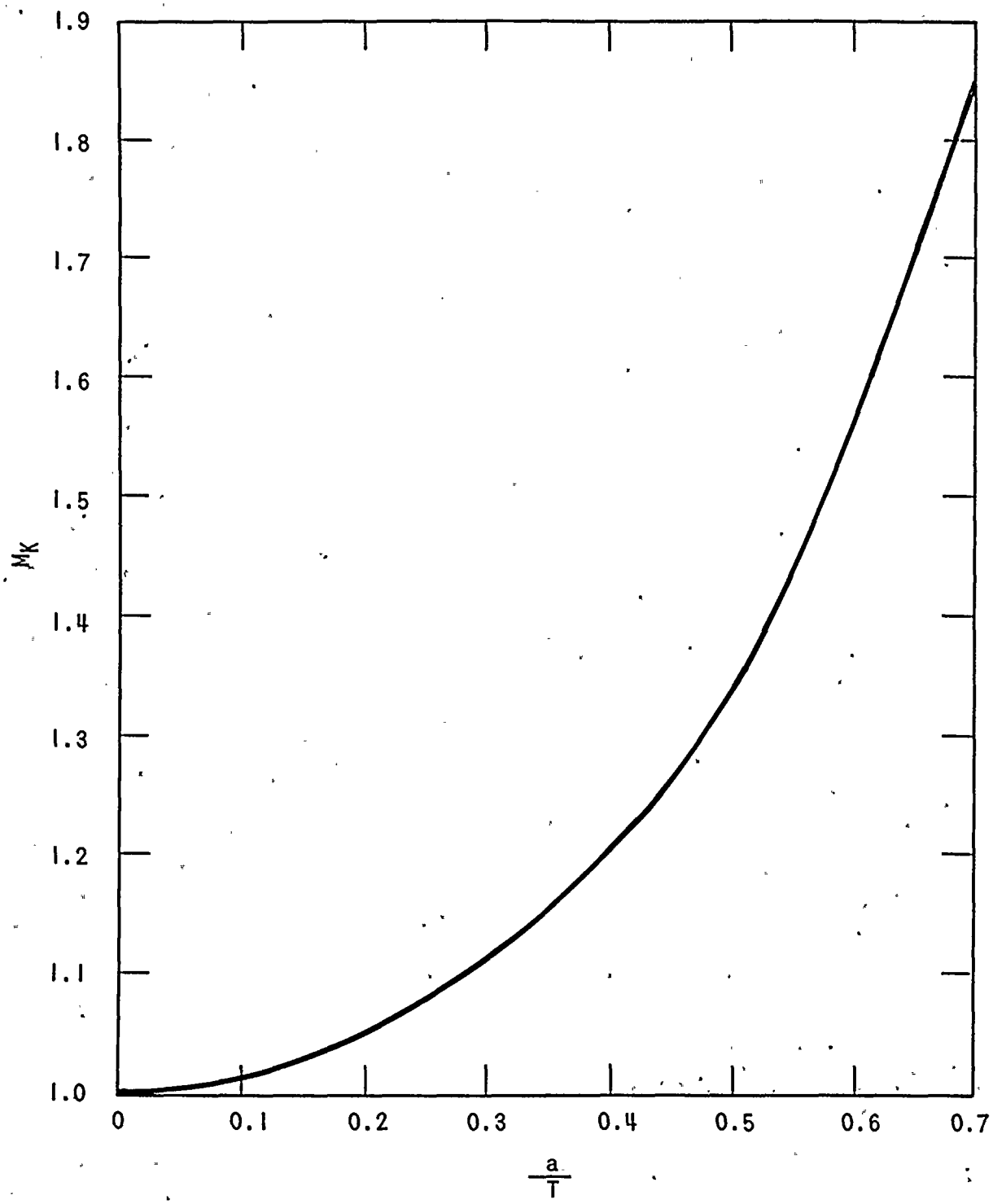

Figure 2-8. M_K versus $(\frac{a}{T})$ Curve

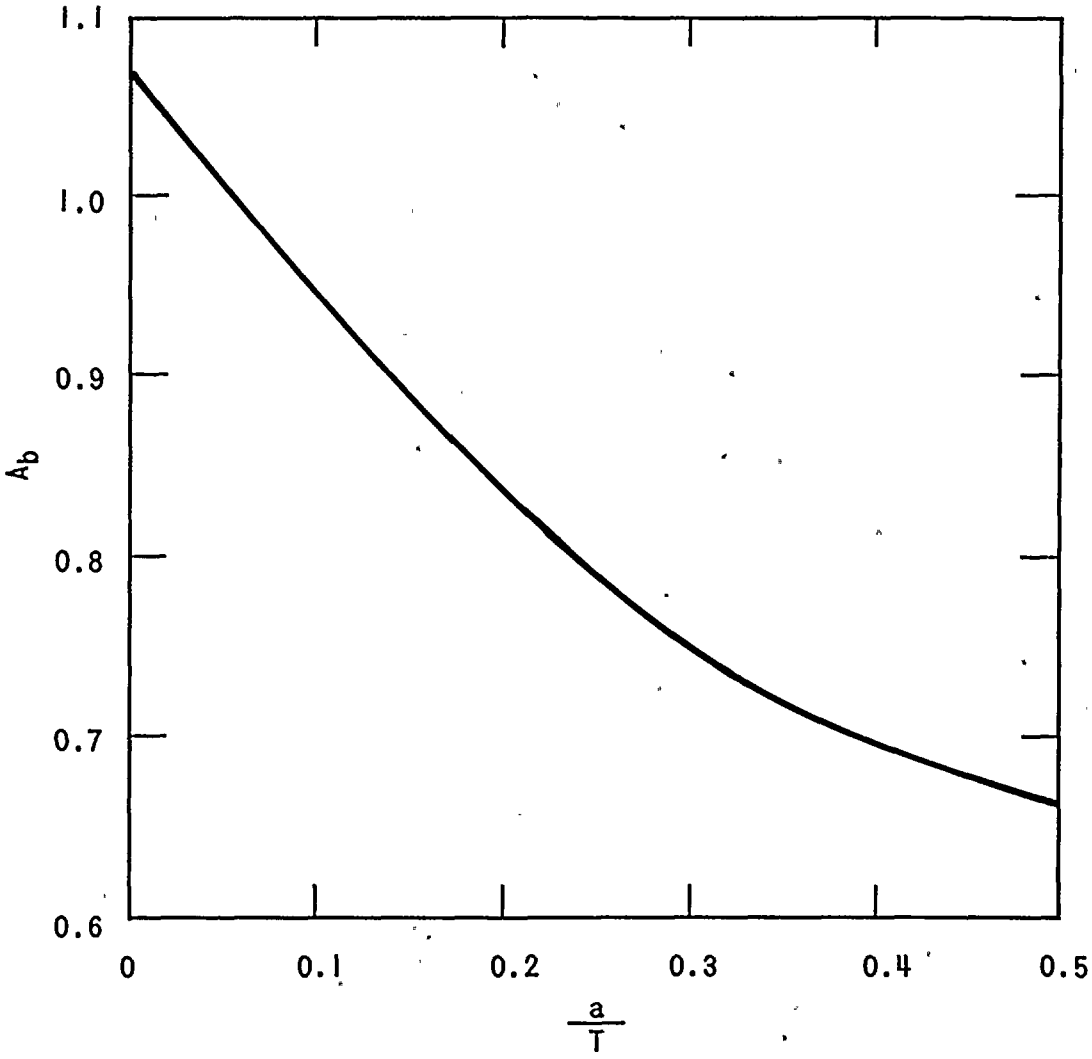

Figure 2-9. A_b versus $(\frac{a}{T})$ Curve

This method is applicable to the outlet nozzle junction of the reactor vessel where a flaw depth of 1/5 is postulated.

2-10. NUMERICAL CALCULATION OF K_I

The geometry and dimensions of the reactor vessels at the four critical locations are shown in detail in figures 2-10 through 2-12. The dimensions used in this analysis were the same as those used in the calculation of the stresses in the reactor vessel stress report.[5] The reactor vessels in Units No. 3 and No. 4 are identical, and because the same design transients apply to both plants, stress values and resultant K_I values are representative of both vessels. Note that this analysis supercedes the previous analysis performed for Unit No. 3.[6]

The numerical calculations of K_I for the four critical locations are provided in five separate tables (tables 2-3 through 2-7). In each table, all load conditions (transients) throughout the life of the vessel have been considered. Only the load stage resulting in the highest K_I for a given transient is listed.

The stress data are based on the original stress reports.[5] The Turkey Point Units No. 3 and No. 4 reports did not contain all the information needed in this analysis. Therefore, the results from a more complete stress report were used where needed. The report used was for the Beaver Valley Unit No. 1 3-loop plant.[7] In the upper head region, the Beaver Valley plant is identical to the Turkey Point plants. For the outlet nozzle region, the plant dimensions are within 2 percent, and in the lower head region, the dimensions are within 5 percent. The stress values used in the K_I calculation were computed by linearizing the inside and outside stresses which are provided in the stress reports. Figure 2-13 illustrates the linearizing process.

The multiplication factors $M_m + M_b$ for the primary and secondary stresses, derived for each region, are based on the highest primary and secondary stresses of all the design transients experienced by each region.

All data related to M_m and M_b calculation are summarized in tables 2-8 and 2-9. These respective M_m and M_b values are entered into tables 2-3 through 2-7 to compute the stress intensity factors, K_I. The combined stress intensity factors are tabulated in the last column of the tables.

2-11. COMPARISON OF THE COMBINED STRESS INTENSITY FACTORS WITH K_{IR} CURVES

Finally, the calculated K_I values for all load transients are plotted versus coolant temperature on the adjusted K_{IR} curves.

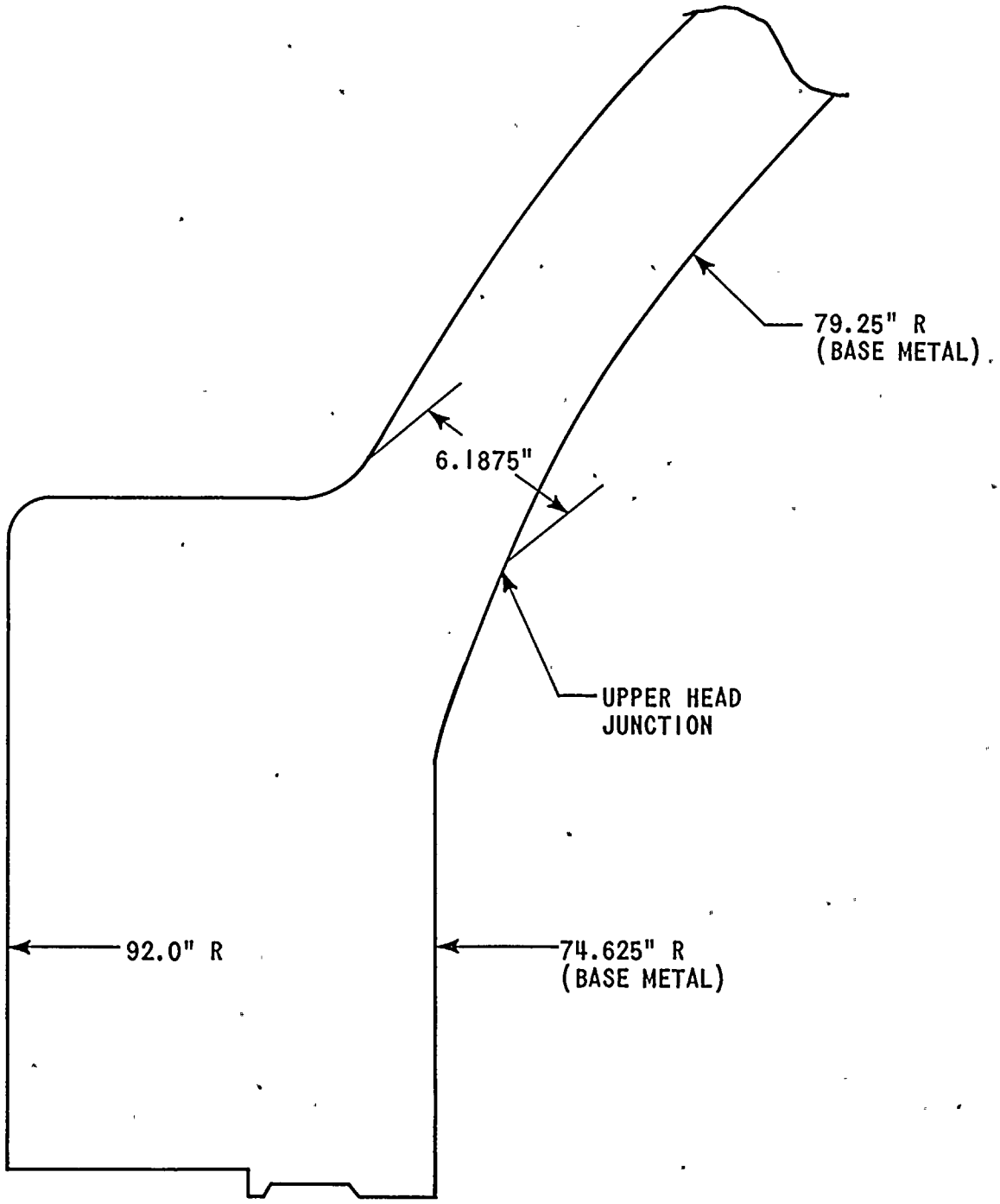

Figure 2-10. Upper Head Region

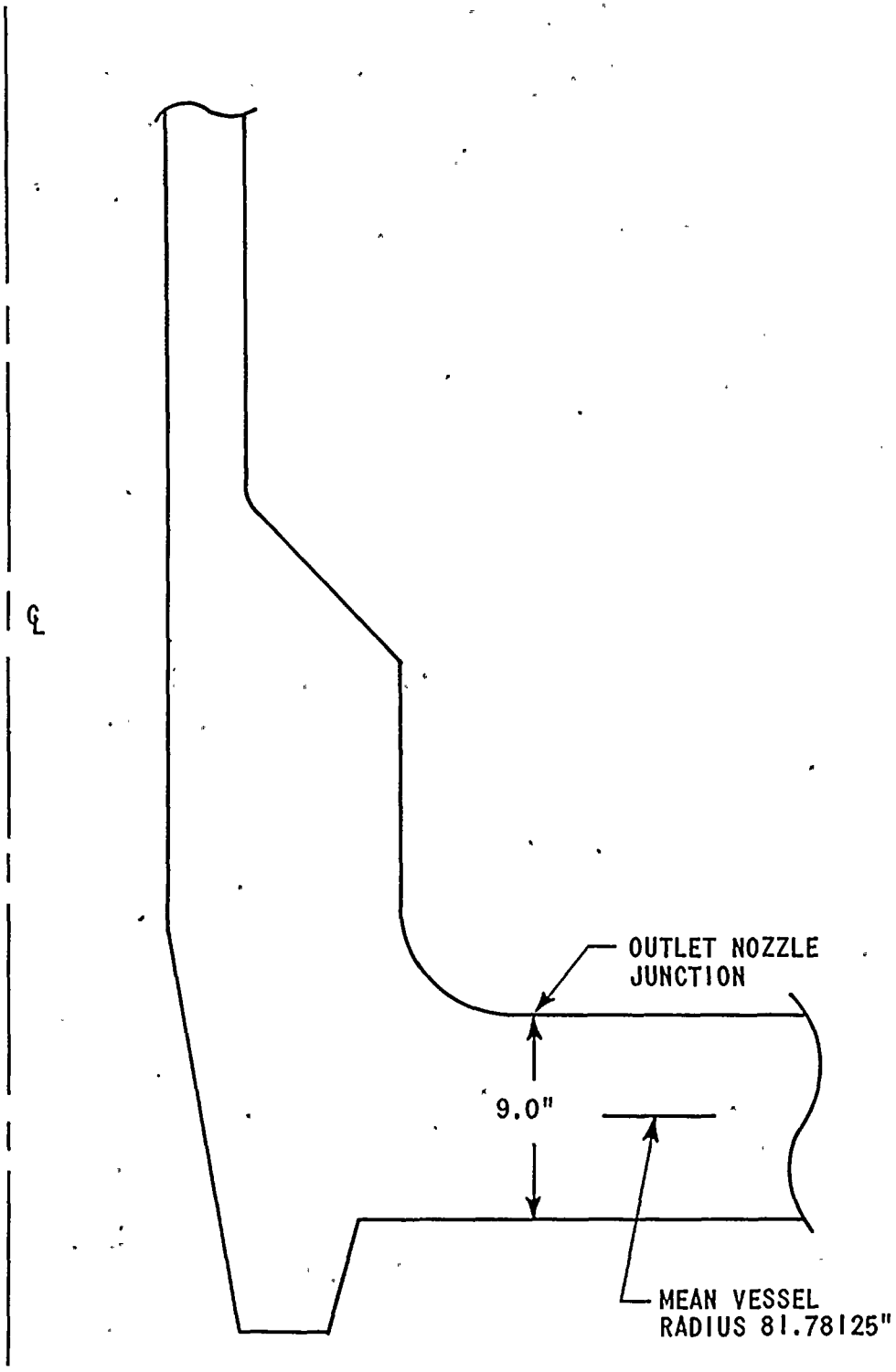

Figure 2-11. Outlet Nozzle Region

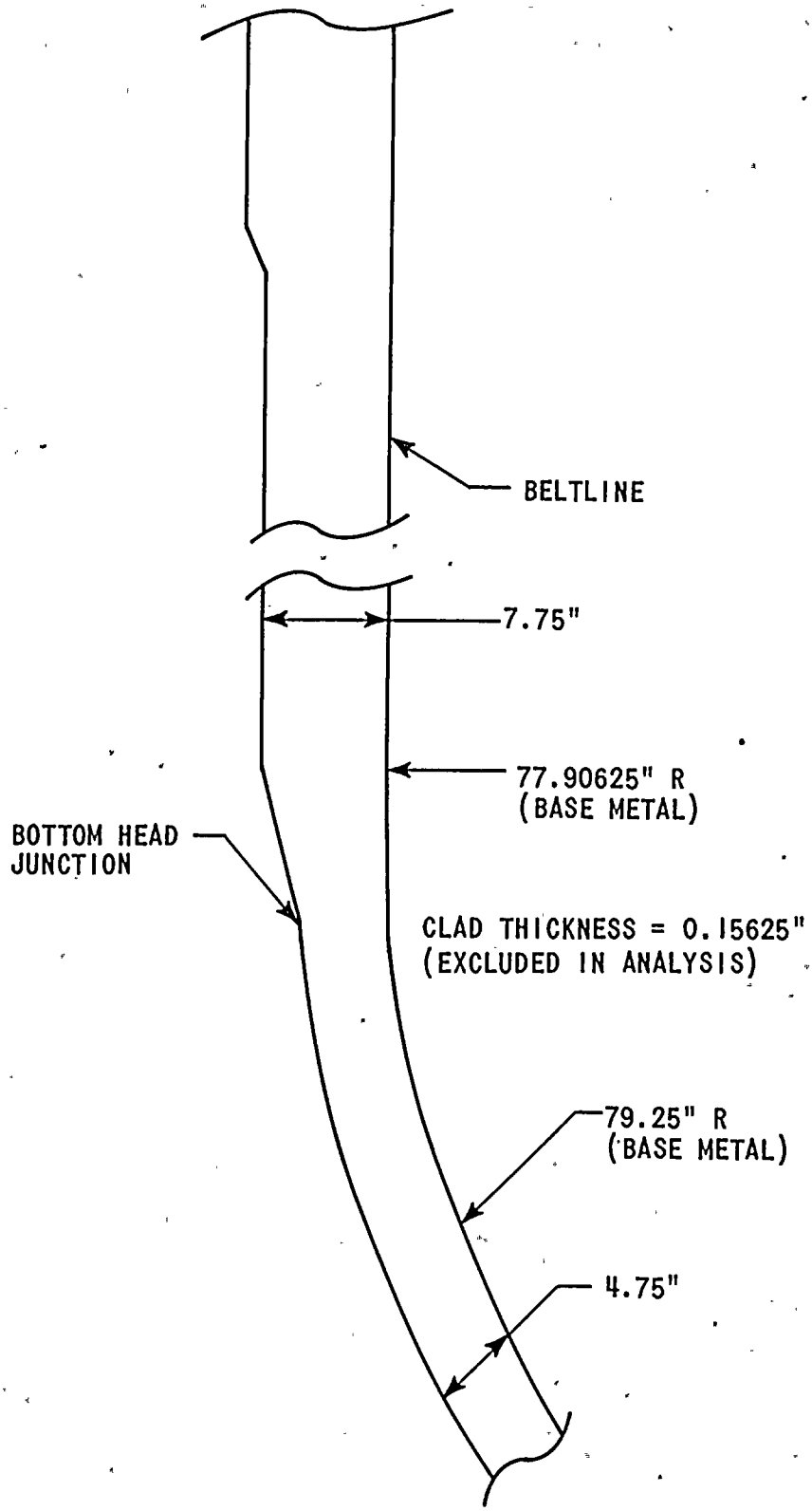

Figure 2-12. Beltline and Lower Head Regions

TABLE 2-3
STRESS AND K_I DATA FOR THE UPPER HEAD JUNCTION

Load Condition	Load Stage	Primary Stresses (ksi)				Secondary Stresses (ksi)				Primary Stress Intensity Factor (ksi$\sqrt{in.}$)		Secondary Stress Intensity Factor (ksi$\sqrt{in.}$)		Combined Stress Intensity Factor (ksi$\sqrt{in.}$)
		σ_i	σ_o [a]	σ_m	σ_b	σ_i	σ_o	σ_m	σ_b	K_{IM}	K_{IB}	K_{IM}	K_{IB}	K_I
Heatup	4.5 hr	-15.01	44.78	14.89	29.89	-6.33	2.81	-1.76	4.57	35.59	47.53	--[b]	7.13	173.37
Cooldown	0 hr	-15.01	44.78	14.89	29.89	0.0	0.0	0.0	0.0	35.59	47.53	0.0	0.0	166.24
Plant loading	20 min	-15.01	44.78	14.89	29.89	-0.88	0.42	-0.23	0.65	35.59	47.53	--	1.01	167.25
Unloading	20 min	-15.01	44.78	14.89	29.89	0.88	-0.42	0.23	-0.65	35.59	47.53	0.54	--	166.78
Small step load increase	220 sec	-14.82	44.89	15.04	29.85	0.54	-0.18	0.18	-0.36	35.95	47.46	0.42	--	167.24
Small step load dec.	35 sec	-14.49	45.10	15.31	29.79	-0.86	0.11	-0.38	0.48	36.59	47.37	--	0.75	168.67
Large step load dec.	2 min	-14.08	45.35	15.64	29.71	-1.35	0.35	-0.50	0.85	37.38	47.24	--	1.33	170.57
Loss of load	10 sec	-11.10	47.20	18.05	29.15	-2.72	0.14	-1.29	1.43	43.14	46.35	--	2.23	181.21
Loss of flow	0 sec	-15.01	44.78	14.89	29.89	0.0	0.0	0.0	0.0	35.59	47.53	0.0	0.0	166.24
Reactor trip from full power	0 sec	-15.01	44.78	14.89	29.89	0.0	0.0	0.0	0.0	35.59	47.53	0.0	0.0	166.24
Turbine roll test	0 min	-15.01	44.78	14.89	29.89	0.0	0.0	0.0	0.0	35.59	47.53	0.0	0.0	166.24
Steady state fluctuation	+fluct	-14.26	45.24	15.49	29.75	-0.63	0.11	-0.26	0.37	37.02	47.30	--	0.58	169.22
Cold hydro test	5 hr	-8.49	48.82	20.17	28.65	0.0	0.0	0.0	0.0	48.21	45.55	0.0	0.0	140.64
Hot hydro test	5 hr	-13.15	45.93	16.39	29.54	-3.78	1.79	-1.00	2.78	39.17	46.97	--	4.34	133.55

a. Due to primary tension (axial stress) on the outside, the flaw is assumed to be on the outside surface.

b. Dashes indicate negative values.

TABLE 2-4
STRESS AND K_I DATA FOR THE OUTLET NOZZLE JUNCTION

Load Condition	Load Stage	Primary Stresses (ksi)				Secondary Stresses (ksi)				Primary Stress Intensity Factor (ksi$\sqrt{in.}$)		Secondary Stress Intensity Factor (ksi$\sqrt{in.}$)		Combined Stress Intensity Factor (ksi$\sqrt{in.}$)
		σ_i	σ_o	σ_m	σ_b	σ_i	σ_o	σ_m	σ_b	K_{IM}	K_{IB}	K_{IM}	K_{IB}	K_I
Heatup	4.5 hr	24.20	23.10	23.65	0.55	-6.33	3.52	-1.41	-4.92	60.54	1.01	—[a]	—	123.10
Cooldown	0 hr	24.20	23.10	23.65	0.55	0.0	0.0	0.0	0.0	60.54	1.01	0.0	0.0	123.10
Plant loading	20 min	24.20	23.10	23.65	0.55	-7.64	3.55	-2.05	-5.59	60.54	1.01	—	—	123.10
Unloading	20 min	24.20	23.10	23.65	0.55	7.64	-3.55	2.05	5.59	60.54	1.01	5.08	9.95	138.13
Small step load increase	220 sec	24.49	23.30	23.90	0.59	0.88	-0.20	0.34	0.54	61.18	1.09	0.84	0.96	126.34
Small step load dec.	35 sec	25.01	23.65	24.33	0.68	-1.84	0.13	-0.86	-0.98	62.28	1.25	—	—	127.06
Large step load dec.	2 min	25.64	24.08	24.86	0.78	-2.72	0.45	-1.14	-1.58	63.64	1.44	—	—	130.16
Loss of load	10 sec	30.25	27.22	28.74	1.51	-10.25	0.14	-5.06	-5.19	73.57	2.78	—	—	152.70
Loss of flow	0 sec	24.20	23.10	23.65	0.55	0.0	0.0	0.0	0.0	60.54	1.01	0.0	0.0	123.10
Reactor trip from full power	0 sec	24.20	23.10	23.65	0.55	0.0	0.0	0.0	0.0	60.54	1.01	0.0	0.0	123.10
Turbine roll test	0 min	24.20	23.10	23.65	0.55	0.0	0.0	0.0	0.0	60.54	1.01	0.0	0.0	123.10
Steady state fluctuation	+fluct	25.35	23.89	24.62	0.73	-1.36	0.13	-0.62	-0.74	63.03	1.34	—	—	128.74
Cold hydro test	5 hr	34.29	29.96	32.13	2.16	0.0	0.0	0.0	0.0	82.25	3.97	0.0	0.0	129.33
Hot hydro test	5 hr	27.08	25.06	26.07	1.01	-3.78	2.36	-0.71	-3.07	66.74	1.86	—	—	102.90

a. Dashes indicate negative values.

TABLE 2-5
HOOP STRESS[a] AND K_I DATA FOR THE BELTLINE

		Primary Stresses (ksi)				Secondary Stresses (ksi)[b]				Primary Stress Intensity Factor (ksi$\sqrt{in.}$)		Secondary Stress Intensity Factor (ksi$\sqrt{in.}$)		Combined Stress Intensity Factor (ksi$\sqrt{in.}$)
Load Condition	Load Stage	σ_i	σ_o	σ_m	σ_b	σ_i	σ_o	σ_m	σ_b	K_{IM}	K_{IB}	K_{IM}	K_{IB}	K_I
Heatup	4.5 hr	23.80	21.55	22.68	1.12	-7.18	7.45	0.14	-7.32	61.46	2.03	0.37	—[c]	127.35
Cooldown	0 hr	23.80	21.55	22.68	1.12	0.0	0.0	0.0	0.0	61.46	2.03	0.0	0.0	126.98
Plant loading	20 min	23.80	21.55	22.68	1.12	1.97	-0.43	0.77	1.20	61.46	2.03	2.01	2.09	131.08
Unloading	20 min	23.80	21.55	22.68	1.12	3.54	-1.18	1.18	2.36	61.46	2.03	3.08	4.11	134.17
Small step load increase	220 sec	24.06	21.79	22.93	1.13	3.34	-0.96	1.19	2.15	62.14	2.05	3.11	3.74	135.23
Small step load dec.	35 sec	24.54	22.22	23.38	1.16	1.53	-0.70	0.42	1.11	63.36	2.10	1.10	1.93	133.95
Large step load dec.	2 min	25.12	22.74	23.93	1.19	0.82	-0.42	0.20	0.62	64.85	2.15	0.52	1.08	135.60
Loss of load	10 sec	29.35	26.57	27.96	1.39	-3.07	-0.65	-1.86	-1.21	75.77	2.52	—	—	156.58
Loss of flow	0 sec	23.80	21.55	22.68	1.12	0.0	0.0	0.0	0.0	61.46	2.03	0.0	0.0	126.98
Reactor trip from full power	0 sec	23.80	21.55	22.68	1.12	0.0	0.0	0.0	0.0	61.46	2.03	0.0	0.0	126.98
Turbine roll test	0 min	23.80	21.55	22.68	1.12	0.0	0.0	0.0	0.0	61.46	2.03	0.0	0.0	126.98
Steady state fluctuation	+fluct	24.85	22.50	23.68	1.17	1.85	-0.69	0.58	1.27	64.17	2.12	1.51	2.21	136.30
Cold hydro test	5 hr	33.05	29.93	31.49	1.56	0.0	0.0	0.0	0.0	85.34	2.82	0.0	0.0	132.24
Hot hydro test	5 hr	26.44	23.94	25.19	1.25	0.49	0.33	0.41	0.08	68.26	2.26	1.07	0.14	106.99

a. The hoop stress is the opening stress for the longitudinal flaw.

b. The secondary stresses include the thermal transient induced stress and the stress produced by radiation heating in the vessel wall.

c. Dashes indicate negative values.

TABLE 2-6
AXIAL STRESS[a] AND K_I DATA FOR THE BELTLINE

Load Condition	Load Stage	Primary Stresses (ksi)				Secondary Stresses (ksi)[b]				Primary Stress Intensity Factor (ksi$\sqrt{in.}$)		Secondary Stress Intensity Factor (ksi$\sqrt{in.}$)		Combined Stress Intensity Factor (ksi$\sqrt{in.}$)
		σ_i	σ_o	σ_m	σ_b	σ_i	σ_o	σ_m	σ_b	K_{IM}	K_{IB}	K_{IM}	K_{IB}	K_I
Heatup	4.5 hr	10.77	10.77	10.77	0.0	-7.18	7.45	0.14	-7.32	28.43	0.0	0.37	--[c]	57.23
Cooldown	0 hr	10.77	10.77	10.77	0.0	0.0	0.0	0.0	0.0	28.43	0.0	0.0	0.0	56.86
Plant loading	20 min	10.77	10.77	10.77	0.0	1.97	-0.43	0.77	1.20	28.43	0.0	2.01	2.09	60.96
Unloading	20 min	10.77	10.77	10.77	0.0	3.54	-1.18	1.18	2.36	28.43	0.0	3.08	4.11	64.05
Small step load increase	220 sec	10.89	10.89	10.89	0.0	3.34	-0.96	1.19	2.15	28.75	0.0	3.11	3.74	64.35
Small step load dec.	35 sec	11.11	11.11	11.11	0.0	1.53	-0.70	0.42	1.11	29.33	0.0	1.10	1.93	61.69
Large step load dec.	2 min	11.37	11.37	11.37	0.0	0.82	-0.42	0.20	0.62	30.02	0.0	0.52	1.08	61.64
Loss of load	10 sec	13.29	13.29	13.29	0.0	-3.07	-0.65	-1.86	-1.21	35.09	0.0	--	--	70.18
Loss of flow	0 sec	10.77	10.77	10.77	0.0	0.0	0.0	0.0	0.0	28.43	0.0	0.0	0.0	56.86
Reactor trip from full power	0 sec	10.77	10.77	10.77	0.0	0.0	0.0	0.0	0.0	28.43	0.0	0.0	0.0	56.86
Turbine roll test	0 min	10.77	10.77	10.77	0.0	0.0	0.0	0.0	0.0	28.43	0.0	0.0	0.0	56.86
Steady state fluctuation	+fluct	11.25	11.25	11.25	0.0	1.85	-0.69	0.58	1.27	29.70	0.0	1.51	2.21	63.12
Cold hydro test	5 hr	14.96	14.96	14.96	0.0	0.0	0.0	0.0	0.0	39.49	0.0	0.0	0.0	59.24
Hot hydro test	5 hr	11.97	11.97	11.97	0.0	0.49	0.33	0.41	0.08	31.60	0.0	1.07	0.14	48.61

a. The axial stress is the opening stress for the circumferential flaw.

b. The axial secondary stresses are assumed essentially equal to the circumferential secondary stresses.

c. Dashes indicate negative values.

TABLE 2-7
STRESS AND K_I DATA FOR THE LOWER HEAD JUNCTION

Load Condition	Load Stage	Primary Stresses (ksi)				Secondary Stresses (ksi)				Primary Stress Intensity Factor (ksi$\sqrt{in.}$)		Secondary Stress Intensity Factor (ksi$\sqrt{in.}$)		Combined Stress Intensity Factor (ksi$\sqrt{in.}$)
		σ_i	σ_o	σ_m	σ_b	σ_i	σ_o	σ_m	σ_b	K_{IM}	K_{IB}	K_{IM}	K_{IB}	K_I
Heatup	4.5 hr	26.27	20.83	23.55	2.72	-2.11	0.70	-0.71	-1.40	50.40	3.89	—[a]	—	108.58
Cooldown	0 hr	26.27	20.83	23.55	2.72	0.0	0.0	0.0	0.0	50.40	3.89	0.0	0.0	108.58
Plant loading	20 min	26.27	20.83	23.55	2.72	-0.94	0.50	-0.22	-0.72	50.40	3.89	—	—	108.58
Unloading	20 min	26.27	20.83	23.55	2.72	0.94	-0.50	0.22	0.72	50.40	3.89	0.45	0.99	110.02
Small step load increase	220 sec	26.56	21.06	23.81	2.75	0.73	-0.33	0.20	0.53	50.95	3.93	0.41	0.73	110.90
Small step load dec.	35 sec	27.08	21.48	24.28	2.80	-1.61	0.30	-0.66	-0.95	51.96	4.00	—	—	111.92
Large step load dec.	2 min	27.73	21.99	24.86	2.87	-2.54	0.86	-0.84	-1.70	53.20	4.10	—	—	114.60
Loss of load	10 sec	32.39	25.69	29.04	3.35	-5.19	0.39	-2.40	-2.79	62.15	4.79	—	—	133.88
Loss of flow	0 sec	26.27	20.83	23.55	2.72	0.0	0.0	0.0	0.0	50.40	3.89	0.0	0.0	108.58
Reactor trip from full power	0 sec	26.27	20.83	23.55	2.72	0.0	0.0	0.0	0.0	50.40	3.89	0.0	0.0	108.58
Turbine roll test	0 min	26.27	20.83	23.55	2.72	0.0	0.0	0.0	0.0	50.40	3.89	0.0	0.0	108.58
Steady state fluctuation	+fluct	27.43	21.76	24.60	2.83	-1.19	0.30	-0.45	-0.74	52.64	4.05	—	—	113.38
Cold hydro test	5 hr	36.48	28.93	32.71	3.77	0.0	0.0	0.0	0.0	70.00	5.39	0.0	0.0	113.09
Hot hydro test	5 hr	29.18	23.15	26.17	3.01	-1.18	0.47	-0.36	-0.82	56.00	4.30	—	—	90.45

a. Dashes indicate negative values.

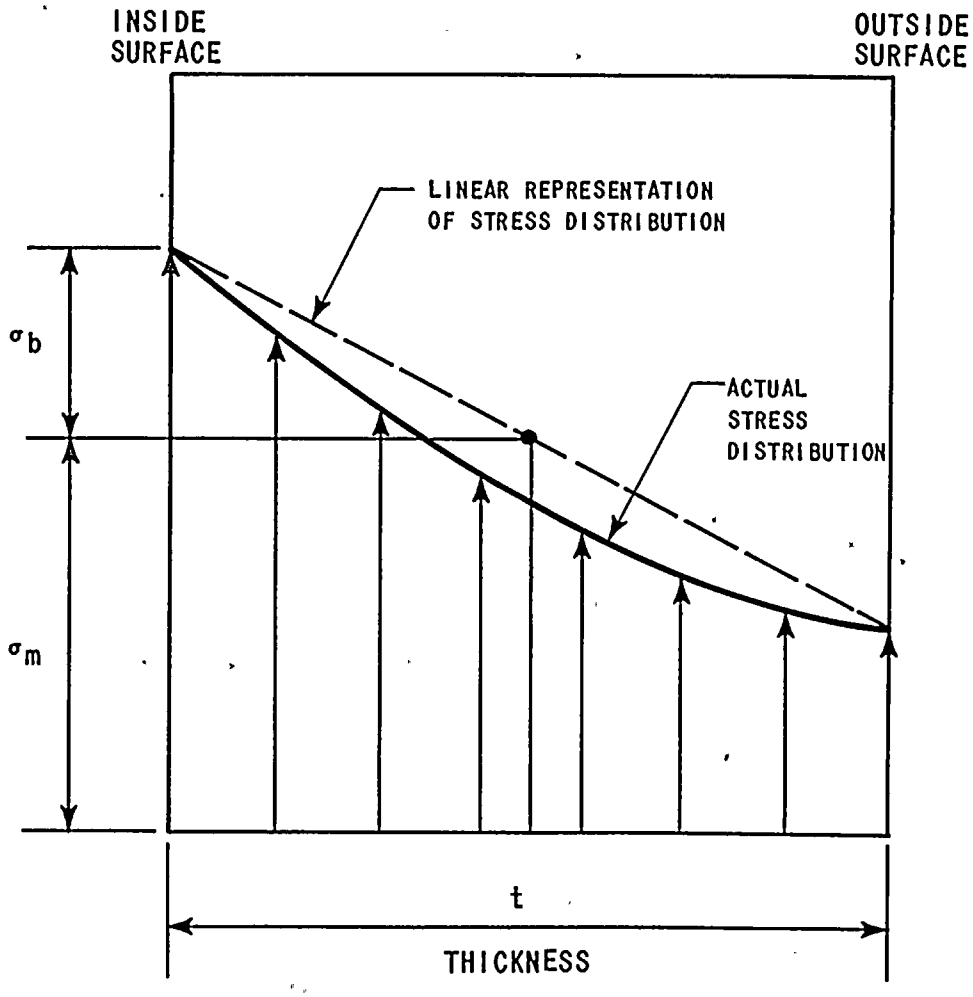

Figure 2-13. Linearized Representation of Stresses

TABLE 2-8

DATA FOR M_m AND M_b CALCULATION BY APPENDIX G CURVE

	Using Figures 2-5 and 2-6						
Stress Intensity Factor Category	T (Inches)	$\sqrt{T}$ (Inches)	σ_y (ksi)	σ_{max} (ksi)	σ_{max}/σ_y	M_m	M_b
Upper Head Junction							
Primary	6.19	2.49	50.0	20.17	0.40	2.39	1.59
Secondary	6.19	2.49	50.0	—[a]	0.10	2.34	1.56
Beltline							
Primary – Hoop	7.75	2.78	50.0	31.49	0.63	2.71	1.81
Primary – Axial	7.75	2.78	50.0	14.96	0.30	2.64	1.76
Secondary	7.75	2.78	50.0	—	0.10	2.61	1.74
Lower Head Junction							
Primary	4.75	2.18	50.0	32.71	0.65	2.14	1.43
Secondary	4.75	2.18	50.0	—	0.10	2.06	1.37

a. Minimum value of σ_{max}/σ_y = 0.10 used.

TABLE 2-9

DATA FOR M_m AND M_b CALCULATION FOR THE OUTLET NOZZLE JUNCTION

Stress Conditions	Using Figures 2-7 and 2-8				Using Figure 2-6				Correction Factors	
	T (Inches)	$\frac{a}{T}$	M_K (ksi)	A_b (ksi)	σ_{max} (ksi)	σ_y (ksi)	σ_{max}/σ_y	Q	M_m	M_b
Primary	9.0	0.20	1.05	0.83	32.13	50.0	0.64	1.15	2.56	1.84
Secondary	9.0	0.20	1.05	0.83	——[a]	50.0	0.10	1.23	2.48	1.78

a. Minimum value of σ_{max}/σ_y = 0.10 used.

2-12. Transients

The load stage chosen for each transient corresponds to the governing pressure and temperature load. The K_I value resulting is thus the highest K_I value for each transient in the four areas analyzed. Table 2-10 shows the load stage temperature and pressure for each transient.

2-13. Maximum Combined K_I Values

The maximum combined K_I values are plotted on each respective end-of-life K_{IR} curve for the four critical locations (figures 2-14 through 2-18). The numerical data for the plots are tabulated in table 2-11. For a justification of the upper shelf value, see appendix A.

2-14. K_I Values

Protection against nonductile failure is conservatively assured since the K_I values are below the K_{IR} curve for all load conditions for each of the critical vessel locations. Note that the K_{IR} curve is indexed to the highest RT_{NDT} at each location in both units. For example, in the upper head, the highest RT_{NDT} is 44°F in Unit No. 3 as compared to 30°F in Unit No. 4.

2-15. CONSERVATISM OF THE ANALYSIS

Protection of the reactor vessel from nonductile failure, ensured by the results of the analysis itself, is still further ensured due to the conservatisms inherent in performing the analysis according to the rules of Appendix G of Code Section III.

2-16. Safety Factors

A safety factor of 2 was applied to the primary stress, as shown in equation (2-5) for normal and upset conditions. A factor of 1.5 was applied for hydrostatic test conditions.

2-17. K_{Ia} Values Included

The K_{IR} curve shown in figure 2-1 is a lower-bound curve determined from crack-arrest toughness values, dynamic fracture toughness data, and static toughness data. Including K_{Ia} values (crack-arrest toughness values) ensures that a flaw as large as the reference flaw will not initiate and that a propagating crack will arrest before it exceeds the size of the reference flaw.

TABLE 2-10
TRANSIENTS[a]

Transients	Time	Cold Leg Temp (°F) for Closure Head, Beltline, Lower Head	Hot Leg Temp (°F) for Outlet Nozzle	System Pressure (psi)
Heatup	4.5 hr	547	547	2250
Cooldown	0 hr	547	547	2250
Plant Loading	20 min	557	612	2250
Unloading	20 min	547	547	2250
Small Step Load Increase	220 sec	555	610	2275
Small Step Load Decrease	35 sec	567	622	2320
Large Step Load Decrease	2 min	560	588	2375
Loss of Load	10 sec	584	658	2775
Loss of Flow	0 sec	559	614	2250
Reactor Trip from Full Power	0 sec	559	614	2250
Turbine Roll	0 min	559	614	2250
Steady State Fluctuations	+fluct	565	620	2350
Cold Hydro[b]	5 hr	—	—	3125
Hot Hydro	5 hr	400	400	2500

a. Transients are taken from the applicable equipment specification. "Turbine Roll" is not listed in the equipment specification, but was included for completeness.

b. The transient temperature is not shown for the cold hydrostatic test condition since the temperature used during this test is determined to ensure compliance with ASME Appendix G requirements and is not specified by the equipment specification.

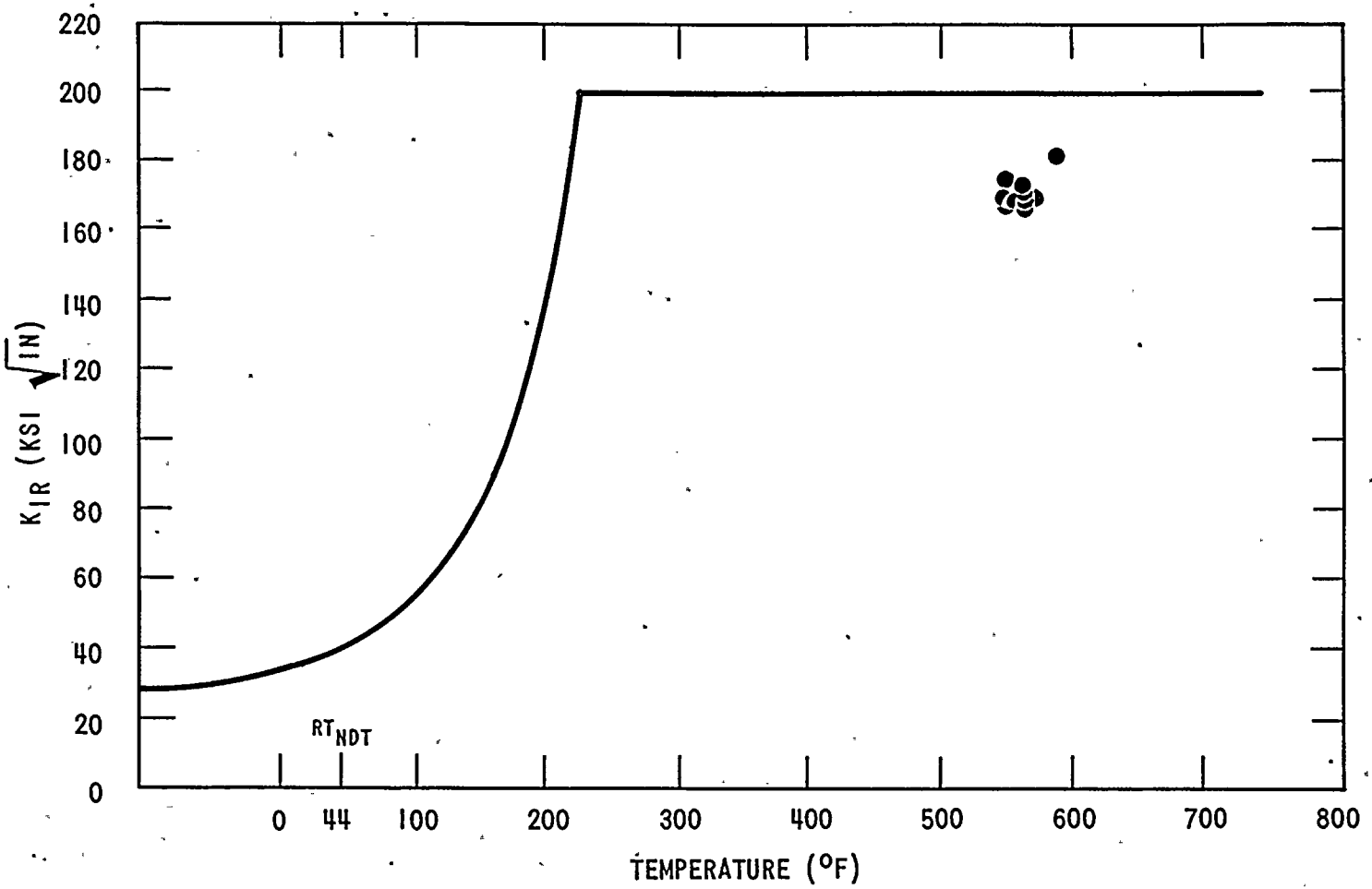

Figure 2-14. K_{IR} versus Temperature Curve for Upper Head Junction

10877-15

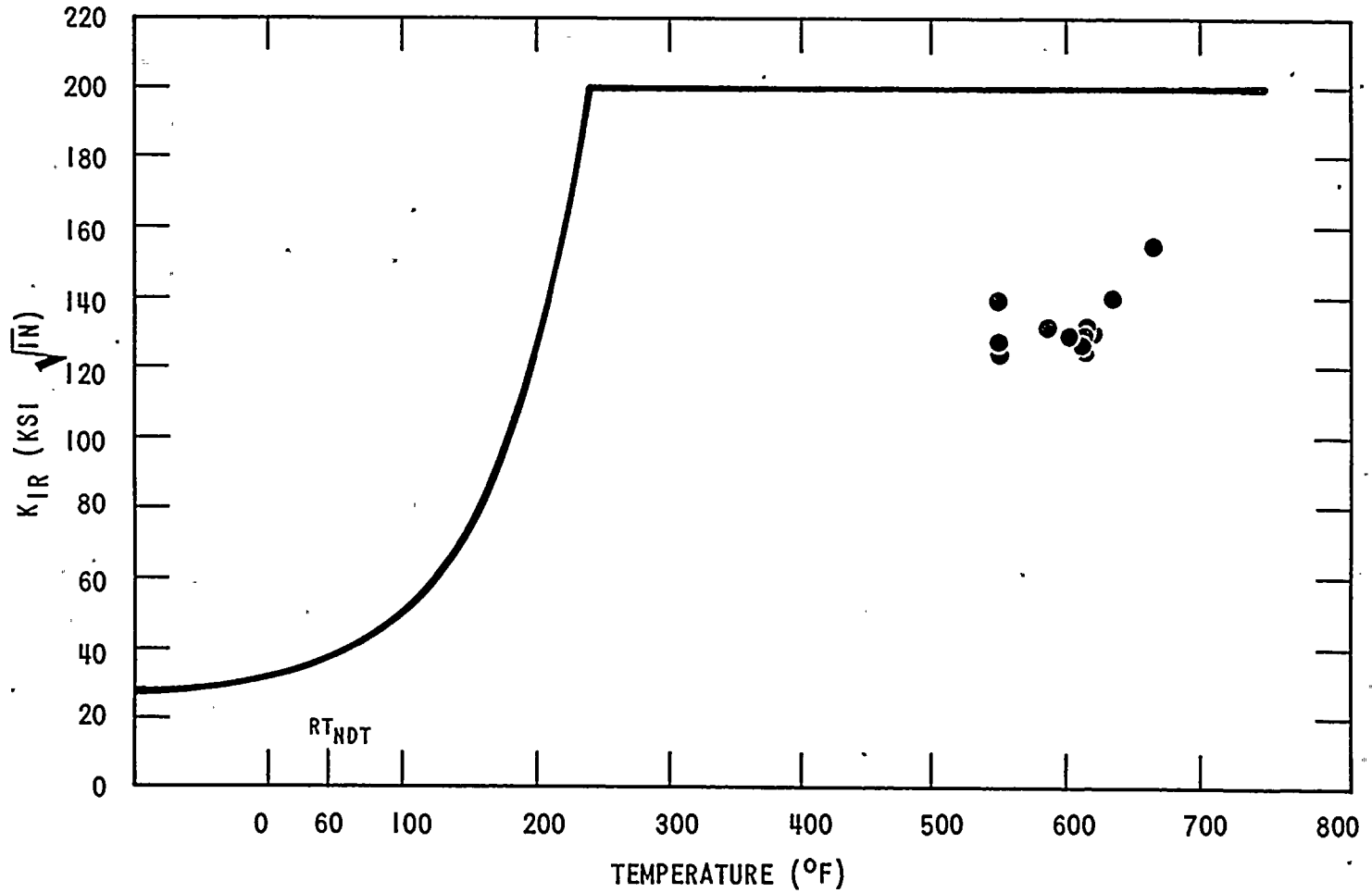

Figure 2-15. K_{IR} versus Temperature Curve for Outlet Nozzle Junction

10877-16

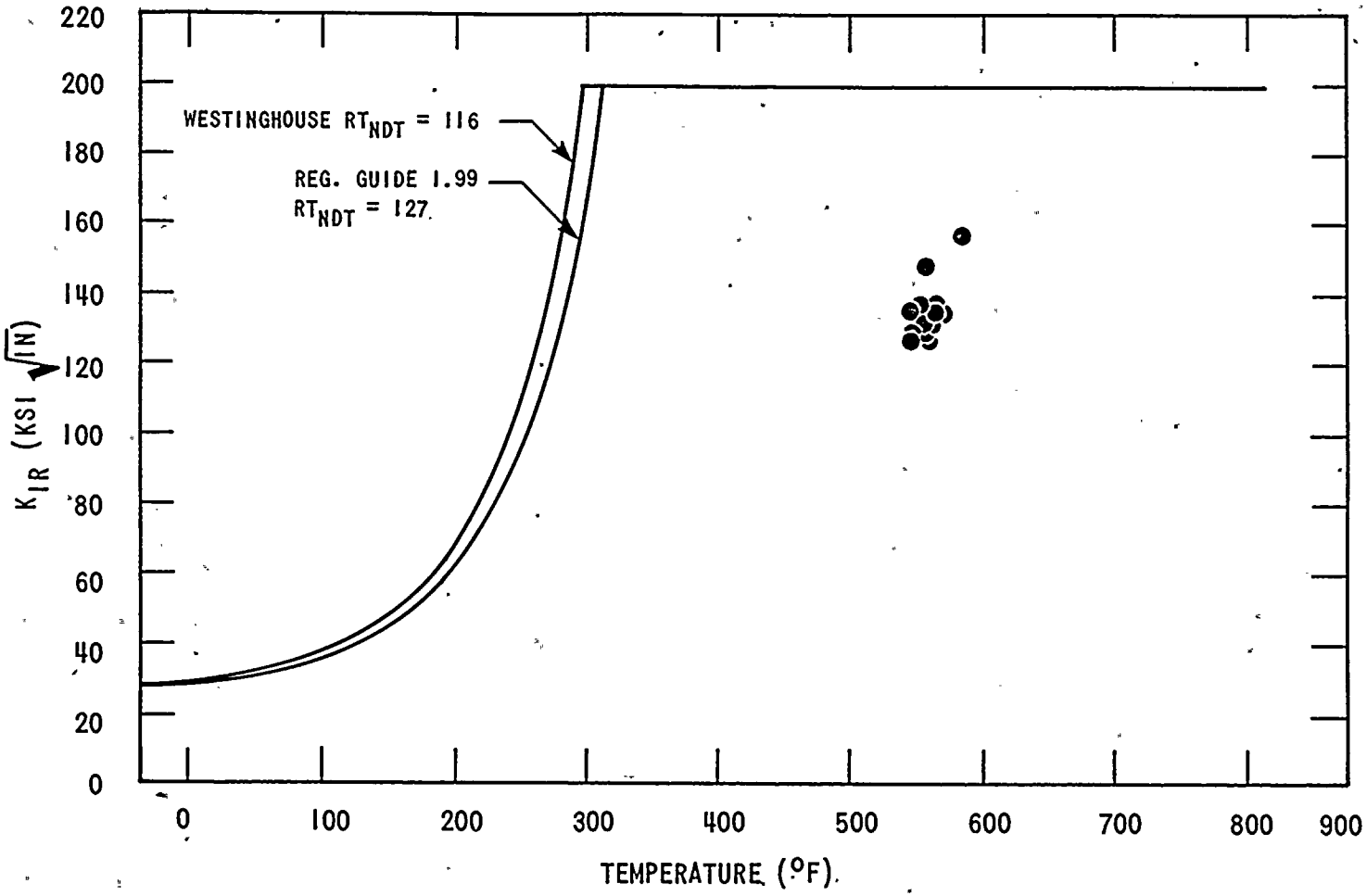

Figure 2-16. K_{IR} versus Temperature Curve for Beltline (Longitudinal Flaw)

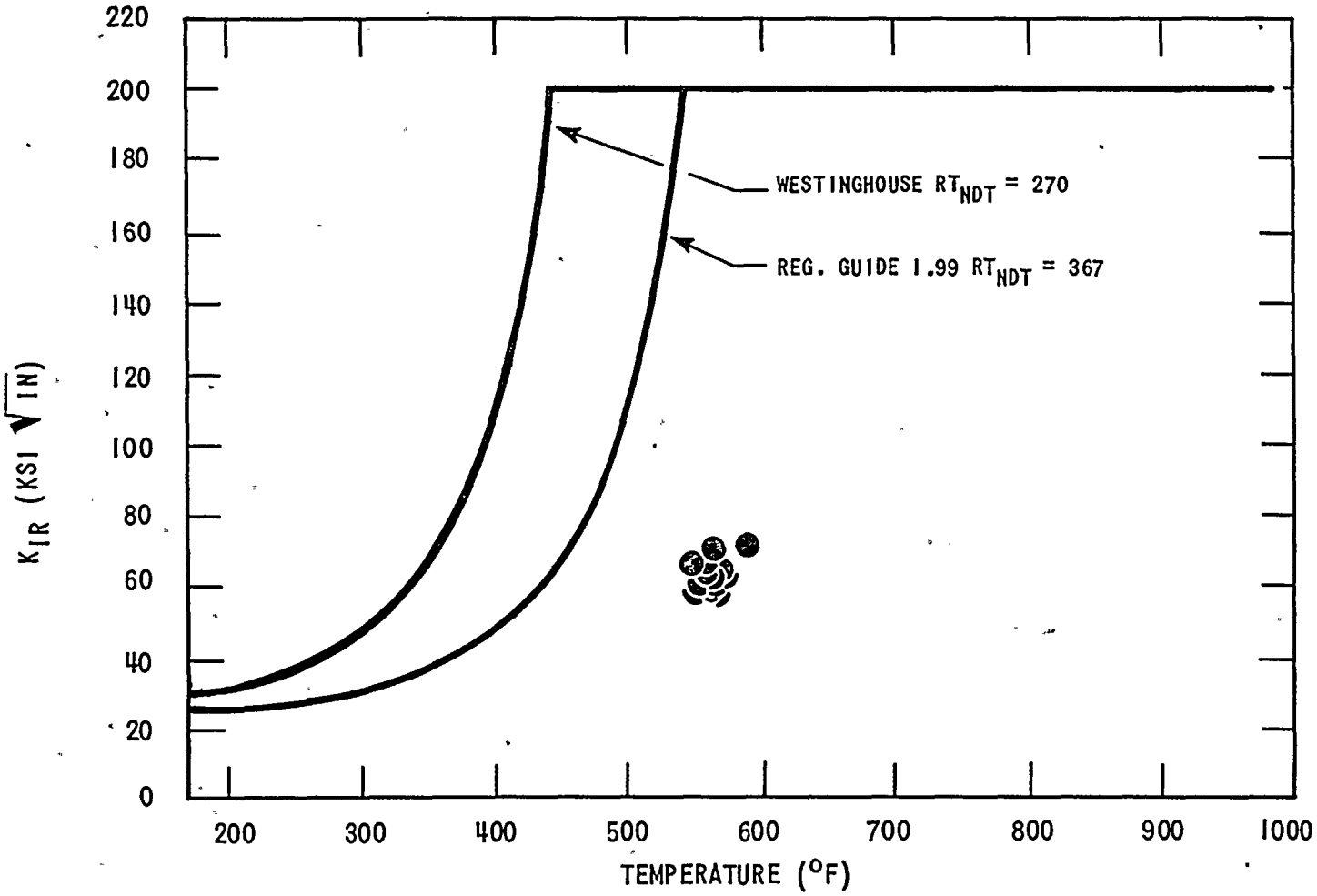

Figure 2-17. K_{IR} versus Temperature Curve for Beltline (Circumferential Flaw)

10877-18

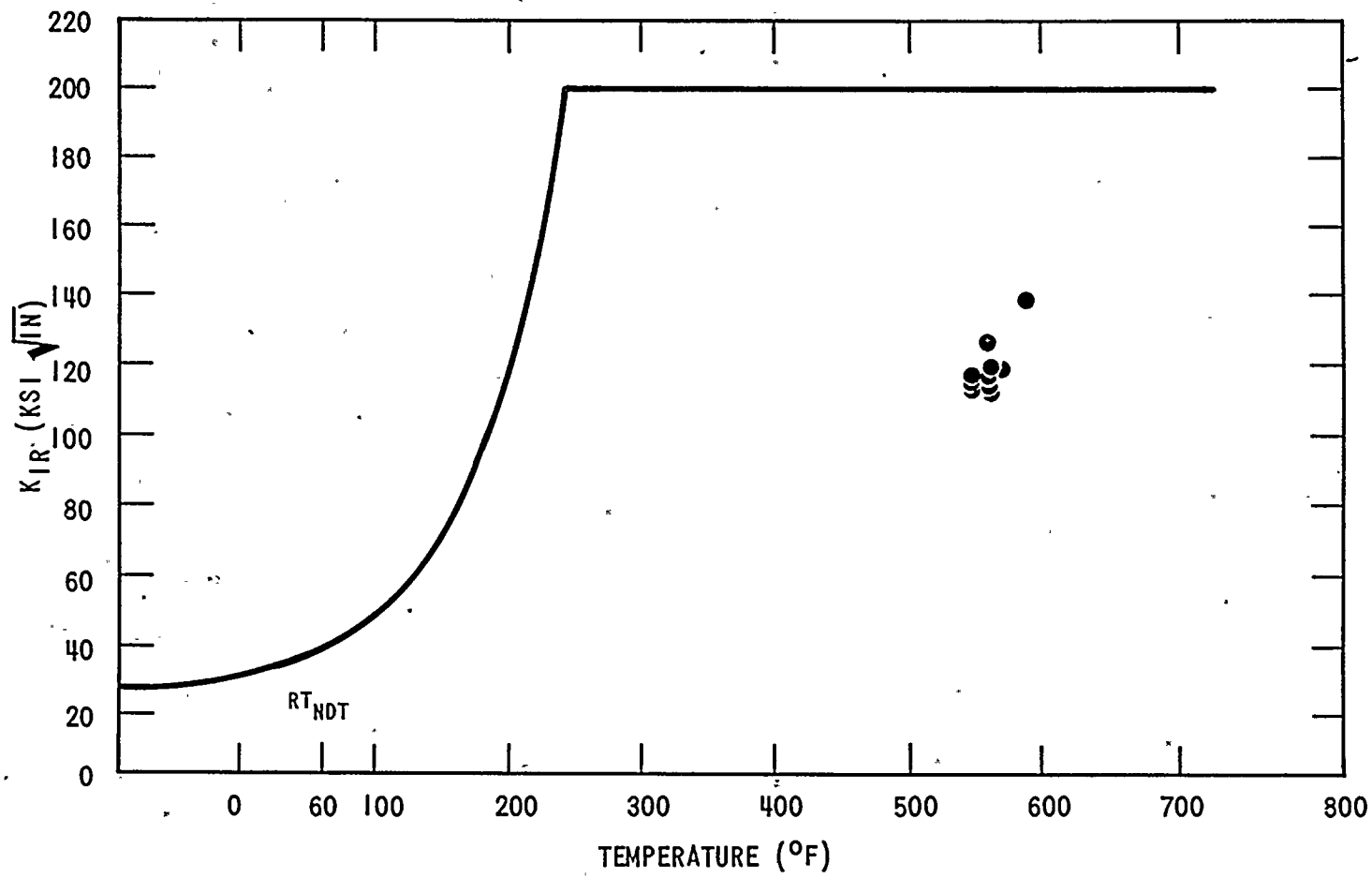

Figure 2-18. K_{IR} versus Temperature Curve for Lower Head Junction

10877-19

TABLE 2-11
TEMPERATURE VERSUS MAXIMUM COMBINED K_I

	Upper Head		Outlet Nozzle		Beltline			Lower Head	
Transients	Temperature (°F)	Maximum Combined K_I (ksi$\sqrt{in.}$)	Temperature (°F)	Maximum Combined K_I (ksi$\sqrt{in.}$)	Temperature (°F)	Maximum Combined K_I (ksi$\sqrt{in.}$)		Temperature (°F)	Maximum Combined K_I (ksi$\sqrt{in.}$)
Heatup	547	173.4	547	123.1	547	127.4[c]	57.2[d]	547	108.6
Cooldown	547	166.2	547	123.1	547	127.0	56.9	547	108.6
Plant Loading	557	167.3	612	123.1	557	131.1	61.0	557	108.6
Unloading	547	166.8	547	138.1	547	134.2	64.1	547	110.0
Small Step Load Increase	555	167.2	610	126.3	555	135.2	64.4	555	110.9
Small Step Load Decrease	567	168.7	622	127.1	567	134.0	61.7	567	111.9
Large Step Load Decrease	560	170.6	588	130.2	560	135.6	61.6	560	114.6
Loss of Load	584	181.2	658	152.7	584	156.6	70.2	584	133.9
Loss of Flow	559	166.2	614	123.1	559	127.0	56.9	559	108.6
Reactor Trip from Full Power	559	166.2	614	123.1	559	127.0	56.9	559	108.6
Turbine Roll	559	166.2	614	123.1	559	127.0	56.9	559	108.6
Steady State Fluctuations	565	169.2	620	128.7	565	136.3	63.1	565	113.4
Cold Hydro Test[a]	—	140.6	—	129.3	—	132.2	59.2	—	113.1
Hot Hydro Test[b]	400	133.6	400	102.9	400	107.0	48.6	400	90.5

a. The K_I values for this transient are not plotted on the end-of-life K_{IR} curves since this is a beginning-of-life transient only.

b. The K_I values calculated for this transient based on the equipment specification temperature of 400°F are conservative since the actual plant transient temperature is determined to ensure compliance with Appendix G.

c. The K_I values in this column are for the longitudinal flaw.

d. The K_I values in this column are for the circumferential flaw.

2-18. Flat Plate Assumed

The expression used to calculate the stress intensity factor was derived for application to a flaw in a flat plate. An axisymmetrical body provides more constraint than a flat plate does. So, the stress intensities calculated by Appendix G will be higher than the actual values in the reactor vessel.

2-19. Stresses Assumed Linear

Linearization of the stresses throughout the wall thickness will generally result in a higher membrane stress than the actual value such as those transients of high radial thermal gradients.

2-20. Largest ΔRT_{NDT}

For each of the critical locations, the material properties used in the calculations were those which gave the largest ΔRT_{NDT} shift to the K_{IR} curve. For example, in the beltline region the weld material properties were used for the circumferential flaw since these properties gave a larger shift to the curve than the surrounding plate material.

2-21. Negative Stresses Not Deduced

The stress intensity factors are computed separately for primary and secondary stresses. In many of the transients, the secondary stresses are negative, and thus act to make the total stress less than the primary stress. The stress intensity factor which results from a negative stress is considered to be zero in the Appendix G procedure. Consequently, the calculated K_I will be greater than actual since the negative stresses are not deducted.

SECTION 3
CONCLUSIONS

In view of the plotted combined K_I values in figures 2-14 through 2-18, it is evident that:

- In the K_{IR} curve for the beltline (figures 2-16 and 2-17) all the maximum combined K_I values are within the upper shelf limit of 200 ksi $\sqrt{in.}$
- Similarly, the maximum combined K_I values of the other three critical regions are below the upper shelf limit conservatively taken as 200 ksi $\sqrt{in.}$ (figures 2-14, 2-15 and 2-18).
- Therefore, the requirements of the rules of Appendix G have been satisfied and protection against nonductile failure is ensured.

SECTION 4
REFERENCES

1. Appendix G of the ASME Boiler and Pressure Vessel Code Section III, "Protection Against Nonductile Failure," 1974 Edition, Winter 1975 Addenda.

2. Potapdvs, J., Hawthorne, J. R., "The Effect of Residual Elements on 550°F Irradiation Response of Selected Pressure Vessel Steels and Weldments." NRL Report 6803, November 1968.

3. Regulatory Guide 1.99, "Effects of Residual Elements on Predicted Radiation Damage to Reactor Vessel Materials," U.S. Nuclear Regulatory Commission, July 1975.

4. "PVRC Recommendations on Toughness Requirements for Ferritic Materials," *Welding Research Council Bulletin #175,* August 1972.

5. "Design Report No. 116," Babcock Wilcox Company, 1966-1970.

6. Phillips, J., et. al., "Fracture Analysis for Normal, Upset, and Test Conditions for Turkey Point III Nuclear Steam Supply System Based on Appendix G, ASME Code Section III," WCAP-8581, October 1975.

7. "Analytical Report for Duquesne Light Company, Beaver Valley Power Station Unit No. 1 Reactor Vessel," Report No. CENC-1183, Combustion Engineering, Inc., July 1972.

8. Yanichko, S. E., et al., "Analysis of Capsule T from the Florida Power and Light Company Turkey Point Unit No. 3 Reactor Vessel Radiation Surveillance Program," WCAP-8631, December 1975.

9. Meeuwis, O., "Material Properties Turkey Point Unit No. 4," Memo Report, SM 13.0 (FLA), October 1976.

10. Meeuwis, O., "Fracture Mechanics Evaluation of the Florida Power and Light Company Turkey Point Units No. 3 and No. 4 Reactor Vessel," WCAP-8945, May 1977.

APPENDIX A
FRACTURE TOUGHNESS VALUES

A large number of fracture toughness tests have been completed on pressure vessel steels and associated welds and weld-heat-affected zones.[1,2,3,4,5,6] Both static and dynamic toughness data have been obtained, and a lower bound for these data in the transition region is given by the reference toughness curve (K_{IR}) in Section III, Appendix G, of the ASME Code. The same curve is also contained in Section XI, Appendix A, of the code along with a curve (K_{IC}) which is a lower bound of static toughness only. The upper shelf toughness for these materials has not been characterized as yet in the ASME Code because of the difficulties involved in testing in this area.

Fracture toughness testing results in two distinct types of fracture behavior. At low and transition temperatures, fracture is by cleavage and the onset of crack extension is abrupt and unambiguous. The maximum load corresponds to the fracture initiation point and there is no stable crack growth. Thus, methods for interpreting data from toughness specimens such as the equivalent energy method[7] and the J-integral method[8] based on the maximum load point in the load-deflection record produce toughness values consistent with those obtained according to the requirements of ASTM procedure E399.[9] Instrumented precracked Charpy test results[4,5,6] obtained in the transition region are also consistent with the other results (figure A-1).

At temperatures higher than the transition temperature, fracture occurs by ductile tearing, and the onset of crack growth cannot be ascertained from the appearance of the load-deflection record. Thus, the methods of toughness determination based on the maximum load point (including precracked Charpy results) lose their validity. The test methods presented in ASTM procedure E399 are impractical for obtaining these upper shelf toughness values because of the size requirements. Results of the Heavy Section Steel Technology Program[1,2,3] have shown that "valid" toughness values cannot be obtained in this region with compact specimens even as large as 12 inches thick. Testing of larger specimens to obtain a valid toughness measurement is both impractical and prohibitively expensive. Therefore, great care must be exercised in interpreting fracture toughness results in the upper shelf region. Two methods are available for reliable determination of upper shelf fracture toughness for reactor pressure vessel steels.

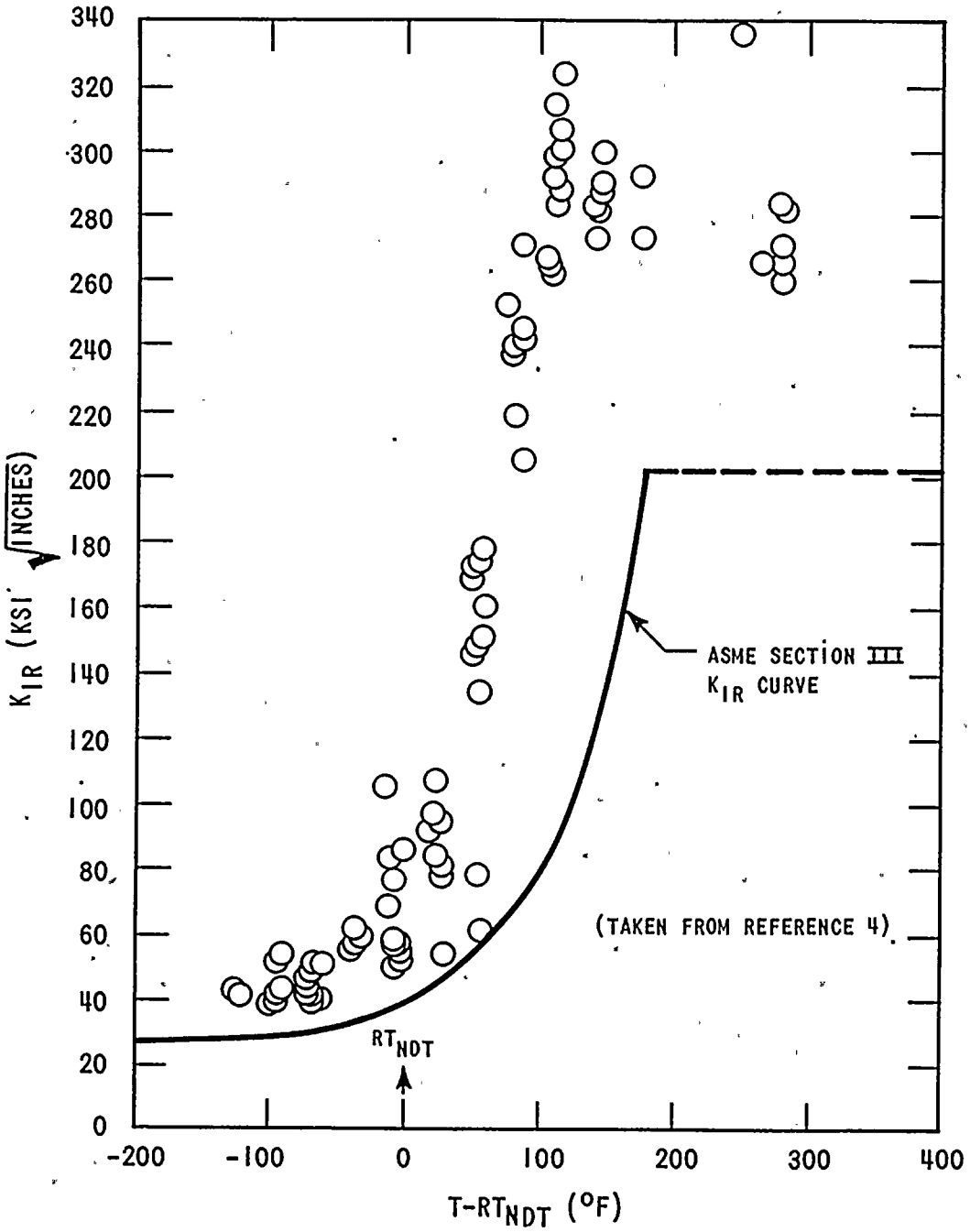

Figure A-1. Instrumented Precracked Charpy Test Results

Data from large compact specimens (2T and 4T) can be used to measure toughness in the transition region based on the maximum load point and will give accurate results as long as the fracture is cleavage-controlled. Both static and dynamic toughness results are available [4,5,6] on unirradiated plate, forging material, welds, and heat-affected zones. Results show that the onset of the upper shelf occurs at toughness values which range from 210 to 250 ksi $\sqrt{in.}$ A careful study of the onset of upper shelf toughness using 1.9 and 4T compact specimens was recently made on irradiated plate and weld material. [10] Results showed that the onset of the upper shelf occurred at values in excess of 215 ksi $\sqrt{in.}$ for the weld material and 220 ksi $\sqrt{in.}$ for the base metal (figure A-2).

Another reliable method of determining upper shelf toughness is the J-integral method proposed recently by Landes and Begley. [11] This method involves measurement and reporting of the actual amount of subcritical crack growth associated with the fracture process. A rather extensive test program has been completed [12] to obtain J_{IC} fracture toughness results for pressure vessel steels. These results can be used to calculate K_{IC} fracture toughness through the relationship

$$J_{IC} = \frac{(1 - \nu^2)}{E} K_{IC}^2$$

In choosing J-integral values which correspond to some minimal crack extension we should therefore obtain toughness values which, when employed in fracture analyses for vessels at upper shelf temperature, predict the conditions for the onset of slow crack growth rather than unstable fracture. In this sense these values will be conservative. Choosing 20 mils as a conservatively small amount of crack extension, we obtain from reference 12 a minimum upper shelf toughness of 200 ksi $\sqrt{in.}$

In conclusion, therefore, the fracture toughness of pressure vessel steels can be conservatively determined from the following procedure:

- In the lower temperature and transition regions use the fracture toughness values given by the ASME code.
- In the upper shelf region, let the fracture toughness be constant and equal to 200 ksi $\sqrt{in.}$ for unirradiated material and 200 ksi $\sqrt{in.}$ for irradiated material.

This interpretation is consistent with the most recent fracture toughness testing results and will provide conservative toughness values throughout the range of temperatures at which the reactor vessel operates.

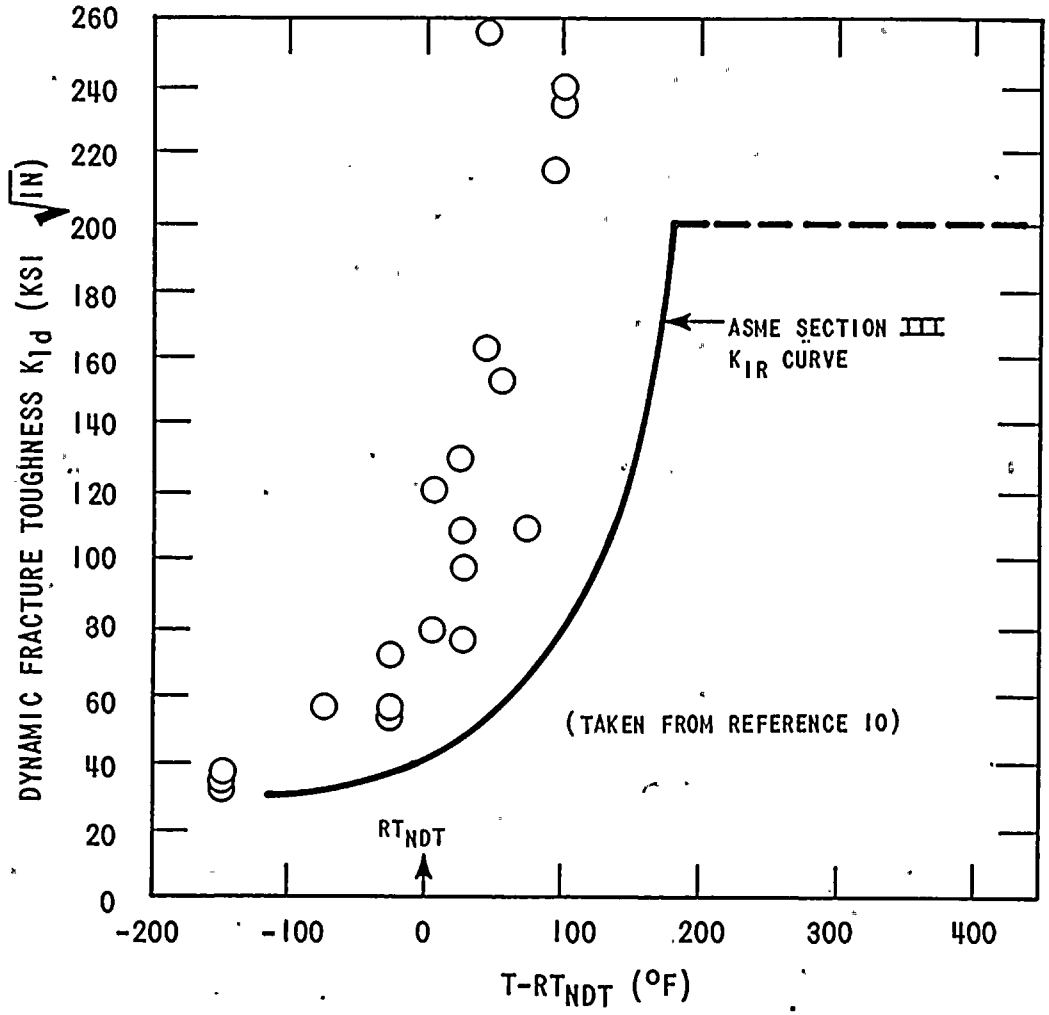

Figure A-2. Irradiated Dynamic Fracture Toughness Results

REFERENCES TO APPENDIX A

1. Shabbits, W. O., Pryle, W. H., and Wessel, E. T., "Heavy Section Fracture Toughness Properties of A533, Grade B, Class 1 Steel Plate and Submerged Arc Weldment," HSST Technical Report 6, WCAP-7414, December 1969.

2. Mager, T. R., "Fracture Toughness Characterization Study of A533, Grade B, Class 1 Steel," HSST Technical Report 10, WCAP-7578, October 1970.

3. Shabbits, W. O., "Dynamic Fracture Toughness Properties of Heavy Section A533, Grade B, Class 1 Steel Plate," HSST Technical Report 13, WCAP-7623, December 1970.

4. Marston, T. U., et al., "Fracture Toughness of Ferritic Materials in Light Water Nuclear Reactor Vessels," EPRI-232-2, December 1975.

5. Wullaert, W. A., et al., "Fracture Toughness of Ferritic Materials in Light Water Nuclear Reactor Vessels," EPRI-232-1, Task B, February 1976.

6. Van der Sluys, W. A., et al., "Fracture Toughness of Ferritic Materials in Light Water Nuclear Vessels," EPRI-232-3 (to be published).

7. Witt, F. J. and Mager, T. R., "A Procedure for Determining Bounding Values on Fracture Toughness K_{IC} at any Temperature," ORNL-TM-3894, October 1972.

8. Begley, J. A. and Landes, J. D., "The J-Integral as a Fracture Criterion," in *Fracture Toughness,* ASTM-STP-514, pp. 1-23, American Society for Testing and Materials, Philadelphia, 1972.

9. ASTM Standard E399-72, "Standard Method of Test for Plane-Strain Fracture Toughness of Metallic Materials," in ASTM Standards, Part 31, pp. 960-979, American Society for Testing and Materials, Philadelphia, 1973.

10. Davidson, J. A., et al., "The Irradiated Dynamic Fracture Toughness of ASTM A533, Grade B, Class 1 Steel Plate and Submerged Arc Weldment," HSST Technical Report 41, WCAP-8775, May 1976.

11. Landes, J. D. and Begley, J. A., "Test Results from J-Integral Studies, an Attempt to Establish a J_{IC} Testing Procedure," in *Fracture Analysis,* ASTM-STP-560, pp. 170-186, American Society for Testing and Material, Philadelphia, 1974.

12. Landes, J. C., Logsdon, W. and Begley, J. A., "Upper Shelf J_{IC} Behavior of A533, Grade B and A508 Class 2 Steels," (Private Communication).

WCAP-8884

WESTINGHOUSE CLASS 3
CUSTOMER DESIGNATED DISTRIBUTION

FATIGUE CRACK GROWTH EVALUATION OF THE FLORIDA POWER AND LIGHT COMPANY TURKEY POINT UNITS NO. 3 AND NO. 4 REACTOR VESSEL

by

J. J. McGowan
P. P. Raju
O. Meeuwis

June 1977

Prepared by Westinghouse for the Florida Power and Light Company

APPROVED: J. N. Chirigos
J. N. Chirigos, Manager
Structural Materials Engineering

Work Performed Under EKDP-300

Although the information contained in this report is nonproprietary, no distribution shall be made outside Westinghouse or its Licensees without the customer's approval.

WESTINGHOUSE ELECTRIC CORPORATION
Nuclear Energy Systems
P. O. Box 355
Pittsburgh, Pennsylvania 15230

ABSTRACT

A fatigue crack growth evaluation of the Turkey Point Units No. 3 and No. 4 Reactor Vessel (specifically, the belt line region) is presented in this report. Concepts of linear elastic fracture mechanics were used in this evaluation. The results of this evaluation indicate that, of those flaws postulated to exist in the belt line region, fatigue crack growth due to normal operating conditions during the design life of the reactor vessel is small.

PREFACE

This report has been technically reviewed and the calculations checked.

W. H. Bamford

TABLE OF CONTENTS

Section	Title	Page
1	INTRODUCTION	1-1
2	THERMAL AND STRESS ANALYSIS	2-1
	2-1. Summary of Method	2-1
	2-2. Finite Element Modeling	2-1
	2-3. Transient Thermal Analysis	2-1
	2-4. Theory of Transient Thermal Analysis	2-5
	2-5. Boundary Conditions	2-5
	2-6. Mechanical and Thermal Properties	2-8
3	DESIGN TRANSIENTS	3-1
4	STRESS INTENSITY FACTOR K_I CALCULATIONS	4-1
5	FATIGUE CRACK GROWTH RATE	5-1
6	FATIGUE EVALUATION	6-1
7	RESULTS AND CONCLUSIONS	7-1

LIST OF ILLUSTRATIONS

Figure	Title	Page
2-1	Turkey Point Units No. 3 and No. 4 Reactor Vessel	2-2
2-2	Turkey Point Units No. 3 and No. 4 Reactor Vessel Belt Line Region	2-3
2-3	Finite Element Model	2-4
2-4	Thermal Boundary Conditions	2-6
2-5	Stress Boundary Conditions	2-7
3-1	End of Heatup - Isothermal Plot	3-4
3-2	End of Cooldown - Isothermal Plot	3-5
3-3	End of Heatup - Hoop Stress Plot	3-6
3-4	End of Cooldown - Hoop Stress Plot	3-7
4-1	Linearized Representation of Stresses	4-4
4-2	Shape Factors for Surface Flaws	4-6
4-3	Membrane Correction Factors for Surface Flaws	4-7
4-4	Bending Correction Factor for Surface Flaws	4-8
5-1	Upper Bound Fatigue Crack Growth Data for Reactor Vessel Steels	5-3

LIST OF TABLES

Table	Title	Page
2-1	Material Properties	2-8
3-1	Transients Used for Fatigue Evaluation	3-2
3-2	Schedule of Reactor Vessel Operating Transients	3-3
4-1	Inside Surface and Mean Stresses and Stress Ranges for the Critical Location of the Turkey Point Units No. 3 and No. 4 Reactor Vessel	4-5
6-1	Stress Intensity Ranges (ΔK_I) Turkey Point Units No. 3 and No. 4 Reactor Vessel Belt Line Region	6-2
7-1	Results of Fatigue Crack Growth Evaluation—Turkey Point Units No. 3 and No. 4 Reactor Vessel Belt Line Region	7-2

SECTION 1
INTRODUCTION

This report presents an evaluation of fatigue crack growth in the reactor vessel belt line region of the Florida Power and Light Company, Turkey Point Units No. 3 and No. 4. This evaluation is based on linear elastic fracture mechanics principles.

Examination of the as-built reactor vessel drawings for Turkey Point Units No. 3 and No. 4 revealed that the belt line regions are identical. All of the system transient, thermal, and mechanical loadings applicable to these units were then studied. In every case the magnitude and number of occurrences of the loadings were the same for both units. The mechanical and thermal properties of the belt line region materials of both units were also the same. Therefore, the fatigue crack growth analysis performed for Unit No. 3 is equally applicable to Unit No 4.

In terms of nonductile fracture, linear elastic fracture mechanics theory provides the most detailed and accurate analytical method for determining the safety margins inherent in thick-walled reactor vessels.

The linear elastic fracture mechanics concept which is applied, is basically a stress intensity consideration for which criteria are established for fracture instability in the presence of a crack-like flaw. Once it has been established that a crack, or crack-like defect exists in the structure being evaluated (either postulated or due to mechanical defect), the approach is to relate the stress field developed in the vicinity of the crack tip to the applied normal stress on the structure, the material properties, and the flaw size necessary to cause fatigue failure. The fatigue crack growth characteristics of the material under service conditions and their dependence on the crack tip stress intensities are important in determining the final flaw size at the end of the service life of a structure.

The fatigue crack growth analysis is performed on the belt line region, which is the most critical from the standpoint of irradiation embrittlement of the material. The initial flaw sizes assumed are conservative upper bounds of the types of flaws which could exist in the reactor pressure vessel. Crack tip stress intensity factors are calculated using finite semielliptical surface flaw expressions, after linearizing the thermal and mechanical stress distributions across the thickness of the belt line. The fatigue crack growth data taken from Section XI[1] of the ASME Code are used in these evaluations.

1. ASME Boiler and Pressure Vessel Code, Section XI, "Rules for Inservice Inspection of Nuclear Power Plant Components," American Society of Mechanical Engineers, New York, 1974.

SECTION 2
THERMAL AND STRESS ANALYSIS

2-1. SUMMARY OF METHOD

This section presents the results of transient thermal and stress analysis of the belt line region of the Turkey Point Units No. 3 and No. 4 reactor vessel. The purpose of this analysis is to determine the stresses in the belt line due to transient, thermal, and mechanical loads identified in the applicable design specification for these reactor vessels.

The analysis was performed in accordance with the requirements of the ASME Code, Section III,[1] and the applicable Westinghouse specification. For calculation of transient temperature fields, a computer program based on a finite difference procedure, was employed.

2-2. FINITE ELEMENT MODELING

In the finite element modeling, the presence of cladding was not considered as per the criteria set forth in Section III[1] of the ASME code. The geometry and the finite element mesh used for the analysis are shown in figures 2-1 through 2-3. The belt line region is represented by a thick-walled cylinder, with 6 elements across the thickness and 53 elements along the axis of symmetry. A single model was used for both the thermal and stress analyses.

Within a given transient the coolant temperature and pressure variations may give opposing variations in the stress distributions through the vessel wall. For such transients it is difficult to determine when the maximum or minimum stress intensity factor would be produced. Therefore, check calculations were performed using an economical one-dimensional finite difference code. This code determines the stresses for a sufficient number of times during the transient to accurately calculate the maximum or minimum stress intensity factor.

2-3. TRANSIENT THERMAL ANALYSIS

The transient heat transfer analysis option of a Westinghouse computer program was used to solve for the nodal point and element temperatures as a function of time. The effect of temperature-dependent material properties was included. This was accomplished by evaluating the material properties based on the most recently calculated temperature. A finite difference was used for integration in the time domain.

1. ASME Boiler and Pressure Vessel Code, Section III, "Nuclear Power Plant Components," American Society of Mechanical Engineers, New York, 1974.

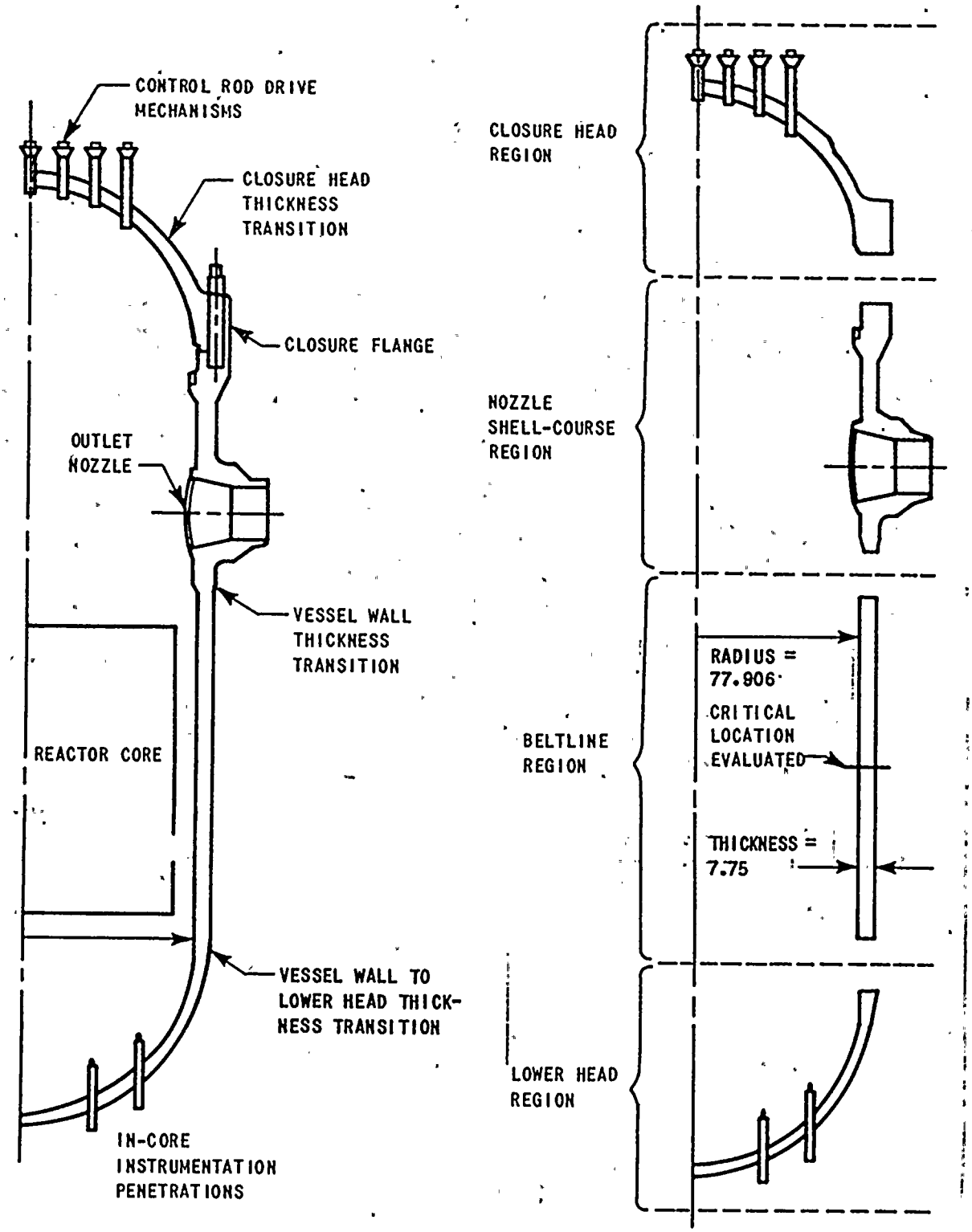

Figure 2-1. Schematic Cross section of the Turkey Point Units No. 3 and No. 4 Reactor Vessel

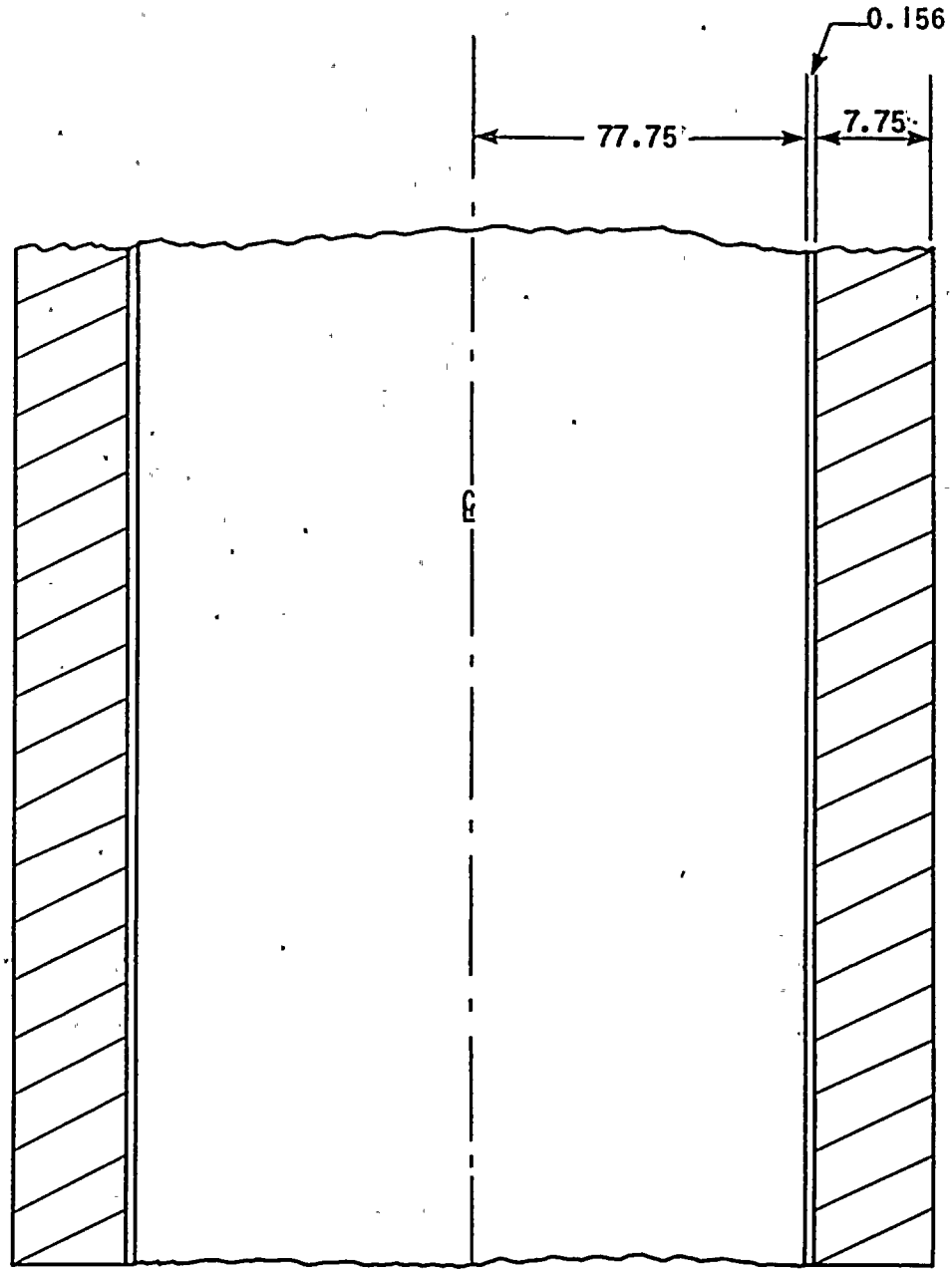

Figure 2-2. Turkey Point Units No. 3 and No. 4 Reactor Vessel Belt Line Region

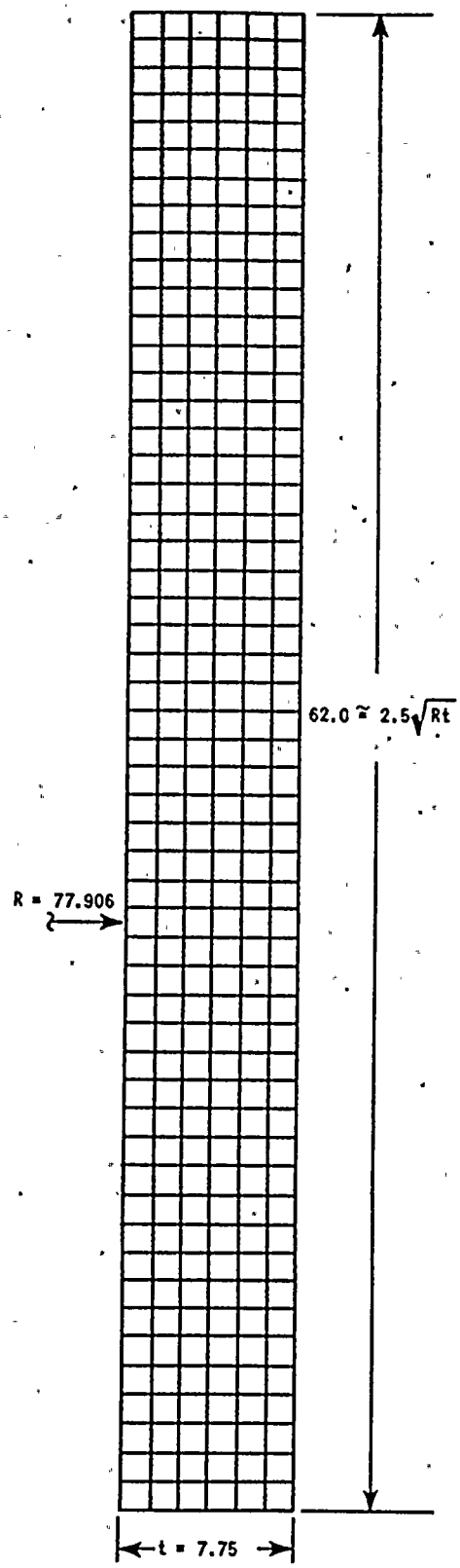

Figure 2-3. Finite Element Model

2-4. THEORY OF TRANSIENT THERMAL ANALYSIS

The basic equation for the transient thermal analysis is

$$[C_pT] \left\{T'\right\} + [K_T] \left\{T\right\} = \left\{Q_{app}\right\} + H \left\{T_o\right\} \qquad (1\text{-}1)$$

where

$\left\{T\right\}$ = the nodal temperature vector

$\left\{T'\right\}$ = the time derivative of the nodal temperature vector

$[C_pT]$ = the specific heat matrix for the entire model

$[K_T]$ = the thermal conductivity matrix including the convection contribution

$\left\{Q_{app}\right\}$ = the applied nodal heat flux vector

$[H]$ = the structure thermal conductivity matrix due to forced convection handled by the element convection surfaces

$\left\{T_o\right\}$ = the bulk temperature.

The time derivative T′ is calculated by a finite difference procedure. The resulting linear simultaneous equations are solved by a wave front equation solver.

2-5. BOUNDARY CONDITIONS

The boundary conditions used in the belt line analysis are as follows.

1) Heat Transfer Analysis

The thermal boundary conditions are clearly defined in figure 2-4. All external surfaces are assumed to be completely insulated. The interior surface is in contact with the primary coolant. A heat transfer coefficient of 2000 Btu/hr-°F-ft^2 is applied at the inside surface. This value is sufficiently high for the calculation of vessel temperature profiles in that the temperature distribution is insensitive to changes in the heat transfer coefficient to values larger than 1000 Btu/hr-°F-ft^2.

2) Stress Analysis

The belt line cross section at the upper end is loaded with a stress distribution

$$Po\left(\frac{a^2}{b^2-a^2}\right)$$

to constrain this edge to remain in its plane and satisfy the equilibrium conditions. The lower edge is allowed to move radially on rollers. No rotation is permitted at this edge. The stress boundary conditions are identified in figure 2-5. Since the region of interest shown on figure 2-5 (section A-A) is away from the upper boundary, the stress values used in the fatigue crack growth calculations are not affected by the boundary conditions.

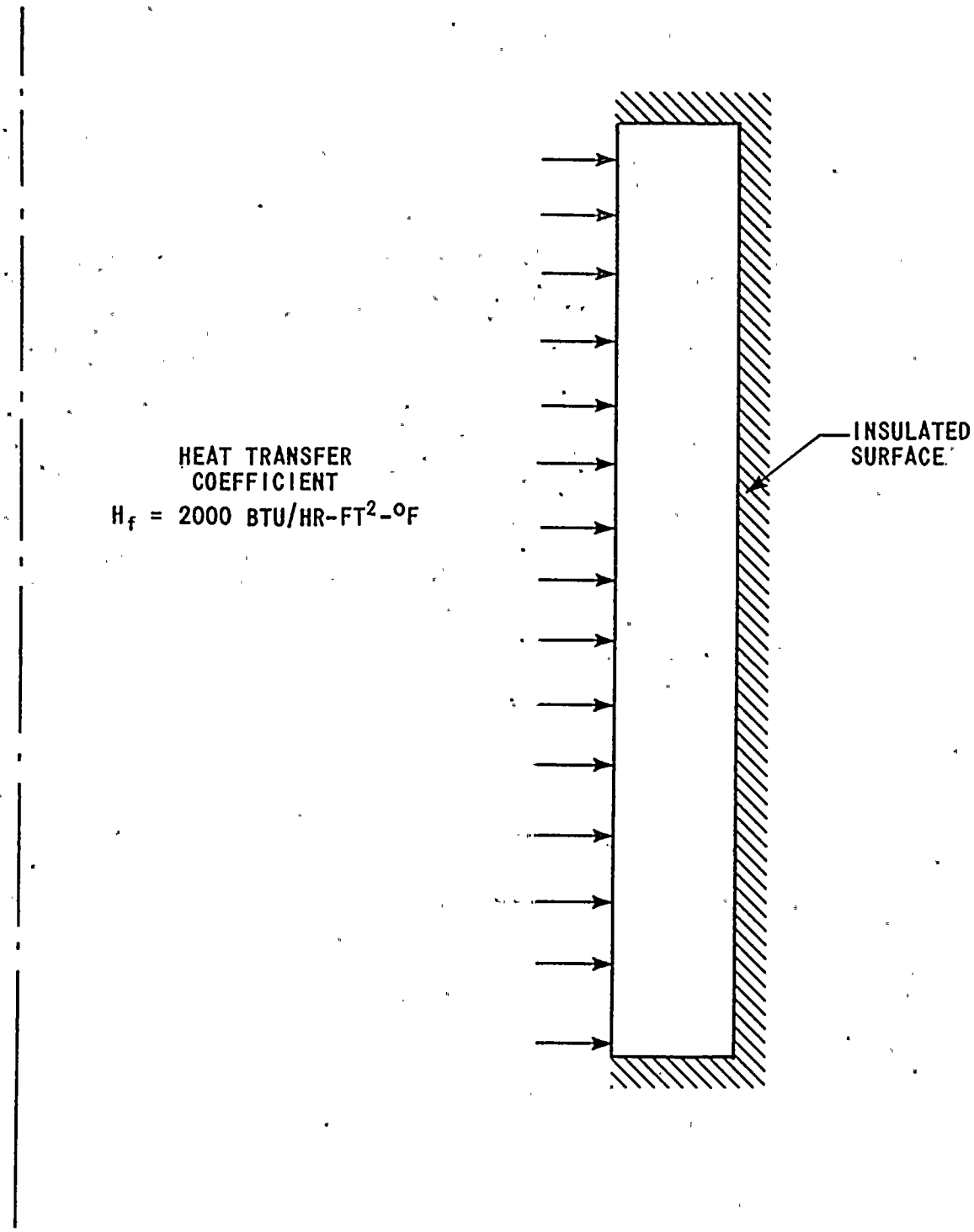

Figure 2-4. Thermal Boundary Conditions

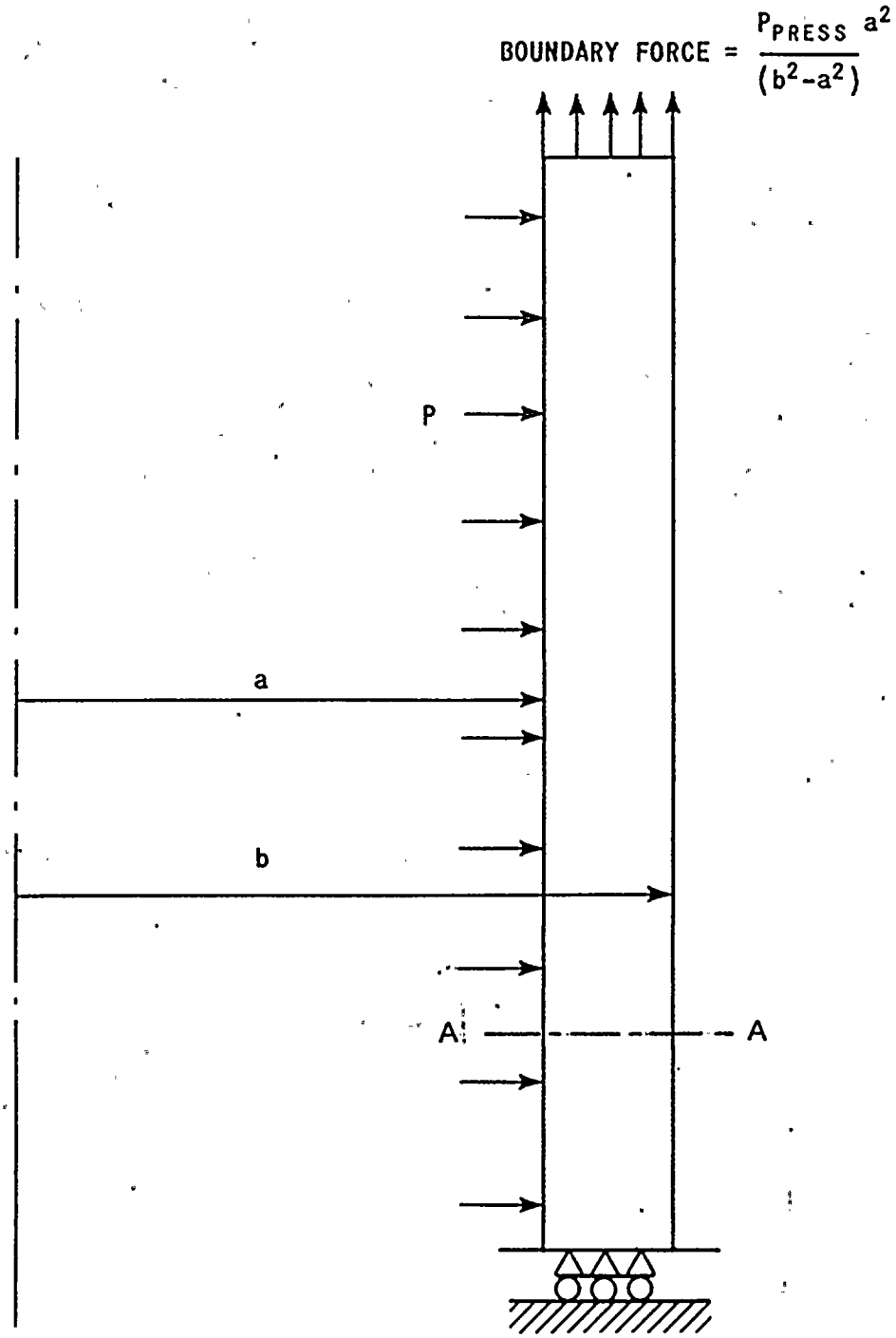

Figure 2-5. Stress Boundary Conditions

2-6. MECHANICAL AND THERMAL PROPERTIES

The material used in the fabrication of the belt line of the reactor vessel is SA-508 Class 2, Table 2-1 furnishes the mechanical and physical properties used in the analysis. Material properties for intermediate temperatures were obtained through interpolation of the data presented in table 2-1.

TABLE 2-1

MATERIAL PROPERTIES

Property	Symbol	Material SA 508 Class 2
Young's modulus (psi)	E_{70}	29.87×10^6
	E_{650}	27.13×10^6
Density (lb/in.^{3})	ρ_{70}	0.2841
	ρ_{650}	0.2797
Conductivity (Btu/hr-in. - °F)	K_{70}	2.208
	K_{650}	1.917
Coefficient of thermal expansion (in/in-°F)	α_{70}	6.10×10^{-6}
	α_{650}	7.35×10^{-6}
Specific heat (Btu/lb-°F)	C_{p70}	0.104
	C_{p650}	0.135

SECTION 3
DESIGN TRANSIENTS

Table 3-1 gives the design transients taken from the applicable Westinghouse specifications used in the evaluation of the reactor vessel belt line region. The transient conditions selected for this evaluation are based on conservative estimates of the magnitude and frequency of the temperature and pressure transients resulting from various operating conditions in the plant and have been updated through operating experience. These are representative of operating conditions which are considered to occur during plant operation and are sufficiently severe or frequent to be of significance to component cyclic behavior. Further, these are regarded as a conservative representation of transients which, when used as bases for component fatigue evaluation, provide confidence that the component is appropriate for its application over the design life of the plant.

The operational transients are broken down into the following categories:

- Normal Condition

  Normal conditions are any conditions noted in the course of system startup, operation in the design power range, hot standby, or system shutdown of the plant, other than Upset, Emergency, Faulted, or Test Conditions.

- Upset Conditions (Incidents of Moderate Frequency)

  Upset conditions are any deviations from normal conditions anticipated to occur often enough that the design has to incorporate a capability to withstand the conditions without operational impairment.

- Test Conditions

  Test conditions are those pressure overload tests including hydrostatic tests and leak tests which occur in the course of testing the system both before and after initial startup.

The total number of cycles for each transient exclusive of the preoperational test cycles has been assumed to be evenly divided over the 40-year operating life of the plant. The assumed schedular distribution of reactor operating transients is shown in table 3-2.

Selective thermal and stress results for the heatup and cooldown transients are presented in figures 3-1 through 3-4.

TABLE 3-1
TRANSIENTS USED FOR FATIGUE EVALUATION

Normal Condition	Occurrences
Heatup and cooldown at 100°F/hr	200
Plant loading and unloading at 5% of full power/min	18400[a]
Step load increase and decrease of 10% from full power	2000
Step load decrease of 50% of full power	200
Steady state fluctuations	1.0×10^6
Upset Conditions	
Loss of load	80
Loss of flow	80
Reactor trip	400
Test Conditions	
Turbine roll[b]	10
Hydrostatic test (3125 psia)	5
Hydrostatic test (2500 psia)	40[c]

a. Although the applicable Westinghouse design specification calls for 14,500 cycles, a conservative estimate of 18,400 cycles was used, based upon operating experience.

b. This transient was not included in the applicable Westinghouse design specification; however, as the plant has undergone this test, it was included for completeness.

c. Although the applicable Westinghouse design specification calls for 5 cycles, a conservative estimate of 40 cycles was used, based upon operating experience.

TABLE 3-2

SCHEDULE OF REACTOR VESSEL OPERATING TRANSIENTS

Transient		Occurrence Table		
	Preoperational Test Cycles	Cycle Type[a] 1	Cycle Type[b] 2	Cycle Type[c] 3
Hydrostatic test (3125 psia)	5			
Turbine roll	10			
Plant heatup/cooldown		1	–	–
Plant loading/unloading		92	–	–
Step load increase/decrease 10% of full power		10	–	–
Step load decrease of 50% of full power		1	–	–
Reactor trip		2	–	–
Steady state fluctuations		5000	–	–
Loss of load			1	–
Loss of flow			1	–
Hydrostatic test (2500 psia)				1

a. Occurrence = 5 cycles/yr
b. Occurrence = 2 cycles/yr
c. Occurrence = 1 cycle/8 yrs

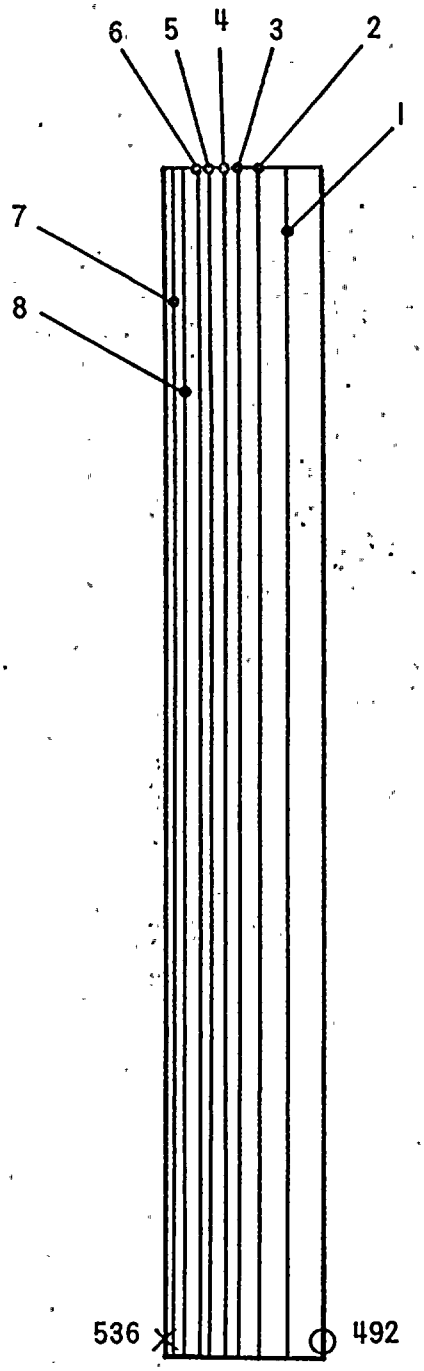

CONTOUR NUMBERS	TEMPERATURES (°F)
1	495
2	501
3	507
4	513
5	519
6	525
7	531
8	534

Figure 3-1. End of Heatup - Isothermal Plot

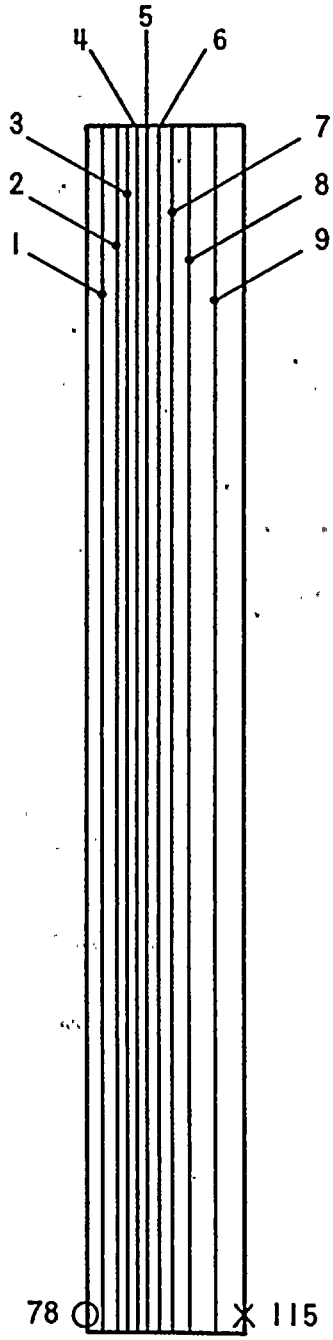

CONTOUR NUMBERS	TEMPERATURES (°F)
1	82
2	86
3	90
4	94
5	98
6	102
7	106
8	110
9	114

Figure 3-2. End of Cooldown - Isothermal Plot

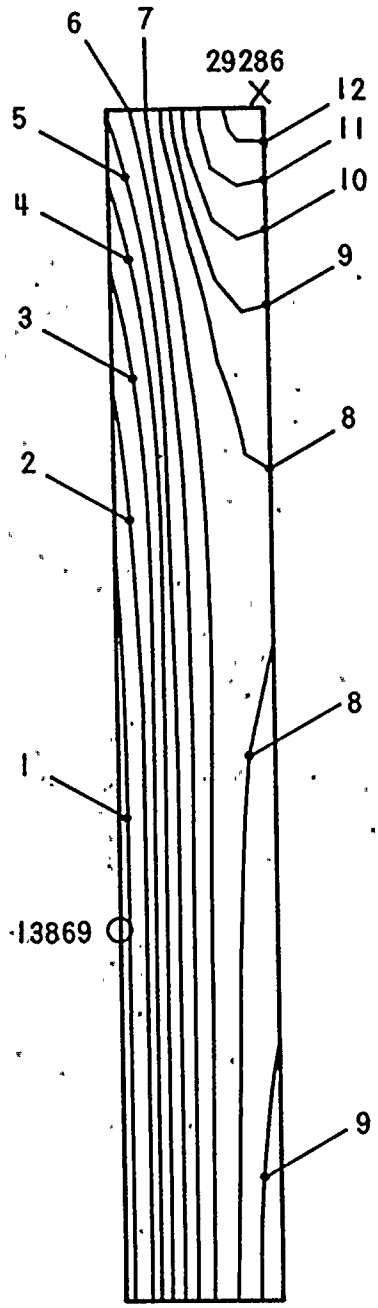

CONTOUR NUMBERS	PSI
1	15000
2	16500
3	18000
4	19500
5	21000
6	22500
7	24000
8	25500
9	26250
10	27000
11	27750
12	28500

Figure 3-3. End of Heatup - Hoop Stress Plot

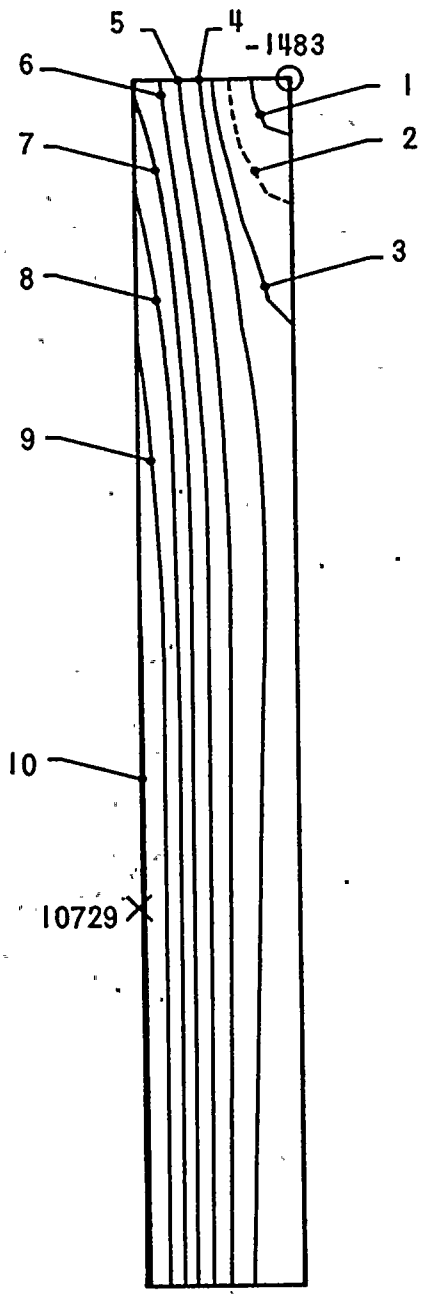

CONTOUR NUMBERS	PSI
1	-750
2	0
3	750
4	1500
5	3000
6	4500
7	6000
8	7500
9	9000
10	10500

Figure 3-4. End of Cooldown - Hoop Stress Plot

SECTION 4
STRESS INTENSITY FACTOR K_I CALCULATIONS

This section describes a method by which the K_I (stress intensity factor) is calculated using the membrane stress and the bending stress as determined by stress analysis. The applied stresses at the flaw location are resolved into membrane and bending stresses with respect to the wall thickness. Pressure, thermal, and discontinuity stresses are considered in the determination of the K_I factors. In the case of a nonlinear stress distribution through the vessel wall, the actual stress distribution is conservatively approximated by using the linearization technique illustrated in figure 4-1. The linearization technique results in higher membrane stresses than would be obtained by using the ASME Code Section XI[1] method. Since the correction factors for membrane stresses (see equation 4-1) are greater than the correction factors for bending stresses, the applied linearization technique results in higher K_I values and consequently, yields conservative results.

Because of the general shape of the calculated stress distribution as shown in figure 4-1, a surface flaw on the inside surface of the belt line is postulated. The surface flaw is considered the worst type of flaw that can be postulated in a reactor vessel. The most critical orientation for this assumed flaw is perpendicular to the direction of maximum principal stress, or axial in this case. A semielliptical configuration with a length-to-depth ratio of 6 and its major axis on the surface is assumed for the shape of the flaw. This flaw geometry is consistent with the type of surface flaw recommended by ASME Code Section III, Appendix G for fracture mechanics evaluation of design transient conditions. The flaw depths varying from 0.125 to 1 inch assumed in this evaluation provide an excellent range of limits for evaluating growth of postulated flaws in the belt line.

For the membrane and bending stresses calculated using the methods described in section 2 and presented in table 4-1, the stress intensity factor at the point of maximum depth is calculated from reference [1]:

1. ASME Boiler and Pressure Vessel Code, Section XI, "Rules for Inservice Inspection of Nuclaer Power Plant Components," American Society of Mechanical Engineers, New York, 1974

$$K_I = \sqrt{\frac{\pi a}{Q}}\ [\sigma_m M_m + \sigma_b M_b] \qquad (4\text{-}1)$$

where:

K_I = Stress intensity factor

σ_m, σ_b = Membrane and bending stress, respectively

a = Minor semiaxis (flaw depth)

Q = Flaw shape parameter, including a plastic zone correction factor, for plane strain conditions. (See figure 4-2.)[1]

$= [\phi_1^2 - 0.212\ (\sigma/\sigma_{ys})^2]$

$$\phi_1 = \int_0^{\pi/2} \sqrt{1 - \left(\frac{b^2 - a^2}{b^2}\right) \cos^2\phi}\ d\phi$$

σ_{ys} = Yield strength of the material

σ = $\sigma_m + \sigma_b$

b = Major semiaxis (1/2 flaw length)

ϕ = Parametric angle of the ellipse

M_m = Correction factor for membrane stresses (see figure 4-3)[1]

M_b = Correction factor for bending stresses (see figure 4-4)[1]

1. ASME Boiler and Pressure Vessel Code, Section XI, "Rules for Inservice Inspection of Nuclear Power Plant Components," American Society of Mechanical Engineers, New York, 1974

The range of stress intensity factor (ΔK_I) for fluctuations of applied stress is determined by replacing σ_m with $\Delta\sigma_m$, and σ_b with $\Delta\sigma_b$. In the analysis, correction factors for bending stresses (M_b) applicable to the point of maximum crack depth ($\beta = 0$) were applied because for cracks with a depth less than approximately 1/4 T, M_b ($\beta = 0$) is greater than M_b ($\beta \neq 0$). However, the amount of conservatism thus introduced is negligible, since the contribution of bending stresses to K_I is very small.

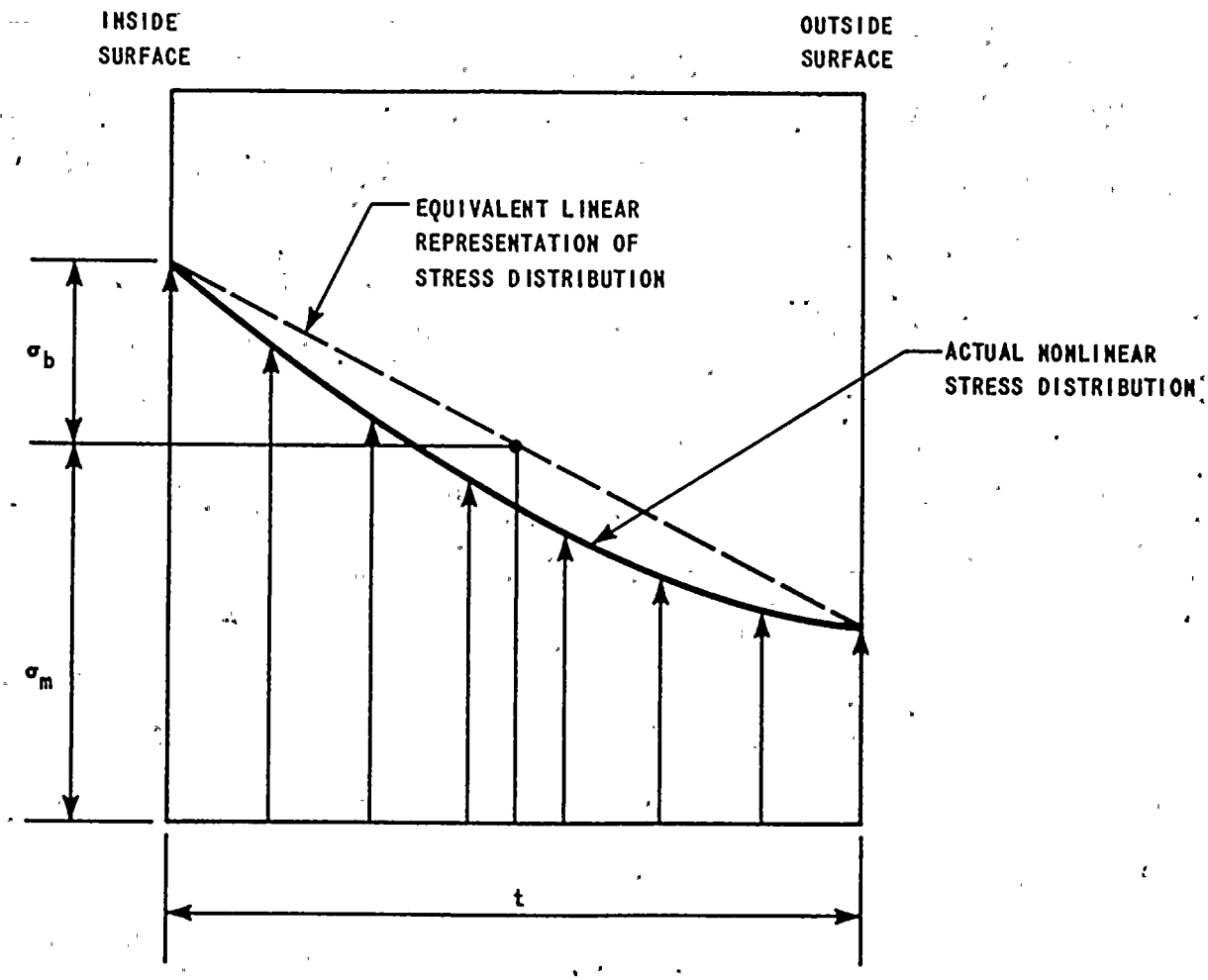

Figure 4-1. Linearized Representation of Stresses

TABLE 4-1

INSIDE SURFACE AND MEAN STRESSES AND STRESS RANGES FOR THE CRITICAL LOCATION OF THE TURKEY POINT UNITS NO. 3 AND NO. 4 REACTOR VESSEL

Transient	σ_{Inside} (ksi)	σ_{Mean} (ksi)	$\Delta\sigma_{Inside}$ (ksi)	$\Delta\sigma_{Mean}$ (ksi)
Hydrostatic test (3125 psia)	32.87	31.33	32.87	31.33
Turbine roll	31.97	22.96	11.83	3.77
Plant heatup/cooldown	27.24	21.18	27.24	21.18
Plant loading/unloading at 5% of full power/min	24.95	22.96	2.64	0.88
Step load increase and decrease of 10% of full power	26.33	23.42	5.74	2.09
Step load decrease of 50% of full power	25.89	22.94	6.62	2.93
Reactor trip	23.64	22.52	4.02	8.83
Steady-state fluctuations	24.89	23.37	2.50	1.69
Loss of load	23.85	23.87	9.91	6.96
Loss of flow	32.99	26.33	13.32	7.59
Hydrostatic test (2500 psia)	26.27	25.04	26.27	25.04

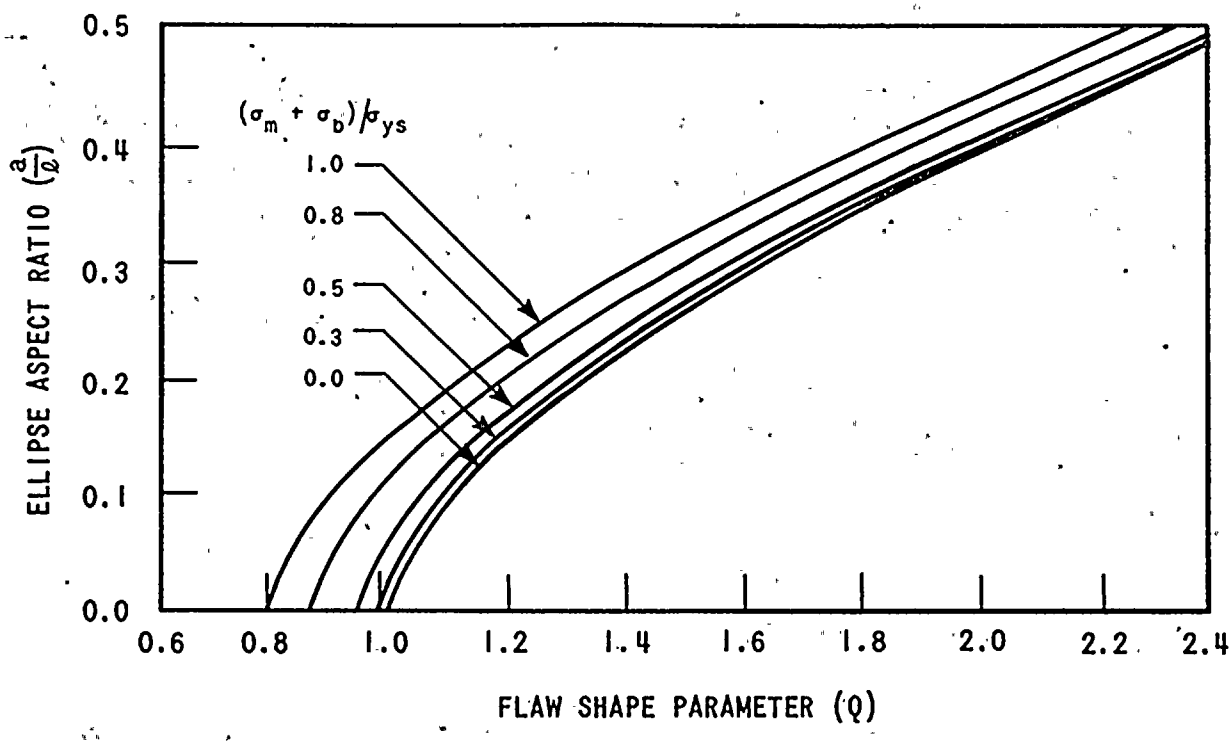

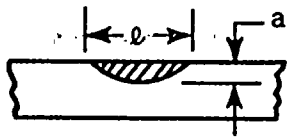

SURFACE FLAW

Figure 4-2. Shape Factors for Surface Flaws

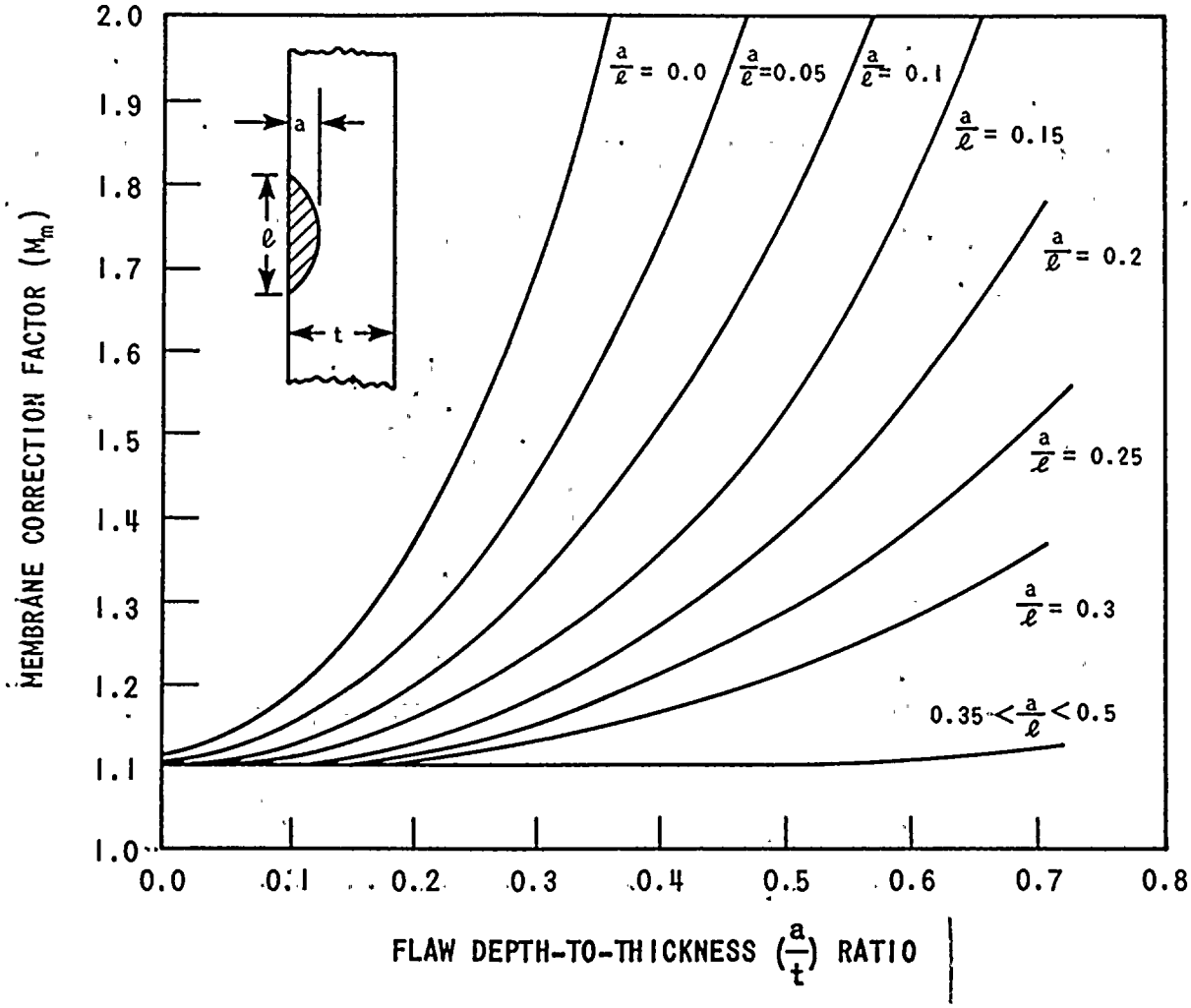

Figure 4-3. Membrane Correction Factors for Surface Flaws

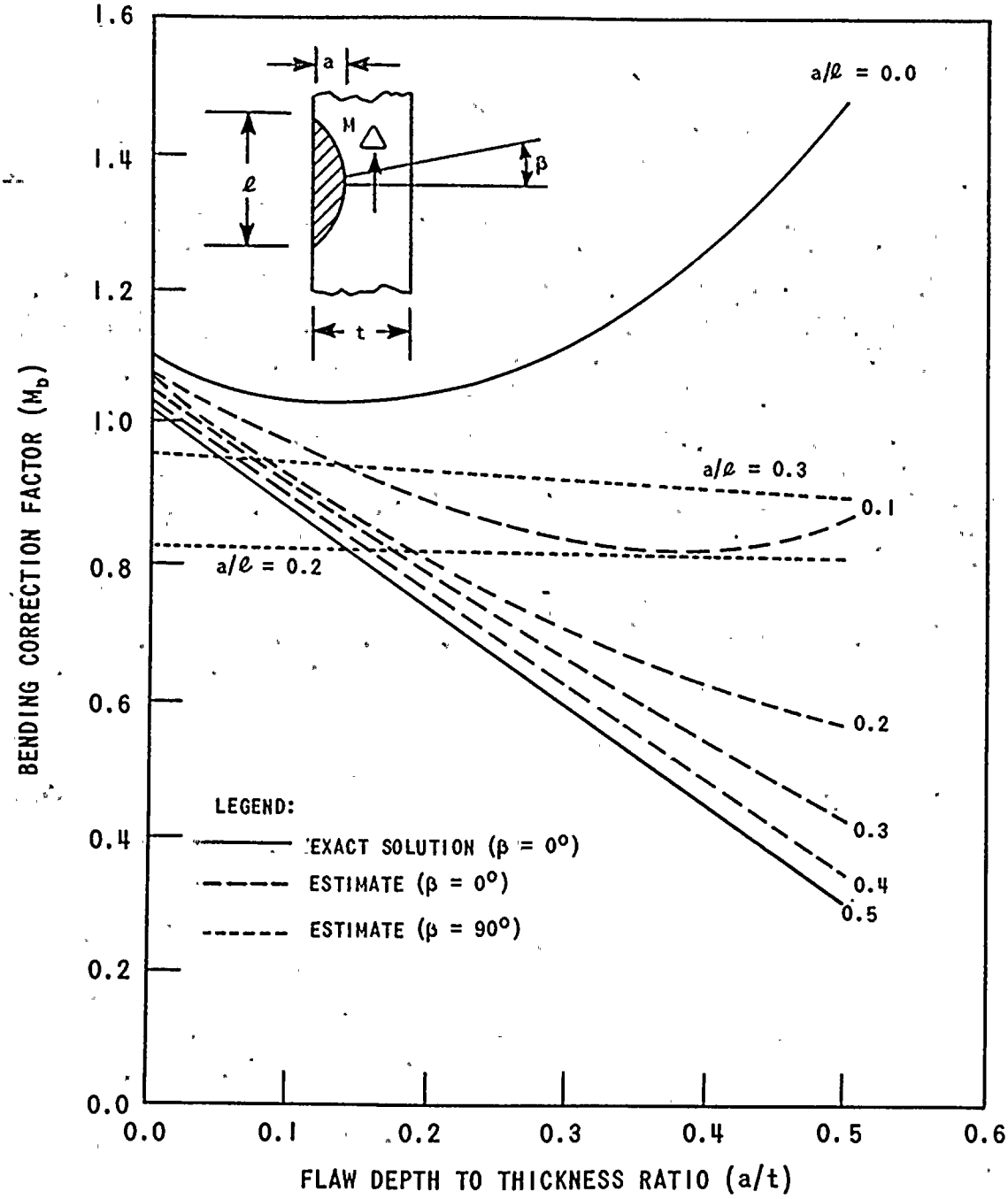

Figure 4-4. Bending Correction Factor for Surface Flaws

SECTION 5
FATIGUE CRACK GROWTH RATE

The fatigue crack growth rate (da/dN) of the material is characterized in terms of the range of applied stress intensity factor (ΔK_I). This characterization is generally of the form:

$$\frac{da}{dN} = C_o \, (\Delta K_I)^n$$

Where n is the slope of the log (da/dN) versus log (ΔK_I) curve, and C_o is a scaling constant. These data should preferably be obtained from specimens of the actual material, taking into account material variability, environment, test frequency, and any other variables that may affect the data. However, for a given flaw or crack size, a wide variation in loading can be considered. Fatigue crack growth data generally do not account for variations in the level of applied loading during cycling. Further, it has been found that when cycles of high amplitude are followed by cycles of low amplitude the crack growth rate for the low amplitude cycles is lower than that predicted by the constant load data. Furthermore, when this order of loading is reversed, the constant load data apply and therefore it is generally conservative to use constant load data.

An upper bound curve for fatigue crack growth data measured on SA-533B-CL1 and SA-508-CL2 steels, including the effects of temperature, frequency, and pressurized water environment and represented by the following expression from Reference [1] is used in the current evaluation.

$$\frac{da}{dN} = (0.3795 \times 10^{-3}) \, (\Delta K_I)^{3.726}$$

where:

$\frac{da}{dN}$ = Crack growth rate, μin./cycle

ΔK_I = Stress intensity factor range, ksi$\sqrt{\text{in.}}$

The curve furnished in figure 5-1 is taken from the ASME Code, Section XI.[1]

1. ASME Boiler and Pressure Vessel Code, Section XI, "Rules for Inservice Inspection of Nuclear Power Plant Components," American Society of Mechanical Engineers, New York, 1974.

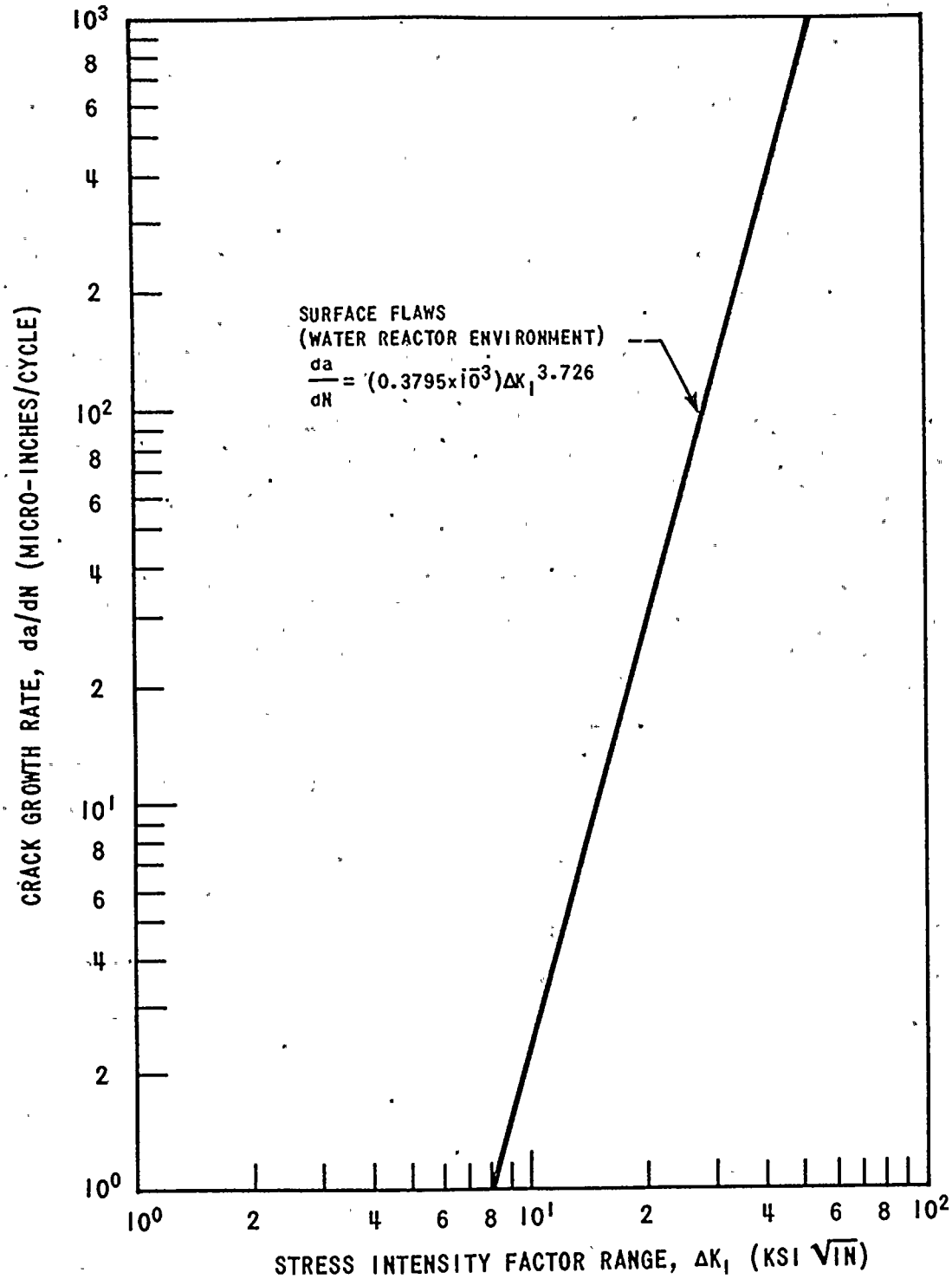

NOTE: THIS FIGURE IS THE SAME AS FIGURE A4300-1, ASME BOILER AND PRESSURE VESSEL CODE, SECTION XI, WINTER 1975, ADDENDA

Figure 5-1. Upper Bound Fatigue Crack Growth Data for Reactor Vessel Steels

Fatigue crack growth data obtained recently by Westinghouse in testing sponsored by the Heavy Section Steel Technology Program[1,2] have shown that the present Section XI curve does not fully describe the crack growth behavior. The crack growth rate displays a double sloped character, with the rate somewhat higher than the Section XI curve at intermediate values of ΔK, and lower than the Section XI curve at very low and very high values of ΔK. Analyses have shown that crack growth determined by use of this new behavior is somewhat less than that calculated from Section XI curve. Since Turkey Point Units 3 and 4 are not subjected to intermediate ΔK's, the analysis for this report has for conservatism used the curve presently in Section XI.

1. Whitman, G. D., "Quarterly Progress Report on the Heavy Section Steel Technology Program for October-December 1975", ORNL/NUREG/TM-3, April 1976.
2. Whitman, G. D., "Quarterly Progress Report on the Heavy Section Steel Technology Program for January-March 1976", ORNL/NUREG/TM-28. July, 1976.

SECTION 6
FATIGUE EVALUATION

The procedure used in applying the linear elastic fracture mechanics concepts to perform a fatigue crack growth analysis of the reactor vessel beltline region is described in this section.

To determine the maximum potential for fatigue crack growth of the postulated flaw during normal operation, a cumulative fatigue crack growth study of the beltline region is performed. All design transients are considered in chronological order according to the assumed schedule prescribed in table 3-2. Stress intensity factors are determined for each transient using the bounding semielliptical flaw model and the methods for K_I determination outlined in section 4.

Each transient is evaluated in the following manner:

1) Determine the maximum range of K_I fluctuation associated with the transient (ΔK_I).

2) Determine the incremental flaw growth (Δa) corresponding to ΔK_I from the fatigue crack growth data.

3) Update the flaw size by assuming the flaw grows to a geometrically similar flaw with a minor half axis ($a + \Delta a$).

4) Proceed to the next transient.

After all transients have been considered, the above procedure yields the expected end-of-life flaw size (a_f). The procedure has been automated using a computer program and from this the crack growth in the critical location of the belt line region has been determined for a period of 10, 20, 30 and 40 years of reactor operation for a number of postulated initial flaw depths. The stress intensity ranges (ΔK_I) associated with the transients are presented in table 6-1.

TABLE 6-1

STRESS INTENSITY FACTOR RANGES (ΔK_I)

TURKEY POINT UNITS NO. 3 AND NO. 4 REACTOR VESSEL BELT LINE REGION

Transient	Postulated Flaw Depth (in.)	ΔK_I ksi $\sqrt{in.}$
Cold hydrostatic test	0.125	20.852
	0.250	29.603
	0.500	42.128
	0.750	51.549
	1.000	59.750
Turbine roll	0.125	7.518
	0.250	10.537
	0.500	14.703
	0.750	17.549
	1.000	19.714
Heatup/cooldown	0.125	17.101
	0.250	24.191
	0.500	34.242
	0.750	41.620
	1.000	47.845
Plant loading/unloading	0.125	1.667
	0.250	2.337
	0.500	3.262
	0.750	3.896
	1.000	4.381
Step load increase and decrease of 10% of full power	0.125	3.456
	0.250	4.848
	0.500	6.776
	0.750	8.103
	1.000	9.126
Step load decrease of 50% of full power	0.125	4.003
	0.250	5.626
	0.500	7.882
	0.750	9.457
	1.000	10.696
Reactor trip	0.125	2.701
	0.250	3.919
	0.500	5.760
	0.750	7.324
	1.000	8.881
Steady-state fluctuations	0.125	1.532
	0.250	2.163
	0.500	3.053
	0.750	3.697
	1.000	4.230

TABLE 6-1 (cont)

STRESS INTENSITY FACTOR RANGES (ΔK_I)

TURKEY POINT UNITS NO. 3 AND NO. 4 REACTOR VESSEL BELT LINE REGION

Transient	Postulated Flaw Depth (in.)	ΔK_I ksi $\sqrt{in.}$
Loss of load	0.125	6.073
	0.250	8.580
	0.500	12.119
	0.750	14.692
	1.000	16.834
Loss of flow	0.125	8.246
	0.250	11.618
	0.500	16.344
	0.750	19.711
	1.000	22.439
Hot hydrostatic test	0.125	16.431
	0.250	23.326
	0.500	33.195
	0.750	40.619
	1.000	47.081

SECTION 7
RESULTS AND CONCLUSIONS

Based on the results of the fatigue crack growth calculations of the Turkey Point Units No. 3 and No. 4 reactor vessel belt line region presented in table 7-1, an initial flaw of 0.125 inch grows to 0.131 inch, and a 1-inch flaw grows to 1.349 inches at the end of 40 years of plant life. The above maximum amount of fatigue crack growth due to normal operating conditions during the design life of the reactor vessel is considered small.

TABLE 7-1

RESULTS OF FATIGUE CRACK GROWTH EVALUATION –
TURKEY POINT UNITS NO. 3 AND NO. 4 REACTOR VESSEL BELT LINE REGION

Postulated Initial Flaw Depth (in.)	Final Flaw Depth (in.) After (___) Years of Reactor Operation			
	10	20	30	40
0.125	0.127	0.128	0.130	0.131
0.250	0.256	0.261	0.267	0.273
0.500	0.522	0.542	0.564	0.588
0.750	0.795	0.840	0.889	0.943
1.000	1.077	1.155	1.245	1.349